PhD in Earth and Marine Sciences
Department of Earth and Marine Sciences (DiSTeM)
Scientific Sector GEO/02

Multi-disciplinary analysis to construct a crustal model of the Sicily Channel using geological and geophysical techniques (data): impacts on geological hazard

PhD STUDENTI
Alessandra Carollo

COORDINATOR
Prof Alessandro Aiuppa

TUTOR
Prof. Attilio Sulli

CO TUTOR
Prof. Raffaele Martorana
Prof. Sebastiano D'Amico

- XXXV CYCLE -
A.A. 2022/2023

CONTENTS

Abstract

To understand the dynamics of crustal deformation and earthquakes in active orogenic systems, it is essential to have a detailed view of the lithospheric structures in three dimensions (3D). Several studies in the literature explain how 3D visualization can enable the recognition of tectonic structures or to be able to establish connections between intraplate volcanoes (*Wu et al., 2016; Lei & Zhao, 2016; Tan et al., 2019*).

This work aims to define and discretize a 1D-velocity model of the Sicily Channel; create a detailed 3D lithospheric model of the Sicily Channel using a multidisciplinary approach to evaluate the geological hazard elements that affect the Iblean foreland integrating bathymetry, heat flow, magnetometric, gravimetric, seismicity, geophysical data, and main active faults. Moreover, it aims to produce a qualitative and quantitative model of Moho, integrating data on the most relevant earthquakes and active faults.

Until now, the information concerning the deep lithospheric structure of the Sicily Channel is not very detailed. Most of the knowledge is generally related to the monitoring of earthquakes (e.g., *Calò & Parisi, 2014; Agius et al., 2020*), seismic surface wave tomography (*Kherchouche et al., 2020; Agius et al., 2020*), the analysis and interpretation of seismic surface profiles (e.g., *Torelli et al., 1995; Corti et al., 2006; Khomsi et al., 2009; Cavallaro et al., 2017; Civile et al., 2018; 2021*), analysis of volcanic system (e.g., *Rotolo et al., 2006*) and plate movement. In addition, the seismic models in the area concern possibly large-scale seismic models that do not cover the total area of the Sicily Channel or are incomplete to be updated.

Three-dimensional lithospheric modeling allows immediate determination of the geometric and kinematic relationships between deep dynamic processes and deformations occurring in the surface crust. Several studies have shown how the three-dimensional model visualization approach, which constrains data of different natures, can be helpful in the study of global tectonics. For example, Wu et al. (2016) performed a tectonic reconstruction of the plates of the Philippine and Asian seas, in which slabs were mapped 3D, allowing them to be quantitatively constructed and

plotted in depth. Lu et al. (2019) developed a three-dimensional visualization technique and produced a lithospheric model below the Tibetan plateau.

Although the Sicily Channel is developed in the Pelagian block, an area considered geologically stable bounded by the southern African plateau and the northern Eurasian plateau, complex geological structures characterize it and are seismically active. This zone is known for its potential seismic hazard, as it is located in a seismically active zone; the area suggests that future seismic events are possible. However, it is essential to note that earthquakes' occurrence and intensity are difficult to predict with certainty; attempts are made to monitor and study the seismic activity in the Mediterranean region. Seismological networks and research institutions work to assess seismic hazards and improve understanding of the geological processes at play. These efforts aim to provide early warning systems and develop an approach for mitigating potential earthquakes' impact.

A 3D geodynamic model of the lithosphere is a theoretical framework to study the processes and movements within Earth’s lithosphere, and it aims to show the dynamics of the lithosphere's evolution over geological timescales.

By defining the geodynamic model of the Sicilian Channel's lithosphere, which contains various components, it is possible to identify, e.g., main seismogenic structures or structures that affect the uplift of deep magmatic fluids.

Overall, 3D lithosphere geodynamic models allow understanding of Earth's dynamic processes better and improve the ability to interpret geological observations. They help to refine knowledge of plate tectonics, seismic hazards, and the long-term evolution of the Earth's surface.

1. CHAPTER - INTRODUCTION

The Sicily Channel is a system of about 500 km offshore rift that develops in the central Mediterranean between Sicily and Tunisia (*Finetti, 1985*). This area is characterized by a multitude of regional tectonic stresses, by normal and strike-slip faults, which have generated the main grabens of Malta, Linosa, and Pantelleria (*Cello, 1987; Jongsma et al., 1985; Boccaletti et al., 1987*).

To understand the dynamics of crustal deformation and earthquakes in active orogenic systems, it is essential to have a detailed view of the lithospheric structures in three-dimensions (3-D). There are several methods for studying lithospheric structures in 3-D, such as seismic tomography, which uses earthquake waves to create images of the Earth's interior. By analyzing how seismic waves travel across the Earth, scientists can infer the properties of the rocks and structures they pass through. This technique can be used to create 3-D models of the lithosphere, revealing the location, shape, and orientation of various features such as faults, fractures, and magma chambers. Another technique for studying lithospheric structures in 3-D is gravity and magnetic imaging. The method uses measurements of the Earth's gravity and magnetic fields to infer the subsurface's distribution of rocks and minerals. By analyzing the variations in these fields, scientists can identify the location and extent of various lithospheric features such as mountain ranges, basins, and faults. In addition to these techniques, various geodetic methods can be used to study lithospheric structures in 3-D. For example, GPS measurements can be used to track the movement of tectonic plates and to infer the location and orientation of faults and other structures. InSAR (Interferometric Synthetic Aperture Radar) can also be used to create detailed maps of ground deformation over time, revealing the location and extent of various features such as fault zones and volcanic centers.

The thesis work is divided into 6 chapters:

Chapter 1 concerns the introduction of this work; the main objectives are described, and the reasons for which this work on Sicily Channel was approached. This work aims to define and discretize a 1D-velocity model of the Sicily Channel; create a detailed 3D lithospheric model of the Sicily Channel using a multidisciplinary approach to evaluate the geo-hazard and geological risk elements that affect the Iblean foreland integrating bathymetry, heat flow, magnetometric, gravimetric,

seismicity, geophysical data, and main active faults. Moreover, produce qualitative and quantitative modeling of a map of Moho, integrating data on the most relevant earthquakes and active faults.

In Chapter 2 is a description of the geodynamic context of the Sicily Channel. It describes the tectonic evolution dating back to 180 Ma with the creation of the Tethys Ocean, describing the main events of compression and continental rifting that led to the current geodynamic structure of the Mediterranean Sea. A study has been made on the historical and recent seismicity through the implementation of several catalogs, to define the general framework of seismicity that affects the Pelagian block. The lithospheric features of heat flow, magnetic anomalies, and magnetometric anomalies are defined for detecting buried magmatic bodies, thus, determining characteristics of Sicily Channel volcanism.

In Chapter 3, the data used in the work are presented. Different data were collected in this study; a good part derives from the ViDEPI project. The CROP multichannel seismic reflection profiles, the Italian commercial zone "G" and the well data were obtained from the online database. Seismic profiles from various authors, Wide-Angle-Reflection-Refraction profiles, and 2D velocity models were consulted. Thus, the 1D- velocity model for the Sicilian Channel calibrated with well data is built and compared with data from the literature. Data on seismic events from January 2005 to December 2021 from the INGV and ISC catalogs, and records of Maltese seismic stations were collected to have a more robust database. There are several examples of the processing phase of seismic signals where it was possible to identify the picking of the P and S phases, and some examples of very noisy signals are also shown. Where possible, a digital filter has been applied to reduce the noise present in seismic signals, thus improving the signal quality.

Chapter 4 describes the methodology used to create the 3D lithospheric model of the Sicily Channel. It describes the phase of interpretation of seismic horizons, of how these were determined in seismic profiles. It describes the conversion phase and the method used to convert seismic profiles from time (TWT) to depth (m).

In Chapter 5, the *b*-value is determined from the Gutenberg-Richter relation to assess earthquake catalogs' quality; the focal mechanisms present in the Sicily Channel are analyzed to provide an estimate of the local stress field; and the relationship between these parameters is described. In addition, describes the geophysical method of

tomography. It defines the concept of seismic tomography, the different applications, and the definition of non-uniqueness of the model that is obtained. It also describes the logarithm of inversion and the velocity model to be used for seismic tomography and for the relocation of earthquakes.

Chapter 6 presents the results obtained. i) The relocation map of earthquakes is shown as a function of the 1D velocity model provided in this work; ii) the 3D crustal model is described, showing and describing the sections that through the Channel of Sicily; iii) the map of Moho 3D the Sicily Channel is represented and described.

Chapter 7 contains the details of the work, and the discussions.

2. CHAPTER - THE GEODYNAMIC FRAMEWORK OF THE SICILY CHANNEL

2.1. Geological and structural setting

The Sicily Channel is a region in the Mediterranean Sea between the island of Sicily, in southern Italy, and the coast of Tunisia, in North Africa. The Sicily Channel is sited in the northern portion of the African continental plate, called the Pelagian Block (*Burollet et al., 1978*), part of the Nubian continental margin extending from the Tunisian Sahel to eastern Sicily. The area is characterized by a complex geologic setting that includes several rock types, structural features, and tectonic activity. The central Mediterranean is composed of two basins with distinctive characteristics: i) the central-eastern portion consists of a predominantly old oceanic lithosphere (about 340 million years ago), ii) the westernmost portion consists of young oceanic lithosphere (30 million years ago). This distinction results from the collision of the Adria plate (promontory of the African plate) with the Eurasian plate (*Blom et al., 2020*).

To understand the present geodynamic structure of the Sicily Channel, it is necessary to examine the global tectonics evolution of the Central Mediterranean region. Around 180 Myr, the continental rupture of the Pangaea (*Jongsma et al., 1985*) and the Tethys Ocean was created between Eurasia and Gondwana. From the Triassic to the Jurassic began the phase of transition from continental rifting to ocean rifting (*Catalano & D'Argenio, 1981*). The Mesozoic times is characterized by the closure of the Tethys Ocean (*Catalano & D'Argenio, 1981; Antonelli et al., 1988; Catalano et al., 2000*), and the Lower Cretaceous is affected by a phase of diffuse extension expanded even to the Sirte Basin in Tunisia (*Stampfli et al., 2001*). In the Upper Cretaceous-Middle Eocene, an NW-SE-oriented compressive event is generated (*Antonelli et al., 1988; Torelli et al., 1995*), contemporary to the change of direction of the African Plate that began to move northward (S*tampfli et al., 2001*). In the Upper Oligocene-Lower Miocene, the main compressional deformation in the central Mediterranean Sea began with the counter-clockwise rotation of the Corsica-Sardinia block and its collision with the African margin creating the collisional system of Sicily (*Catalano et al., 2004*). The orogenesis occurred concerning the westward subduction of the Adriatic, northern African, and

Ionian lithosphere beneath the Corsica-Sardinia block. During the Upper Messinian, the evolution of the central Mediterranean was blocked due to the closure of the Mediterranean Basin and the consequent separation from the Atlantic Sea, an event defined as the "Messinian Salinity Crisis" (*Butler et al., 1995*), thus causing the emergence of most of the submarine volcanoes which incurred widespread erosion effects (*Civile et al., 2014; 2015*). During the Lower Pliocene, the extensional event led to Malta, Linosa, and Pantelleria graben formation with WNW-ESE direction (*Grasso et al., 1999; Corti et al., 2006; Calò & Parisi, 2014; Civile et al., 2021*). This event appears to have occurred at the same time as the evolution of the Sicilian-Fold-and-Thrust-Belt (SFTB) located in the central part of the Mediterranean, representing a curve segment of the Apennine-Maghrebian Chain (*Catalano et al., 2013; Napoli et al., 2015)*.

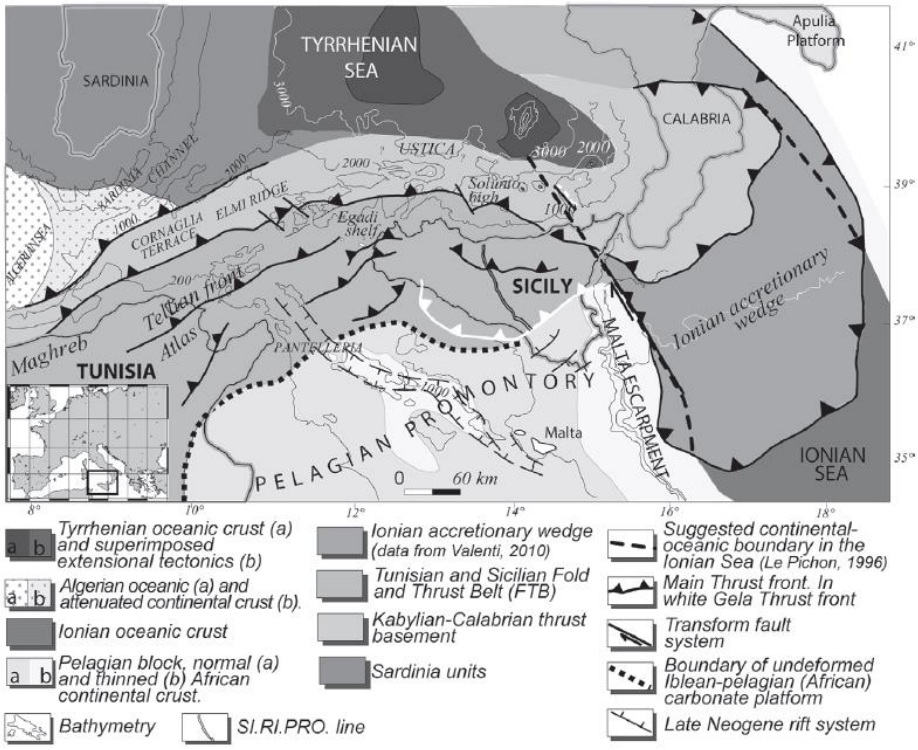

FIGURE 1. SCHEMATIC STRUCTURAL MAP OF THE CENTRAL MEDITERRANEAN AREA. THE MAP DISPLAYS THE PANEL OF THE STUDY AREA. THE MAIN THRUST FRONTS ARE SHOWN IN BLACK, AND THE FRONT OF GELA IS IN WHITE (FROM *Catalano et al., 2013*).

Three elements characterize the collisional system of Sicily and offshore areas (Fig. 1):

i. An E and SE-vergent fold and thrust belt (SFTB) that outcrops in northern Sicily, constituted by Peloritani Units, Sicilide Units, and Maghrebian-Sicilian Units (*Catalano & D'Argenio, 1981; Finetti, 2005*);
ii. a WNW-ESE trending foredeep which expand from the southern Sicily offshore (Gela Basin) to the Ionian margin of Sicily;
iii. a foreland area that outcrops in the Hyblean Plateau and is submersed in the Pelagian Sea and the adjacent Ionian Sea, defined by continental and oceanic crust (*Catalano et al., 2001*).

2.2. Lithological and lithostratigraphic setting

The area of the Sicily Channel is characterized by a set of lithostratigraphic units of the Trapanese-Saccense and Hyblean domains, belonging to the paleogeographic domains of the Sicilian mainland (*Catalano et al., 1989*). The facies Trapanese-Saccense extends from the Northern Adventure bank to Agrigento offshore, while in the southern sector, sequences belong to the Pelagian block (Tunisian-Malta). Antonelli et al. (1988) represented a lithostratigraphic scheme of this area based on the integration of well and seismic reflection data acquired on the northern coast of the Sicily Channel (Fig. 2).

In detail, the Trapanese-Saccense facies expand from the Adventure Bank and offshore Agrigento; Triassic-Eocene carbonates and marls below Oligocene-Quaternary clastic deposits characterize these. The carbonate sequences are platform carbonates of the Trias-Lias age (Sciacca and Inici formations) that pass, from bottom to top, to limestone and deep marls (Buccheri, Chiaramonte, Hybla and Amerillo formations). In comparison, the clastic sequences are sedimentary rocks of the coastal and external platform (Fortuna, Ain Grab, Corleone, Terravecchia, and Ribera formations) mixed with open platforms and shallow water marl and limestone (San Cipirello, Mahmoud, and Nilde formations) and evaporitic deposits.

The Hyblean domains extend between the Ragusa-Malta Plateau and offshore of the Agrigento coast.

The sequence presents deep sea and platform carbonate and sedimentary rocks of Trias-Lias age (Gela, Noto, Streppenosa, Siracusa, and Modica formations) that pass from bottom to top to pelagic and deep-sea rocks (Buccheri, Chiaramonte,

Hybla, and Amerillo formations). This sequence is covered by external platform carbonates, marl, and evaporitic deposits of the Oligocene-Miocene age and clastic deposits of the Plio-Quaternary age (Ribera formation).

In the southern sector of the Sicily Channel, however, sequences belong to the outward domains of the Pelagian block (Tunisian and Malta). The Tunisian area has shallow platforms (Jurassic) and pelagic carbonates compared to Trapanese and Iblean sequences (Siracusa and Buccheri formations), passing to deep marine carbonates deposits and clastics (Sidi Kralif, Fahden, Aleg, Abiod, El Haria, and Souar formations). Above, there are Oligo-Quaternary deposits like those of the Trapanese domain. Malta facies have shallow marine carbonate deposits (Gela, Alexia, and Siracusa formations, Naxxar and Malta Groups, Upper Coralline Limestone) that develop in the southern area of the Ragusa-Malta Plateau (*Jongsma et al., 1985*).

As shown in Figure 3, we can synthesize the tectonic evolution of the area in four main phases along a hypothetical south-north transect from offshore Tunisia, Malta, and Sicily (*Lipparini et al., 2009*).

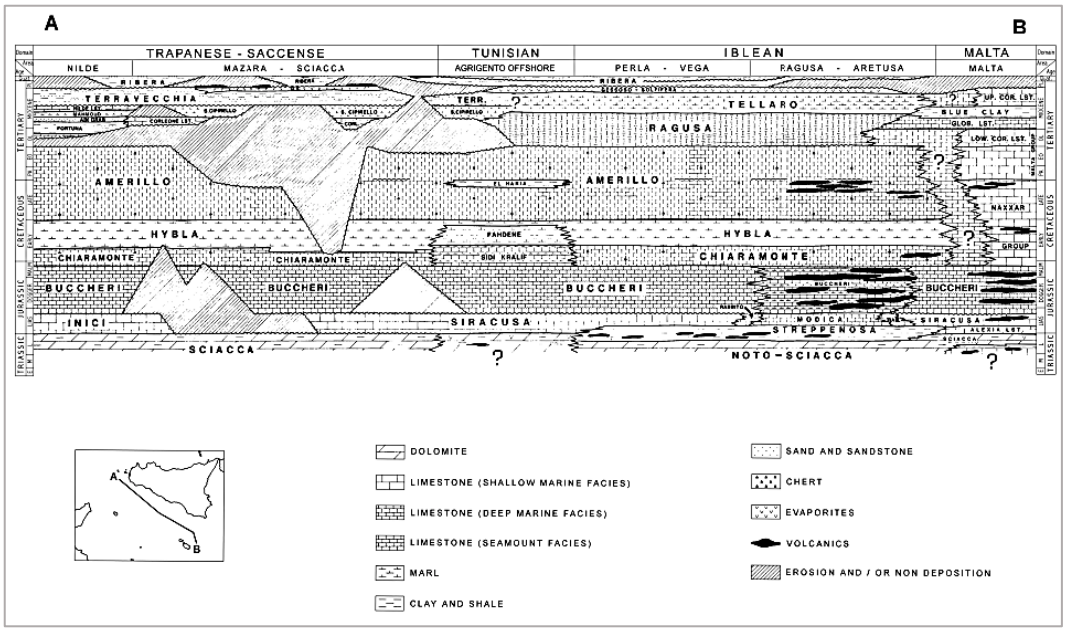

FIGURE 2. LITHOSTRATIGRAPHIC CORRELATION CHART ALONG THE CENTRAL AND EASTERN PART OF THE NORTHWEST SICILY CHANNEL. THE CORRELATIONS BETWEEN THE TRAPANESE-SACCENSE, TUNISIAN, HYBLEAN, AND MALTESE LITHOSTRATIGRAPHIC SEQUENCES ARE DESCRIBED IN SECTION A-B (FROM *Antonelli et al., 1988*).

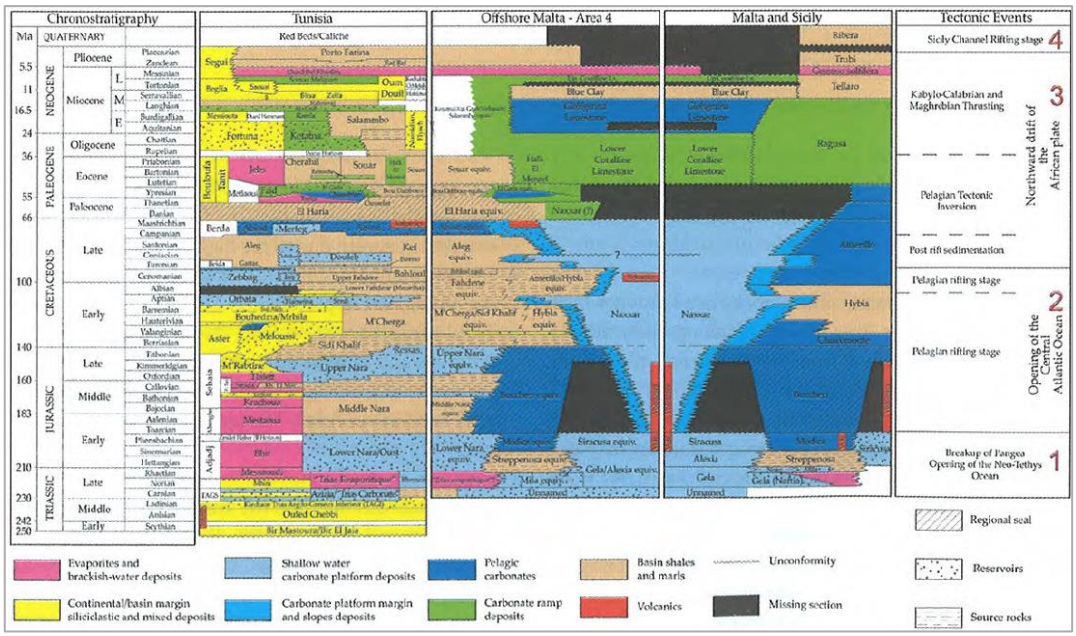

FIGURE 3. REGIONAL STRATIGRAPHY AND TECTONICS CHART: MAIN DEPOSITIONAL ENVIRONMENTS DEVELOPED ALONG A HYPOTHETICAL SOUTH-NORTH TRANSECT FROM OFFSHORE TUNISIA TO SICILY AND MAIN TECTONIC EVENTS (FROM *Lipparini et al., 2009*).

2.3. Morphostructural and structural background

The central Mediterranean area is characterized by a large shelf (Fig. 4) that expands from the southwestern Sicilian offshore in the Adventure bank and reaches the maximum extension to the Malta escarpment.

The Sicily Channel is a shallow sea where the water depth is, on average, less than 400 m and reaches a depth between 1300 and 1700 m in the Pantelleria, Linosa and Malta graben, WNW-ESE-oriented. These basins divide into secondary grabens such as Malta-Medina and Medina-Melita grabens separating the Maltese plateau respectively from the Medina bank and Medina bank from the Melita bank. Such graben is the result of a continental rifting event from the Neogene-Quaternary affecting the African lithosphere (*Finetti, 1984; Jongsma et al., 1985; Boccaletti et al., 1987; Dart et al., 1993; Reuther et al., 1993; Argnani, 2009; Ventura et al., 2014*).

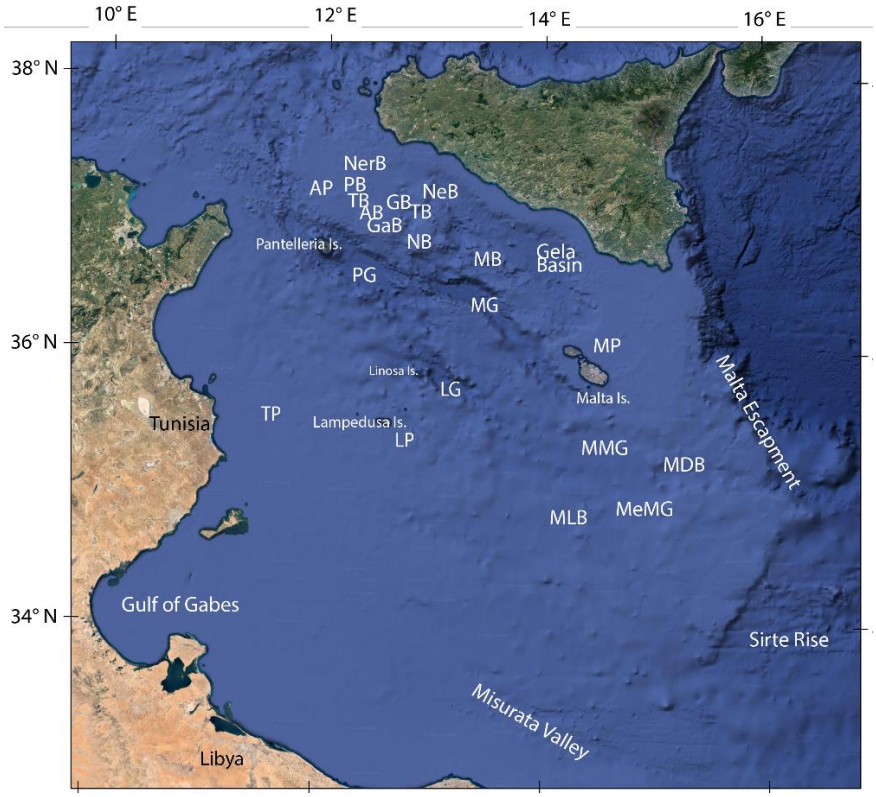

FIGURE 4. BATHYMETRY MAP OF SICILY CHANNEL WITH THE LOCATION OF THE MAIN SEDIMENTARY BANKS. **AP:** ADVENTURE PLATEAU; **NERB:** NEREO BANK; **PB:** PANOPE BANK; **TB:** TETIDE BANK; **AB:** ANTIFTITE BANK; **GAB:** GALATEA BANK; **NEB:** NERITA BANK; **GB:** GRAHAM BANK; **TB:** TERRIBLE BANK; **NB:** NAMELESS BANK; **MB:** MADREPORE BANK; **PG:** PANTELLERIA GRABEN; **MG:** MALTA GRABEN; **MP:** MALTA PLATEAU; **LG:** LINOSA GRABEN; **LP:** LAMPEDUSA PLATEAU; **MMG:** MALTA-MEDINA GRABEN; **MEMG:** MEDINA-MELITA GRABEN; **MDB:** MEDINA BANK; **MLB:** MELINA BANK. (QGIS SOFTWARE).

Another Morphostructural element is the N-S alignment that separates the Pantelleria Graben from the Linosa and Malta Graben, resulting from an alternation of basins and high structural (*Civile et al., 2021*). Furthermore, the basin is influenced by rifting of volcanic activity represented by the volcanic islands of Pantelleria and Linosa and by a sequence of magmatic manifestations NNE-SSWoriented from the island of Linosa to the edges of the Nameless and Graham banks along the Sicilian coast (*Peccerillo, 2005; Rotolo et al., 2006*). One of the main morphotectonic structures of the Sicily Channel area is the steep Malta escarpment, bounded by the western Ionian basin. In general, intense seismic activity in the northern part of the escarpment is recorded in recent instrumental catalogs (*Chiarabba et al., 2005*) and historical databases (*Boschi et al., 1995*).

2.4. Historical seismicity

The seismicity of the Sicily Channel derives mainly from tectonic processes that have influenced this area, much of the movement of convergence between the African and Euro-Asian plates. The seismic history of a site constitutes a chronological list of the effects caused by near and remote earthquakes expressed in macroseismic intensity and represents the essential basis for considering the possible effect of the earthquake on the territory in time. Through the reconstruction of the seismic history, it is possible to evaluate the hazard to the site using recently developed analytical methods.

For the historical construction of the seismic events that have characterized the area of the Sicily Channel used several databases:

i. Catalogue of Strong Earthquakes in Italy (461 BC-1997) and in the Mediterranean area (760 BC-1500) (CFTI5Med);
ii. Italian Historical Macroseismic Archive (ASMI);
iii. Macroseismic Database (DBMI15 v4.0);
iv. Parametric Catalogue of Italian Earthquake (CPTI15 v4.0).

The CFTI5Med, or the “Catalogue of Strong Earthquakes in Italy (461 BC-1997) and in the Mediterranean area (760 BC-1500)” (*Guidoboni et al., 2018; 2019*), reports the seismic history of many areas of the Mediterranean listing earthquakes with indications of the various macroseismic intensities (MCS) estimated for the site where the event took place. In the catalog, three events in Tunisia are identified with magnitude 6.2 Me (equivalent magnitude calculated on macroseismic observations) dating back to before 900 (Fig. 5). The epicentral parameters of these events were calculated on a single intensity data from the "Catalogue of ancient earthquakes in the Mediterranean area until the 10th century" (*Guidoboni et al., 1994*), where the effects of seismic events on buildings and sanctuary/temples of Tunisia are described.

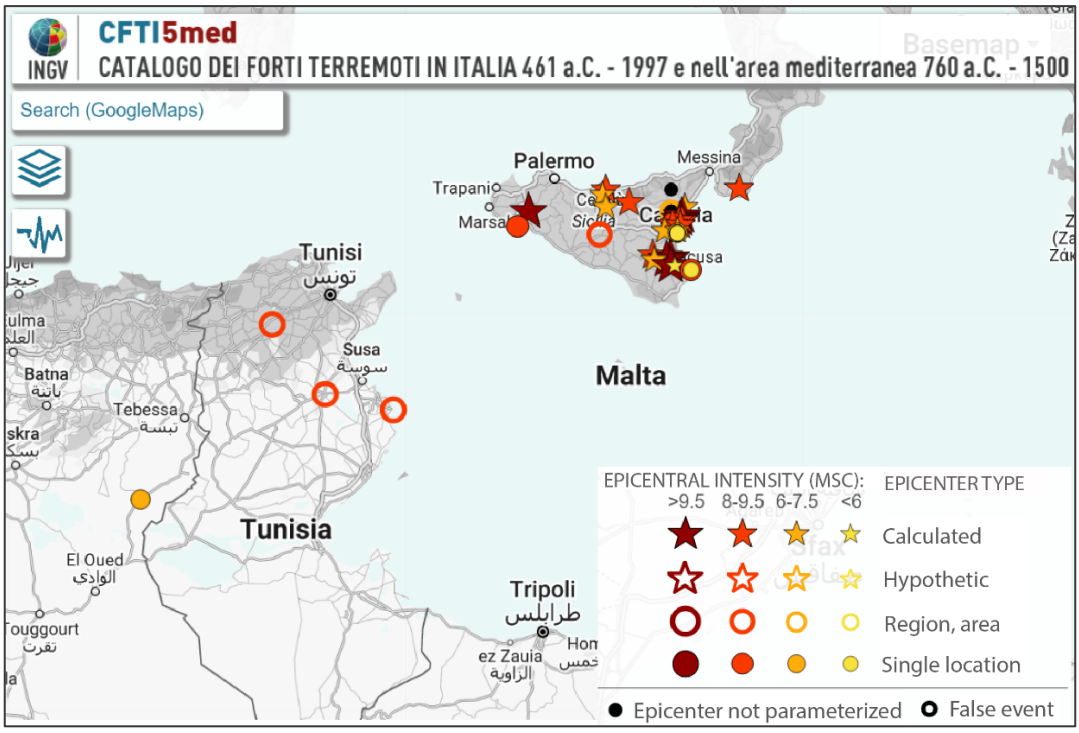

FIGURE 5. MAP OF SICILY CHANNEL HAS REPORTED THE HISTORICAL SEISMIC EVENTS DETERMINED BY THE CATALOG CFTI5MED (FROM -760 TO 1997). THERE ARE THREE MAGNITUDE EVENTS 6.2 ME WITH EPICENTRAL INTENSITY 9.2 (MCS) IN THE TUNISIAN AREA (CIRCLED IN RED). IN THE LEGEND, THE EPICENTER TYPES ARE DIFFERENTIATED ACCORDING TO THE EPICENTRAL INTENSITY (FROM YELLOW TO BORDEAUX): I) WITH FULL STARS, THE EPICENTRAL LOCATION IS CALCULATED FROM A SUFFICIENT NUMBER OF SITES WITH MACROSEISMIC INTENSITY; II) WITH EMPTY STARS, THE LOCATION IS PRESUMED, SINCE THE ONLY DISTRIBUTION OF SITES WITH MACROSEISMIC INTENSITY DOES NOT ALLOW A CALCULATION; III) WITH EMPTY CIRCLES, THE LOCATION TAKES PLACE IN THE CENTRAL ZONE OF A REGION OR AN AREA BASED ON HISTORICAL SOURCES WHERE THE MOST SIGNIFICANT EFFECTS HAVE OCCURRED BUT WITHOUT REFERENCES TO INDIVIDUAL LOCATIONS; IV) WITH FULL CIRCLES, THE LOCATION IS AT A SINGLE LOCATION/SITE WHERE A DEGREE OF INTENSITY IS AVAILABLE.

The ASMI catalog, or "Italian Historical Macroseismic Archive" (*Rovida et al., 2017*), documents 1112 historical (Fig. 6) events located within a radius of about 300 km from the center of Sicily Channel (36.625° N – 13.082° E); of these, only 10 have relevant magnitudes (≥ 6):

- 0853.08.31, Messina, 38.183° N - 15.550° E, M_w 6.10;
- 1169.02.04 07:00, southern Sicily, 37.215° N - 14.949° E, M_w 6.50 (± 0.46);
- 1542.12.10 15:15, southern Sicily, 37.215° N - 19.944° E, M_w 6.68 (± 0.24);
- 1693.01.09 21:00, southern Sicily, 37.141° N - 15.035° E, M_w 6.07 (± 0.23);
- 1693.01.11 13:30, southern Sicily, 37.140° N - 15.013° E, M_w 7.32 (± 0.10);
- 1786.03.10 14:10, Gulf of Patti, 38.102° N - 15.021° E, M_w 6.14 (± 0.19);

- 1818.02.20 18:15, Catania, 37.603° N - 15.140° E, M_w 6.28 (± 0.10);
- 1908.12.28 20:27, Strait of Sicily, 38.146° N - 15.687° E, M_w 7.10 (± 0.18);
- 1968.01.15 02:01:09, Belice Valley, 37.756° N - 12.981° E, M_w 6.41 (± 0.09), depth: 3 km;
- 1978.04.15 23:33:48, Gulf of Patti, 38.685° N - 15.086° E, M_w 6.03 (± 0.10); depth: 18 km.

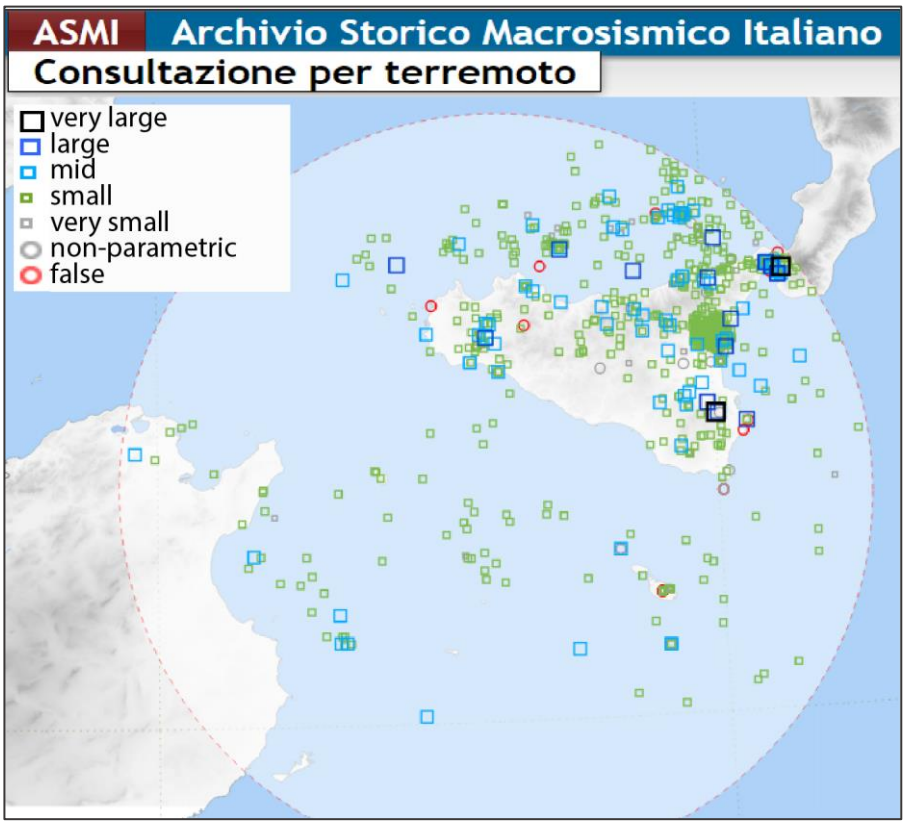

FIGURE 6. MAP OF SICILY CHANNEL, THE SEISMIC EVENTS FROM 400 TO 2021.12.24 ARE IDENTIFIED BY THE CATALOG ASMI (ARCHIVIO STORICO MACROSISMICO ITALIANO). IN THE CIRCLE IS THE STUDY AREA.

The information derived from the ASMI and CFTI5Med catalogs has also been integrated with those derived from the CPTI15 catalogs (Italian Earthquake Parametric Catalogue) and the DBMI15 (Italian Macroseismic Database) (*Locati et al., 2022*). The CPTI15 catalog (emidius.mi.ingv.it/CPTI15-DBMI15/query_eq/) returns homogeneous parametric, macroseismic, and instrumental data for earthquakes with maximum intensity (Io) ≥ 5 or magnitude ≥ 4 from 1000 to 2020. The DBMI15 catalog (emidius.mi.ingv.it/CPTI15-DBMI15/query_place/), on the other hand, provides a homogeneous set of macroseismic intensities deriving from several sources for earthquakes with a maximum intensity ≥ 5, from 1000 to 2020.

Considering a radius of 300 km relative to a central point of coordinates 36.617°N-13.167°E, from the CPTI15 catalog were filtered 892 events (Fig. 7), while from the DBMI15, 1145 locations have been determined on 15343 (Fig. 8).

Table 1 lists the events of the several events recorded with a magnitude greater than ≥ 5.5 (23 seismic events). It reports the date, the epicentral area in which the event occurred, the origin time (UTC), geographical coordinates, the data of macroseismic intensity (NMDP – number of Macroseismic Data Point), the maximum intensity epicentral scale MCS (Io), the moment magnitude (Mw) and depth (km).

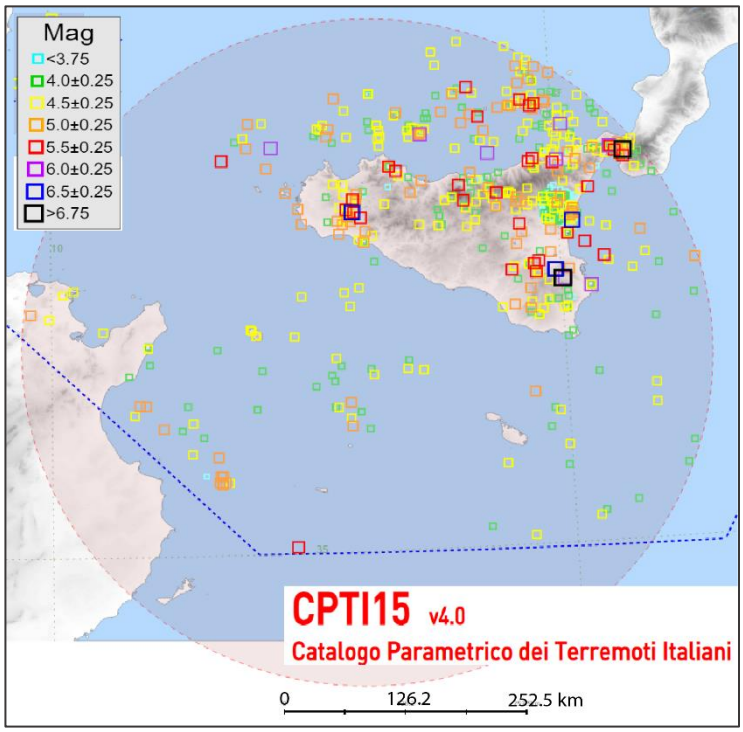

FIGURE 7. MAP OF SICILY CHANNEL SHOWS THE AREA'S SEISMIC HISTORY EXTRACTED FROM THE CPTI15 V4.0 (CATALOGO PARAMETRICO DEI TERREMOTI ITALIANI) FROM 1000 TO 2020. MAGNITUDES DIVIDED INTO DIFFERENT CLASSES ARE REPORTED. THE CIRCLE CORRESPONDS TO THE STUDY AREA WHERE 892 EVENTS WERE IDENTIFIED.

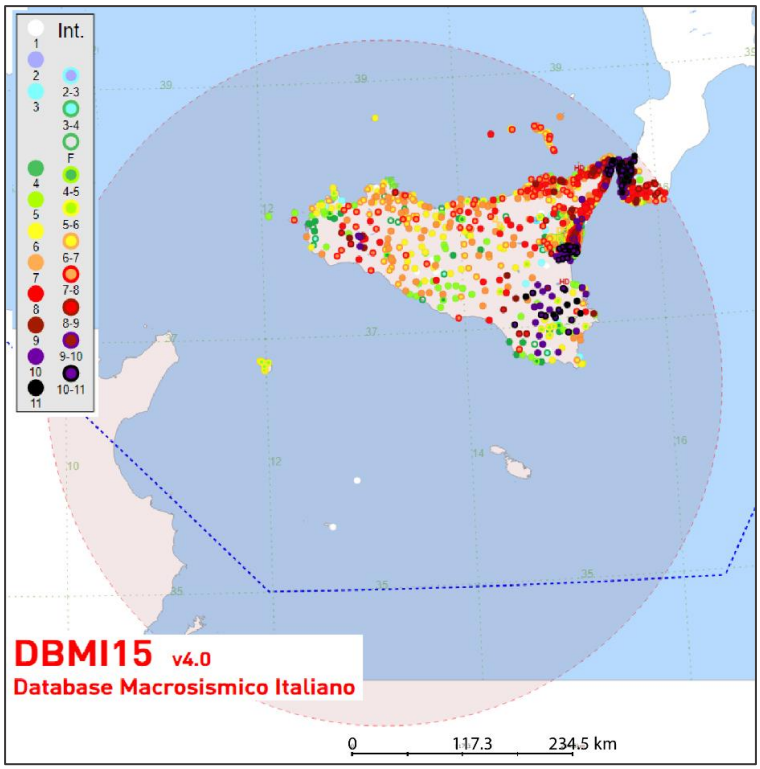

FIGURE 8. MAP OF SICILY CHANNEL SHOWS THE AREA'S SEISMIC HISTORY EXTRACTED FROM THE DBMI15 V4.0 (DATABASE MACROSISMICO ITALIANO) FROM 1000 TO 2020. MACROSEISMIC INTENSITIES ARE REPRESENTED WITH DIFFERENT COLOURS FROM VALUE 1 (LESS INTENSITY) TO 11 (MAXIMUM INTENSITY). THE CIRCLE CORRESPONDS TO THE STUDY AREA WHERE 1145 LOCATIONS HAVE BEEN DETERMINED ON 15343.

TABLE 1. THE TABLE SHOWS THE SEISMIC HISTORY OF THE SICILY CHANNEL EXTRACTED FROM THE PARAMETRIC CATALOGUE ITALIAN EARTHQUAKE (CPTI15) FOR THE MOST SIGNIFICANT EVENTS WITH MAGNITUDE ≥ 5.5, FROM 1000 TO 2020.

Region	Date	Time (UTC)	Lat	Lon	Depth (km)	Io	NMDP	Mag (Mw)
Siracusa	1125.06.07	11:00:00	37.073	15.286	-	8-9	1	5.80
SE-Sicily	1169.02.04	07:00:00	37.215	14.949	-	10	8	6.50
Messina	1172.09.26	13:40:00	38.185	15.555	-	8	1	5.56
Strait of Sicily	1509.02.25	22:20:00	38.099	15.684	-	8	4	5.56
SE-Sicily	1542.12.10	15:15:00	37.215	14.944	-	10	32	6.70
Nebrodi Mt.	1613.08.25	05:00:00	38.122	14.788	-	8	2	5.56
Iblean Mt.	1624.10.03	17:00:00	37.270	14.742	-	8	3	5.60
SE-Sicily	1693.01.09	21:00:00	37.141	15.035	-	8-9	30	6.70
SE-Sicily	1693.01.11	13:30:00	37.140	15.013	-	11	179	7.30
Iblean Mt.	1698.01.01	-	37.292	14.789	-	7-8	6	5.66
Messina	1749.08	-	38.185	15.555	-	8-9	1	5.80
Gulf of Patti	1786.03.10	10:14:10	38.102	15.021	-	9	10	6.14
Catania	1818.02.20	18:15:00	37.603	15.140	-	9-10	128	6.30

Iblean Mt.	1818.03.01	02:45:00	37.204	14.756	-	7.-8	24	5.57
Tyrrhenian sea	1823.03.05	16:37:00	38.185	14.344	-	8	107	5.81
Aspromonte	1907.10.23	20:28:19	38.086	15.958	-	8-9	274	5.96
Strait of Sicily	1908.12.28	04:20:27	38.146	15.687	-	11	772	7.10
Tyrrhenian sea	1941.03.16	16:35:02	38.300	12.200	-	7	-	5.91
Belice Valley	1968.01.15	02:01:90	37.756	12.981	3	10	162	6.4
Gulf of Patti	1978.04.15	15:23:33	38.385	15.086	17.9	8	330	6.03
Tyrrhenian sea	1980.05.28	19:51:20	38.483	14.270	18.9	5-6	44	5.66
Ionian sea	1990.12.13	00:24:25	37.306	15.429	10	-	304	5.61
Tyrrhenian sea	2002.09.06	01:21:27	38.364	13.687	9.6	6	132	5.92

From the several data accessible, can see that the completeness of the historical catalog decrease going back in time; for past events, there is no information about the epicentral depth of the time event. In particular, the 1968 seismic sequence in the Belice Valley is the most significant event in which more information has been recorded (Table 1 is the first event for which is reported a value of hypocentre depth of the event). The area of the Belice Valley has hit by a seismic sequence (more than 300 events) from 14 to 15 January 1968. These severely damaged fourteen villages, four of which were devastated, Gibellina, Poggioreale, Salaparuta, and Montevago (*Bottari, 1973; Rovida et al., 2011*).

2.5. Recent seismicity

This large belt shows evidence of active deformation defined by tectonic bathymetry, volcanic, and magnetic features (*Palano et al., 2020*). Seismic activity around the Sicily Channel is moderate, the magnitude of earthquakes being generally under 5.0; however, the coverage of the instrumental network was (in the past) generally insufficient to well locate and capture all the earthquakes. Active faults of the rift zone mainly control seismicity in this area. Based on seismological studies, two fundamental areas of seismic fault zones are identified; they extend east and west of the Gela Thrust System and continue offshore. The fault zone placed to the west of the Gela Thrust System is an alignment with NNE-SSW direction, corresponds to the Capo Granitola-Sciacca Fault Zone (CGSFZ) extending from the coast of Sicily (near Sciacca) towards the Lampedusa island.

This alignment separates, thus, the rift system into two sectors: the Pantelleria Graben to the west and the Linosa and Malta Graben to the east.

The other zone of fault to the east of the Gela Thrust System is the Scicli-Ragusa Fault (SRF), extending from the south-eastern sector of Sicily, from Ragusa to the Sicily Channel offshore, with an indeterminate length (Fig. 9).

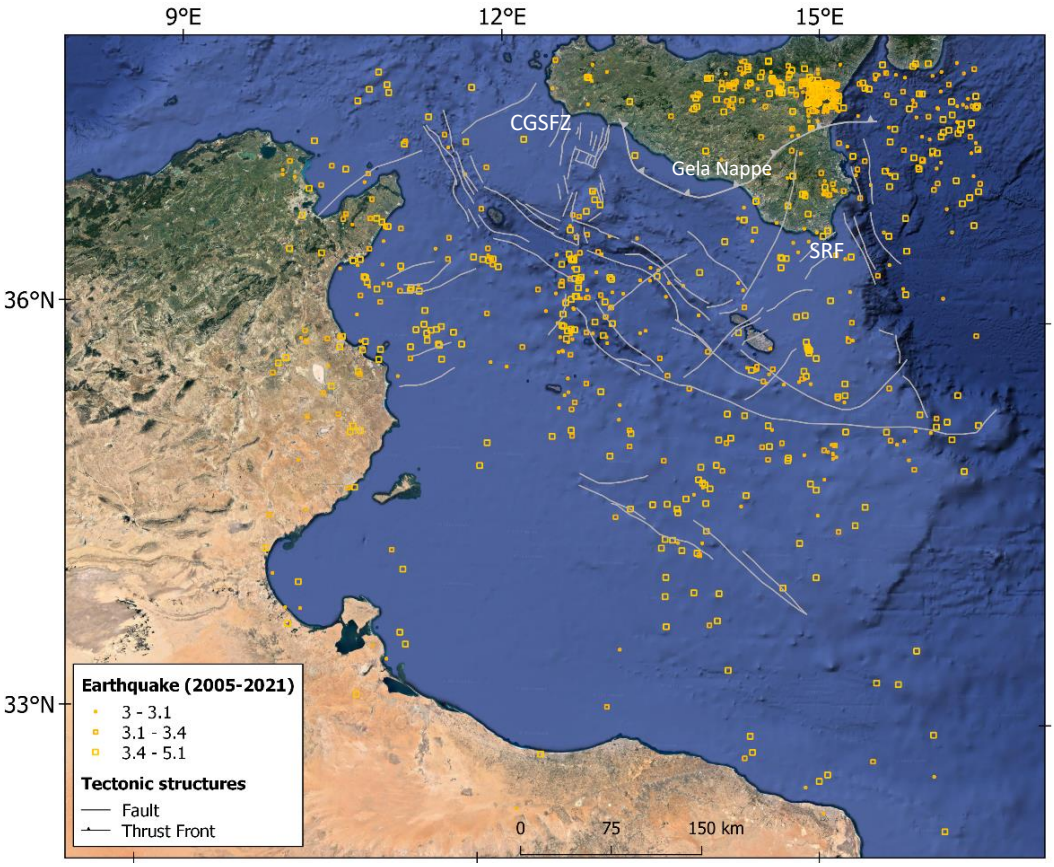

FIGURE 9. THE SEISMOLOGICAL-TECTONIC MAP. THE SEISMIC EVENTS RECORDED FROM 2005-2021 (FROM THE INGV-ISC CATALOGS) ARE REPORTED IN THE GIS ENVIRONMENT (QGIS SOFTWARE). THE MAIN TECTONIC STRUCTURES ARE OUTLINED. CGSFZ: CAPO GRANITOLA-SCIACCA FAULT ZONE; SRF: SCICLI-RAGUSA FAULT.

Previous studies have also shown that the instrumental seismicity is mainly concentrated along the NS-oriented belt, characterized by moderate magnitude (up to 4.7) with a prevalence of earthquakes between 10 and 20 km depth (*Chiarabba et al., 2005; Galea, 2007; Calò & Parisi, 2014*), but occasionally deeper events occur (*Palano et al., 2020*). The Malta and Linosa graben are also seismically active, with a high density of seismic activity at about 20 km and between 80-120 km SSE from the coast of Malta (*Agius et al., 2020*), thanks to the integration of a new seismic catalog for the offshore Maltese island.

2.6. Volcanism

Many volcanic centers are present in the Sicily Channel. The magmatic activity in the Sicily Channel began with the formation of the volcanic islands of Pantelleria and Linosa (age of 300-150 ka) (*Argnani et al., 1990; Argnani et al., 2009; Civile et al., 2010*). The oldest magmatic rocks emerged on the island of Pantelleria, dating back to Trias, and have an alkaline composition (*Mahood & Hildreth, 1983*); while the island of Linosa emerged in the Quaternary age and it is also characterized by the presence of alkaline rocks (*Romagnoli et al., 2020*).

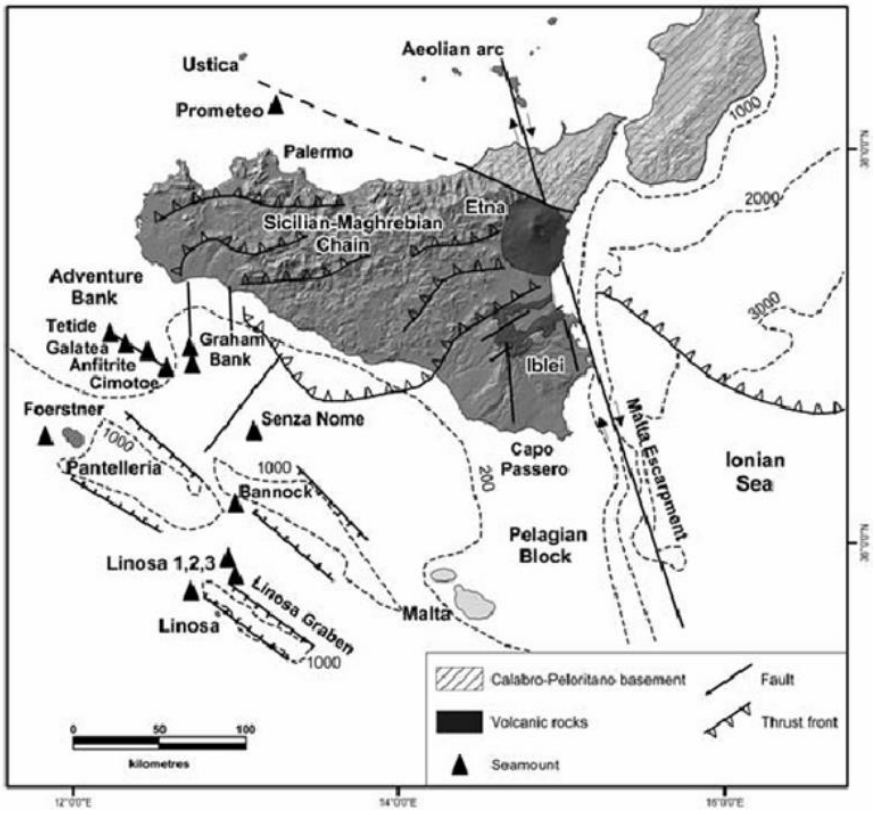

FIGURE 10. LOCAL MAP OF SICILY VOLCANOES. THE BLACK TRIANGLES REPRESENT THE SEAMOUNTS IN THE SICILY CHANNEL, AND SEVERAL CONES RISE ALONG NW-SE AND N-S TRENDING FAULTS (FROM *Peccerillo, 2005*).

In general, the volcanic activity produced in the Sicily Channel is concentrated mainly in the western area (Neogene age), and a similar activity of age but affinity has occurred in the Hyblean Plateau and on Mt. Etna (*Calanchi et al., 1989*). In particular, the Sicily Channel's north-western sector is characterized by intense magmatic activity (Fig. 10), which developed mainly in the Quaternary and was defined by a series of submerged volcanic edifices (*Coltelli et al., 2016*). Most of these volcanoes are located inside shallow banks known as Adventure, Graham,

Nameless, and Terrible banks, which are situated on an almost N-S-shaped belt (Fig. 11) called the "Separation Belt" (*Argnani et al., 1990*). Tetide, Galatea, Amphitrite, and Cimotoe determine a row of centers aligned in an NW-SE direction on the eastern margin of the Adventure bank, while a significant activity occurred in the recent past (1831) with the formation of Ferdinandea island in the Graham bank (*Washington, 1909; Colantoni et al., 1975*). This eruption occurred about 5 km northwest of Pantelleria island and is the only volcanic activity documented in historical times in this area of the Channel.

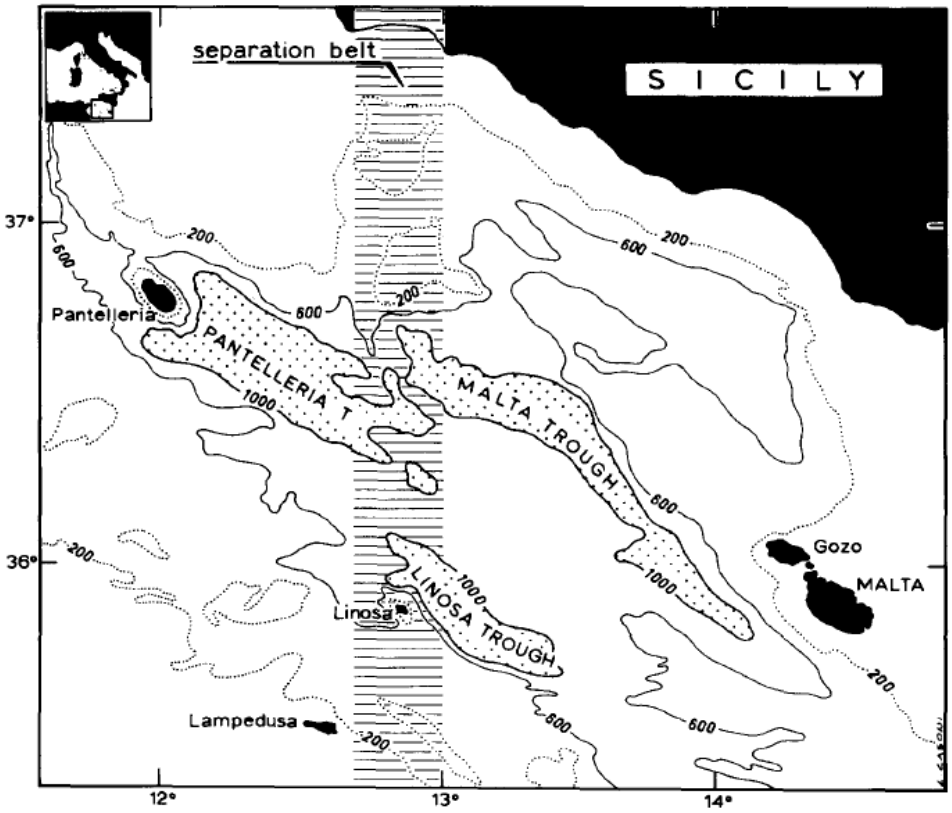

FIGURE 11. BATHYMETRIC MAP OF SICILY CHANNEL. THE POSITION OF THE MAIN GRABEN (TROUGH) AND THE SEPARATION BELT IS SHOWN (FROM *Argnani et al., 1990*).

2.7. Definition of lithospheric features

2.7.1. Bouguer gravity anomalies

The Bouguer anomaly is a gravitational anomaly that detects density changes within the Earth, calculated with the magnitude of the anomaly proportional to the density contrast and the thickness of the anomalous body. It is considered an

excellent tool for determining the main structural elements and delineating geological elements at a regional scale. In the Sicily Channel, several positive values of Bouguer's anomaly are located just off the south-eastern coast of Pantelleria island, between +40 and +80 mGal (*Morelli, 1975; Boccaletti et al., 1987; Cello, 1987; Scarascia et al., 1994; 2000; Belguith et al., 2013*). Instead, the maximum values of +80 mGal are reached near the Nameless, Graham, and Adventure banks (Fig. 12). According to Lodolo et al. (2012) and Jongsma et al. (1985), these anomalies coincide with the presence of buried magmatic bodies, and in such areas, there is a rising of the Moho discontinuity at depths between 17-18 km (relatively low compared to the surrounding area) (*Finetti et al., 2005; Civile et al., 2008*). Negative anomalies, -40 mGal, are recorded at the Gela Thrust System, whose deformation extends from the central-northern sector of the Sicily Channel (*Milano et al., 2020*). This data is presumably related to the deepening of Moho at about 35 km depth (*Finetti, 2005*).

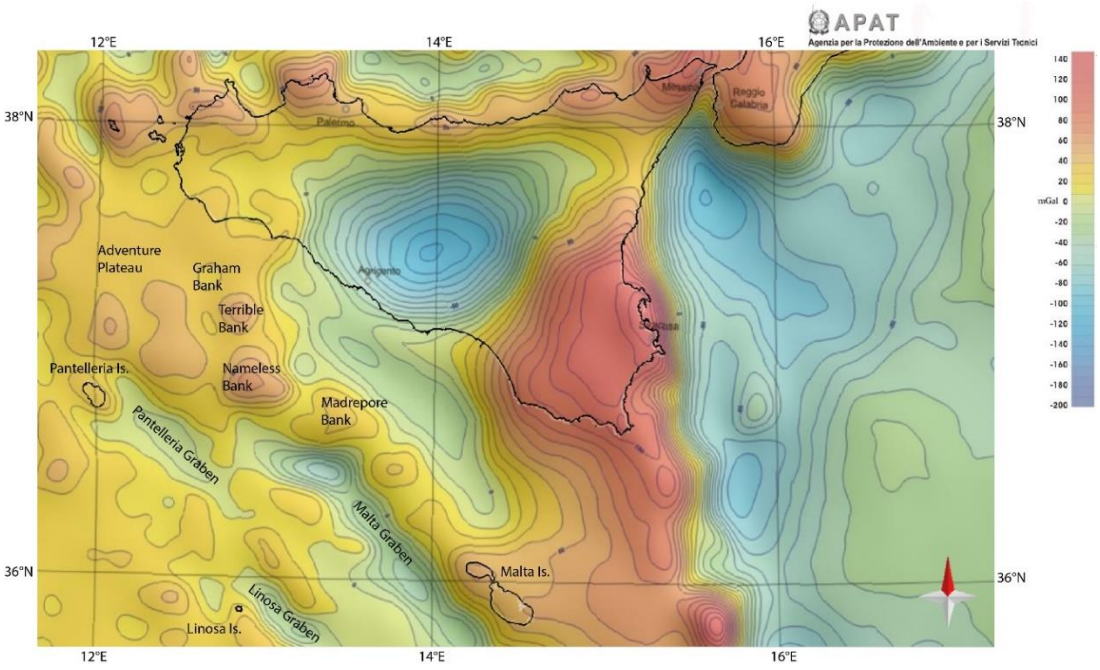

FIGURE 12. EXTRACT OF THE ITALIAN GRAVITY MAP, SCALE 1:1.250.000 (*APAT, 2005*).

2.7.2. Magnetic data

High-resolution aeromagnetic investigations can be used to trace geological processes that are not quickly derived from other geophysical techniques. The

magnetic field of the central Mediterranean shows low amplitude anomalies in the southwestern zone of the Pelagian Sea. On the other hand, significant magnetic anomalies are located along the Pantelleria Graben axis and along a wide N band that extends from the Linosa island to the eastern edge of the Nameless bank (*Lodolo et al., 2012*). This band corresponds to an N-trend lithospheric transfer zone placed in the central part of the Sicily Channel, which separates the fracture system into two independent areas (*Argnani et al., 1986; Argnani et al., 1990*): Pantelleria Graben to the west and Malta and Linosa to the east (*Civile et al., 2014; 2018*). Significant anomalies are also found east of the Pelagian Sea, within Malta, the Malta-Medina graben, and above the Medina bank (*Jongsma et al., 1985*). High-frequency magnetic anomalies are recorded along the Malta escarpment and in the Sirte basin, where pillow lavas (Jurassic) have been found (*Finetti, 1982; Reuther & Eisbacher, 1985*). The presence of high-frequency magnetic anomalies at existing volcanic plexuses can only confirm the presence of volcanic activity in other areas with high-frequency anomalies. The area of the Sicily Channel is characterized by a residual magnetic field with high-frequency anomalies up to 1200 nT, connected to the presence of buried volcanic bodies (*Chironi et al., 2000*).

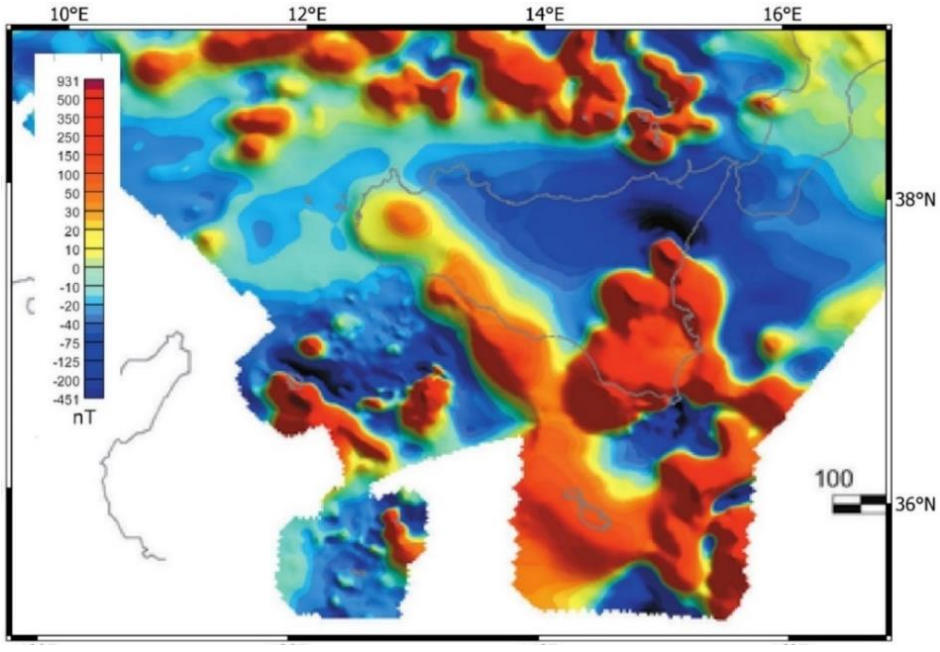

FIGURE 13. COLOR-SHADED RELIEF MAP OF THE AEROMAGNETIC ANOMALY FIELD (FROM *Caratori Tontini et al., 2004*).

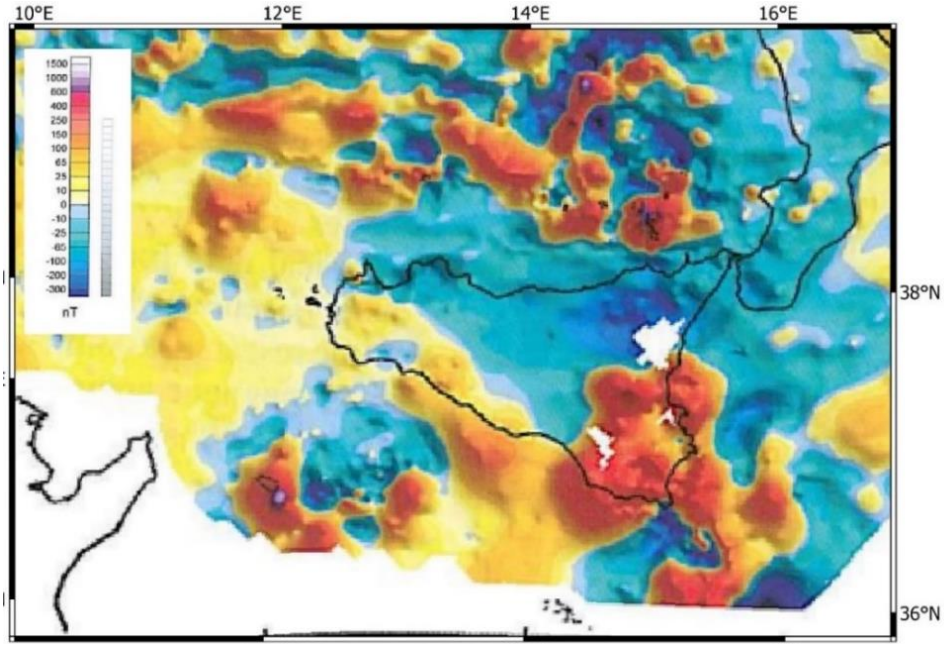

FIGURE 14. MAP OF A MAGNETIC ANOMALY IN RELIEF-SHADED ITALY (FROM *Chiappini et al., 2000*).

The two aeromagnetic maps (Fig. 13, 14) show insufficient information concerning the Sicily Channel; in both maps, the information is lost in the central area of the Pelagian block. Particularly in the map of Caratori Tontini et al. (2004), the high magnetic anomaly in Malta island is evident. Compared to the previous maps, these appear to have an original view of the tectonic elements concerning the global context. There is a good correlation between magnetic anomalies and regional geology, in fact, it is optimal to make deep interpretations.

2.7.3. Heat flow data

The temperature distribution within the crust is a relevant parameter of the physical properties of rocks and fluids. In the western part of the Sicily Channel, along the alignment Lampedusa-Sciacca Shear Zone oriented N-S, characterized by a deformation left-lateral strike-slip, there is a high heat flow up to 130 mW/m^2 (*Della Vedova et al., 1995; 2001*). This, associated with active magmatism and thinned continental crust, describes the relatively ductile rheology of the lithospheric crust (Fig. 15). In the eastern part, however, low heat flow values are found. High heat values were found predominantly along the Malta and Pantelleria graben (*Granath & Casero, 2004*). An anomalous heat flow value was measured in

the Linosa graben (50 mW/m^2), slightly above average (average value is 42 mW/m^2), probably due to the thick graben sedimentary cover (*Jongsma et al., 1985*).

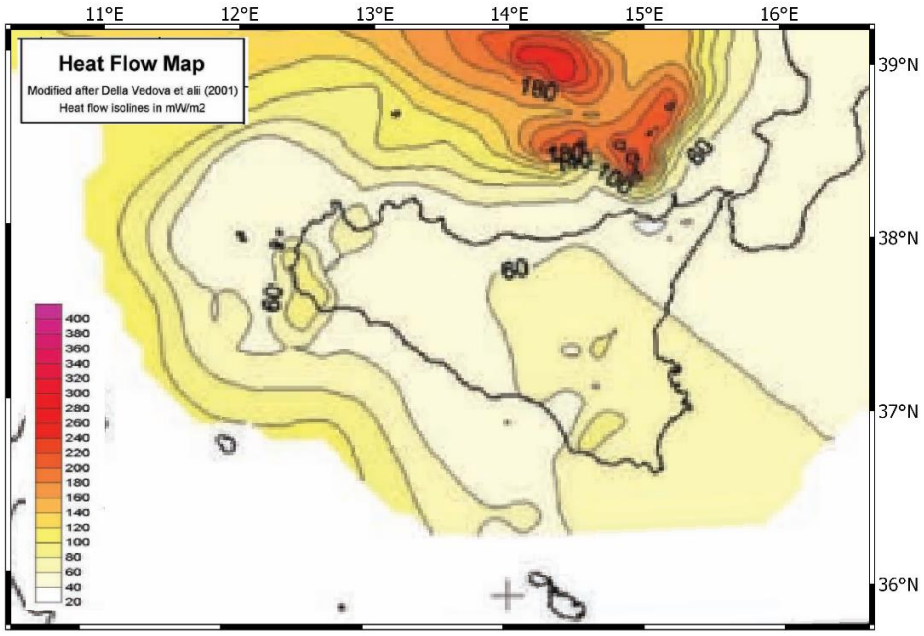

FIGURE 15. EXTRACT HEAT FLOW MAP, MODIFIED AFTER Della Vedova et al. (2001).

Generally, the Sicily Channel is characterized by a thinned continental lithosphere (about 60-70 km), with a relatively high heat flow between 60-130 mW/m^2 (*Della Vedova et al., 1989; 1995*). Significant volcanic activity in the area can be described by combining relatively high heat flow values with positive Bouguer and magnetic anomalies.

2.7.4. Seismic reflection data

Seismic reflection, one of the most used techniques in marine areas, is used to obtain information on tectonic characteristics and stratigraphic environment.

Several acquisitions of seismic reflection were made in Italy and in the offshore areas, aiming to produce different crustal sections and a map of the depth profile of Moho. Most of the profiles were executed with land recording stations, in some cases, were also used recordings on the seabed (OBS – Ocean-Bottom Seismometer).

Figure 16 shows the crustal sections' positions from Scarascia et al. (1994) and Cassinis et al. (2005).

The HH section (Fig. 17a) starts from the island of Pantelleria and crosses Sicily (from Sciacca to Termini Imerese) towards the island of Salina (Aeolian islands). Along this profile is observed a deepening of the African crust from 20 km below Pantelleria to 40 km under Sicily.

The LL section (Fig. 17b) extends along the southern coast of Sicily, starting from the Egadi islands, crossing Capo Passero, crossing the Malta escarpment, and continuing to the Ionian Sea. Along the section, the thickness of the crust varies from 35 to 40 km, while the horizon of the upper crust at the Caltanissetta basin deepens up to 20 km deep. Towards SE, the Moho decreases and reaches 17 km offshore Capo Passero; in the area, the Moho reaches 12 km depth. In the marine part of the Ionian Sea, data were acquired with OBS (*Makris et al., 1986*).

Section 11c (Fig. 17c) starts from eastern Tunisia, crossing the Pantelleria island towards Sicily. To realize this section were used 15 OBS and explosive sources were used both onshore and offshore. By interpreting these data, we determine the depth of the Moho below the Pantelleria island at about 20 km deep; in this area, in particular, the upper mantle is characterized by a P-wave velocity of 7.6 km/s (low velocity compared to normal values). While under the Sicilian and Tunisian coast, the velocity of the upper mantle is about 8.1 km/s, compared with the structure of the Rift area of the Sicily Channel.

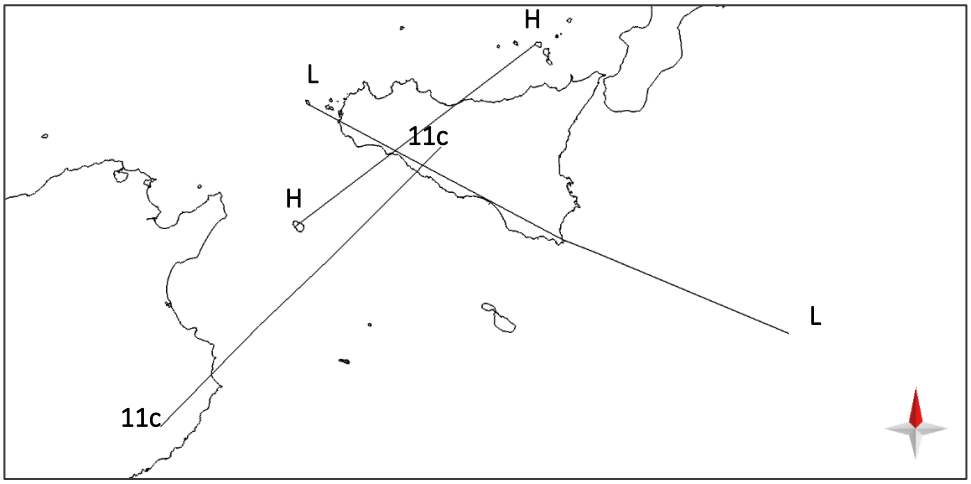

FIGURE 16. TRACES OF THE CRUSTAL SECTION RESULTING FROM THE D.S.S. SEISMIC PROFILES. SECTION HH AND SECTION LL (*Scarascia et al., 1994*), SECTION 11C (*Cassinis et al., 2005*) (MOVE SOFTWARE).

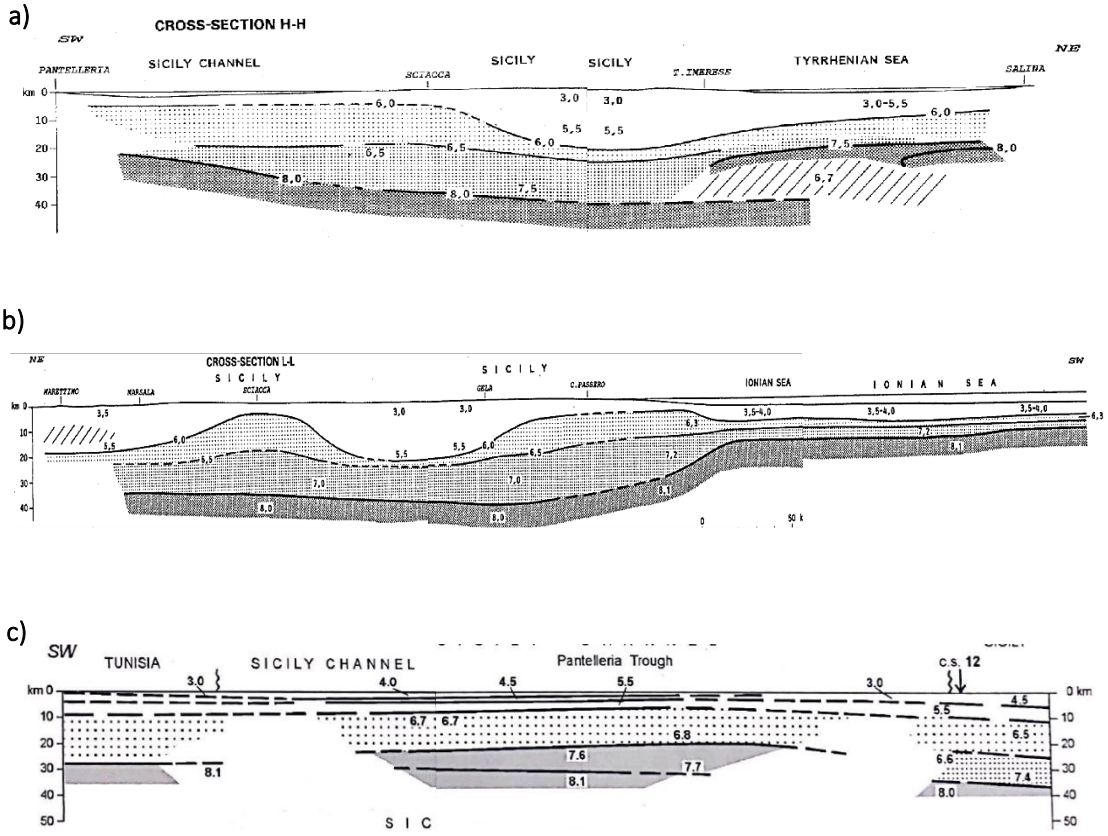

FIGURE 17. A) CROSS-SECTION HH, STARTING FROM PANTELLERIA ISLAND, SCIACCA, TERMINI IMERESE TO SALINA; **B)** CROSS-SECTION LL, STARTING FROM AEOLIAN ISLAND, MARSALA, SCIACCA, GELA, CAPO PASSERO, TO IONIAN SEA; **C)** CROSS-SECTION 11C, STARTING FROM TUNISIA, SICILY CHANNEL, PANTELLERIA, TO SICILY (*Scarascia et al., 1994; Cassinis et al., 2005*). IN ORDER TO BETTER UNDERSTAND THE CRUSTAL STRUCTURES, DIFFERENT PATTERNS ARE REPRESENTED AS A FUNCTION OF THE P-WAVES VELOCITY: **I)** EMPTY/WHITE PATTERN FOR LAYERS WITH A VELOCITY LESS THAN 6.0 KM/S; **II)** CLEAR SHADED PATTERN FOR LAYERS WITH A VELOCITY BETWEEN 6.0 AND 6.5 KM/S, CORRESPONDING TO THE UPPER CRUST; **III)** DARK SHADED PATTERN, FOR LAYERS WITH A VELOCITY VALUE BETWEEN 6.5 AND 7.5 KM/S, CORRESPONDING TO THE LOWER CRUST; **IV)** FULL DARK PATTERN, FOR LAYERS WITH A VELOCITY SUPERIOR TO 7.5 KM/S. DASHED LINES INDICATE VELOCITY REVERSALS.

3. CHAPTER - MATERIALS

3.1. Data selection

Different data were collected in this study (Fig. 18); a good part derives from the ViDEPI project. The CROP multichannel reflection seismic profiles were obtained from the online database, the Commercial Zone "G" and the well data (www.videpi.com/videpi/videpi.asp). In addition, data from seismic profiles were integrated with works previously published by authors who have explored different sectors of the Sicily Channel.

Instrumental seismic data from January 2005 to December 2021 from "Seismic Bulletin" INGV - National Institute of Geophysics and Volcanology (terremoti.ingv.it/iside) and the "ISC Bulletin" International Seismological Centre (www.isc.ac.uk/iscbulletin/) were collected. Events with epicentres in the area between 30.0° N and 38.0° N of latitude and between 10.0° E and 16.5° E of longitude were selected, including all depths and magnitude $M \geq 3$. The database has also been integrated with recordings from the Malta Seismic Network (MSN), which has expanded over the last few years the network on the island (a total of 13 stations).

Data collection has been implemented on the tectonic structures that affect the Sicily Channel area, including digitizing data in the GIS project. The aim is to create a complete detailed database of the area to have a complete picture of the geodynamics that affects the Sicily Channel.

The following seismic profiles were used:

- CROP Profiles: M3, M21, M23, M24, M25, M39 (collected from the ViDEPI project online database www.videpi.com/videpi/videpi.asp). They are high penetration profiles whose recording time is 17 s in two-dimensional traveltime (TWT). Have been consulted the interpretations of several authors who have illustrated and discussed the structure of the tectonostratigraphic crustal Sicily Channel (*Catalano et al., 2000; Chironi et al., 2000; Finetti & Del Ben, 2005; Corti et al., 2006*).
- Seismic reflection profiles: cross-section B, cross-section C, cross-section D (*Jongsma et al., 1985*); Profile1 (*Makris et al., 1986*); CN95-84-2, CN95-84-14, C1034, CS89-01, CN115-84-7 (*Torelli et al., 1995*); A-B (*Corti et al., 2006*); Line-L1, Line-L2, Line-L3 (*Khomsi et al., 2009*); PANT2, PANT3 (*Civile et al., 2010*); Profile-AA, Profile-CC (*Fink et al., 2012*); G82-117, G82-121, G82-127, G82-129, G82-131, G82-143, CS71-SC15 (*Cavallaro et al., 2017*); G82-141, G82-142, FASTMIT05, BC-34 (*Civile et al., 2018*); Profile 1 (*Micallef et al., 2018*); C-1007, C81-33, Line Sciacca4 (*Ferranti et al., 2019*); G145, PANT1 (*Civile et al., 2021*);
- MS seismic lines: MS-19, MS-116, MS-118B, MS119. Seismic lines acquired during the Mediterranean Sea Project (MS Project) (*Civile et al., 2021*);

- 2D velocity models: M25 seismic model, F32 profile of Pantelleria-Gargano DSS, M39 seismic model (*Chironi et al., 2000*); DYP1 (*Dellong et al., 2018*);
- Seismic Wide-Angle-Reflection-Refraction Profile (WARR) or also called Deep Seismic Sounding (DSS): section LL, section HH (*Scarascia et al., 1994*); section 11c (*Cassinis et al., 2005*);
- Crustal seismic reflection profile: SI.RI.PRO. Project (Deep Reflection Seismic Multidisciplinary Project of field geology, seismic reflection, gravimetry, and magnetotellurics, with recording times up to 19 s (TWT) which allowed to find a link between the deep crustal domains and the shallow thrust structure (*Accaino et al., 2011; Catalano et al., 2013*).

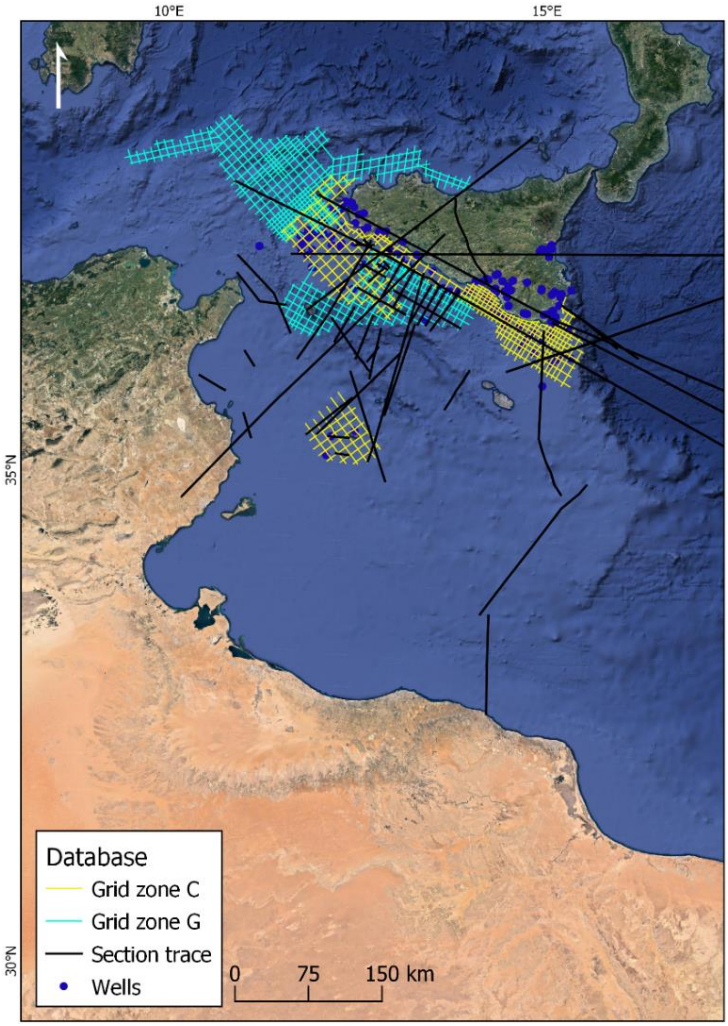

FIGURE 18. DATABASE LOCATION MAP. THE BLUE DOTS ARE THE WELLS THAT ARE LOCATED NEAR THE SICILIAN COAST. THE GRID ZONES BELONG TO THE ITALIAN COMMERCIAL ZONES "C" AND "G" ACQUIRED BY AGIP. IN BLACK, THE SECTION IS UTILIZED IN THIS WORK (QGIS SOFTWARE).

3.2. Well-log database

The numerous prospective wells are available along the Sicilian coast and in the Sicily Channel derived from decades of exploration through several oil campaigns published on the open-source sites of the GeoThopica and ViDEPI Project (geothopica.igg.cnr.it/index.php/it/, www.videpi.com/videpi/pozzi/consultabili.asp). These boreholes, in general, provide direct sampling data of the composition of the upper crust (the depth is approximately 3-5 km) and data on density, temperature, rock porosity, and fluid pressure.

152 wells were analyzed based on the lithological characteristics, and two horizons were discriminated (Fig. 19); the facies belonging to the soft sedimentary rocks and the facies belonging to the hard sedimentary rocks.

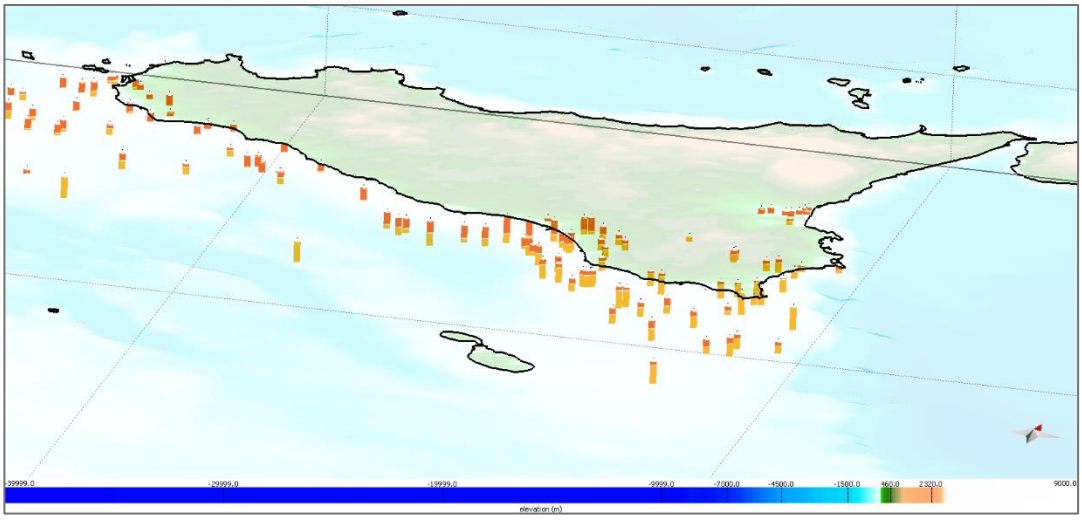

FIGURE 19. THE LOCATION WELLS MAP WITHIN THE SOFTWARE 3D MOVE SUITE V. 2017.2 (VERTICAL EXAGGERATION = 1.5). IN WELLS, THE RED COLOUR CORRESPONDS TO THE SOFT SEDIMENTARY ROCK FACIES, WHILE THE ORANGE CORRESPONDS TO THE HARD SEDIMENTARY ROCK FACIES.

A database was created with well data:

i. Name (name of the mention well);
ii. geographical coordinates (latitude and longitude values);
iii. rotary table depth (the distance from the rotary table to the seabed. The rotary table is installed on the base of the drilling machine);
iv. the bottom below the rotary table (the bottom depth compared to the rotating table);

v. the seabed (measured by the difference between rotation table depth and the seabed under the rotary table);
vi. the total drilling depth (the sum of the thickness values for different formations);
vii. lithological characteristics (lithological description of stratigraphic levels);
viii. age (the geologic time for stratigraphic levels);
ix. formations (the name of the formations identified);
x. horizon (describes the horizon of belonging between soft and hard sedimentary rocks).

The uploaded information in the 3D software includes the name, geographical coordinates with the Project Reference System, the seabed depth, and the identification of sedimentary horizons (Table 2). The project reference system is ETRS89 "European Terrestrial Reference System 1989", EPGS 4258, coordinate system type: geographic, semi-major axis 6378137.0 m and semi-minor axis 6356752.3 m, spheroid: GRS 1980 (EPGS 7019), projection type: UTM, zone: 33, Hemisphere North. The ETRS89 is a geodetic Cartesian reference where the Eurasian plate is considered static.

TABLE 2. EXCERPT FROM THE DATABASE WAS IMPORTED INTO THE 3D SOFTWARE (MOVE SUITE V. 2017.2) WITH THE WELL NAME, GEOGRAPHICAL COORDINATES, THE SEABED DEPTH, TOTAL DRILLING DEPTH, HORIZONS, AND GEOLOGICAL FORMATIONS.

Well name	X (E)	Y (N)	Z	Horizon	Formation
ACATE-001-DIR	442086	4094343.1	3	Top soft sediment	FM RIBERA/RAGUSA
ACATE-001-DIR	442086	4094343.1	-1492.1	Top hard sediment	FM AMERILLO/HYBLA/CHIARAMONTE/BUCCHERI/MODICA/STREPPENOSA/GELA
ACATE-001-DIR	442086	4094343.1	-3380.1	fondo pozzo	fondo pozzo
ACATE-002	441072.9	4095398.1	2	Top soft sediment	FM RIBERA/GESS SOLFIFERA/TELLARO/RAGUSA
ACATE-002	441072.9	4095398.1	-1553.1	Top hard sediment	FM AMERILLO/HYBLA/CHIARAMONTE/BUCCHERI/MODICA/STREPPENOSA/GELA
ACATE-002	441072.9	4095398.1	-3366.1	fondo pozzo	fondo pozzo
ACATE-003	439203	4097321.7	5	Top soft sediment	FM RIBERA/GESS SOLFIFERA/TELLARO/RAGUSA
ACATE-003	439203	4097321.7	-1760.5	Top hard sediment	FM AMERILLO/HYBLA/CHIARAMONTE/BUCCHERI/MODICA/STREPPENOSA/GELA
ACATE-003	439203	4097321.7	-3181.5	fondo pozzo	fondo pozzo
ALFA-001	255907.9	4148127.3	-60	Top soft sediment	FM RIBERA/TERRAVECCHIA/CALC CORLEONE
ALFA-001	255907.9	4148127.3	-2239.5	Top hard sediment	FM BOU DABBOUS/EL HARIA/ABIOD/ALEG/ALLAM
ALFA-001	255907.9	4148127.3	-2715.5	fondo pozzo	fondo pozzo
ARCHIMEDES-001	467819.5	4054456.6	-71.5	Top soft sediment	FM RIBERA/GESS SOLFIFERA/TELLARO/RAGUSA
ARCHIMEDES-001	467819.5	4054456.6	-1002.5	Top hard sediment	FM AMERILLO/HYBLA/CHIARAMONTE/BUCCHERI/MODICA/STREPPENOSA
ARCHIMEDES-001	467819.5	4054456.6	-5020.5	fondo pozzo	fondo pozzo
ARETUSA-001	495445	4038791	-83	Top soft sediment	TOP GESSI/GESS SOLFIFERA/TELLARO/RAGUSA
ARETUSA-001	495445	4038791	-1202	Top hard sediment	FM AMERILLO/HYBLA/CHIARAMONTE/BUCCHERI/MODICA/STREPPENOSA
ARETUSA-001	495445	4038791	-3728	fondo pozzo	fondo pozzo
AVOLA-001	505771.3	4091674.3	503	Top soft sediment	FM PALAZZOLO/TELLARO/RAGUSA
AVOLA-001	505771.3	4091674.3	-260.7	Top hard sediment	FM AMERILLO/CALC PORTO PALO/AMERILLO/HYBLA/CHIARAMONTE/BUCCHERI/RABBITO/STREPPENOSA
AVOLA-001	505771.3	4091674.3	-1958.7	fondo pozzo	fondo pozzo
BIDDINE-001	456157.8	4101606.4	240	Top soft sediment	FM RIBERA/GESS SOLFIFERA/TRIPOLI/TELLARO/RAGUSA
BIDDINE-001	456157.8	4101606.4	-777.35	Top hard sediment	FM AMERILLO/HYBLA/CHIARAMONTE/BUCCHERI/MODICA/STREPPENOSA/NOTO
BIDDINE-001	456157.8	4101606.4	-2105.35	fondo pozzo	fondo pozzo

Clay land from the Oligo-Miocene to the Pleistocene age are discriminated as soft sedimentary rocks (Ragusa, Corleone, S. Cipirello, Tellaro, Palazzolo, Terravecchia, Gessoso Solfifera, Ribera formations). Hard sedimentary rocks correspond to the carbonatic facies from the Triassic to the Cretaceous (Sciacca, Streppenosa, Modica, Buccheri, Chiaramonte, Hybla, Porto Palo limestone,

Amerillo formations). The horizons in wells were identified based on the lithological characteristics of the Sicilian and Tunisian facies. A subdivision of lithostratigraphic units identified in the wells and the correlation between the formations is shown in Table 3.

TABLE 3. THE TABLE SHOWS THE SUBDIVISION OF THE LITHOSTRATIGRAPHIC UNITS IN THE WELLS SELECTED IN THIS WORK.

Tunisian facies	Sicilian facies	Lithology	Age
RAF RAF	RIBERA	Fossiliferous clay, sandy	Plio/Pleistocene
PORTO FARINA			
OUM DOUIL	GESSOSO SOLFIFERA	Gypsum limestone, clay	Miocene (Messiniano)
SAQUAF			
MELUART			
Q BEL KHEDIM			
NILDE	TERRAVECCHIA	Clay, sand	Miocene
	PALAZZOLO	Fossiliferous clay, sand	Upper Miocene
MAHMOUD	TELLARO	Fossiliferous clay, sand	Middle Miocene
MAHMOUD	S. CIPIRELLO	Marl, clay	Low Miocene
AINGRAB	CORLEONE	Packstone/wackestone	Low Miocene
FORTUNA	RAGUSA	Fossiliferous mudstone/wackestone	Oligo/Miocene
SALAMMBO			
HALK EL MENZEL	AMERILLO (Alcamo) / PORTO PALO LIMESTONE	Fossiliferous limestone	Cretaceous/Eocene
SOUAR			
METLAOUI			
BOU DABBOUS			
EL HARIA			
ABIOD			
ALEG			
GEBEL NEHAL	HYBLA (Alcamo)	Mudstone marl	Lower Cretaceous
ALLAM			
FAHDENE			
HAMEIMA			
SERDJ			
SIDI AICH			
BOU HEDMA			
SIDI KHALIF	LATTIMUSA (m.bro Busambra) / CHIRAMONTE (Alcamo)	Cherty mudstone, chalk	Jurassic (Malm)
NARA	BUCCHERI (Giardini)	Fossiliferous wackestone	Jurassic (Dogger/Malm)
	MODICA/ RABBITO/ SIRACUSA/ INICI	Mudstone/wackestone	Jurassic (Lias)
	STERPPENOSA	Mudstone recrystallized, dolomite	Upper Trias
	SCIACCA/ NOTO/ GELA/ TAORMINA	Dolomite	Trias

Below are the names of the wells, in alphabetical order, consulted for this work:

Acate-001_dir, Acate-002, Acate-003, Alfa-001, Archimedes-001, Aretusa-001, Avola-001, Biddine-001, Biddusa-001, Biddusa-002, Bimmisca-001, Campobello-001, Capo Negro-001, Carla-001, Carrubo-001, Cassibile-001, Catania-011, Catania-012, Catania-013, Catania-014, Cernia-001, Chelbi-001, Cianciana-001, Cisina-001, Contrada Triglia-001, Contrada Ulmo-001, Corvi, Corvina Mare-001, Cozzo Scalia-001, Delfino-001, Dittaino-001, Egeria-001, Eraclea Sicilia-001, Ermione-001, Eva-001, Gabbiano-001, Genziana-001, Genziana-001_Dir_A, Giada-001, Leone-001, Lucata-001, Maddalena-001, Manfria-002, Marinella-001, Marinella-002, Marinella-003, Marzamemi-001, Menfi-001, Merluzzo Mare-001, Mila-001, Mila-002, Mila-002_Bis, Mila-003, Mila-004, Mila-004_Dir, Mila-005, Mila-006, Mila-006_Dir, Mila-007_Dir, Mila-008_Dir, Mila-009, Monterosso-001, Mozia-001, Ms-A1, Nada-001, Naila-001, Nanda-001, Narciso-001_Dir, Narciso-001_Dir_A, Narciso-002, Narciso-003, Nausicaa-001, Nella-001, Nerian-001, Nettuno-001, Nilde-001, Nilde-001_Bis, Nilde-002, Nilde-003, Nilde-003_Bis, Nilde-004_Dir, Nilde-005, Nilde-006, Nilde Ovest-001, Ninfea-001, Niobe-001, Noemi-001, Nora Nord-001, Norma-001, Nuccia-001, Nunzia-001, Olga-001, Onda-001, Oreste-001, Orione Est-001, Orlando-001, Orlando-002, Oscar Ovest-001, Pachino-004, Palazzolo-001, Palma-001, Palma-002, Palma-003, Pamela-001, Pamela-001_Bis, Pancrazio Sud-001, Paola Est-001, Patty Est-001, Pellicano Ovest-001, Perla-001, Perla-002, Piera-001, Pilade Est-001, Pina-001, Plinio Sud-001, Poggi-003, Polpo-001, Ponte Olivo-001, Porto Palo-001, Prezioso-001, Rabbito-001, Remo Nord-001, Riccio Sud-001, Rigolizia-001, Rizzo-002, Rizzo-003, Rosa-001, S. Croce Camerina-001, S. Croce Camerina-002, S. Demetrio-001, Samanta-001, Santuzza-001, Scicli-001, Scicli-002, Settefarine-001, Simeto-001, Siracura-001, Sirio-001, Sofia-001, Spada Mare-001, Spigola Mare-001, Tullia-001, Ulisse-001, Ursitto-001, Valle Torta-001, Vallo-001, Venere-001, Vera-001, Vittoria-003, Vittoria-004, Vittoria Ovest-001, Zagara-001.

The final list of well data is available as Additional Information (Table A1) with coordinates.

3.3. Tectonic structures

A map of the tectonic structure that affected the Sicily Channel from Sicily to the Tunisian coast has been created. A database has been created in a GIS environment, where data has been imported and digitized (Fig. 20).

From the work of Antonelli et al. (1988) discriminated mainly two sectors of Sicily Channel: i) the northern sector offshore the Egadi islands in which are located the Drepano Thrust Front, and Inner Maghrebian thrust front ENE-SWS direction, and normal faults displace the NW-SE direction. This sector corresponds to the most internal and deformed part of the western segment of the Maghrebide Chain and is formed by tectonic units stacked partially compatible with the internal units of western Sicily and northern Tunisia. ii) the sector of the Pelagian block and the Malta plateau. This area is the stable area of the foreland and is affected by extensional structures that dislocate shallow marine carbonate deposits of Malta facies.

Jongsma et al. (1985) show a general deformation pattern of the central Sicily Channel area, characterized by a main dextral strike-slip deformation, E-W direction, extending from Tunisian towards Malta-Medina graben and continuing towards the Ionian Sea. A divergent movement near the Pantelleria, Malta, and Linosa graben causes the opening of these graben. In the easternmost area, the Medina plateau is characteristic of a convergent deformation with folds parallel to the strain's primary tensional axis. NNE-SSW inverse faults are derived from offsetting the grabens (*Winnock & Bea, 1979*) and observations mapped in Malta (*Illies, 1981*).

In the Adventure plateau, the north-western sector of Sicily Channel (*Civile et al., 2014*) is clearly visible the front of the push of the orogenic Apenninic-Maghrebian domain, Egadi Thrust Front, NE-SW direction. This area has two different tectonic processes: the construction of the Sicilian-Maghrebian Chain and, hand, the process of a continental rift that generated the Adventure plateau (do not exceed 150 m depth).

In particular, the Adventure plateau is affected by normal N-W faults linked to the continental rifting of the North African margin, which generated the graben of Pantelleria. Based on analyzing several seismic profiles, these faults tend to submerge several hundred meters to S-W.

To the east of the Adventure bank is the deformation zone (or transfer zone), the Capo Granitola-Sciacca Fault Zone (CGSFZ), which is over 60 km wide from 28 to 38 km.

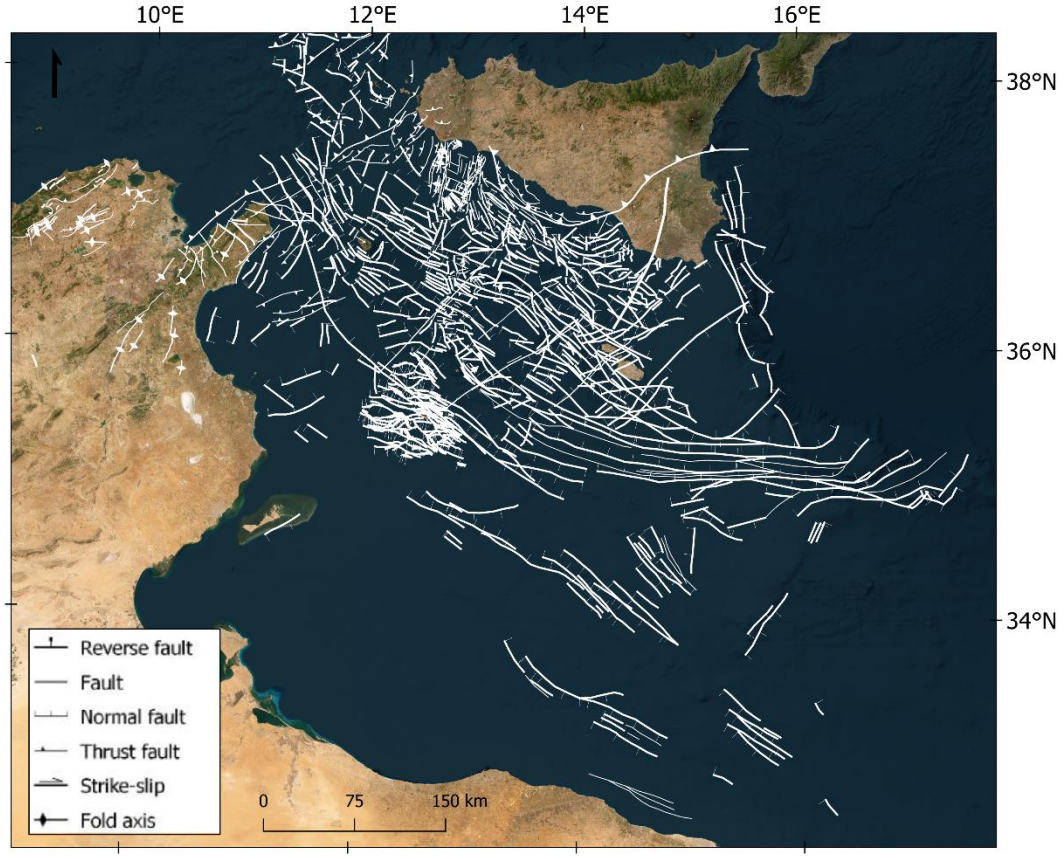

FIGURE 20. MAP OF THE TECTONIC STRUCTURES OF THE SICILY CHANNEL AREA (QGIS SOFTWARE V. 3.10.12-A CORUÑA). DATA HAS BEEN COLLECTED BY SEVERAL AUTHORS WHO HAVE EXAMINED THE CENTRAL MEDITERRANEAN AREA. AS THE LEGEND SHOWS, NORMAL FAULTS, REVERSE FAULTS, THRUST, STRIKE-SLIP, AND FOLDING AXIS ARE DISTINCT.

Two fault systems border this area, Capo Granitola Fault System (CGFS) to the west and Sciacca Fault System (SFS) to the east, characterized by transpressive and transtensive structures, N-S trending (*Civile et al., 2018; Ferranti et al., 2019*). NNE-oriented extensional faults predominantly characterize this zone, and sub-vertical N-S faults are found.

In the offshore sector, the Agrigento coast, along the south-central coast of Sicily, is a deformative zone of about 80 km characterized by a system of faults WNW-ESE to NW-SE-oriented (*Cavallaro et al., 2017*). Within this area, normal faults (Miocene age) reactivated later in strike-slip (Zancleano-Piacenziano age). The process of continental rifting, which occurred between the Neogene-Quaternary, which affected the Sicily Channel, produced the main graben with WNW trend,

which are controlled on the margins by normal faults, well visible from seismic profiles (*Grasso et al., 1992; Civile et al., 2010; Lodolo et al., 2012; Civile et al., 2021*). Therefore, due to the convergence between the African and Eurasian plates, the Tunisian block has developed several systems of faults and push folds with vergence towards the south (*Fink et al., 2012; Jallouli et al., 2013; Gaidi et al., 2020*) along the coast and the Tunisian offshore (*Boccaletti et al., 1987*).

Studies of multichannel seismic reflection profiles, calibrated with well data, conducted analyses in the areas surrounding the Lampedusa and Lampione islands (*Torelli et al., 1995*). A detailed analysis has been made in this area, noting the main structures developed since the Late Miocene age (*Grasso et al., 1993*). The overall pattern around the two islands is characterized by WNW-ESE faults, associated with minor faults that take a trend of NNW-SSE, NW-SE, and NE-SW. As a result of the continental rift, a series of horsts and grabens with WNW-ESE direction are noted.

The map of tectonic structures has been implemented in the GIS environment and has been subsequently "simplified" in such a way as to have a general framework of the study area for the realization of maps and the lithospheric model for the Pelagian block.

3.4. The seismic velocity of the continental crust

It is essential to describe and define the crust's composition and how the division into upper, middle, and lower crusts is based. Even today, there are many discussions on the lithological composition of the continental crust; the main reason is linked to the difficulty of estimating the composition of the deep crust because of the trouble of sampling significant portions. In situ, studies on the lower crust require geophysical analysis to determine regional phenomena. Petrological and geochemical analyses of the deepest portion of the continental crust are connected to the study of high-grade metamorphic lithologies, the granulite. The joint study of high-resolution geophysical and geochemical data can lead to robust constraints on the lower crust composition.

Numerous studies have shown that the depth and thickness of the lower continental crust vary regionally and in different geological contexts.

Conrad's discontinuity corresponds seismically to the lower crust but may not be present. From the lithological point of view, the upper continental crust has a granitoid composition (rich in SiAl lithophile elements). In contrast, the lower crust has an intermediate-acidic composition, granulitic type (rich in SiMa ferromagnesian elements), intermediate or basic with amphiboles.

The first seismic studies on the crust date back to the period between 1900 and 1970, where the main limitations referred to the techniques of use, which produced preliminary results on the structure of the crust. Except for some interpretations, these data were interpreted with two or more homogeneous layers, entrusting to the upper layer a granitic composition (with Vp = 6.0 km/s) and the lower layer a basaltic composition (with Vp = 6.5 km/s) (*Mooney et al., 2010*). A greater understanding of the crust's seismic structure occurred by introducing deep seismic reflection profiles and acquiring wide-angle seismic refraction and reflection data (WARR). These studies have shown that the crust is laterally and vertically heterogeneous (*Holbrook et al., 1992*). Traditionally, seismic studies of the deep continental crust are classified into two categories according to the physical parameters to be acquired, seismic refraction analysis and seismic reflection analysis. The two analyses are complementary in that the data of seismic reflection produces a structural image of the crust, while the data of seismic refraction provides an estimate of the velocity distribution of the seismic ray paths within the crust.

In the past, Conrad (1925) was the first to define the concept of the lower crust, analyze the path of seismic waves, and identify a layer over the Moho discontinuity with a seismic wave velocity between 6.0 and 8.0 km/s, that is, between the upper crust and upper mantle.

Subsequently, Holbrook et al. (1992) analyzed the portion of the lower crust in detail, a study based on the acquisition of wide-angle seismic field and laboratory measurements. This work is based on the compilation of velocity data from over 90 wide-angle refraction seismic studies compared with the velocity values of the rocks analyzed in the laboratory, particularly the lower crust. A summary of the continental seismic velocities of the middle and lower crust is presented in different tectonic environments: Precambrian shields, cratonal platforms, continent-continent collision zones, volcanic plateaus, continental rift zones, continental and island arcs, forearc regions, passive continental margins. A database of several works

published in the last decade has been created, with different seismic properties differentiating the lower crust from the middle crust. The P-waves velocity, S-waves velocity, Poisson ratio, and thickness values were reported. The P-wave velocities are between 6.0 to 7.5 km in the lower crust and Vp from 5.4 to 7.3 km/s in the middle crust. The ranges of these velocities vary according to the mineralogical composition of the rocks, including compositions from felsic to ultramafic and metamorphic to granulite and eclogite. The relationship between the P and S waves velocity (Vp and Vs) for a rock or a particular mineral can be expressed as a Poisson ratio:

$$\sigma = \frac{Vp^2 - 2Vs^2}{2\,(Vp^2 - Vs^2)} \quad (1)$$

assuming the material is isotropic and homogeneous. It is a very diagnostic lithological indicator, as it is sensitive to the content of quartz in rocks and allows us to distinguish the rocks rich in quartz (such as quartzites) from those poor in quartz (such as serpentinites). This value varies on average from 0.23 to 0.35 for the most common rock types. For the lower crust, a range of values is obtained between 0.24 and 0.29, while for the average crust between 0.24 and 0.27.

From the results obtained, comparing the acquisitions performed in the field with the laboratory analyses, it has been seen that the lower crust is characterized by a wide range of the P-waves velocity, therefore presuming that different types of rock characterize it. Figure 21a shows that 90 % of the P-wave velocity data is between 6.0 and 6.8 km/s, with a peak between 6.5 and 6.8 km/s corresponding to the metagabbro for the middle crust. Whereas for the lower crust (Fig. 21b), it is recognized a bimodal distribution of the P-waves velocity is in the ranges between 6.7 and 6.8 km/s and between 7.0 and 7.2 km/s, corresponding to the granulitic composition; this indicate that about 2/3 of the global lower crust has an average P-wave velocity within these ranges and that about half of this has a velocity equal to or greater than 7.0 km/s. The histograms were created by assigning a weighting factor to each velocity value based on the relationship between the different tectonic environments' investigated crustal area and the individual environments' volumetric abundance.

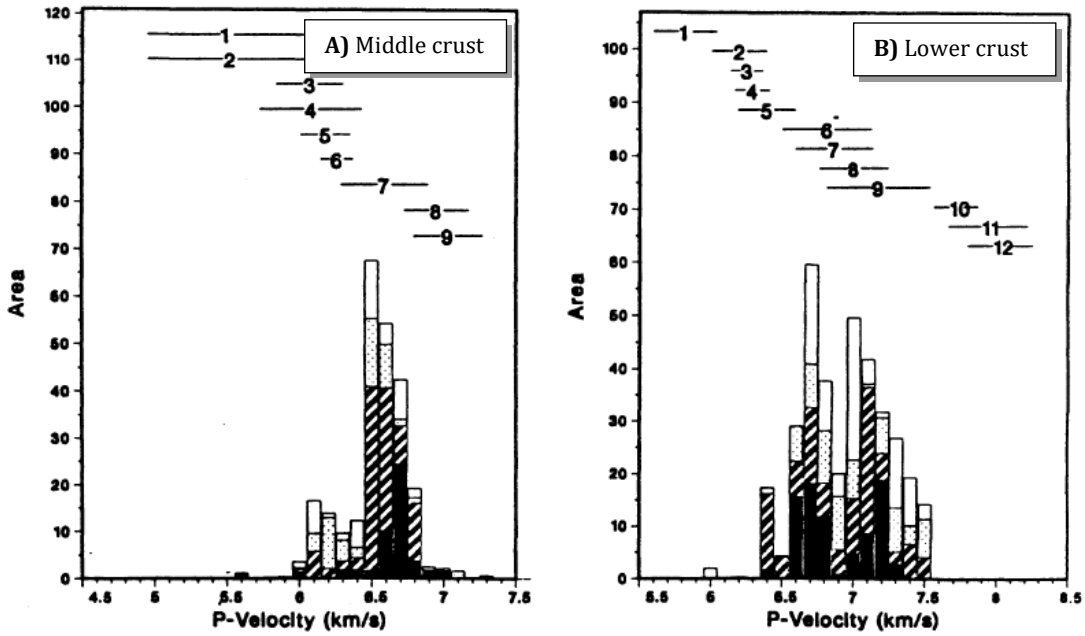

FIGURE 21. HISTOGRAM OF THE CROSS-SECTIONAL AREA OF CRUST (IN KM^2 X 10^3) AND P-WAVE VELOCITY FOR THE LOWER CRUST IN ALL TECTONIC ENVIRONMENTS. BARS ON TOP SHOW THE VELOCITY RANGE FOR THE POSSIBLE ROCK TYPE. FOR THE MIDDLE CRUST **A) 1:** SERPENTINITE; **2:** QUARTZITE; **3:** GRANITE; **4:** GRANODIORITE; **5:** FELSIC AMPHIBOLITE FACIES; **6:** SCHIST; **7:** METAGABBRO; **8:** GABBRO; **9:** AMPHIBOLITE. FOR THE LOWER CRUST **B) 1:** QUARTZITE (GRANULITE); **2:** FELSIC AMPHIBOLITE FACIES GNEISS; **3:** FELSIC GRANULITE; **4:** SCHIST; **5:** INTERMEDIATE GRANULITE; **6:** ANORTHOSITE; **7:** MAFIC GRANULITE; **8:** AMPHIBOLITE; **9:** FELSIC AND INTERMEDIATE GARNET GRANULITE; **10:** PYROXENITE; **11:** ECLOGITE; **12:** DUNITE/PERIDOTITE (*Holbrook et al., 1992*).

3.4.1. Velocity model

To determine the horizons in the individual seismic profiles, a velocity value was assigned to discriminate the different geological formations. A comparison has been made (Table 4) between velocity values proposed by different authors (*Torelli et al., 1995; Mooney et al., 1998; Catalano et al., 2000; Bello et al., 2000; Civile et al., 2014; Meccariello et al., 2017*) calibrating data, in this work, with seismic CROP profiles, and well data. Particularly, Catalano et al. (2000) have analyzed the structures of central-western Sicily; the P-wave velocity has been obtained by calibrating the data of wells associated with the sedimentary bodies identified. Six sedimentary deposits have been identified below:

i) Carbonate platform succession (Trias/Lias age) with a velocity of 5000 m/s; ii) carbonate platform succession (Dogger/Malm age) with a velocity of 4500 m/s; iii) basin and slope to basin carbonate succession, with a velocity 4000 m/s; Numidian

quarzarenites (Upper Oligocene/Lower Messinian age) with a velocity 3500 m/s; terrigenous deposits predominantly clayey and marly (Serravallian/Messinian age) with 3000 m/s and sandy deposits (Plio/Pleistocene age) with velocity 2000 m/s. Civile et al. (2014) analyzed the seismic-stratigraphic sequence of the Adventure bank area by processing 2D seismic profiles and well data. In this case, the velocity considered is (from the most ancient successions) 3350 m/s for the Trias sequence, 3200 m/s for the Jurassic succession, 3100 m/s for the Cretaceous succession, 2750 m/s for the Cretaceous/Eocene succession, 2500 m/s for the Oligo/Miocene succession, 2150 m/s for the Miocene succession (Messinian), 1900 m/s for the Pliocene succession and 1500 m/s for the water.

Based on the velocity analysis, a geological interpretation was carried out in this work according to the global crustal model CRUST 5.1 (at 5° x 5°) determined by Mooney et al. (1998). This crustal model was made on seismic refraction data published between 1948 and 1995 and on a detailed sediment and ice thickness analysis. The P-waves velocity were measured directly in the field, while empirical Vp-Vs and Vp-density relationships estimated the S-waves velocity. The choice to use this new crustal model resides in extending to a significantly larger database than the previous ones, and the new constraints derived from archives and laboratory studies are explicitly specified. Mooney defines 14 primary crustal types (Fig. 22) for the CRUSTAL 5.1 model construction, each of which is divided into seven layers, and Vp, Vs, and density are specified in each layer. In this work, six horizons have been recognized according to the lithological properties and P-waves velocity values.

In particular, the CRUST 5.1 model is characterized by 2592 cells, 5° x 5°, where eight layers are identified to describe the crust and the upper mantle: 1) ice, 2) water, 3) soft sedimentary rocks, 4) hard sedimentary rocks, 5) upper crust, 6) middle crust, 7) lower crust, and 8) upper mantle.

TABLE 4. DIAGRAM OF THE SICILIAN AND TUNISIAN FORMATIONS ANALYZED BY CALIBRATION OF WELLS. DIFFERENT AUTHORS PROPOSED VELOCITY VALUES: MOONEY ET AL. (1998); MECCARIELLO ET AL. (2017); TORELLI ET AL. (2000); CATALANO ET AL. (2000); CIVILE ET AL. (2014); BELLO ET AL. (2000).

<table>
<tr><th rowspan="2">Age</th><th rowspan="2">Equivalent Tunisian formations</th><th rowspan="2">Sicilian formations</th><th colspan="6">Velocity m/s</th></tr>
<tr><th>This work, from Mooney et al., 1998</th><th>Meccariello et al., 2017</th><th>Torelli et al., 1995</th><th>Catalano et al., 2000</th><th>Civile et al., 2014</th><th>Bello et al., 2000</th></tr>
<tr><td rowspan="2">Plio/Pleistocene</td><td>Porto Farina</td><td rowspan="2">Ribera</td><td rowspan="11">1600 / 3200 (2400)</td><td rowspan="2">2750</td><td rowspan="2">1910</td><td rowspan="2"></td><td rowspan="2"></td><td rowspan="2"></td></tr>
<tr><td>Raf Raf</td></tr>
<tr><td rowspan="5">Miocene up</td><td>Q bel Khedim</td><td rowspan="4">Gessoso Solfifera</td><td rowspan="4">3300</td><td rowspan="4"></td><td rowspan="4"></td><td rowspan="5">2150</td><td rowspan="4">2500</td></tr>
<tr><td>Melquart</td></tr>
<tr><td>Saouaf</td></tr>
<tr><td>Oum Douil</td></tr>
<tr><td>Nilde</td><td>Terravecchia</td><td rowspan="2">2800</td><td rowspan="2"></td><td rowspan="3">3000</td><td rowspan="3"></td></tr>
<tr><td>Miocene middle</td><td>Mahmoud</td><td>San Cipirello</td></tr>
<tr><td>Miocene low</td><td>Aingrab</td><td>Corleone</td><td>3000</td><td></td><td>2500</td></tr>
<tr><td rowspan="3">Oligo/Miocene</td><td>Fortuna</td><td rowspan="2">Ragusa</td><td>3300</td><td></td><td rowspan="6">3500 / 4000</td><td rowspan="3">2750 / 3100</td><td rowspan="2"></td></tr>
<tr><td rowspan="2">Salammbo</td><td>3500</td><td></td><td rowspan="9">5500</td></tr>
<tr><td rowspan="8">Cretaceous up/Eocene</td><td>Halk El Menzel</td><td rowspan="8">Amerillo</td><td rowspan="15">4000 / 5300 (4600)</td><td rowspan="8">4800</td><td rowspan="8">5960</td></tr>
<tr><td>Souar</td></tr>
<tr><td>Metlaoui</td></tr>
<tr><td>Boudabbous</td></tr>
<tr><td>ElHaria</td></tr>
<tr><td>Abiod</td></tr>
<tr><td>Aleg</td></tr>
<tr><td rowspan="8">Cretaceous low</td><td>Gebel Nehal</td><td rowspan="8">Hybla</td><td rowspan="8">5600</td><td rowspan="8">6280</td><td rowspan="9">4500</td><td rowspan="4">3100</td></tr>
<tr><td>Allam</td></tr>
<tr><td>Fahdene</td></tr>
<tr><td>Hamemia</td></tr>
<tr><td>Serdj</td></tr>
<tr><td>Sidi Aich</td></tr>
<tr><td>Boud Hedma</td></tr>
<tr><td>Jurassic (Malm)</td><td>Sidi Khalif</td><td>Chiaramonte</td><td rowspan="5">3200</td></tr>
<tr><td>Jurassic (Dogger/Malm)</td><td rowspan="2">Nara</td><td>Buccheri</td><td rowspan="4"></td><td rowspan="4"></td></tr>
<tr><td>Jurassic (Lias)</td><td>Modica</td></tr>
<tr><td>Trias up/Jurassic low</td><td></td><td>Streppenosa</td></tr>
<tr><td rowspan="3">Trias</td><td rowspan="3"></td><td rowspan="3">Sciacca</td><td>5400</td><td></td><td rowspan="3">5000</td></tr>
<tr><td></td><td></td><td rowspan="2">3350</td></tr>
<tr><td>5800</td><td></td></tr>
</table>

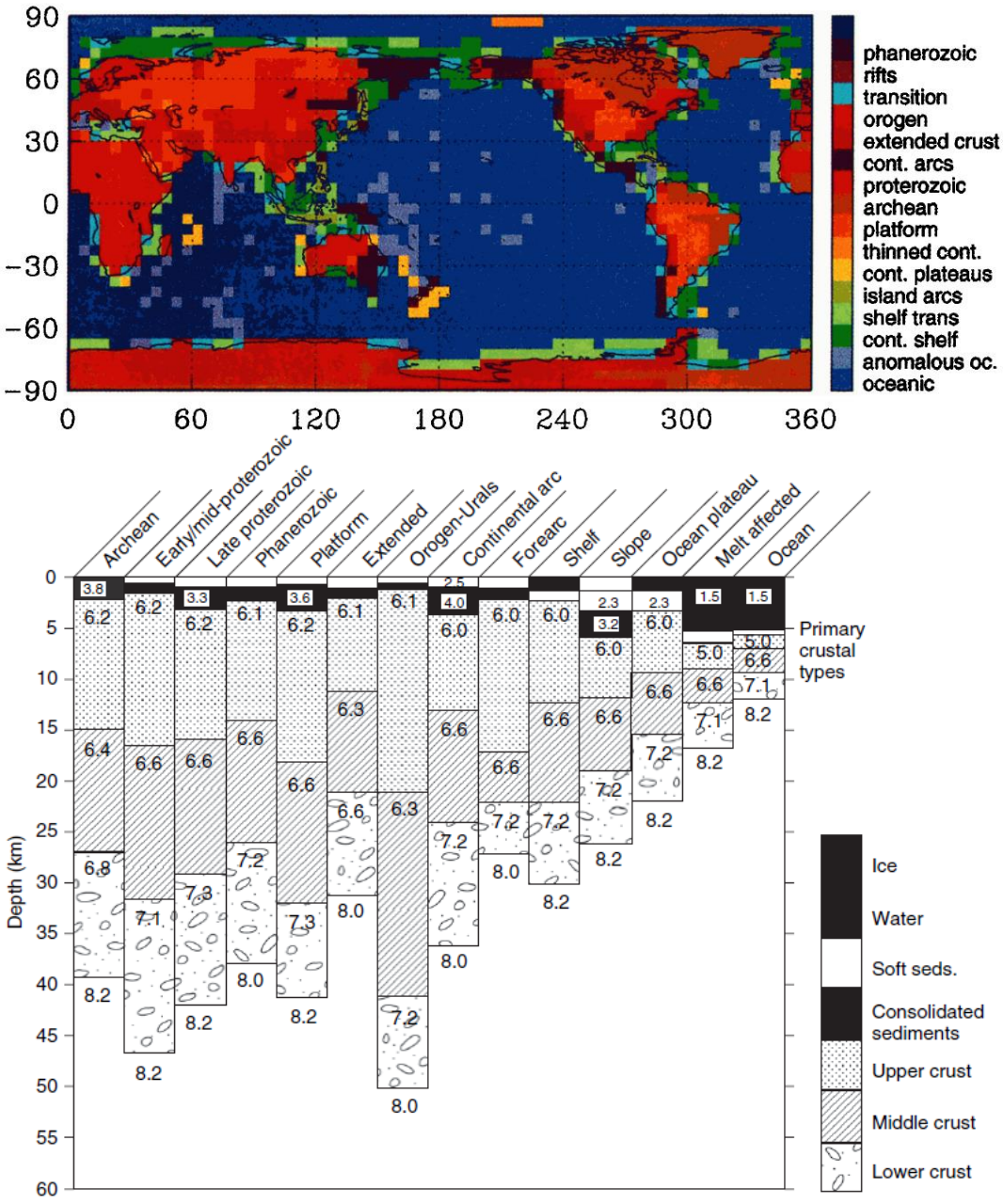

FIGURE 22. THE TOP FIGURE SHOWS THE CRUST TYPE DISTRIBUTION USED TO DETERMINE THE CRUSTAL MODEL AT 5° X 5° - CRUST 5.1. THE FIGURE BELOW SHOWS THE P-WAVE VELOCITIES OF THE INDIVIDUAL HORIZONS; THE VELOCITIES REFER TO THE TOP OF THE INDIVIDUAL HORIZONS, UP TO THE UPPER MANTLE (*Mooney et al., 1998; 2010*).

A comparison of the P-waves velocity from previous works from the analysis of the lithological characteristics of the wells analyzed identified six horizons, from top to bottom (Fig. 23):

1) Soft sedimentary rocks (unconsolidated) with a P-wave velocity of 2.4 km/s;
2) hard sedimentary rocks (consolidated) with a P-wave velocity of 4.6 km/s;

3) upper crystalline crust with a P-wave velocity of 6.0 km/s;
4) middle crystalline crust with a P-wave velocity of 6.5 km/s;
5) lower crystalline crust with a P-wave velocity of 7.1 km/s;
6) uppermost mantle with a P-wave velocity of 8.2 km/s.

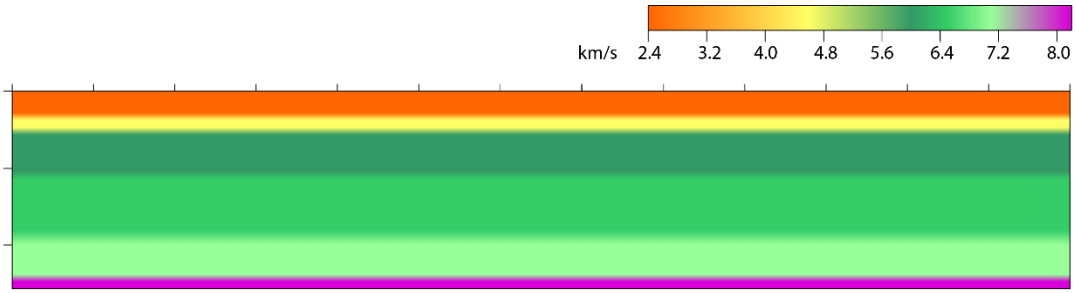

FIGURE 23. 1D-VELOCITY MODEL DISCRETIZATION. THE SURFER GOLDEN SOFTWARE (V. 20.2.218) WAS USED TO BUILD THE MODEL.

The 1D-velocity model has been discretized with constant velocity for different seismic horizons to have the model's lateral and vertical heterogeneity. The discretization of a 1D-velocity model involves dividing it into discrete intervals or grid points, where each represents a specific depth or position along the 1D model. The 1D model was built with the Surfer Golden software, the cell spacing is 0.9 (x-y spacing) for 20244 total nodes (28 rows by 723 columns).

3.5. Seismic network monitoring

The area of the Sicily Channel is considered a low seismicity area, but this is substantially related to the limited instrumental coverage of the whole central Mediterranean. For this reason, the location of earthquakes in the Sicily Channel, particularly in the North African part, is difficult.

The Rete Sismica Nazionale (RSN) controls seismic monitoring in Italy and is managed by the Istituto Nazionale di Geofisica e Vulcanologia (INGV). The Umbria-Marche earthquake in 1997 is a point of Italy's recent monitoring system development. In the 80s and 90s, the Italian National Network integrated the installation of seismic stations with modern instrumentation capable of rendering high-resolution images of the active faults (*Amato & Mele, 2008*). In 1997, the RSN had 90 stations and limited coverage. The problems were mainly related to the low precision of the location of earthquakes and the response in time; in fact, for

earthquakes of minor intensity, it took at least 5 minutes to obtain reliable hypocentral positions. In 1995, the digital broadband seismic network was introduced throughout the Mediterranean (MedNet Project); stations were installed between Pantelleria, Linosa, and Malta islands, managed by the Istituto Nazionale di Geofisica e Vulcanologia (*Boschi & Morelli, 1994*).

In the last 30 years, the INGV has expanded the seismic network, which has grown numerically and (*Amato & Mele, 2008*) today, it has more than 600 stations (Fig. 24).

Malta's seismic network has also expanded the seismic network in region in recent years, currently includes six permanent broadband stations, and between June 2017 and September 2018, six more temporary short-period stations (for the FASTMIT project) were implemented (*Bozionelos et al., 2019*). The main objectives of the FASTMIT project, financed by the Italian government and managed by OGS (Istituto Nazionale di Oceanografia e di Geofisica Sperimentale, Sezione Centro Ricerche Sismologiche, Italy) concern the analysis and monitoring of seismicity in the Italian seas to increase knowledge on fault systems present and determine the evolution of this within the geodynamic complex of the Sicily Channel.

The six short-period stations installed on Malta island are equipped with Lennartz sensors and RefTek digitizers to supplement Malta's permanent network. Four of these stations, FM01, FM02, FM04, and FM06, are located on the globigerina or inferior coral limestone surfacing, while the other two stations, FM03 and FM05, are located on the formation of the superior coral limestone (*Bozionelos et al., 2019*).

It was chosen a radius of about 400 km from a central point of the Sicily Channel (36.66° N – 12.83° E) to determine the stations from which to obtain the recordings of seismic events (Fig. 25). The research was carried out by the site ISC from the International Registry of Seismograph Stations (IR). Tables 5 and 6 show the lists of stations on the island of Malta and on the coast of Tunisia and Algeria, respectively.

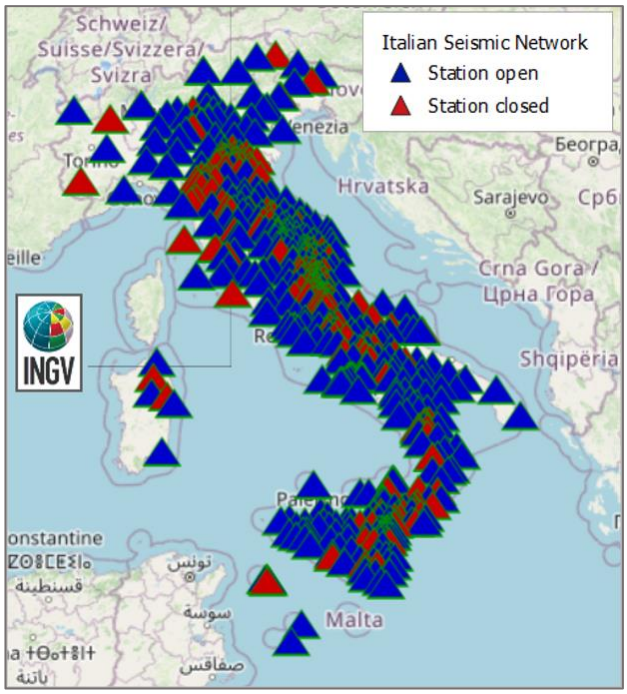

FIGURE 24. THE ITALIAN SEISMIC NETWORK MAP OF THE ISTITUTO NAZIONALE DI GEOFISICA E VULCANOLOGIA HAS MORE THAN 600 SEISMIC STATIONS. THE STATION ILLUSTRATED WITH BLUE TRIANGLES ARE ACTIVE STATIONS, WHILE THE RED TRIANGLES ARE CLOSED STATIONS (http://terremoti.ingv.it/instruments).

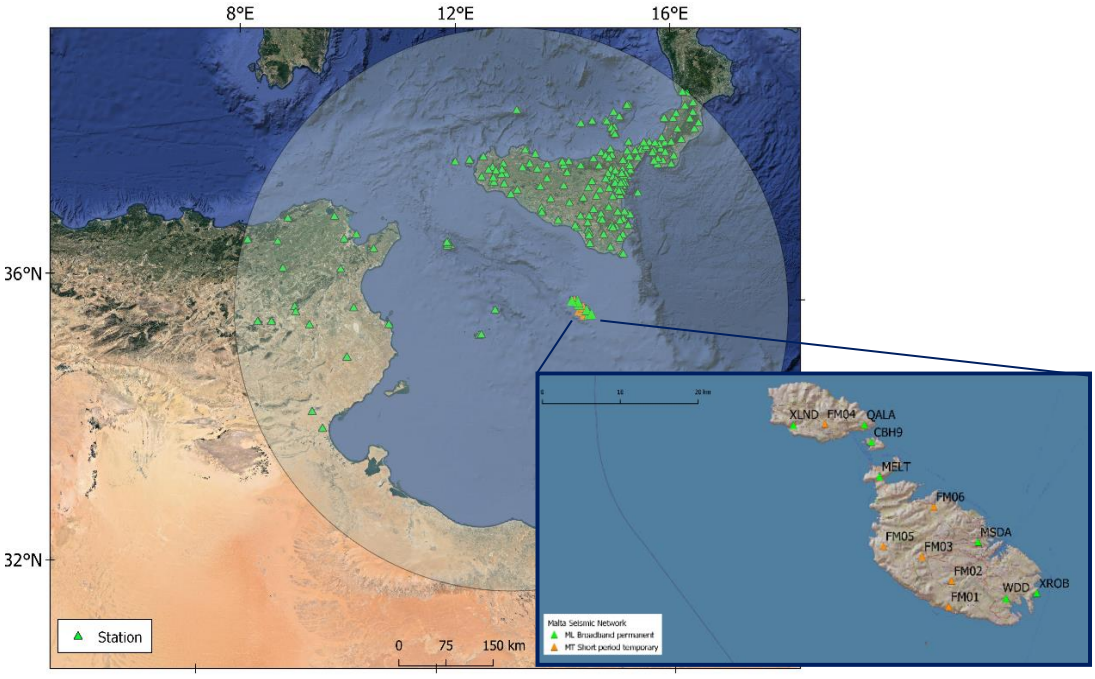

FIGURE 25. MAP OF SEISMIC STATIONS USED IN THIS WORK. FOR THE ISLAND OF MALTA, THE STATIONS ARE ILLUSTRATED WITH ORANGE TRIANGLES THE SIX SHORT-PERIOD OGS STATIONS, AND THE GREEN TRIANGLES ARE FROM THE SIX PERMANENT STATIONS OF THE MALTA SEISMIC NETWORK (QGIS SOFTWARE).

TABLE 5. OVERVIEW OF STATIONS INSTALLED BY THE MALTA SEISMIC NETWORK (MSN), SHORT-PERIOD TEMPORARY AND BROADBAND PERMANENT STATIONS.

Station Code	Long (E°)	Lat (N°)	Elevation (m)	Outcropping geology	Network
CBH9	14.331	36.014	28	up coralline limestone	MALTA broadband permanent
FM01	14.443	35.828	128	low coralline limestone	MALTA short period Temporary
FM02	14.447	35.857	95	globigerina limestone	MALTA short period Temporary
FM03	14.404	35.885	190	up coralline limestone	MALTA short period Temporary
FM04	14.265	36.034	105	globigerina limestone	MALTA short period Temporary
FM05	14.349	35.896	205	up coralline limestone	MALTA short period Temporary
FM06	14.421	35.941	6	low coralline limestone	MALTA short period Temporary
MELT	14.343	35.975	98	up coralline limestone	MALTA broadband permanent
MSDA	14.484	35.901	48	globigerina limestone	MALTA broadband permanent
QALA	14.321	36.034	92	up coralline limestone	MALTA broadband permanent
WDD	14.524	35.837	44	low coralline limestone	MALTA broadband permanent
XLND	14.22	36.032	15	low coralline limestone	MALTA broadband permanent
XROB	14.568	35.843	26	low coralline limestone	MALTA broadband permanent

For Tunisian stations, much of it is part of the Tunisian SBS seismic network (Table 6) managed by INM (National Meteorology Institute). The SBS seismic network comprises 15 single-component seismological stations and 4 digital stations (*Ksentini & Romdhane, 2013*); in this work, 11 were selected. While the Tunisia BB Network (TT_Net) manages three stations (www.fdsn.org/networks/detail/TT/), 2 of the three are inserted in the database to acquire seismic signals; they are open and accessible.

TABLE 6. OVERVIEW OF STATIONS INSTALLED IN TUNISIA AND ALGERIA.

Station Code	Station name	Region	Lat (N°)	Long (E°)	Elevation (m)	Status	Network
AYNT	El Ayoun	Tunisia	35.57372	8.92925	1100	Open	
BKLT	Bekalta	Tunisia	35.6186	10.9965	25	2010-2021	
BLIT	Baltah	Tunisia	36.713	8.95283	225	1993-2021	SBS Seismic Network
BTHT	Jabal bu Thady	Tunisia	35.13233	10.28517	240	2010-2021	SBS Seismic Network
CBOGS	Bougous	Algeria	36.707	8.416	207	2017-2022	
GFA	Gafsa (1989-1999)	Tunisia	34.3382	9.7265	250	1990-1996	SBS Seismic Network
HANT	Hania	Tunisia	35.8333	10.3635	165	2010-2021	
I48TN	Kesra Infrasonic array reference point	Tunisia	35.8052	9.323	848	Open	
KCHT	Kechabta	Tunisia	37.11	9.94	565	Open	SBS Seismic Network
KEST	Kesra	Tunisia	35.73178	9.34603	885	Open	
KRIT	Krib	Tunisia	36.3383	9.07483	640	Open	SBS Seismic Network
MBZ	Menzel Bouzelfa	Tunisia	36.68	10.67	220	1976-2021	SBS Seismic Network
MEDT	Meda	Tunisia	34.1082	9.92033	90	Open	SBS Seismic Network
SBS	Sidi-Bou-Said	Tunisia	36.87	10.35	125	1973-1992	SBS Seismic Network
TAMR	Tamra	Tunisia	37.0469	9.1091	93	Open	Tunisia BB Network (TT_Net)
THA	Thala	Tunisia	35.5603	8.69972	1080	2008-2008	SBS Seismic Network
THTN	Thala	Tunisia	35.5616	8.6881	1095	Open	Tunisia BB Network (TT_Net)
TROT	Trozza	Tunisia	35.5617	9.60017	900	Open	SBS Seismic Network
TUN	Tunis	Tunisia	36.8	10.1333		1933-1957	
ZGN	Zaghouan	Tunisia	36.37	10.1	720	Open	SBS Seismic Network

3.5.1. Earthquake data

In this work, the arrival times of the P and S phases obtained from the "Seismic Bulletin" INGV - National Institute of Geophysics and Volcanology

(terremoti.ingv.it/iside) and the "ISC Bulletin" International Seismological Centre (www.isc.ac.uk/iscbulletin/) were used. The data refer to earthquakes recorded from January 2005 to December 2021. Events with epicentres in the area between 30.0° N and 38.0° N of latitude and between 10.0° E and 16.5° E of longitude were selected, including all depths and magnitude $M \geq 3$.

The INGV bulletin provides the list of earthquakes closest to the Italian territory, while the ISC database is more complete for sources located towards the Tunisian coast. To expand, therefore, the information on seismic events from the ISC catalog was implemented with events recorded by Tunisian stations and was also integrated with events recorded by Malta stations.

A dataset of seismic events (915 events) has been realized, which are reported (Table 7), the area, date, origin time (UTC – Coordinated Universal Time), latitude, longitude, depth (m), magnitude, and magnitude type.

TABLE 7. EXAMPLES OF SEISMIC EVENTS ARE REPORTED. THE INTEGRATION OF THE INGV AND ISC DATABASES CREATED THE DATABASE.

Region	Date	Origin time (UTC)	Lat	Lon	Depth (m)	Magni tude	
Canale di Sicilia meridionale (MARE)	2005-01-02	02:05:56.99	35.858	13.055	10000	3.0	ML
Tunisia [Sea]	2005-01-05	21:16:50.10	36.4237	10.7593	10000	3.6	MD
Costa Ragusana (Ragusa)	2005-01-08	16:59:15.53	36.622	14.759	5000	3.1	MD
Malta (MALTA)	2005-01-15	01:08:51.84	35.696	14.429	10000	3.2	MD
Tunisia [Sea]	2005-02-07	20:05:39.00	36.2907	10.8155	14000	4.9	Mw
Tunisia [Sea]	2005-02-07	20:46:26.91	36.2556	10.8317	10000	5.1	Mw
Tunisia [Sea]	2005-02-07	22:50:07.60	36.2228	10.8528	8400	3.1	MD
Tunisia [Sea]	2005-02-08	01:24:49.10	36.1138	10.9598	10000	3.2	MD
Tunisia [Sea]	2005-02-08	01:49:39.30	36.1558	10.7762	26400	3.2	MD
Tunisia [Sea]	2005-02-08	18:40:04.60	36.2092	10.9243	300	4.2	MD
Tunisia [Sea]	2005-02-10	19:15:23.80	36.2527	10.9805	10000	3.0	MD
Tunisia [Sea]	2005-02-13	18:40:37.50	33.6885	10.2515	10000	3.4	MD
Tunisia [Sea]	2005-02-23	04:42:55.85	36.7584	10.6086	10000	3.3	ML
Central Mediterranean Sea	2005-02-27	01:55:21.89	33.749	13.6314	10000	3.5	mb
Mar Ionio Meridionale (MARE)	2005-03-17	18:57:15.95	37.411	15.963	10041	3.1	ML
Costa Ragusana (Ragusa)	2005-03-20	02:18:17.08	36.634	14.38	10000	3.0	MD
Tunisia [Sea]	2005-03-22	09:51:53.70	36.413	10.6932	19100	3.4	MD
Tunisia [Sea]	2005-04-09	09:55:32.30	34.0043	10.3283	5200	3.5	MD
Mar Ionio Meridionale (MARE)	2005-04-13	13:19:19.88	37.504	16.333	23962	3.4	ML

Different magnitude types have been found from the consultation of the ISC Bulletin: ML, Md, Mw, mb, mb1, mb1mx, mbtmp, ms, ms1, ms1mx. The choice in this work of cataloging (for the magnitude type) was to prefer the events with magnitude Mw (moment magnitude), mb (short-period body-wave magnitude), and ML (local -Richter- magnitude) in this priority order.

The final list of earthquakes is available as Additional Information (Table A2).

3.5.2. Analysis of earthquake data

855 events were analyzed from the Maltese dataset. Starting from the total of 915 events identified in the Sicily Channel, 60 events were not recorded as the stations were turned off. This phase of the work has led to the analysis of the seismic signals recorded by Maltese stations to accurately identify the arrival times of P and S waves (picking).

A total of 2441 signals recorded by the Maltese stations were analyzed; a general framework of the signals acquired by the individual stations is shown in Table 8.

The data from the monitoring stations have been analyzed individually to detect signals relevant to seismic or acoustic disturbances.

TABLE 8. SUMMARY DIAGRAM OF THE ANALYZED SIGNALS RECORDED BY THE STATIONS OF MALTA (FOR 855 SEISMIC EVENTS).

MALTA STATIONS	WDD	XLND	MELT	QALA	FM01	FM02	FM03	FM04	FM05	FM06	CBH9	XROB
SIGNALS RECORDED	799	359	288	147	63	63	52	63	55	60	201	76

The processing of the data was carried out manually, and the noise-affected events were discarded. Particular attention was paid to applying the appropriate filters and time windows for the different sampling frequency streams. In general, the filters act on the input signal to produce a different signal at the output. They are used for different cases, for example, to correct the instrument's response, to correct the effects related to aliasing (sampling distortion or undersampling), and to separate the frequencies of the signal "desired" from the unwanted ones, that is, the noise. For the three components (HHE, HHN, HHZ), a Butterworth band-pass filter (BPF) with a frequency range of 0.1-10.0 Hz was generally used. It was possible to attenuate the signals' frequencies and pick the P and S phases using this frequency range.

Several examples are shown of the processing (Swarm software v. 3.1.0) of seismic signals, where the waveform of the earthquake and the spectrogram are reported for the three components, HHE, HHN, and HHZ. Figure 26 (1a), for example, shows that the event occurred on 2006.11.25 (18:56:53.42 UTC) at N-E of Malta island; in

this case, picking the P and S waves for the event recorded by the WDD station was possible. Picking was carried out in both diagrams or rather, thanks to spectrograms, it was possible to have an additional constraint for determining seismic phases. Other examples of seismic events in distinct parts of the Sicily Channel, several km away from the Maltese stations, are shown in the following figures (Fig. 27, 28, 29, 30). There are also several events where picking the P and S phases was impossible. The earthquake that occurred on 2016.10.11 (07:38:14.60 UTC) at NW from Malta island along the Tunisian coast (Fig. 31-2a), about 300 km away from the XLND station, is an example of a noisy signal. The band-pass filter [0.1 - 10.0 Hz] was applied, but it was impossible to pick the seismic phases. The analysis of the data shows that most events are at a great distance (even 400 km away), but even for some events at a relatively small distance, it was difficult to detect the seismic phases; for example, earthquakes from the central part of the Sicily Channel (SE of Pantelleria island) are known to be highly attenuated probably due to the high temperatures present under the grabens.

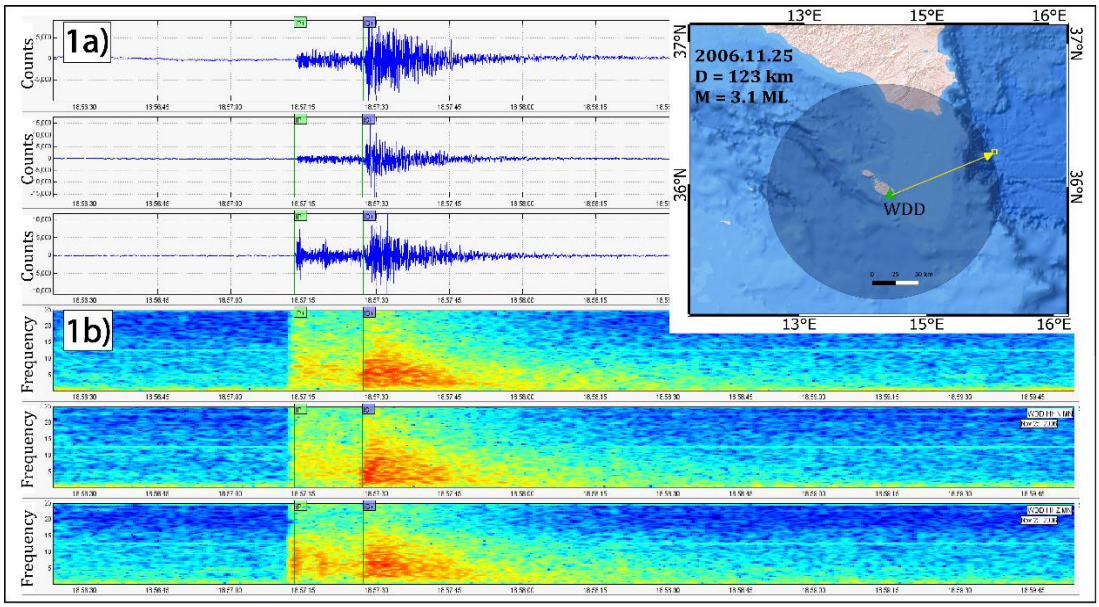

FIGURE 26. EARTHQUAKE RECORDED BY WDD STATION (2006.11.25 – 18:56:53.42 UTC – MAGNITUDE 3.1 ML – EPICENTER DISTANCE 123,97 KM), P AND S PICKING PHASE WAS CARRIED OUT. **1a)** THE EARTHQUAKE WAVEFORM OF THE THREE COMPONENTS; **1b)** THE SPECTROGRAM OF THE THREE COMPONENTS. THE TOP RIGHT IS THE EARTHQUAKE MAP (SWARM SOFTWARE).

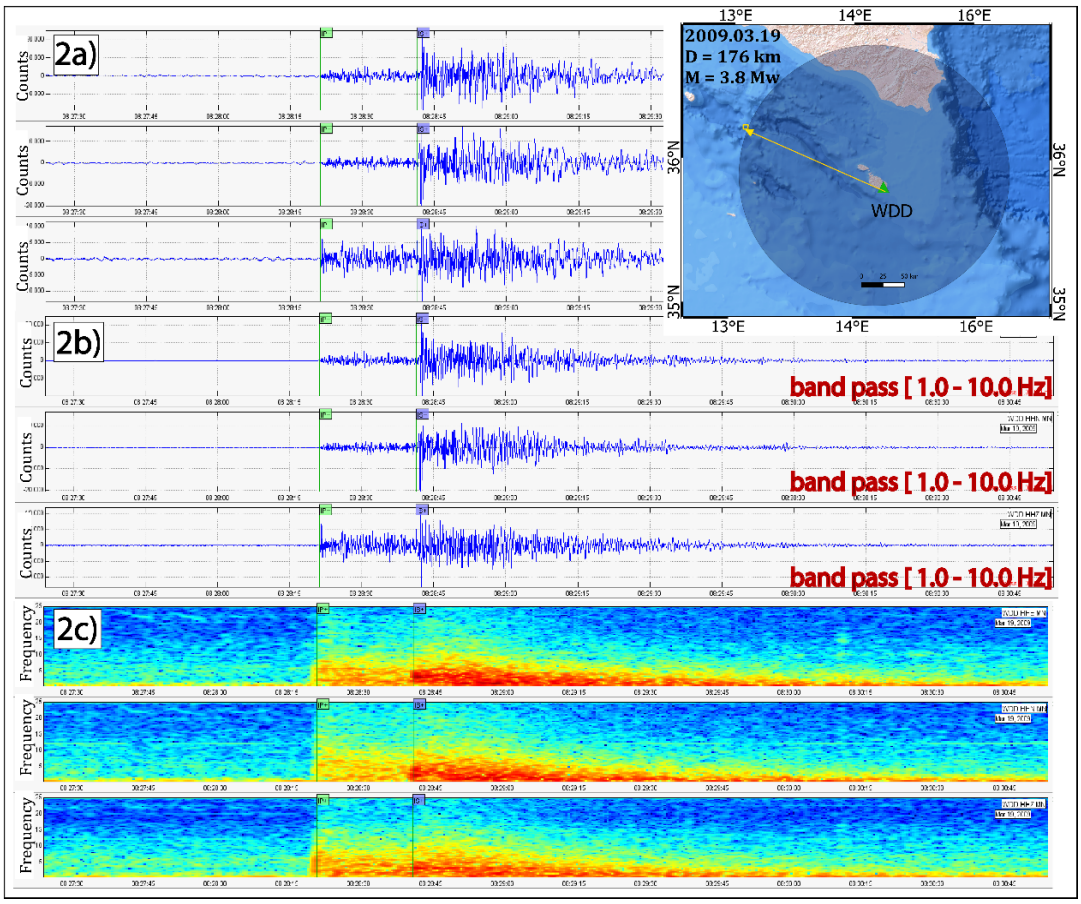

FIGURE 27. THE EARTHQUAKE RECORDED BY WDD STATION (2009.03.19 – 08:27:54.02 UTC – MAGNITUDE 3.8 MW – EPICENTER DISTANCE 176 KM), P AND S PICKING PHASE WAS CARRIED OUT. **2a)** THE EARTHQUAKE WAVEFORM OF THE THREE COMPONENTS; **2b)** THE FILTERED WAVEFORM [BAND-PASS 0.1-10.0 HZ] OF THE THREE COMPONENTS; **2c)** THE SPECTROGRAM OF THE THREE COMPONENTS. THE TOP RIGHT IS THE EARTHQUAKE MAP (SWARM SOFTWARE).

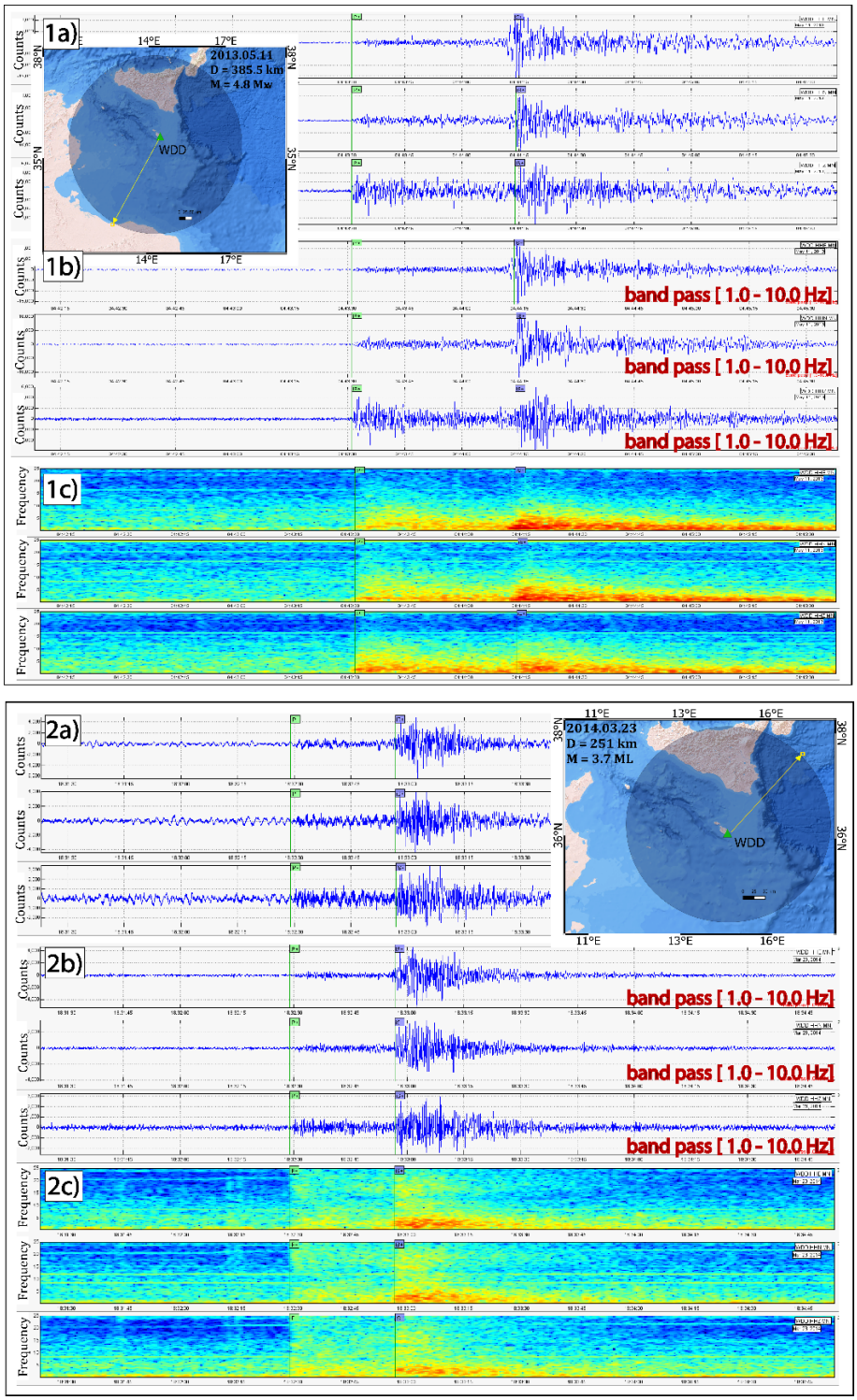

FIGURE 28. 1) EARTHQUAKE RECORDED BY WDD STATION (2013.05.11 – 04:42:38.14 UTC – MAGNITUDE 4.8 MW – EPICENTER DISTANCE 385.5 KM), P AND S PICKING PHASE WAS CARRIED OUT. **1a)** THE EARTHQUAKE WAVEFORM OF THE THREE COMPONENTS; **1b)** THE FILTERED WAVEFORM [BAND-PASS 0.1-10.0 HZ] OF THE THREE COMPONENTS; **1c)** THE SPECTROGRAM OF THE THREE COMPONENTS. THE TOP LEFT IS THE EARTHQUAKE MAP. **2)** THE EARTHQUAKE RECORDED BY WDD STATION (2014.03.23 – 18:31:53.02 UTC – MAGNITUDE 3.7 ML – EPICENTER DISTANCE 251 KM), P AND S PICKING PHASE WAS CARRIED OUT. **2a)** THE EARTHQUAKE WAVEFORM OF THE THREE COMPONENTS; **2b)** THE FILTERED WAVEFORM [BAND-PASS 0.1-10.0 HZ] OF THE THREE COMPONENTS; **2c)** THE SPECTROGRAM OF THE THREE COMPONENTS. THE TOP RIGHT IS THE EARTHQUAKE MAP (SWARM SOFTWARE).

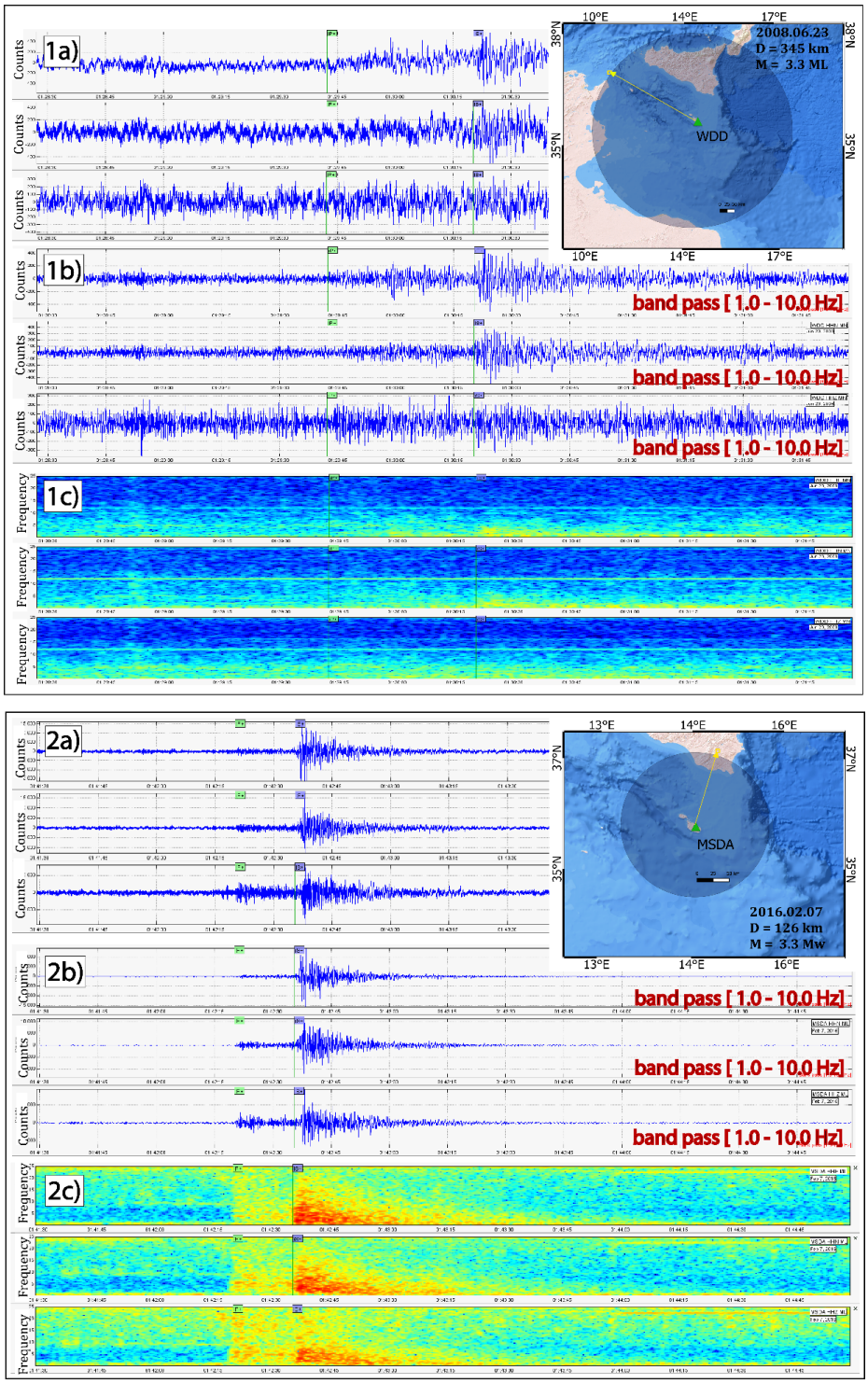

FIGURE 29. 1) EARTHQUAKE RECORDED BY WDD STATION (2008.06.23 – 01:28:57.11 UTC – MAGNITUDE 3.3 ML – EPICENTER DISTANCE 345 KM), P AND S PICKING PHASE WAS CARRIED OUT. **1a)** THE EARTHQUAKE WAVEFORM OF THE THREE COMPONENTS; **1b)** THE FILTERED WAVEFORM [BAND-PASS 0.1-10.0 HZ] OF THE THREE COMPONENTS; **1c)** THE SPECTROGRAM OF THE THREE COMPONENTS. THE TOP RIGHT IS THE EARTHQUAKE MAP. **2)** THE EARTHQUAKE RECORDED BY MSDA STATION (2016.02.07 – 01:41:59.14 UTC – MAGNITUDE 3.3 MW – EPICENTER DISTANCE 126 KM), P AND S PICKING PHASE WAS CARRIED OUT. **2a)** THE EARTHQUAKE WAVEFORM OF THE THREE COMPONENTS; **2b)** THE FILTERED WAVEFORM [BAND-PASS 0.1-10.0 HZ] OF THE THREE COMPONENTS; **2c)** THE SPECTROGRAM OF THE THREE COMPONENTS. THE TOP RIGHT IS THE EARTHQUAKE MAP (SWARM SOFTWARE).

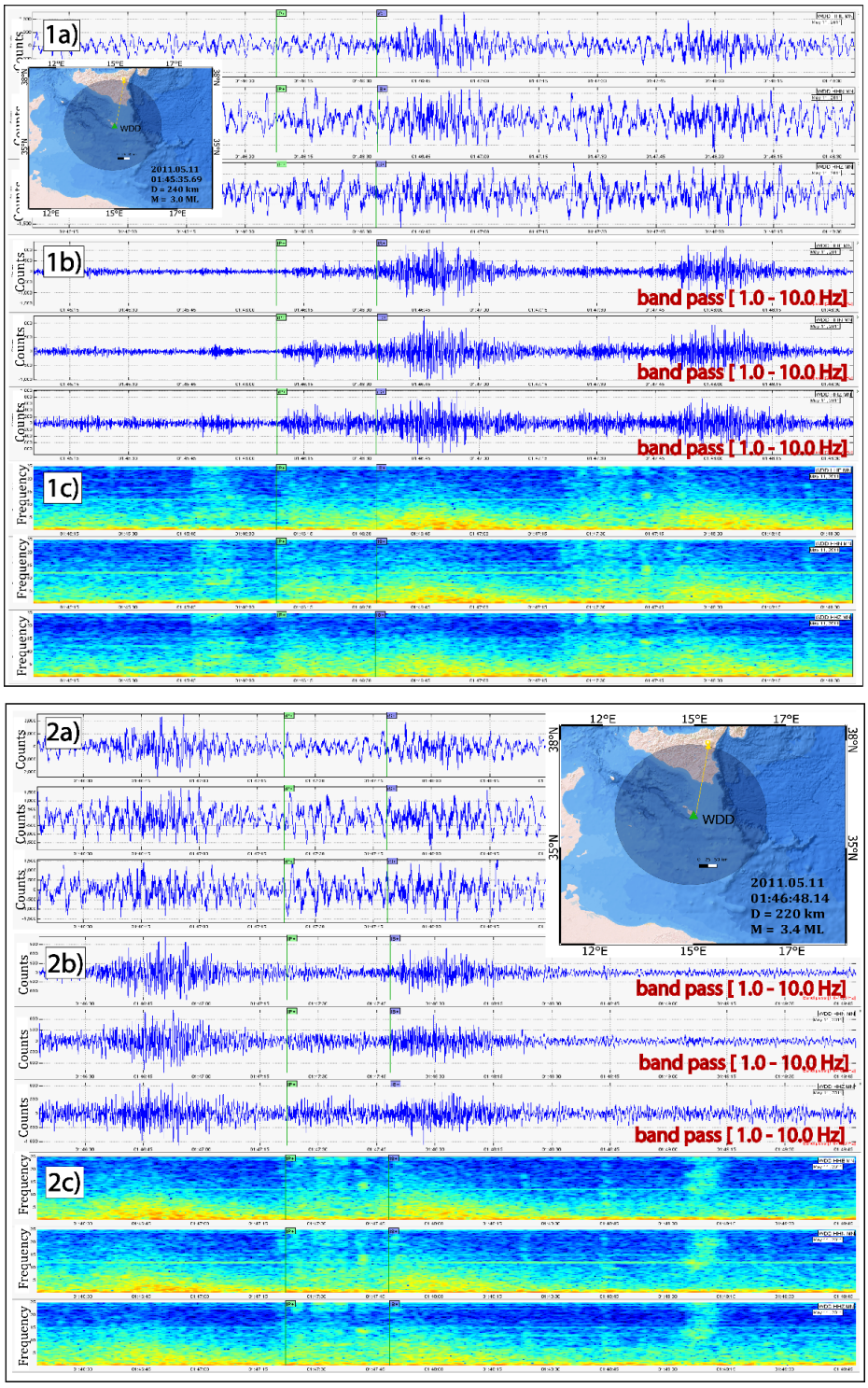

FIGURE 30. 1) EARTHQUAKE RECORDED BY WDD STATION (2011.05.11 – 01:45:35.69 UTC – MAGNITUDE 3.5 ML – EPICENTER DISTANCE 240 KM), P AND S PICKING PHASE WAS CARRIED OUT. **1a)** THE EARTHQUAKE WAVEFORM OF THE THREE COMPONENTS; **1b)** THE FILTERED WAVEFORM [BAND-PASS 0.1-10.0 HZ] OF THE THREE COMPONENTS; **1c)** THE SPECTROGRAM OF THE THREE COMPONENTS. THE TOP LEFT IS THE EARTHQUAKE MAP. **2)** THE EARTHQUAKE RECORDED BY WDD STATION (2011.05.11 – 01:46:48.14 UTC – MAGNITUDE 3.5 ML – EPICENTER DISTANCE 220 KM), P AND S PICKING PHASE WAS CARRIED OUT. **2a)** THE EARTHQUAKE WAVEFORM OF THE THREE COMPONENTS; **2b)** THE FILTERED WAVEFORM [BAND-PASS 0.1-10.0 HZ] OF THE THREE COMPONENTS; **2c)** THE SPECTROGRAM OF THE THREE COMPONENTS. THE TOP RIGHT IS THE EARTHQUAKE MAP (SWARM SOFTWARE).

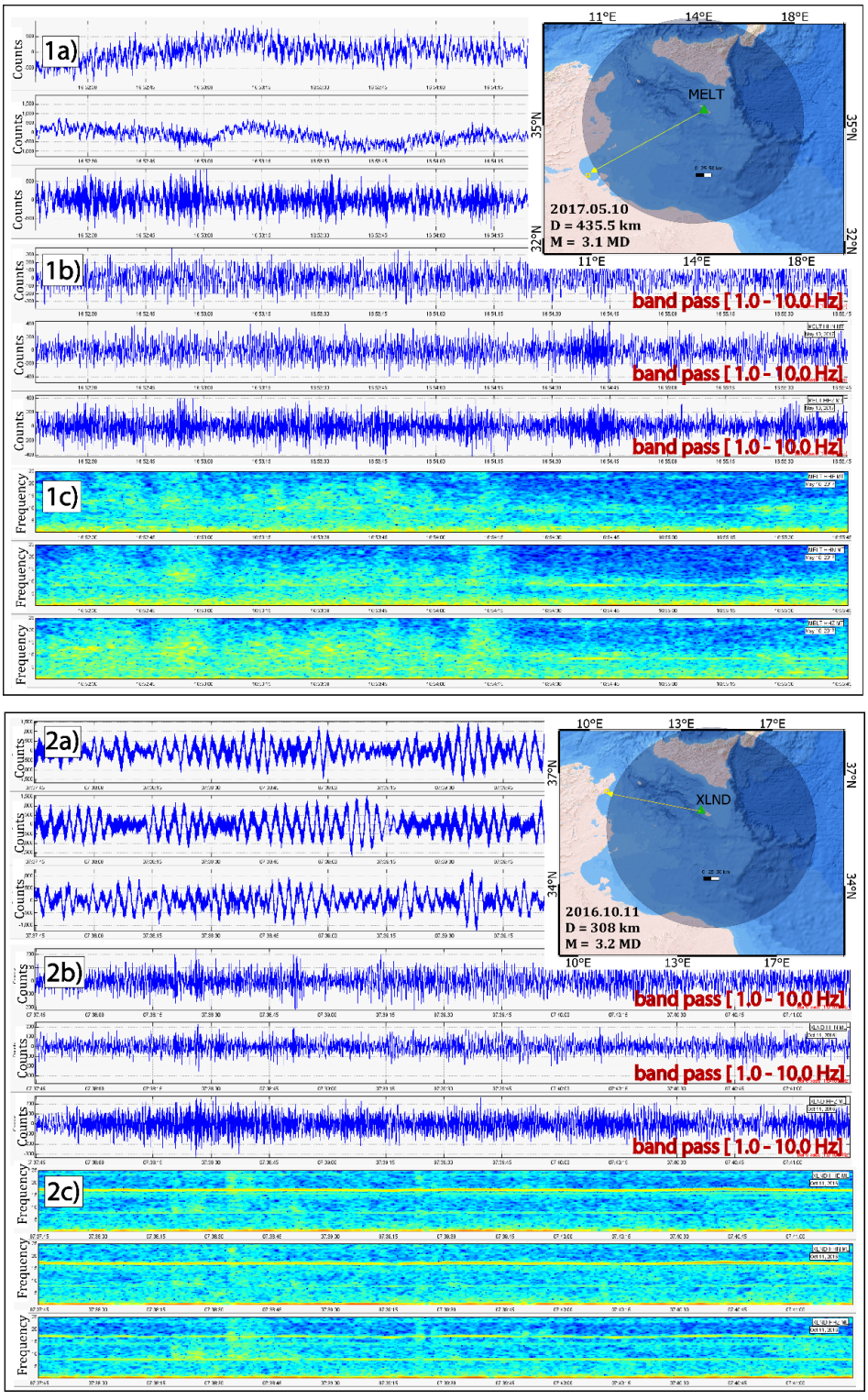

FIGURE 31. 1) EARTHQUAKE RECORDED BY MELT STATION (2017.05.10 – 16:52:46.4 UTC – MAGNITUDE 3.1 MD – EPICENTER DISTANCE 240 KM), A NOISY SIGNAL. **1a)** THE EARTHQUAKE WAVEFORM OF THE THREE COMPONENTS; **1b)** THE FILTERED WAVEFORM [BAND-PASS 0.1-10.0 HZ] OF THE THREE COMPONENTS; **1c)** THE SPECTROGRAM OF THE THREE COMPONENTS. THE TOP RIGHT IS THE EARTHQUAKE MAP**. 2)** THE EARTHQUAKE RECORDED BY XLND STATION (2016.10.11 – 07:38:14.60 UTC – MAGNITUDE 3.2 MD – EPICENTER DISTANCE 308 KM), A NOISY SIGNAL. **2a)** THE EARTHQUAKE WAVEFORM OF THE THREE COMPONENTS; **2b)** THE FILTERED WAVEFORM [BAND-PASS 0.1-10.0 HZ] OF THE THREE COMPONENTS; **2c)** THE SPECTROGRAM OF THE THREE COMPONENTS. THE TOP RIGHT IS THE EARTHQUAKE MAP (SWARM SOFTWARE).

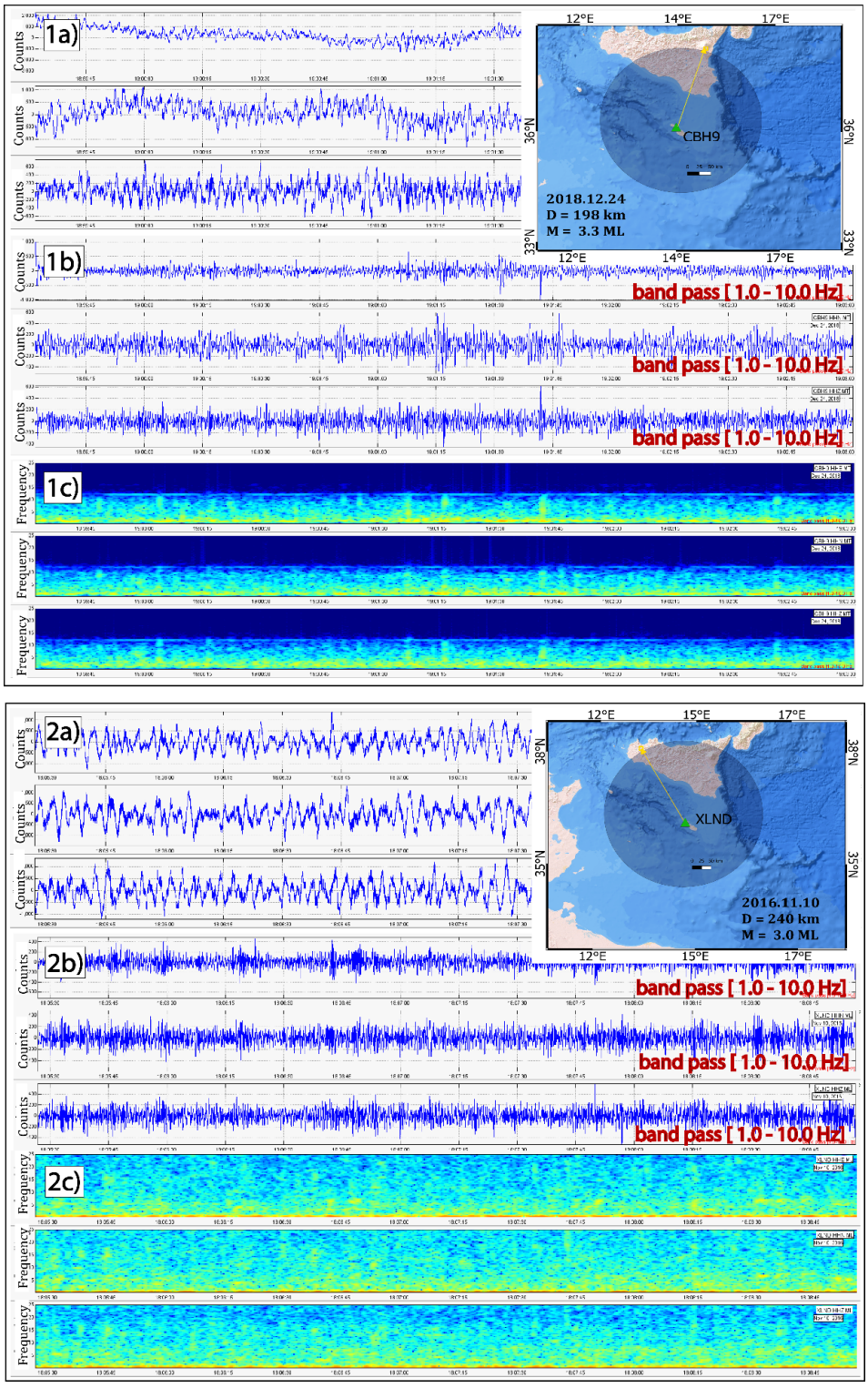

FIGURE 32. 1) EARTHQUAKE RECORDED BY CBH9 STATION (2017.05.10 – 19:00:02.00 UTC – MAGNITUDE 3.3 ML – EPICENTER DISTANCE 198 KM), A NOISY SIGNAL. **1a)** THE EARTHQUAKE WAVEFORM OF THE THREE COMPONENTS; **1b)** THE FILTERED WAVEFORM [BAND-PASS 0.1-10.0 HZ] OF THE THREE COMPONENTS; **1c)** THE SPECTROGRAM OF THE THREE COMPONENTS. THE TOP RIGHT IS THE EARTHQUAKE MAP. **2)** THE EARTHQUAKE RECORDED BY XLND STATION (2016.11.10 – 18:05:56.83 UTC – MAGNITUDE 3.0 ML – EPICENTER DISTANCE 240 KM), A NOISY SIGNAL. **2a)** THE EARTHQUAKE WAVEFORM OF THE THREE COMPONENTS; **2b)** THE FILTERED WAVEFORM [BAND-PASS 0.1-10.0 HZ] OF THE THREE COMPONENTS; **2c)** THE SPECTROGRAM OF THE THREE COMPONENTS. THE TOP RIGHT IS THE EARTHQUAKE MAP (SWARM SOFTWARE).

The epicentral distance (Fig. 33) has also been calculated according to the relation:

$$D = \frac{S-P\ lag\ time}{\{\frac{1}{Vs} - \frac{1}{Vp}\}} \quad (2)$$

Where,

$$S-P\ lag\ time = D\ \{1/Vs\ - 1/Vp\} \quad (3)$$

The *lag time* is the time difference between the arrival of the P-waves and the arrival of S-waves, increasing as the waves travel further from their origin.

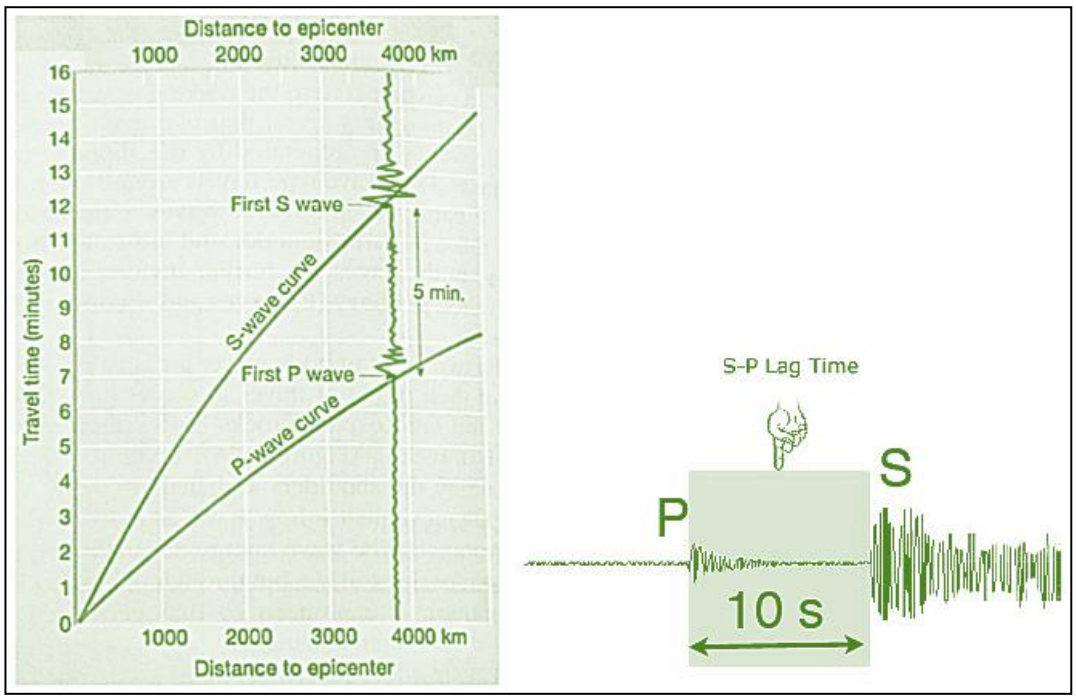

FIGURE 33. EPICENTER DISTANCE/TRAVELTIME GRAPH AND GRAPHIC REPRESENTATION OF S-P LAG TIME.

For the values of Vp and Vs, average values were given, respectively, of 6.7 km/s and 3.8 km/s. For example, for the event shown in Figure 26, the S-P time of 14,06s provides 123.97 km from the WDD station.

4. CHAPTER - METHODOLOGY FOR THE REALIZATION OF THE 3D LITHOSPHERIC MODEL AND MOHO MAP

4.1. Seismo-stratigraphic analysis

Based on the correlation with well and stratigraphic data, a seismic-stratigraphic analysis has been made on the seismic reflection profiles collected for this work. The first phase of interpreting profiles (in raster format) was done using Adobe Illustrator CC (2018). Subsequently, the profiles were imported and georeferenced in two software, QGIS (v. 3.10.12-A Coruña) and Move Suite (v. 2017.2) software.

The surface reflectors were mapped according to the lithological characteristics obtained from the wells. The i) soft sedimentary rocks are the successions related to Ribera, Gessoso Solfifera, Terravecchia, Palazzolo, Tellaro, San Cipirello, Corleone, and Ragusa formations (Table 9); ii) hard sedimentary rocks are the successions relate to Amerillo, Porto Palo limestone, Hybla, Lattimusa, Chiaramonte, Buccheri, Siracusa, Streppenosa, Sciacca formations (Table 10).

TABLE 9. SUMMARY SCHEME OF SICILIAN AND TUNISIAN FACIES BELONGING TO THE HORIZON SOFT SEDIMENTARY ROCKS.

Tunisian facies	Sicilian facies	Lithology	Age	Horizon
Raf Raf	Ribera	Fossiliferous clay, sandy	Plio/Pleistocene	**Soft sedimentary rocks**
Porto Farina				
Oum Douil	Gessoso Solfifera	Gypsum limestone, clay	Miocene (Messiniano)	
Saquaf				
Meluart				
Q Bel Khedim				
Nilde	Terravecchia	Clay, sand	Miocene	
	Palazzolo	Fossiliferous clay, sand	Miocene up	
Mahmoud	Tellaro	Fossiliferous clay, sand	Miocene middle	
	S. Cipirello	Marl, clay	Miocene low	
Aingrab	Corleone	Packstone/wackestone	Miocene low	
Fortuna	Ragusa	Fossiliferous mudstone/wackestone	Oligo/Miocene	
Salammbo				

The calibration with the wells has been implemented on the lithological characteristics of the Sicilian facies and the Tunisian facies, are discriminated as soft sedimentary rocks (unconsolidated) the clayey soils from the Oligo-Miocene to

the Pleistocene age and as soft sedimentary rocks the carbonatic facies from the Triassic to Cretaceous age.

TABLE 10. SUMMARY SCHEME OF SICILIAN AND TUNISIAN FACIES BELONGING TO THE HORIZON HARD SEDIMENTARY ROCKS.

Tunisian facies	Sicilian facies	Lithology	Age	Horizon
Halk El Menzel	Amerillo (Alcamo) / Porto Palo Limestone	Fossiliferous limestone	Cretaceous/Eocene	**Hard sedimentary rocks**
Souar				
Metlaoui				
Bou Dabbous				
El Haria				
Abiod				
Aleg				
Gebel Nehal	Hybla (Alcamo)	Mudstone marl	Lower Cretaceous	
Allam				
Fahdene				
Hameima				
Serdj				
Sidi Aich				
Bou Hedma				
Sidi Khalif	Lattimusa (m.bro Busambra) / Chiaramonte (Alcamo)	Cherty mudstone, chalk	Jurassic (Malm)	
Nara	Buccheri (Giardini)	Fossiliferous wackestone	Jurassic (Dogger/Malm)	
	Modica/ Rabbito/ Siracusa/ Inici	Mudstone/wackestone	Jurassic (Lias)	
	Streppenosa	Mudstone recrystallized, dolomite	Upper Trias	
	Sciacca/ Noto/ Gela/ Taormina	Dolomite	Trias	

The calibration done with the wells concerns the most superficial part, about 4000 m of depth, in fact it has been extremely useful in discriminating the top of the soft sedimentary rocks and hard sedimentary rocks.

The CROP (CROsta Profonda) project interpreted the deep crust reflection seismic profiles to map the deepest crustal reflectors. This project was born in the late 90s in collaboration with CNR-ENI and CNR-ENEL; it represents a multidisciplinary research study on geophysical data today to understand geodynamic processes, the definition of geological hazard, and the search for energy resources that affect the Italian peninsula. About 10000 km of seismic reflection on land and marine profiles have been acquired (about 1250 km on land and about 8700 km at sea). The given bank is available and accessible online for consultation (www.videpi.com/videpi/videpi.asp).

The CROP profiles covering the Sicily Channel are shown in Figure 34.

The interpretations of the deep seismic lines have generated a crustal profile (geological) along about 900 km that crosses the central Mediterranean starting from the Algerian Sea towards the Ionian Sea. The interpretation of the seismic-stratigraphic horizons has been compared with the analysis of the seismic profiles carried out by different authors (*Catalano et al., 2000; Chironi et al., 2000; Finetti & Del Ben, 2005*).

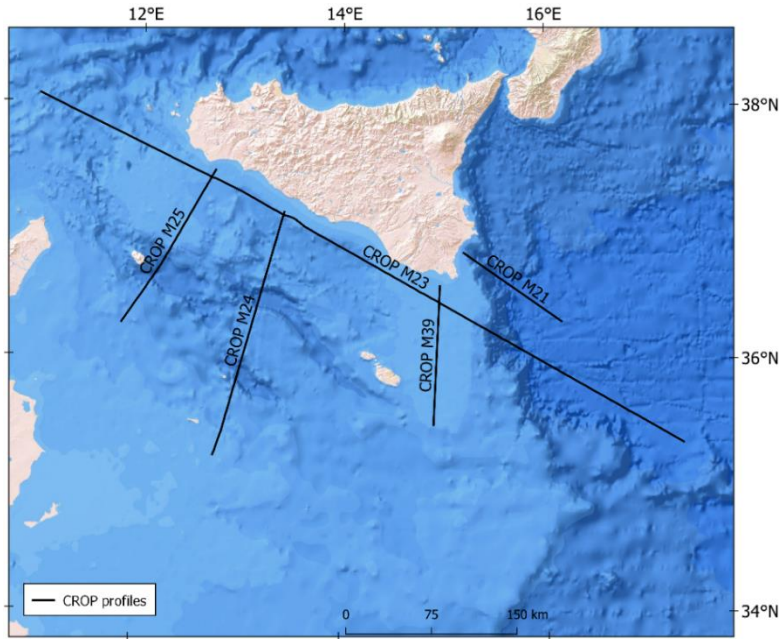

FIGURE 34. MULTICHANNEL SEISMIC REFLECTION PROFILE'S LOCATION MAP: M21, M23, M24, M25, AND M39 - CROP PROJECT (QGIS SOFTWARE).

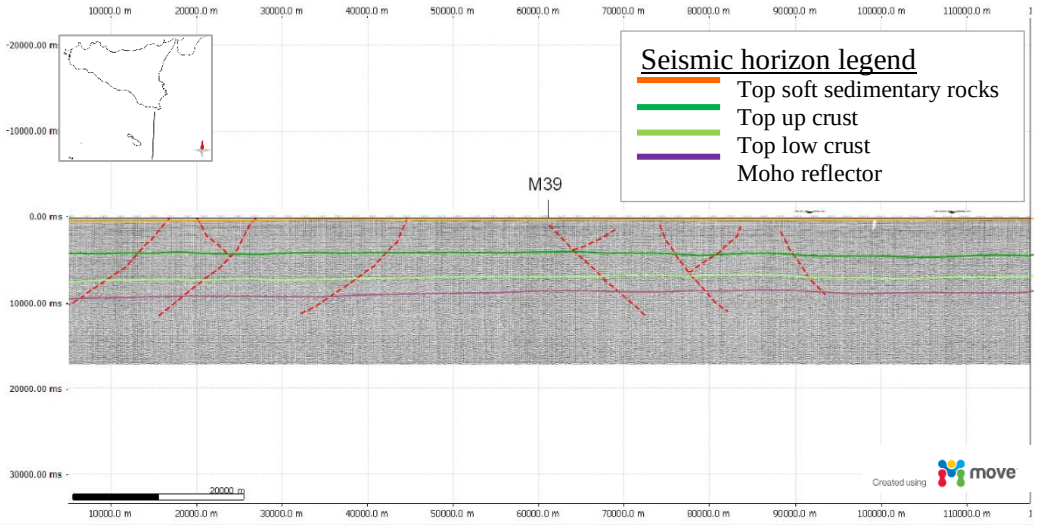

FIGURE 35. ANALYSIS OF THE SEISMIC PROFILE CROP M39 (S/TWT) EXTENDS ALONG THE EASTERN MARGIN OF THE PELAGIAN SEA. SEISMIC HORIZONS AND MAIN TECTONIC STRUCTURES ARE RECOGNIZED. VERTICAL EXAGGERATION = 1. (MOVE SOFTWARE).

The interpretation of the CROP M39 profile is shown (Fig. 35), in agreement with Chironi et al. (2000) and Finetti & Del Ben (2005), the passage between the upper and lower crust can be found at about 7s/TWT.

From the analysis of some multichannel seismic profiles belonging to the Italian Commercial Zone "G", available within the ViDEPI project, it was possible to discriminate the surface horizons. Multichannel seismic profiles show good penetration up to about 5 s/TWT (Fig. 36).

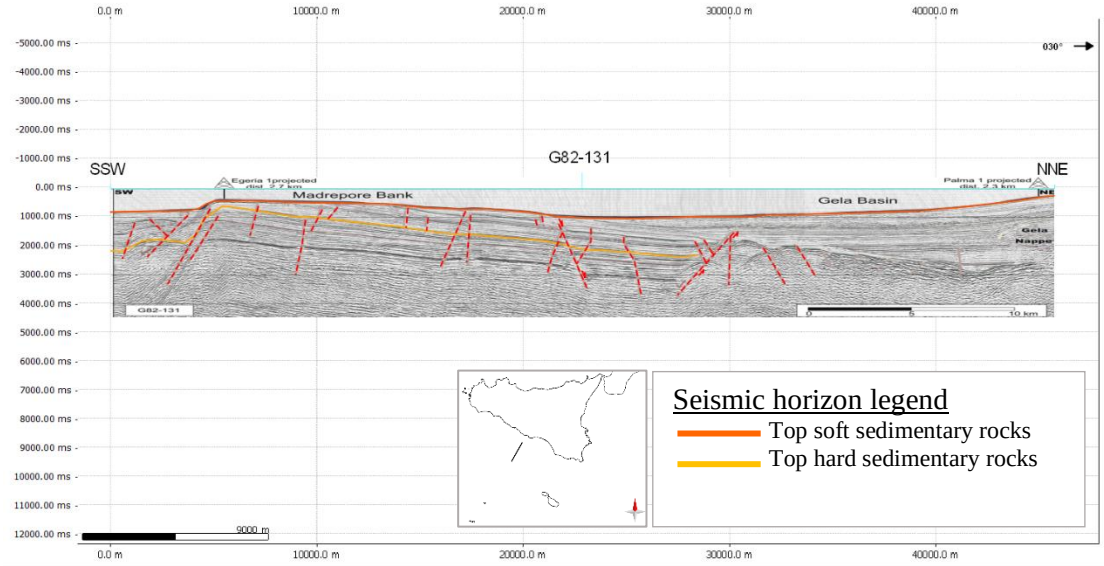

FIGURE 36. MULTICHANNEL SEISMIC PROFILE (G82-131) BELONGING TO THE ITALIAN COMMERCIAL ZONE. PROFILE ACROSS THE GELA BASIN AND THE MADREPORE BANK. VERTICAL EXAGGERATION = 1.5. (MOVE SOFTWARE).

A visible reflector is a reflector that discriminates the top of hard sedimentary rocks, representing the top of the Cretaceous-Eocene limestone of the Amerillo formation.

4.2. Time-to-depth conversion

Once the individual horizons were detected from the seismic profiles, the conversion of the vertical profile scale from seconds (TWT – Two Way Traveltime) to meters (m) was conducted using Move Suite software (v. 2017.2).

Four methods can be used to perform the time-to-depth conversion process:

1. Fixed method: it is presumed that the velocity of seismic waves increases with depth, according to the equation:

$$Z = V_0\ (e^{kt} - 1)/k \quad (4)$$

where: Z is the layer thickness (m), V_0 is the initial velocity (m/s), k is a coefficient that describes the velocity variation with depth, t is the traveltime (s);

2. Equation method: the tool allows us to choose from different equations the best model to describe the velocity behaviour with depth. This approach is useful when the trend is non-linear and not linear;
3. User defined table/checkshot: allows to import of a velocity model in ASCII format with two columns, which can be i) time (y) - depth (x), ii) depth (y) - time (x), iii) velocity (y) - depth (x), iv) velocity (y) - time (x);
4. Database method: this method uses the same equation (3) used for the fixed method, but in this case, can vary the initial velocity (V_0) and the k variation coefficient. Depending on the lithological properties, these values are added to the software database.

All conversion methods have been tested, and the most certain result has been obtained by arbitrarily setting values through the Move software database (Fig. 37). Different velocity values were assigned for each horizon, porosity values, density, Young modulus, Poisson ratio, and cohesion, and on the lithological characteristics, it was possible to determine the percentage of sandstone, shale, and limestone. The assigned velocity values refer to the velocity model described in paragraph 3.4.1 (velocity model).

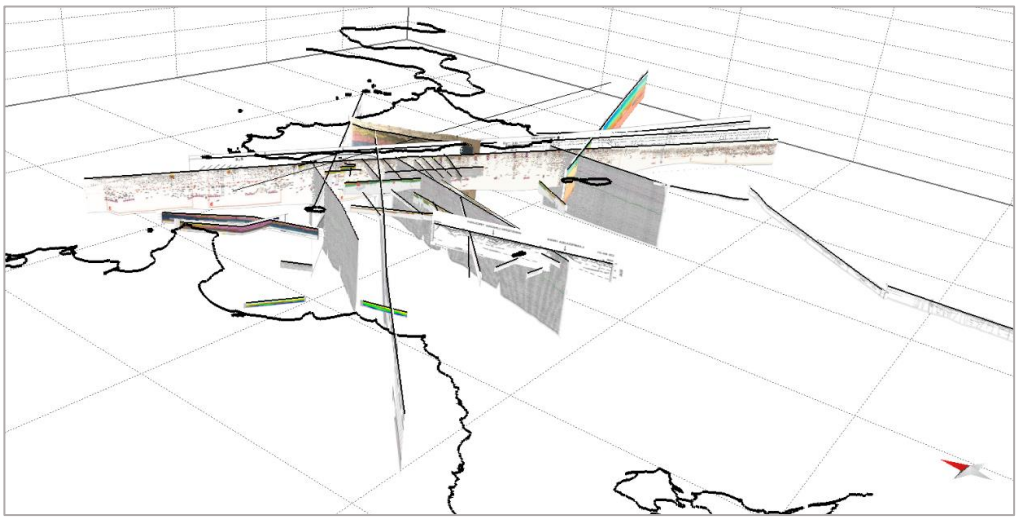

FIGURE 37. IMPORT THE SECTIONS OF THE SEISMIC PROFILES CONVERTED IN DEPTH (m) INTO THE 3D ENVIRONMENT WITH VERTICAL IMAGES (MOVE SOFTWARE).

4.3. Calibration and interpolation of seismic horizons

The next step was to interpolate data (horizons and well data) and create surfaces for the individual horizons (6 surfaces). Using the tool of Move software, it is possible to generate a surface from a point/well marker.

There are six methods to create the surface:

1) Delaunay Triangulation;
2) Multilevel B-Spline Approximation;
3) Inverse Distance Weighting (IDW);
4) Ordinary Kriging;
5) Advancing Front;
6) Alpha Contour.

After a series of tests, the data was interpolated using the Delaunay Triangulation method. This method makes the geometry of triangles (Fig. 38) in a grid more uniform than the other methods avoiding creating narrow triangles; what is obtained is an almost uniform mesh.

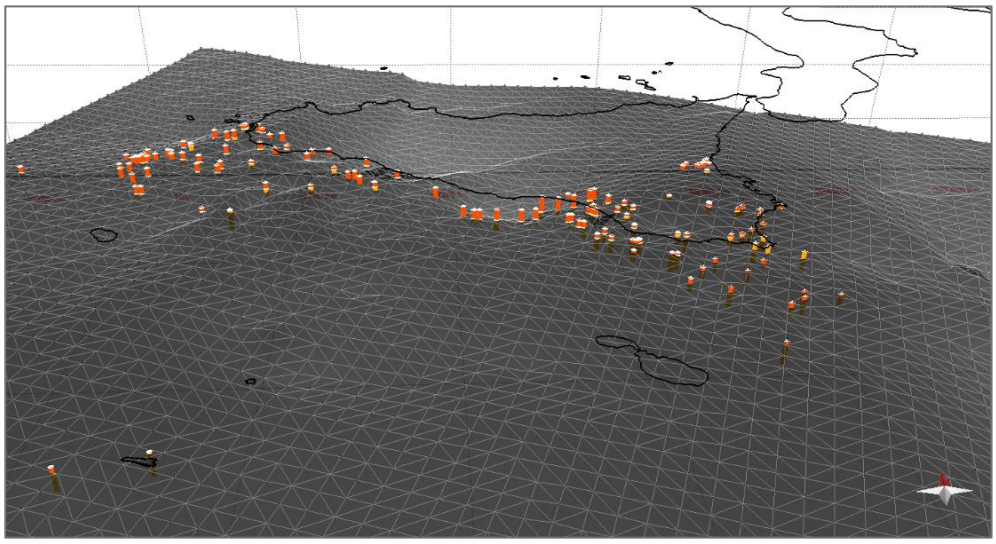

FIGURE 38. RESULT OF INTERPOLATION OF SEISMIC HORIZONS AND WELL DATA, USING THE DELAUNAY TRIANGULATION METHOD (MOVE SOFTWARE).

After building the surfaces, a dense grid is built, 30 km x 30 km, enclosing the mash created for different horizons. In this way, multiple sections were created by the intersection of previously realized surfaces (Fig. 39a). A resampling of the horizons was done, also calibrating the well data (Fig. 39b) for the surface horizons.

This process allowed to adapt the surfaces better, avoiding possible overlaps between the data.

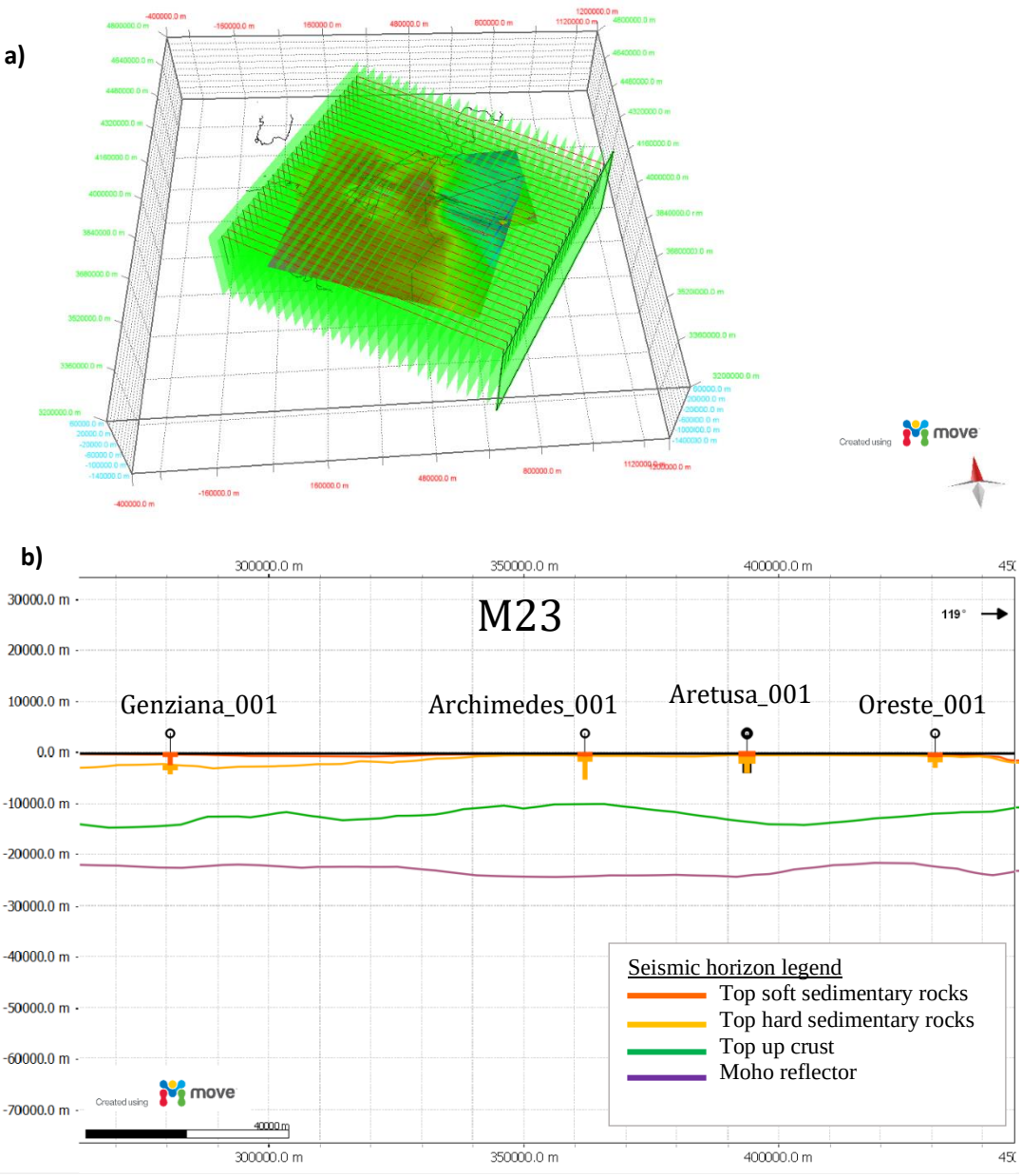

FIGURE 39. a) CONSTRUCTION OF A DENSE GRID OF CELLS 30 KM X 30 KM; **b)** CALIBRATION OF SEISMIC HORIZONS (SOFT AND HARD SEDIMENTARY ROCKS) WITH WELL DATA PROJECTED ON THE M23 SECTION, LINE CROP (MOVE SOFTWARE).

5. CHAPTER - SEISMICITY CHARACTERIZATION

5.1. Gutenberg-Richter relationship

In this paper, the Gutenberg-Richter relationship of the distribution between the magnitude distribution and the total number of earthquakes (*Ishimoto & Iida, 1939; Gutenberg & Richter, 1944*) was applied to earthquakes recorded in the survey area, according to the report:

$$\log_{10} N\,(M) = \; a - b\,M \tag{5}$$

where N is the number of seismic events of a particular magnitude $> M$, M is the minimum magnitude, a and b are constants. The b-value is typically nearly 1.0 for seismically active regions; the change in value is influenced by several factors. For example, high b-values are obtained for high thermal gradients and heterogeneity of rocks, whereas lower b-values are obtained for increments of ineffective and shear stress (*Rodríguez-Pérez et al., 2020*). The b-value graphically represents the slope of the line and measures the relative abundance between small and large earthquakes, while the a-value corresponds to the total seismicity rate of the studies region.

Determining the b-value is essential for seismotectonic studies and seismic risk analysis. Figure 40 shows the trend of the Gutenberg-Richter law for Sicily Channel data. 1662 seismic events were selected, from 1985 to 2021, with magnitude ≥ 3 located in the area between 30.0° N and 38.0° N of latitude and 10.0° E and 16.5° E of longitude. The b-value has been calculated using the method of Max Curvature (*Wiemer & Wyss, 2000*) through the Maximum Likelihood Estimator of Aki (1965), and the magnitude of completeness (Mc) was estimated, which corresponds to the limit value of magnitude below which there is no certainty on the origin and reliability of the data. A value of Mc > 3.0 has been estimated, and the events have been analyzed with M ≥ Mc to assurance the data's consistency and stability. A b-value of 1.16 (± 0.03) was obtained, close to the average of the seismically active regions (approximately 1.0). The ZMAP software (v. 7.1) package was used in MATLAB code to perform all calculations (*Wiemer, 2001; Reyes & Wiemer, 2019*); the software was mainly used to evaluate earthquake catalogs' quality.

The *a*-value strongly depends on the *b*-value and returns indications on the maximum expected magnitude in the study region; in this case, the value is 6.7 for a data set that covers more than 30 years. This value may be overestimated due to magnitude errors (it may also be related to the fact that magnitudes < 3 were not considered in this work); the value that has been determined is greater than the maximum effective magnitude that has been measured in this area. The maximum magnitude measured in this area, from the INGV and ISC catalogs, was 5.1 on 2005.02.07 (20:46:26.91 UTC) off the coast of Tunisia.

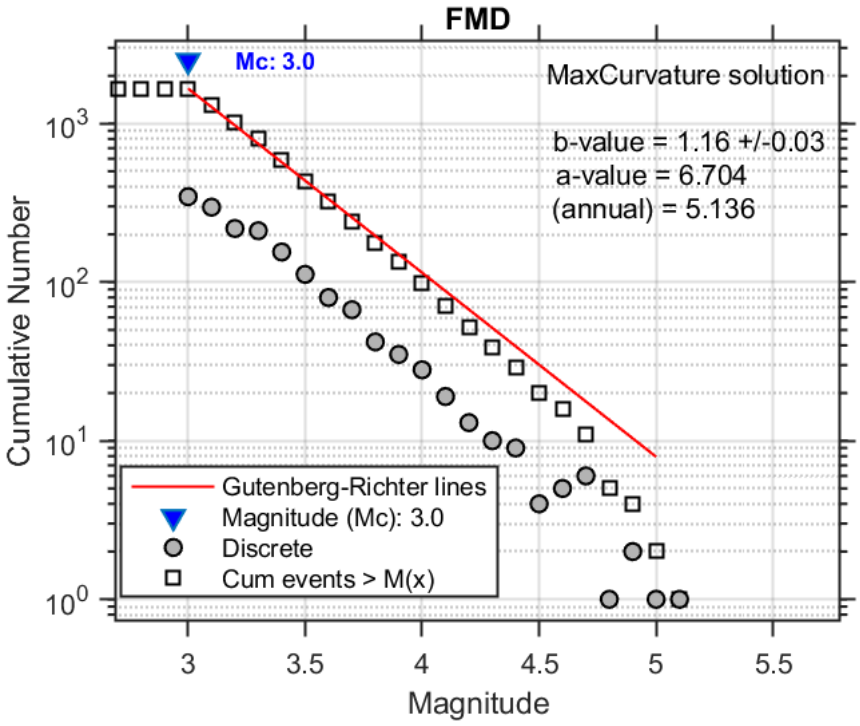

FIGURE 40. FREQUENCY-MAGNITUDE DISTRIBUTION (FMD) OF EARTHQUAKES FROM 1985 TO 2021 (WHITE SQUARES, CUMULATIVE; GREY CIRCLES, NON-CUMULATIVE) AND RELATIVE GUTENBERG-RICHTER LINE (RED LINE) FOR THE EVENTS OF MAGNITUDE MW LARGER THAN THE (M_C) COMPLETENESS MAGNITUDE (ZMAP SOFTWARE).

One of the main problems for the study of seismicity in the Sicily Channel is related to the distance epicenter-seismic stations installed in the study area. Several authors have analyzed this area, in the work of Calò & Parisi (2014), a *b*-value of 1.05 has been defined for the data set covering a portion of the Sicily Channel, the separation belt N-S between the Pantelleria graben, on one side, and the Linosa and Malta grabens on the other side. Agius et al. (2020) obtained a *b*-value of 1.05 for the offshore survey area on Malta island, even if the obtained value is an orientation value since the observation period has not been long enough and the observed

magnitudes have been considered ≥ 3. Pondrelli et al. (2011) determined a value of 1.13 (± 0.05) in the study area of the European-Mediterranean region. The *b*-value obtained in this work is well in agreement with studies that have been done in this area.

From the histograms shown in Figure 41, the earthquake depth range in the Sicily Channel is 0-45 km, with a peak between 5-10 km, where more earthquakes are recorded. The frequency of occurrence of earthquakes is a function of magnitude, a higher frequency of earthquakes is observed for a magnitude between 3-3.5, while a lower frequency of earthquakes is observed for a greater magnitude between 4-4.5.

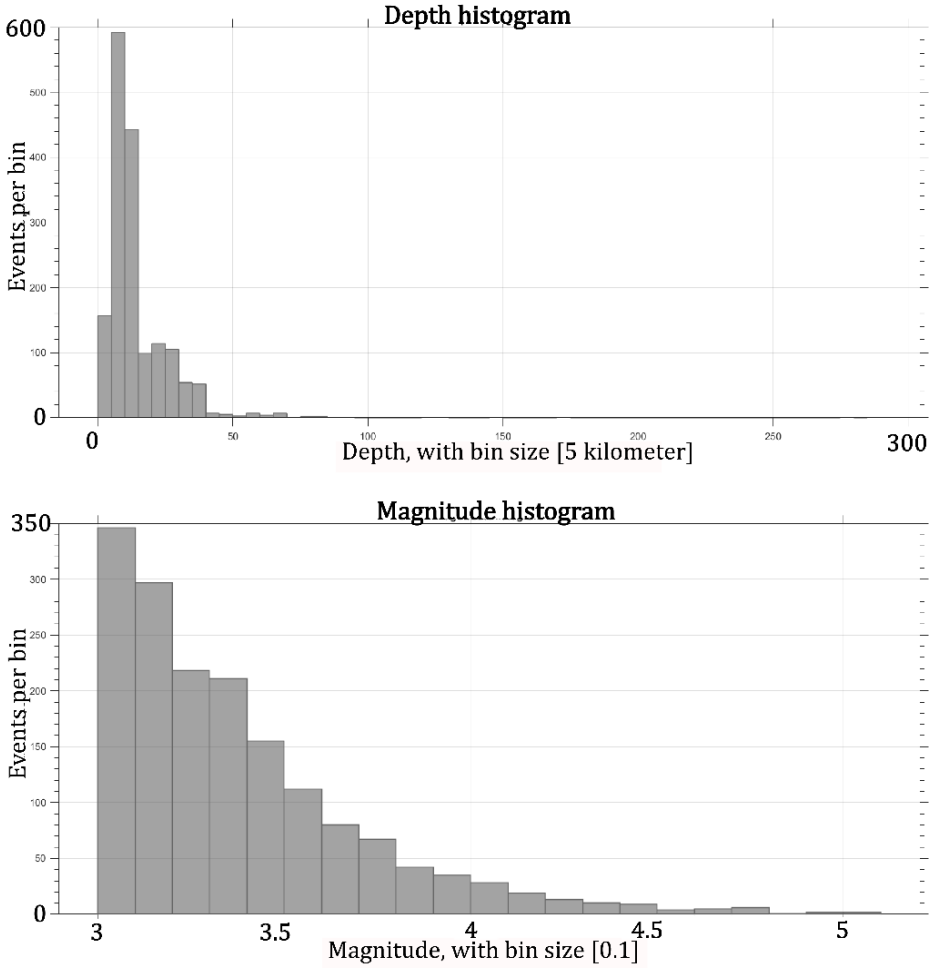

FIGURE 41. AT THE TOP, THE DEPTH (km) HISTOGRAM WITH EVENTS PER BIN AND DEPTH WITH A BIN SIZE OF 5 KM. AT THE BOTTOM, THE MAGNITUDE HISTOGRAM WITH EVENTS PER BIN AND MAGNITUDE WITH A BIN SIZE OF 0.1 (ZMAP SOFTWARE).

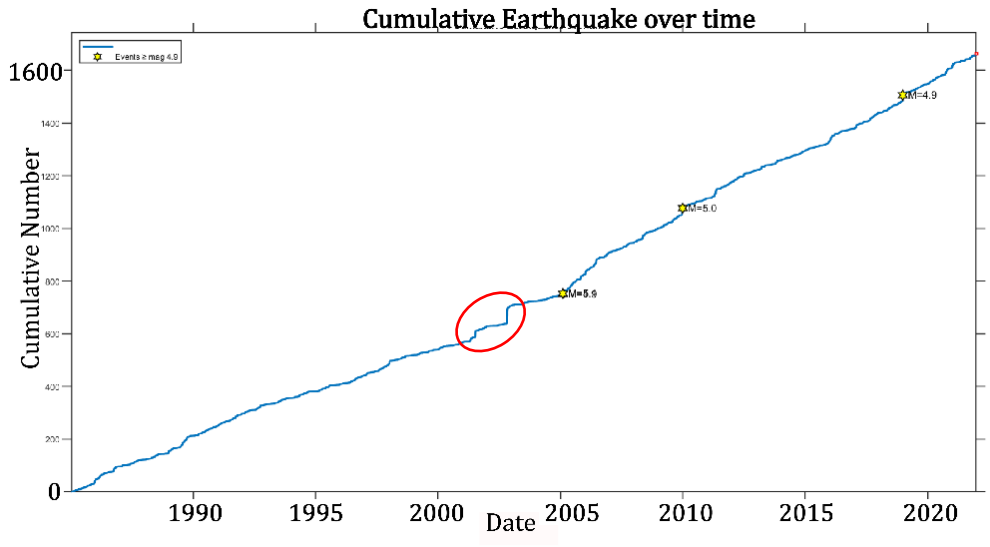

FIGURE 42. CUMULATIVE EARTHQUAKE OVER TIME, WITH MAGNITUDE (M_C) > 3 FOR THE INGV – ISC CATALOGS (1985-2021). THERE ARE TWO PEAKS (IN THE RED CIRCLE): THE FIRST BETWEEN 2001.07.13 AND 2001.07.22; THE SECOND BETWEEN 2002.10.28 AND 2002.11.06, BOTH SEQUENCES RECORDED IN ETNA MT. A CHANGE IN SLOPE HAS BEEN OBSERVED SINCE 2005 DUE TO THE INCREASE OF SEISMIC STATIONS INSTALLED IN THE ITALIAN PENINSULA (ZMAP SOFTWARE).

From the cumulative curve (Fig. 42) of the earthquakes recorded from 1985.01.01 to 2021.12.31, two peaks corresponding to the seismic sequences recorded in the areas of Etna Mt. (Zafferana Etnea) are identified; the first between 2001.07.13 and 2001.07.22, the second between 2002.10.28 and 2002.11.06. There is also a variation in the slope of the cumulative curve since 2005, probably linked to the implementation of seismic stations by the Rete Sismica Nazionale. This is evident in Figure 43. Observing the spatial-temporal variation (Fig. 43) of the magnitude and depth distribution (range of 20 years) shows that since 2005 there has been an increase in earthquakes, given by the expansion of the Rete Sismica Nazione in the Italian territory. Note an increase in the recording of seismic events at different depths, with four events ≥ 4.9.

Authors such as Schorlemmer et al. (2005) and Rodríguez-Pérez & Zúñiga (2018) demonstrate that there is a dependency between the *b*-value and the focal mechanism. The *b*-value, however, is affected by many factors and can also be influenced locally; for example, it may differ between unrelated fault zones (*Schorlemmer & Wiemer, 2005*) or even for variations in time and space (*Nuannin et al., 2005*) or suffers from dehydration processes where interstitial pressures increase and stress is reduced, for example as has been seen in Japan in subduction zones (*Wyss et al., 2001*).

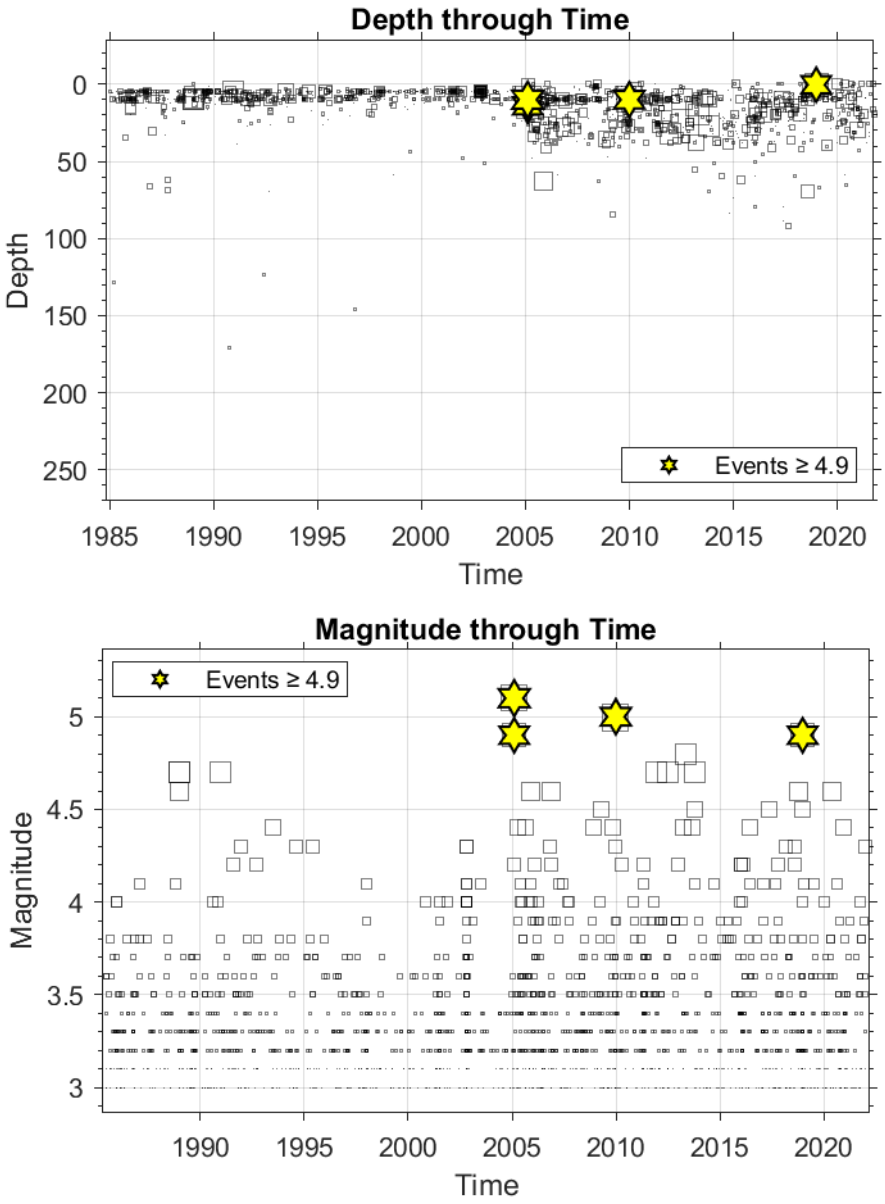

FIGURE 43. (UPPER PANEL) PLOT DEPTH THROUGH TIME FROM 1985 TO 2021. (LOWER PANEL) PLOT MAGNITUDE THROUGH TIME FROM 1985 TO 2021. THE YELLOW STARS ARE EVENTS OF MAGNITUDE ≥ 4.9. SQUARES ARE SEISMIC EVENTS AT DIFFERENT DEPTHS; DIMENSIONS ARE A FUNCTION OF THE MAGNITUDE. (ZMAP SOFTWARE).

5.1.1. Dependency between the *b*-value and the focal mechanism

To determine the stress regime of a tectonic region, it is essential to study the focal mechanisms that characterize it. The focal mechanism consists of the graphic representation of the seismic moment tensor, corresponding to the system of equivalent forces acting on a point seismic source.

For the area of the Sicily Channel was consulted the "European-Mediterranean Region Centroid-Moment Tensor catalog - RCMT" (*Pondrelli et al., 2002* - rcmt2.bo.ingv.it/searchRCMT.html), the "Time Domain Moment Tensor catalog - TDMT" (*Scognamiglio et al., 2006* - http://terremoti.ingv.it/tdmt), the "Global Centroid-Moment Tensor catalog - GCMT" (*Dziewonski et al., 1981; Ekström et al., 2012* - www.globalcmt.org/CMTcite.html), and the "International Seismological Centre catalog – ISC" (*Lentas et al., 2018; 2019* - www.isc.ac.uk/iscbulletin/search/fmechanisms/interactive/) from 1985.01.01 to 2021.12.31. 54 seismic events have been catalogued in the area between 30.0° N and 37.5° N of latitude and between 9.5° E and 16.0° E of longitude, including all depths. The final list of focal mechanisms is available as Additional Information (Table A3).

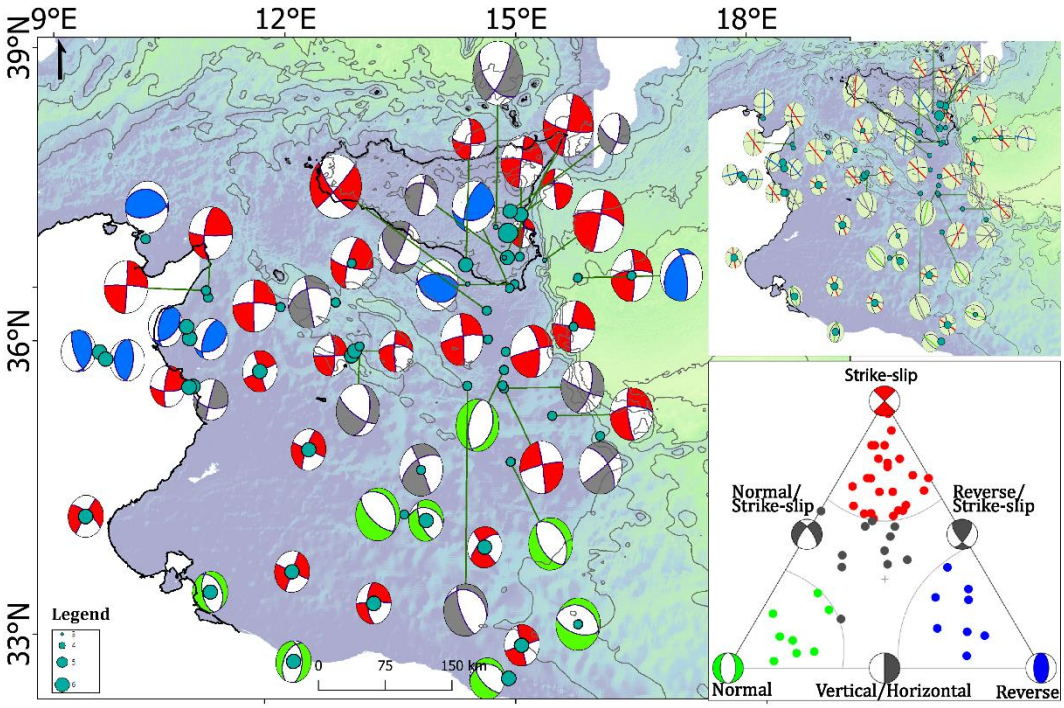

FIGURE 44. MAP OF FOCAL MECHANISMS IN THE SICILY CHANNEL AREA FROM 1985 TO 2021 (ARCGIS SOFTWARE V. 10.7.1). THE FOCAL MECHANISMS (BEACHBALLS) HAVE BEEN DESIGNED TO INDICATE THE DIFFERENT TYPES OF SLIP OF EARTHQUAKE: NORMAL, STRIKE-SLIP, AND REVERSE (THRUST). THE GREEN DOTS IDENTIFY THE EXACT POSITION OF THE FOCAL MECHANISMS, AND THE DIMENSIONS CORRESPOND TO THE VALUES OF THE MAGNITUDES (FROM 3 TO 6 MW). THE BALLS ARE CONNECTED WITH THE ARROWS TO THE ASSOCIATED EPICENTER. THE ORIENTATION OF THE MAXIMUM HORIZONTAL STRESS (SH-MAX) IS SHOWN AT THE TOP RIGHT, AND PLOTTED DATA WITHIN THE TRIANGLE DIAGRAM (*Frohlich, 1992*) TO DISPLAY SIMILARITIES AND DATA DENSITY ("TRIANGLEPLOT.M", MATLAB CODE TO THE CLASSIFICATION OF SOURCE FOCAL MECHANISMS). THE VERTICES OF THE TRIANGLE REPRESENT EARTHQUAKES: NORMAL MECHANISMS (WITH VERTICAL P AXES), STRIKE-SLIP MECHANISMS (WITH VERTICAL B AXES), AND REVERSE MECHANISMS (WITH VERTICAL T AXES).

To perform the tectonic analysis of the area, the “beachballs” have been built in the map of the Sicily Channel (Fig. 44) according to the values of strike1 (0° - 360°), dip1 (0° - 90°), and rake1 (0° - 360°), for the 54 events catalogued (in environment ArcGIS). From the data obtained from the database, note a predominance of strike-slip mechanisms in the Sicily Channel; several thrust-type mechanisms develop along the Sicilian coast and the Tunisian coast (SHmax orientation mainly towards NW-SE, and some E-W), while normal mechanisms are recorded in the S-E zone of the Sicily Channel (with SHmax orientation NW-SE).

To visualize the data more quickly and to determine the proportions of the thrust movement, the focal mechanisms have been plotted in the ternary graph or "triangular diagram" of Frohlich (1992), where the vertices correspond to the normal focal mechanisms (green), strike-slip (red), reverse (blue), and the intermediate areas of normal/strike-slip, reverse/strike-slip, and vertical/horizontal (grey). The script of the triangular diagram "TrianglePlot.m" was used, an open-source code on MATLAB, to classify source focal mechanisms (strike-slip, normal, and reverse) and plot the triangle diagram.

The distribution of events in the central Mediterranean is predominant towards the vertex of the strike-slip and for strike-slip/normal and strike-slip/reverse mechanisms. A range of magnitude of the predominant moment of the area between 4.2 and 4.7 can be determined (Fig.45)

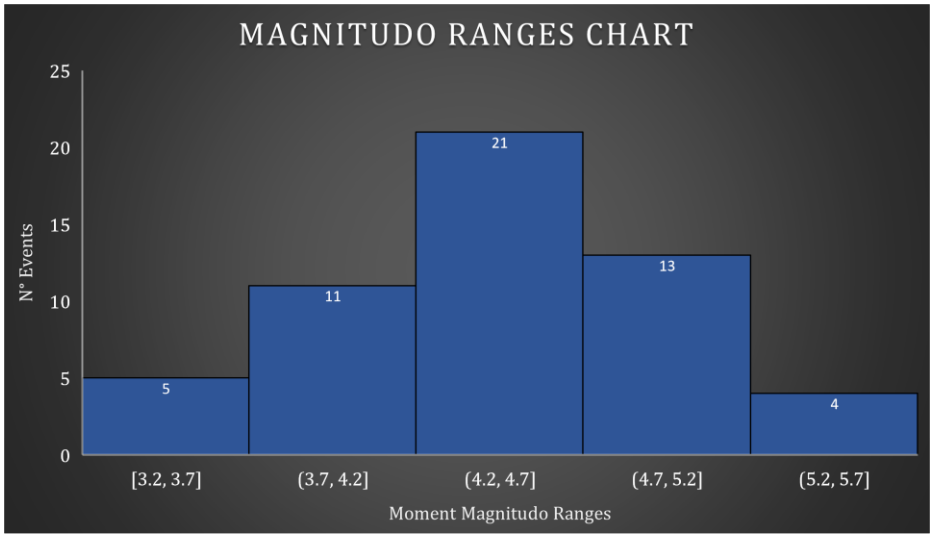

FIGURE 45. THE MOMENT MAGNITUDE RANGES CHART HAS BEEN CONSTRUCTED FOR THE NUMBER OF EVENTS (54). ARE FOUND IN THE MAJORITY, 21 EVENTS WITH A MAGNITUDE BETWEEN 4.2 AND 4.7.

Typically, the *b*-value, calculated from the Gutenberg-Richter relationship, is used to describe the occurrence of small and large events (a low *b*-value indicates a higher proportion for large events, and vice versa, high *b*-values indicate a higher proportion of small events). For this reason, the relationship between the *b*-value and the different fault styles can be summarized (Fig. 46). High values of *b* (1.1 ÷ 1.2) are obtained for events of normal faults, low values for inverse faults (0.85 ÷ 0.95), and intermediate values for strike-slip events (0.95 ÷ 1.15). The value of *b* that has been calculated in this work confirms the strike-slip/normal style of the area of the Sicily Channel.

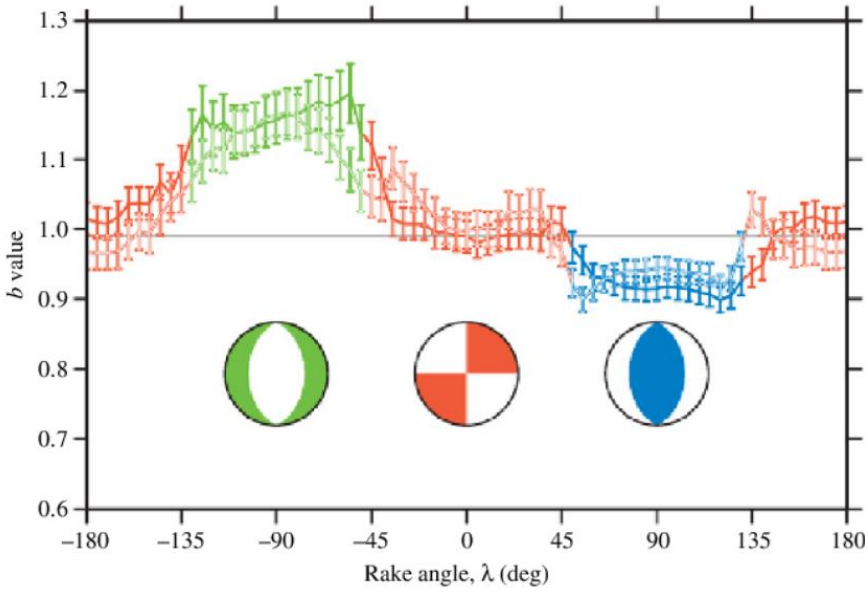

FIGURE 45. GRAPH OF *B*-VALUE WITH RAKE ANGLE (λ). THE *B*-VALUE RANGE VERSUS THE DIFFERENT FAULT STYLES IS SHOWN. THE GREEN, RED, AND BLUE LINES CORRESPONDINGLY REPRESENT THE *B*-VALUE FOR NORMAL, STRIKE-SLIP, AND REVERSE EVENTS (FROM *Schorlemmer et al., 2005*).

5.2. Stress field analysis

An analysis of the stress inversion for the area of the Sicily Channel was made based on the seismic focal mechanisms to refine the geometry and kinematics that affect this zone. The stress analysis was performed with the software "STRESSINVERSE" (v. 1.1), developed by Vavryčuk (2014); a package open source used in MATLAB code, run by a script called "StressInverse.m". Strake1, dip1, and rake1 values of focal mechanisms were used (available as Additional Information in Table A3). The inversion algorithm is based on Michael's (1984,

1987) method and the instability criterion that Lund & Slunga (1999) suggested. By inversion, it is possible to determine four parameters (Fig. 46) of the stress tensor: three angles characterizing the main stress directions (σ_1, σ_2, and σ_3), and the shape ratio (*Gephart & Forsyth, 1984*), expressed by the relation:

$$R = \frac{\sigma 1 - \sigma 2}{\sigma 1 - \sigma 3} \tag{6}$$

where, σ_1, σ_2, and σ_3 are the main stresses, compressive, intermediate, and less compressive, respectively; the shape ratio can take values $0 \leq R \leq 1$.

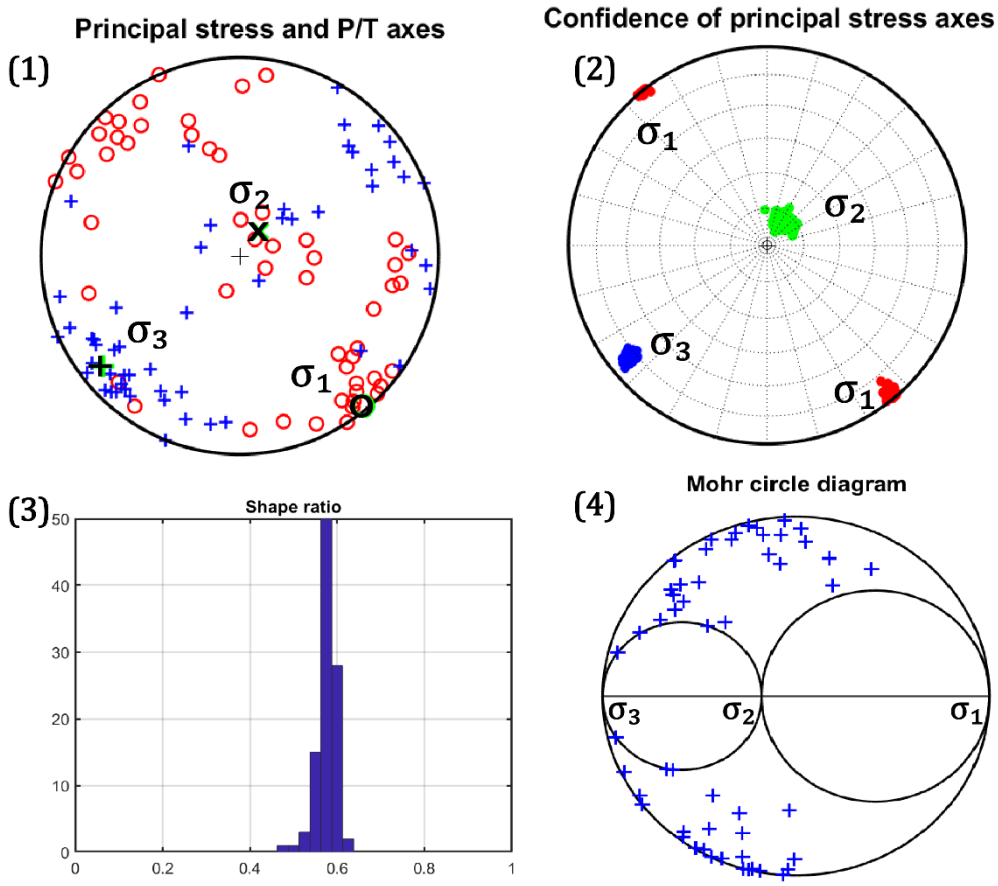

FIGURE 46. RESULTS OF THE STRESS INVERSION FOR THE SICILY CHANNEL. **[1]** PLOT OF A FOCAL SPHERE WITH THE PRINCIPAL STRESS AND P/T AXES. THE RED CIRCLES REPRESENT PRESSURE (P AXES), WHILE THE BLUE CROSSES REPRESENT TENSION (T AXES); **[2]** PLOT WITH THE CONFIDENCE OF PRINCIPAL STRESS AXES (σ_1, σ_2, σ_3). σ_1, IN RED, INDICATES THE MAXIMUM COMPRESSIVE STRESS; σ_2, IN GREEN, INDICATES THE INTERMEDIATE COMPRESSIVE STRESS; σ_3, IN BLUE, INDICATES THE MINIMUM COMPRESSIVE STRESS; **[3]** SHAPE RATIO HISTOGRAM = 0.6; **[4]** MOHR CIRCLE DIAGRAM WITH THE POSITION OF FAULTS (BLUE CROSSES).

The objective of the inversion is to determine the tensor of the efforts affecting the Sicily Channel. The inversion used 54 focal mechanisms with a magnitude > 3.2, and at least 20 focal mechanisms are needed to achieve adequate stress results (*Martínez-Garzón et al., 2016; Jia et al., 2018*). The estimated principal stress axes indicate that the maximum compressive stress axis σ_1 has an azimuth of 140.5° and a plunge of 2.5°, while the minimum compressive stress axis σ_3 has azimuth and plunge values of 231°/12°; the intermediate stress axis is almost vertical with azimuth and plunge values of 39.8°/77°. When deformation occurs, we speak of "seismogenic volume", it is not a single fault that generates the rupture of a volume of rock but is considered a 'around, it means that you generate a network of faults associated with the main that generated the deformation, and may also present different orientations.

The results of the σ_1 orientation obtained from the stress analysis generally agree with the World Stress Map (WSM) project (*Heidbach et al., 2016*), which proposes a stress map where other maximum stress orientation (SHmax) is applied (Fig. 47).

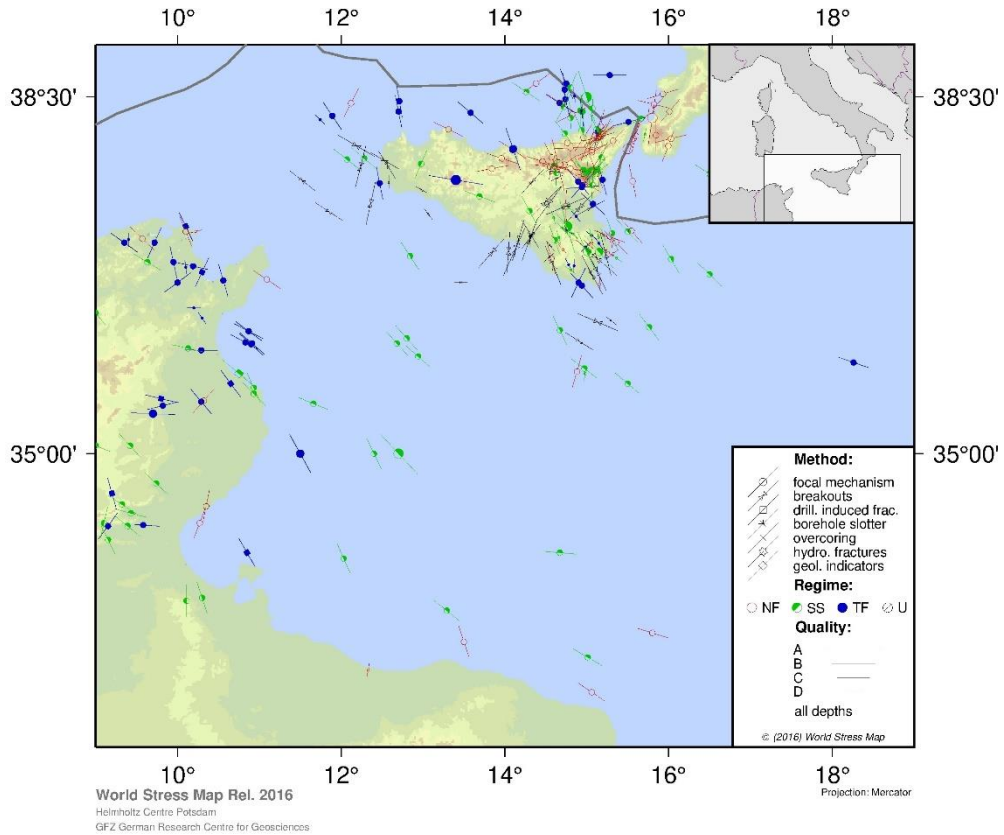

FIGURE 47. THE STRESS MAP OF THE WORLD STRESS MAP (WSM) PROJECT OF THE SICILY CHANNEL AREA. THE PROJECT PROVIDES A GLOBAL COMPILATION OF INFORMATION ON THE CRUSTAL STRESS FIELD. THE DATA DEPTH RANGE IS 0-40 KM (*Heidbach et al., 2016*).

5.3. Seismic Tomography and Local Earthquake Tomography

Tomography is a technique for imaging two or three-dimensional Earth. Seismic tomography is a geophysical method that analyzes earthquake-related seismic waves to have a simplified basement model. The use of different waves for tomographic models, P (primary compression waves), S (secondary shear waves), and surface waves (Love and Rayleigh), depends on the wavelength of the seismic wave and the distance between the source and the receiver. After the signals from the receiver (seismometer) are acquired, they are used to solve the "inverse problem," thus determining the positions of reflection and refraction of the travel time of the seismic waves. The solution to the inverse problem consists in comparing the travel times of the seismic waves acquired by the seismometers with an initial velocity model of the Earth; this model is modified (n. times) until the best fit between the calculated and predicted data of the initial model is found.

Local Earthquake Tomography (LET) is used to obtain images of the elastic properties of the Earth using the natural seismicity generated by local sources. The method consists of picking the seismic waves, then determining the P-waves' and S-waves' first arrival time on a seismometer network to map the positive and negative anomalies concerning the initial velocity model (*Kissling, 1988*). The subsurface model is discretized into cells in which seismic waves travel time, and the velocity depends on the seismic velocities of all cell's crossover by the seismic radius. A necessary condition is that a high density of seismic rays crosses the crustal volume to limit the anomalies determined by the velocity of the deep seismic wave and reduce the problem's non-uniqueness (*Thurber, 1993*). The solution of an inverse problem is not univocal, as a definite set of experimental parameters can correspond to infinite inverse models interpretative compatible, other than the fact that the number of parameters of the model is generally greater than the number of measures, so the uniqueness of the solution is inevitable (the problem is defined underdetermined). Several models solve the inverse problem; choosing the model by comparing experimental data with those acquired is essential.

The solution to the inverse problem of Local Earthquake Tomography must take into consideration i) the position of the receivers (which must be determined within the inversion process), ii) and the geometry of the seismic rays; this means that the function that regulates wave arrival times is not linear of the velocity of the medium

in which it propagates (*Thurber, 1993*). In particular, the non-linearity function that connects the arrival times of waves and earthquakes depends on the paths of the seismic rays, the velocity, and the position of the earthquakes.

5.3.1. Inversion algorithms and velocity model

Several inversion algorithms exist to perform Local Seismic Tomography inversion of earthquakes, such as code LOTOS-07 (*Koulakov, 2009*); this algorithm uses a joint inversion of the P and S wave velocity and the coordinates of the stations. In recent decades, several Local Earthquake Tomography (LET) inversion algorithms have been created, and one of the most used is the SIMULPS12 code. Thurber's SIMULPS12 inversion algorithm performs a joint inversion of the primary wave velocity (Vp), primary/secondary wave velocity ratio (Vp/Vs) parameters, and hypocentral parameters. Thurber inversion is mainly used with local earthquakes and is a full matrix inversion of the least-square damping factor (*Evans, 1994*) least-square damping, means that the norm of the model is computed and weighted with the quadratic misfit of the acquired data, such that this value is minimized at each iteration.

In this work, the code was used SIMULPS12, compared to the LOTOS-07 code; the choice of this algorithm lies in the fact that it presents an improvement in the optimization phase of the 1D-velocity model. Moreover, this algorithm allows more uniform coverage of the seismic rays as the parameterization grid is not fixed, and it is possible to free the path of the rays from the nodes.

Several tests have been made, starting from the initial dataset (from 2005.01.01 to 2021.12.31), the P and S phases of the individual events were determined, and a first skimming of the data was made; the area has also been narrowed trying to exclude the area of Sicily where there is Mount Etna in which most of the seismic events are recorded. Excluding this data, it was decided to extend the database from 1985.01.01 until 2021.12.31 to obtain a richer database. To perform the inversion tomography of the P-velocity and the Vp/Vs ratio, 437 seismic events from 1985.01.01 to 2021.12.31, between 10.35° E and 15.58° E of longitude and between 34.70° N and 37.60° N of longitude, depths up to 40 km, and magnitude > 3 have been considered. For each seismic event, the readings of the P and S phases

were determined (considering at least seven readings to earthquake), thus obtaining an average of readings superior to 15. To make the inversion, two files were made, one with the readings of the phases P and S for each event and the other with the number (total 292) and the list of seismic stations to consider (Fig. 47).

The next step is to define the optimal 1D-velocity model. The parameterization of the initial model is the most crucial part of this process, in which a value of Vp and Vp/Vs is assigned to each node of the SIMULP12 three-dimensional velocity model. The 1D velocity model has been created based on the global crustal model CRUST 5.1 defined by Mooney et al., 1998. The P-waves velocities were measured directly in the field, while empirical Vp-Vs and Vp-density relationships estimated the velocities of the S-waves.

```
160113 1701 29.18  36.070000   14.790800  15.20 4.2
WDD   IP 0   7.290WDD    S     5.230HPAC  IP 0  13.410HMDC  IP 0  16.610HMDC   S    12.710HAVL  IP 0  17.520
HAVL   S    13.100MEU   IP 0  19.050MEU    S    14.870HVZN  IP 0  19.760HVZN   S    15.770SSY   IP 0  20.420
SSY    S    16.000AGST  IP 0  21.760AGST   S    17.060RAFF  IP 0  21.810RAFF   S    17.010HLNI  IP 0  22.140
HLNI   S    17.880HAGA  IP 0  22.150HAGA   S    16.970CLTA  IP 0  22.580FAVR  IP 0  26.120ECNV  IP 0  28.010
ESML  IP 0  28.010EPOZ  IP 0  28.500CAGR  IP 0  28.720GALF  IP 0  29.000ESLN  IP 0  29.400RESU  IP 0  30.660
LPDG  IP 0  30.720EPZF  IP 0  31.280EMSG  IP 0  31.280PETRA IP 0  32.360ALJA  IP 0  32.400MNO   IP 0  32.560
AIO   IP 0  32.610NOV   IP 0  33.320MUCR  IP 0  33.460MSFR  IP 0  33.490MMGO  IP 0  33.590CSLB  IP 0  33.680
MCSR  IP 0  33.680GIB   IP 0  34.550CORL  IP 0  35.270MPNC  IP 0  35.600SOLUN IP 0  36.670SOI   IP 0  36.830
MSRU  IP 0  37.570IVPL  IP 0  37.840MPG   IP 0  38.580JOPP  IP 0  43.140PLAC  IP 0  44.110GRI   IP 0  48.400

160120 0357 57.54  36.476000   12.707700  22.20 3.4
CLTB  IP 0  20.510FAVR  IP 0  21.240FAVR   S    13.930CLTA  IP 0  22.350CLTA   S    15.900CMDO  IP 0  25.530
CORL  IP 0  25.800CORL   S    19.750FAVR  IP 0  26.290RAFF   S    19.340WDD   IP 0  26.430WDD    S    22.160
HMDC  IP 0  28.750HMDC   S    21.730SOLUN IP 0  29.380SOLUN  S    21.960MPG   IP 0  29.460MPG    S    22.690
RESU  IP 0  29.780CSLB  IP 0  30.840CSLB   S    23.300MEU   IP 0  30.880MEU    S    22.490HLNI  IP 0  32.000
HLNI   S    23.220HAVL  IP 0  32.550HAVL   S    24.450SSY   IP 0  33.450SSY    S    25.420PLLN  IP 0  33.700
PLLN   S    24.250GALF  IP 0  33.780GALF   S    23.680

160207 0141 59.14  36.994000   14.861000   4.60 3.3
HMDC  IP 0   1.880HMDC   S     1.180MEU   IP 0   3.160MEU    S     2.200HVZN  IP 0   4.380HAVL  IP 0   5.240
HAVL   S     4.120SSY   IP 0   5.820HPAC  IP 0   6.850HLNI  IP 0   7.050HLNI   S     5.740HAGA  IP 0   7.930
HAGA   S     6.630AGST  IP 0   8.270AGST   S     7.090RAFF  IP 0   9.020RAFF   S     8.540ESML  IP 0  12.740
ESML   S    10.320ECNV  IP 0  12.920CAGR  IP 0  14.510ESLN  IP 0  14.520ESLN   S    11.040CLTA  IP 0  15.010
EPOZ  IP 0  15.080GALF  IP 0  15.600EMSG  IP 0  17.270EPZF  IP 0  17.550RESU  IP 0  19.010MNO   IP 0  19.420
AIO   IP 0  19.820FAVR  IP 0  20.100MUCR  IP 0  20.520PETRA IP 0  20.560NOV   IP 0  20.560MSFR  IP 0  20.700
MCSR  IP 0  21.020CSLB  IP 0  21.620PLLN  IP 0  22.260MTTG  IP 0  22.630MPNC  IP 0  22.720ALJA  IP 0  22.790
GIB   IP 0  22.850MILZ  IP 0  25.110MSRU  IP 0  25.120IVPL  IP 0  25.290SOI   IP 0  25.480ILLI  IP 0  27.880
IFIL  IP 0  27.900IACL  IP 0  27.960SOLUN IP 0  28.170MPG   IP 0  29.970ISTR  IP 0  31.130JOPP  IP 0  31.610
PLAC  IP 0  33.020USI   IP 0  35.770GRI   IP 0  37.850
```

```
 292
ACATE      37.024000     14.500700  201 0.00 0.00  0
ACL        38.533100     14.355600  140 0.00 0.00  0
AGST       37.256530     15.227140   70 0.00 0.00  0
AIO        37.971190     15.233000  751 0.00 0.00  0
ALJA       37.749000     13.753700  700 0.00 0.00  0
AQ6*       38.485560     14.931670      0.00 0.00  0
ATN        38.159470     15.464720 1130 0.00 0.00  0
AUG1       37.243200     15.255500    0 0.00 0.00  0
AYNT       35.573720      8.929250 1100 0.00 0.00  0
BKLT       35.618600     10.996500   25 0.00 0.00  0
BLIT       36.713000      8.952830  225 0.00 0.00  0
BTHT       35.132330     10.285170  240 0.00 0.00  0
CAGR       37.622000     14.499900  548 0.00 0.00  0
CAT        37.514200     15.097200   20 0.00 0.00  0
CAVT       37.678830     12.755600  158 0.00 0.00  0
CBH9       36.014000     14.331400   27 0.00 0.00  0
CBOGS      36.707000      8.416000  207 0.00 0.00  0
CDI1       37.503200     14.647300    1 0.00 0.00  0
CEL        38.259390     15.893890  690 0.00 0.00  0
```

FIGURE 48. (UPPER PANEL) EXAMPLE FILE OF THREE SEISMIC EVENTS (2016.01.13-2016.01.20-2016.02.07), THE READINGS OF THE P AND S PHASES RECORDED TO THE SEISMIC STATIONS ARE REPORTED. (LOWER PANEL) EXAMPLE FILE OF THE LIST OF SEISMIC STATIONS (NAME STATION, LAT, LON, ELEVATION IN METERS).

The choice to use this new crustal model resides in extending to a significantly more extensive database than the previous ones, and the new constraints derived from archives and laboratory studies are explicitly specified.This work recognizes six horizons according to the lithological properties and P-waves velocity values (definite in paragraph 3.4.1). The identified horizons, from top to bottom: (1) Soft sedimentary rocks with a P-wave velocity of 2.4 km/s; (2) hard sedimentary rocks with a P-wave velocity of 4.6 km/s; (3) upper crystalline crust with a P-wave velocity of 6.0 km/s; (4) middle crystalline crust with a P-wave velocity of 6.5 km/s; (5) lower crystalline crust with a P-wave velocity of 7.1 km/s; (6) uppermost mantle with a P-wave velocity of 8.2 m/s.

The SIMULP12 code uses the built-in 1D velocity model and, as a first iteration, optimizes a model depending on the data imported. The peculiarity of this algorithm is that it performs the inversion phase with different orientations of the grid (0°, 22°, 45°, and 67°), and the results obtained by these grids are mediated and plotted in a regular mesh used as a velocity model for following iterations.

After optimizing the model, use this as the initial model and start the real tomographic inversion to obtain the final 3D model. Following several iterations, the model of P and S velocity anomalies is obtained, defined by a regular 3D grid.

As for the results of the seismic tomography, problems occurred in the data conversion phase to reconstruct the velocity model of the Sicily Channel.

The problem is connected to the fact that the inversion is not linked to small-distance events, as most of the stations are in Sicily, and few are located in the smaller islands (although there has been the implementation of the seismic network, for example, for the island of Malta). The major readings that can be obtained in the Sicily Channel are P and S phase readings with large distances. If there are not enough rays to sample the volume under investigation, no constraint is necessary for the reconstruction of the velocity model; the algorithm works with a distance cut-off within which data of a certain quality moves. For events occurring in the Sicily Channel, the algorithm automatically discards stations with a distance greater than 250 km (most are located at high distances). By automatically discarding this data, the number of readings available has been reduced, thus lowering the data quality; for this reason, it is impossible to obtain a reliable result. Unfortunately, this determines a high data gap, and the reversal of tomography does not converge.

6. CHAPTER – RESULTS

6.1. Earthquake relocation

Given the difficulty obtained by seismic tomography because, unfortunately, the distances are high between the stations and the seismic events, earthquakes have been relocated. Several localization tests have been carried out using different inversion algorithms, such as the HypoDD algorithm, to obtain a localization of the hypocentres with the double-difference algorithm (DD) of Waldhauser & Ellsworth (2000); with this algorithm and the geometric network of seismic stations, unfavorable did not allow localizing all events, but only a third. Other tests were carried out, even with the LOTOS-07 algorithm, but this algorithm was not suitable because it discarded much more data, not reaching the sufficient number of rays for the volume investigated.

The relocation was carried out using the code SIMULPS12 (*Evans, 1994*) to reconstruct the seismic rays' raytracing. Considering the geographical limits between 34.7° N and 37.6° N of latitude and between 10.35° E and 15.6° E of longitude, the depths up to 40 km, and the magnitude ≥ 3; 437 earthquakes were inverted derived from the INGV catalog (Fig. 49). The readings of the phases P and S (minimum 7 readings per seismic event) were determined, obtaining an average number of readings > 15. The inversion was made starting from a 1D velocity model, whose model results from the integration of different types of seismic velocity data available in the literature for the southern Italy area. Starting from the integration of multiple datasets and constraints (e.g. velocity patterns from seismic profiles and/or tomographies, Moho depth estimates) and following a procedure derived to the one already successfully applied in the area about a decade ago (*Orecchio et al., BGTA 2011*), we obtained the 3D velocity model that clearly shows the first-order structural features of the area, in agreement with the complex puzzle of lithospheric units. This model has been used for a depth between 0-30 km, integrating the 1D velocity model described in paragraph 3.4.1 for the greater depths.

Figure 50 is shown the depth representation of seismic events; it is noted that the relocated events are deeper, and more distributed in space; most of the input data

(from the INGV bulletin) show a fixed depth between 5 and 10 km, and there is an alignment of seismic events.

The final list of earthquake relocation is available as Additional Information (Table A4).

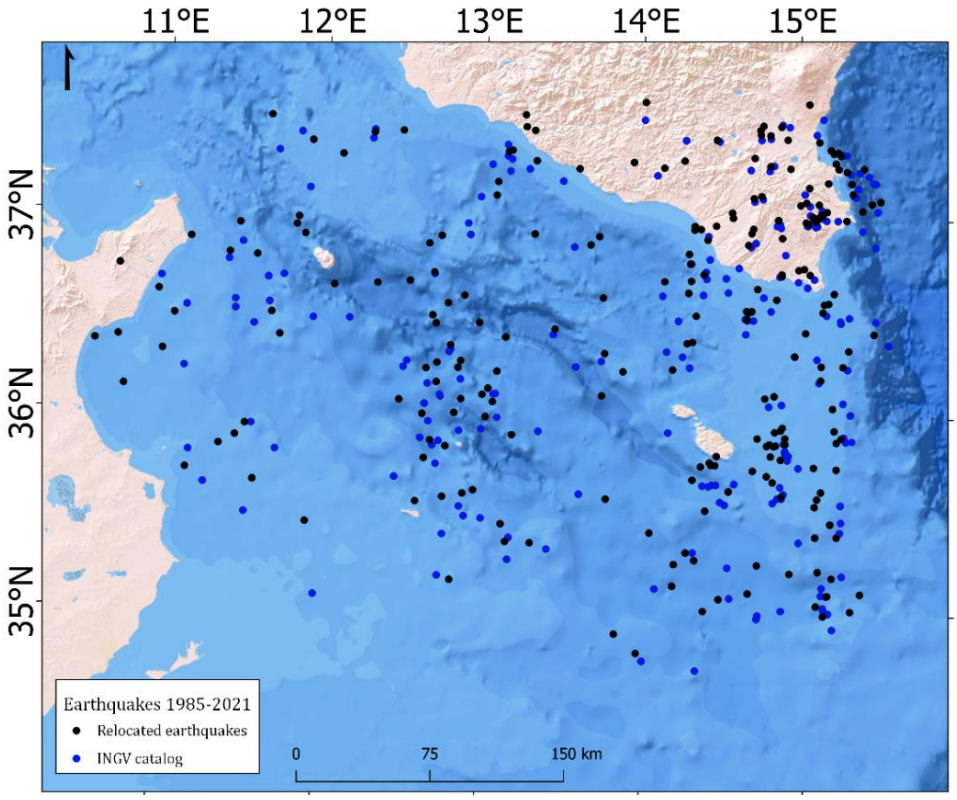

FIGURE 49. MAP OF RELOCATED EARTHQUAKES OF THE SICILY CHANNEL. THE DATASET IS DERIVED FROM THE INGV CATALOG, FOR RECORDED SEISMIC EVENTS FROM 1985.01.01 TO 2021.12.31 (34.7° N – 37.6° N AND 10.35° E – 15.6° E). BLUE DOTS ARE EVENTS FROM THE INGV DATABASE; BLACK DOTS ARE EARTHQUAKES RELOCATED IN THIS STUDY (QGIS SOFTWARE).

The INGV seismic bulletin localization system is a large-scale localization system that uses a 1D velocity model for the whole national territory and tends to lose constraints if it does not have a suitable geometry (because depth is the most complicated parameter to constrain); if do not have a suitable network geometry, this parameter is set to fixed depth (that is why events are located more at 5 and 10 km of depth). As a result of the relocation is observed, therefore, a distribution of the events is more concentrated (black dots in Fig. 49) than the events of the INGV catalog (blue dots), the seismic events are more aggregated in space just for the relocation carried out, small clusters are formed in the Sicily Channel in correspondence of the main tectonic structures.

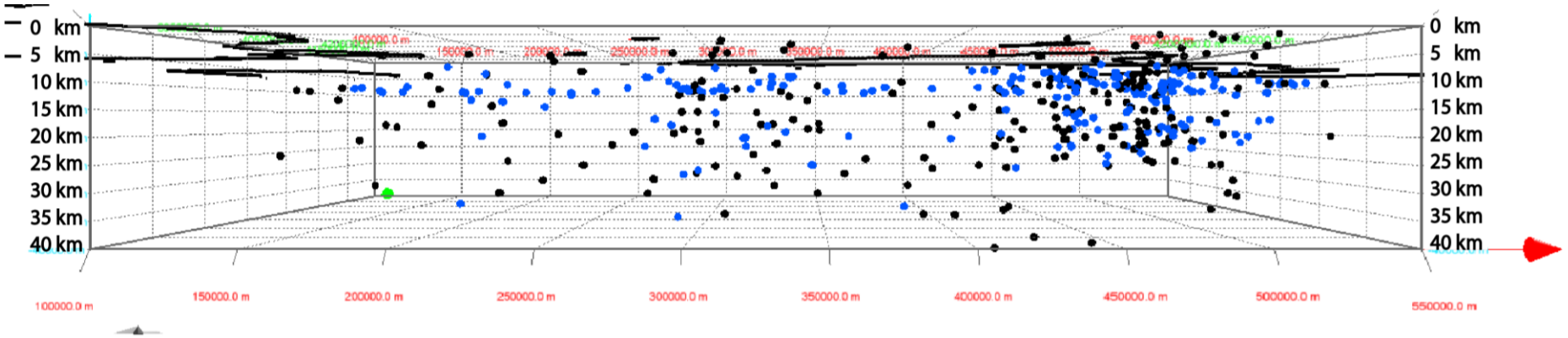

FIGURE 50. 3D VISUALIZATION OF SEISMIC EVENTS, THE MAXIMUM DEPTH REACHED IS ABOUT 40 KM (233 SEISMIC EVENTS HAVE BEEN RELOCATED). BLUE DOTS ARE EVENTS FROM THE INGV DATABASE, AND BLACK DOTS ARE EARTHQUAKES RELOCATED IN THIS STUDY. SEISMIC ALIGNMENTS FOR BLUE EVENTS AT A FIXED DEPTH OF 5 AND 10 KM. VERTICAL EXAGGERATION = 2 (MOVE SOFTWARE).

6.2. 3D Lithospheric model

Developing a 3D lithospheric model involves representing the lithosphere as a three-dimensional grid or mesh. The model includes physical parameters such as the geometry and mechanical properties of the lithosphere and the underlying mantle. The results presented in this paper come from a joint interpretation of seismic-stratigraphic and structural on a large set of seismic data to create a crustal model of the Sicily Channel and, thus, to obtain a key to an understanding of the geological complexity of the collision area between the African and European plates. In the volumetric view, the Sicily Channel's lithospheric model has been constructed to discriminate the several horizons of the crust (upper, middle, and lower) and the thickness. Several sections within the lithospheric 3D model have been created to detail the crustal thicknesses below the reference sections (Fig. 51).

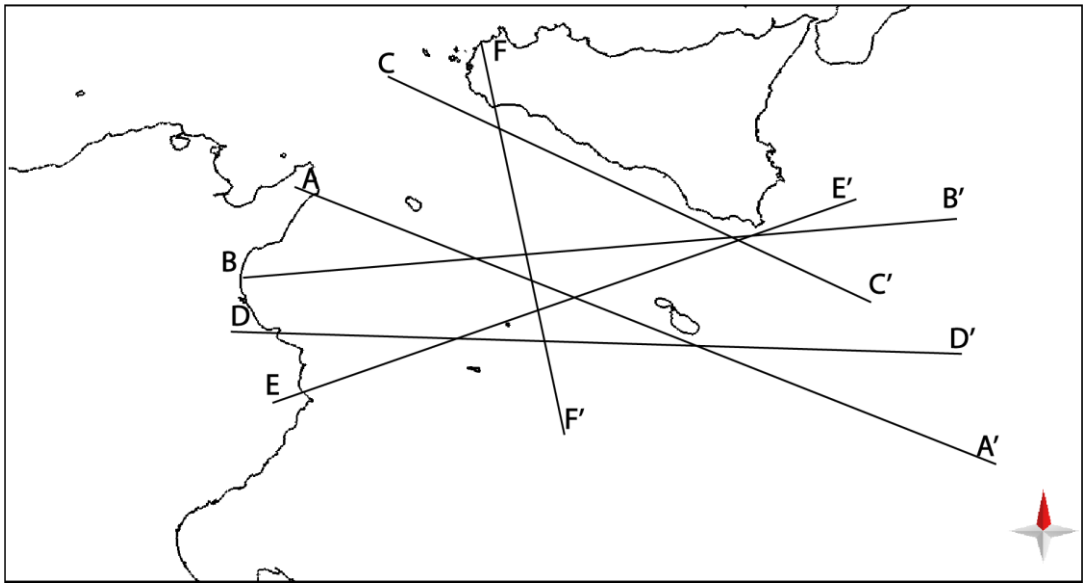

FIGURE 51. THE SECTIONS' LOCALIZATIONS ARE DRAWN WITHIN THE 3D MODEL OF THE SICILY CHANNEL (MOVE SOFTWARE).

Section A-A' shown in Figure 52, oriented NW-SE, starts from the Tunisian coast, crosses the island of Malta, and extends towards the Malta escarpment. Under Malta, it is possible to identify the individual crustal horizons, the thickness of about 2 km of soft sedimentary rocks, 5 km of hard sedimentary rocks, 8 km of the upper crust, about 1 m of middle crust, 7.5 km for the lower crust (total thickness of 23 km). A progressive crustal thickening towards SE is observed in correspondence

with the Malta escarpment, where the layer of the intermediate crust is easily visible.

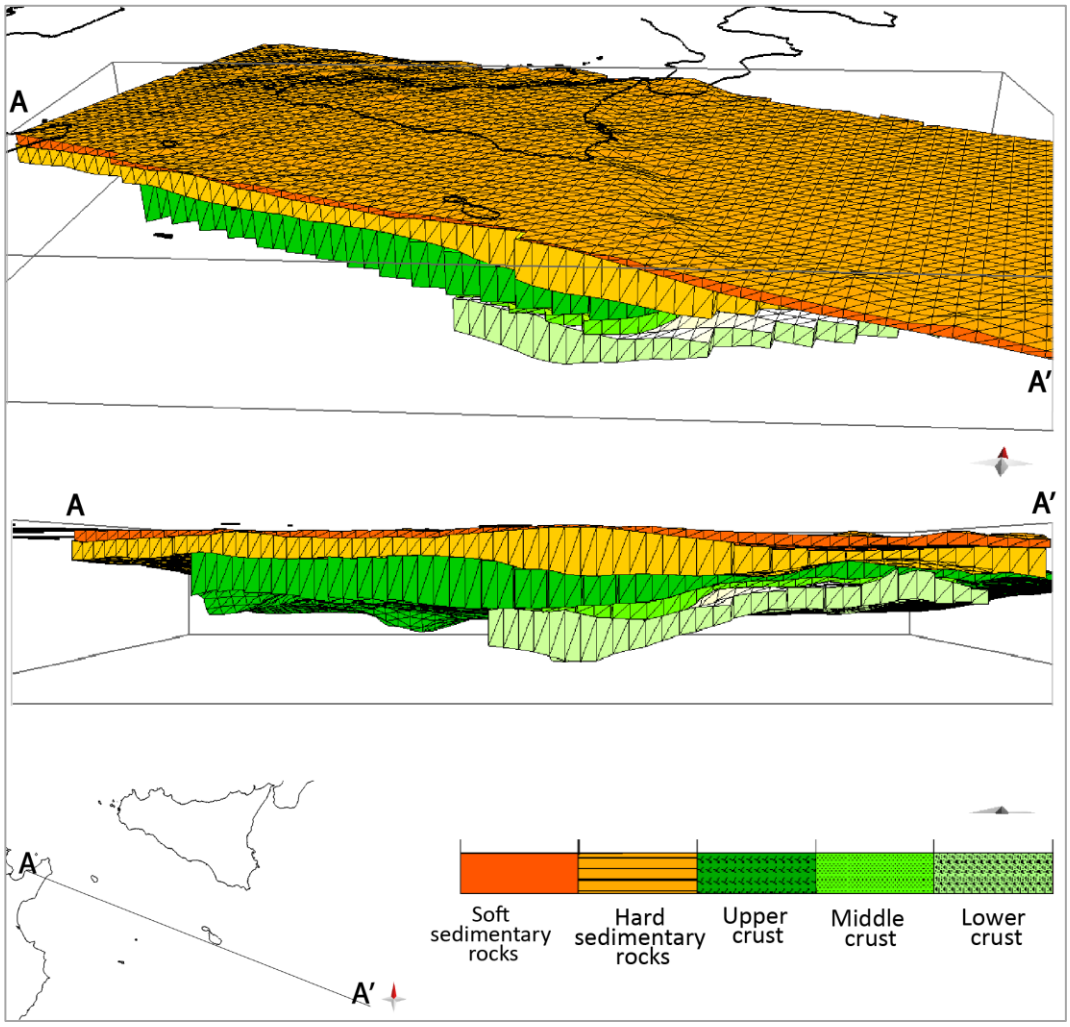

FIGURE 52. THE 3D LITHOSPHERIC MODELS OF THE SICILY CHANNEL. **SECTION A-A'** STARTS FROM THE TUNISIAN COAST, CROSSES THE ISLAND OF MALTA AND EXTENDS TOWARDS THE MALTA ESCARPMENT. THE LEGEND DIFFERENTIATES THE HORIZONS ACCORDING TO COLOUR AND PATTERN (SOFT AND HARD SEDIMENTARY ROCKS, UPPER, MIDDLE, AND LOWER CRUST). AT THE BOTTOM LEFT IS THE LOCATION MAP OF THE SECTION. VERTICAL EXAGGERATION = 3 (MOVE SOFTWARE).

Another Section in Figure 53, B-B' oriented NW-SE, which starts from the Tunisian coast towards ENE, crosses the Pantelleria graben, approaches the Sicilian coast, and continues towards the Ionian Sea. Here we can observe a crustal thinning at the graben and a progressive thickening in the Sicilian offshore. It is not clearly visible, but all the crustal levels (lower, middle, and upper) are identified in the section, even if with less detail.

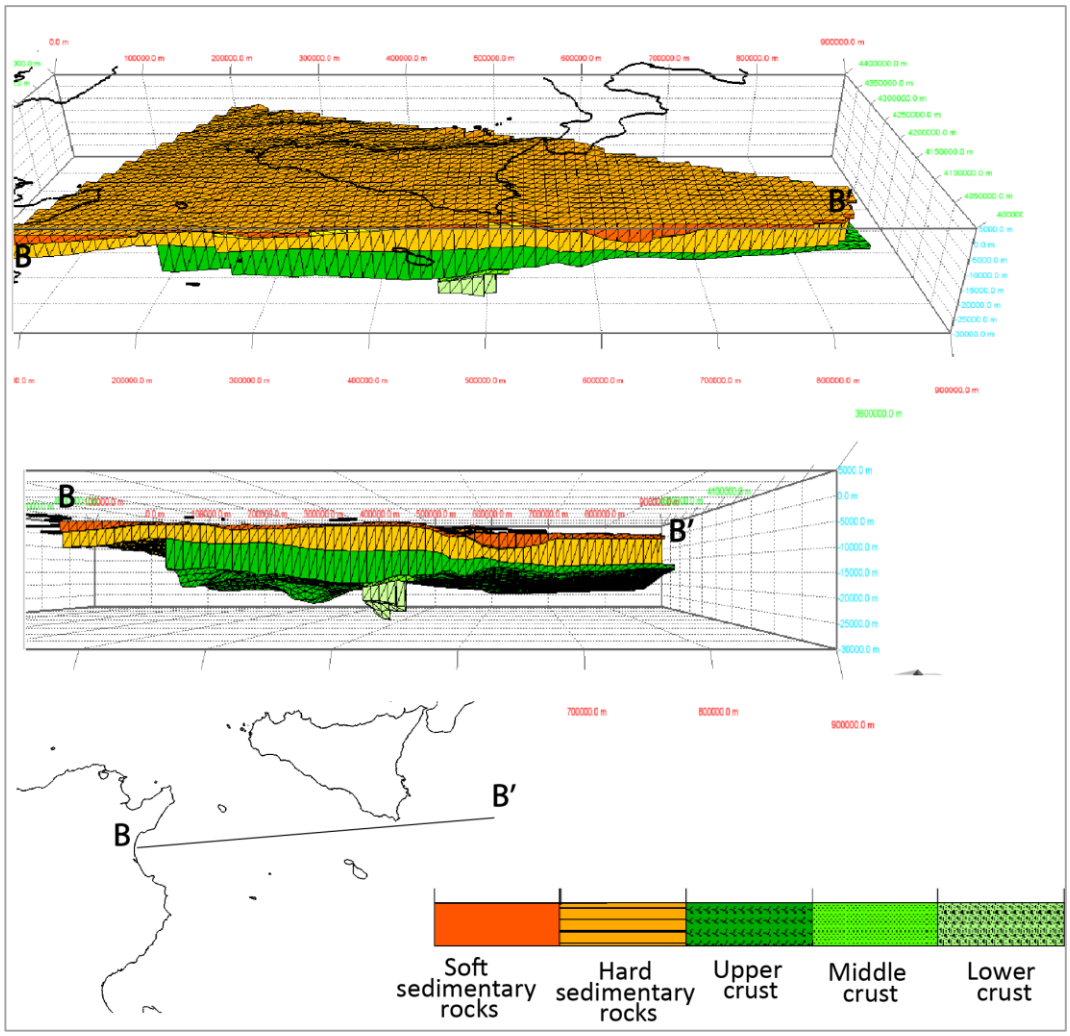

FIGURE 53. THE 3D LITHOSPHERIC MODELS OF THE SICILY CHANNEL. **SECTION B-B'** STARTS FROM THE TUNISIAN COAST AND EXTENDS TOWARDS THE MALTA ESCARPMENT UNTIL THE IONIAN SEA. THE LEGEND DIFFERENTIATES THE HORIZONS ACCORDING TO COLOR AND PATTERN (SOFT AND HARD SEDIMENTARY ROCKS, UPPER, MIDDLE, AND LOWER CRUST). AT THE BOTTOM LEFT IS THE LOCATION MAP OF THE SECTION. VERTICAL EXAGGERATION = 3 (MOVE SOFTWARE).

Section C-C' oriented NW-SE (Figure 54), extends near and parallel to the southern Sicilian coastline, starting from the Adventure bank, passes through the Gulf of Gela, passing the escarpment of Malta, and ending in the Ionian Sea. This section coincides with the CROP M23 profile that was created for the ViDEPI project. We observe along this section a crustal thickening, where the total depth reached is about 25 km; we observe a thickness almost constant of the upper crust (green pattern) strongly deformed.

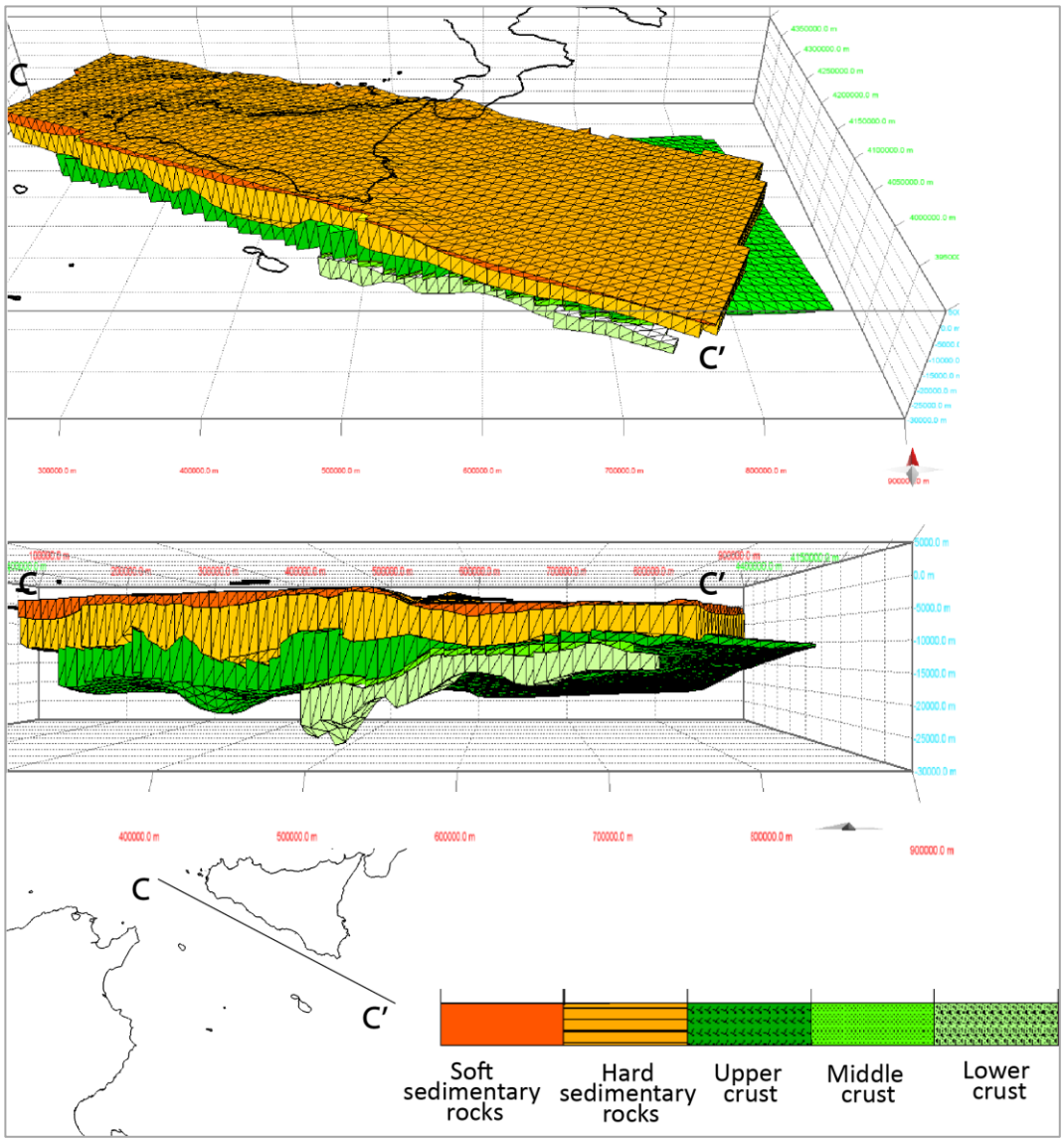

FIGURE 54. THE 3D LITHOSPHERIC MODELS OF THE SICILY CHANNEL. **SECTION C-C'** STARTS FROM THE ADVENTURE BANK AND EXTENDS TOWARDS THE MALTA ESCARPMENT (SECTION COINCIDING WITH THE CROP M23 PROFILE OF THE VIDEPI PROJECT). THE LEGEND DIFFERENTIATES THE HORIZONS ACCORDING TO COLOR AND PATTERN (SOFT AND HARD SEDIMENTARY ROCKS, UPPER, MIDDLE, AND LOWER CRUST). AT THE BOTTOM LEFT IS THE LOCATION MAP OF THE SECTION. VERTICAL EXAGGERATION = 3 (MOVE SOFTWARE).

The section D-D' oriented WSW-ENE, in Figure 55, extends from the Tunisian coast, passes under the Lampedusa island, extends south of the island of Malta, and continues towards the Malta escarpment. This section gives a different perspective than the previous sections. Small thicknesses are determined for soft sedimentary rocks (due to the information from the calibration data), the crustal thickness along

the section is about 22 km, and crustal levels (lower, middle, and upper) can be differentiated, about 1 km thick for the middle level.

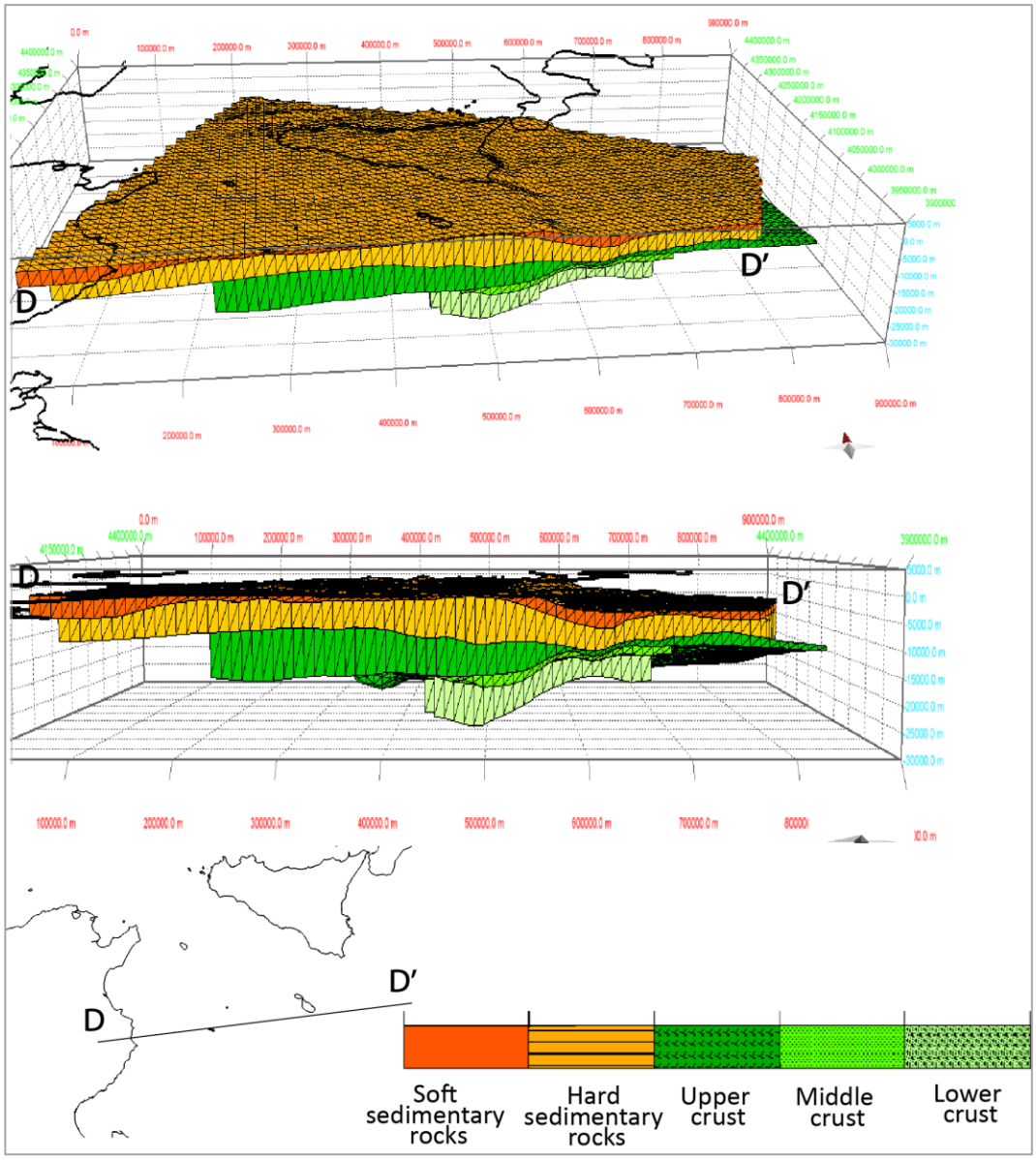

FIGURE 55. THE 3D LITHOSPHERIC MODELS OF THE SICILY CHANNEL. **SECTION D-D'** STARTS FROM THE TUNISIAN COAST, CROSSES LAMPEDUSA ISLAND, AND CONTINUES TOWARDS MALTA ISLAND, UP TO THE MALTA ESCARPMENT. THE LEGEND DIFFERENTIATES THE HORIZONS ACCORDING TO COLOUR AND PATTERN (SOFT AND HARD SEDIMENTARY ROCKS, UPPER, MIDDLE, AND LOWER CRUST). AT THE BOTTOM LEFT IS THE LOCATION MAP OF THE SECTION. VERTICAL EXAGGERATION = 3 (MOVE SOFTWARE).

The E-E' section, shown in Figure 56, starts from the Tunisian coast and crosses the Linosa and Malta graben towards the Sicilian coast. A crustal thinning is identified

in correspondence of the two graben, more significant in the coincidence of the Linosa graben. In this section, the average crustal thickness is about 20 km and the rise of the Moho discontinuity. There is a general thinning of crustal and sedimentary horizons.

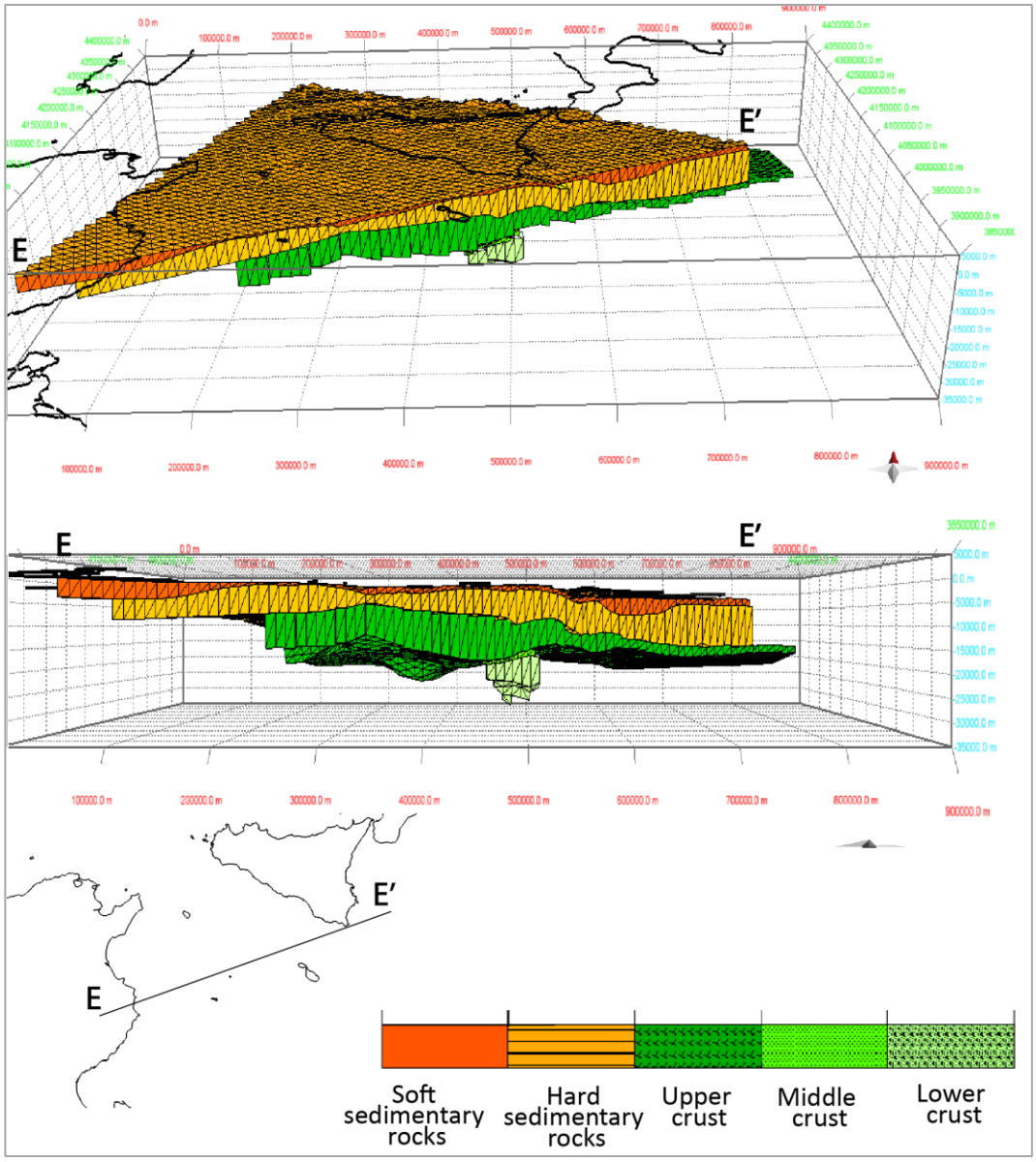

FIGURE 56. THE 3D LITHOSPHERIC MODELS OF THE SICILY CHANNEL. **SECTION E-E'** STARTS FROM THE TUNISIAN COAST, CROSS LINOSA ISLAND, AND CONTINUES TOWARDS THE PLATEAU HYBLEAN. THE LEGEND DIFFERENTIATES THE HORIZONS ACCORDING TO COLOUR AND PATTERN (SOFT AND HARD SEDIMENTARY ROCKS, UPPER, MIDDLE, AND LOWER CRUST). AT THE BOTTOM LEFT IS THE LOCATION MAP OF THE SECTION. VERTICAL EXAGGERATION = 3 (MOVE SOFTWARE).

Section F-F' (in Figure 57) is oriented about NW-SE, starting from the Sicilian coast from the area of Mazara del Vallo, crossing the Pantelleria and Linosa graben, and continuing towards the Libyan coast. This section is representative in the Sicilian offshore, a progressive crustal thinning is observed from N to S, below the two graben.

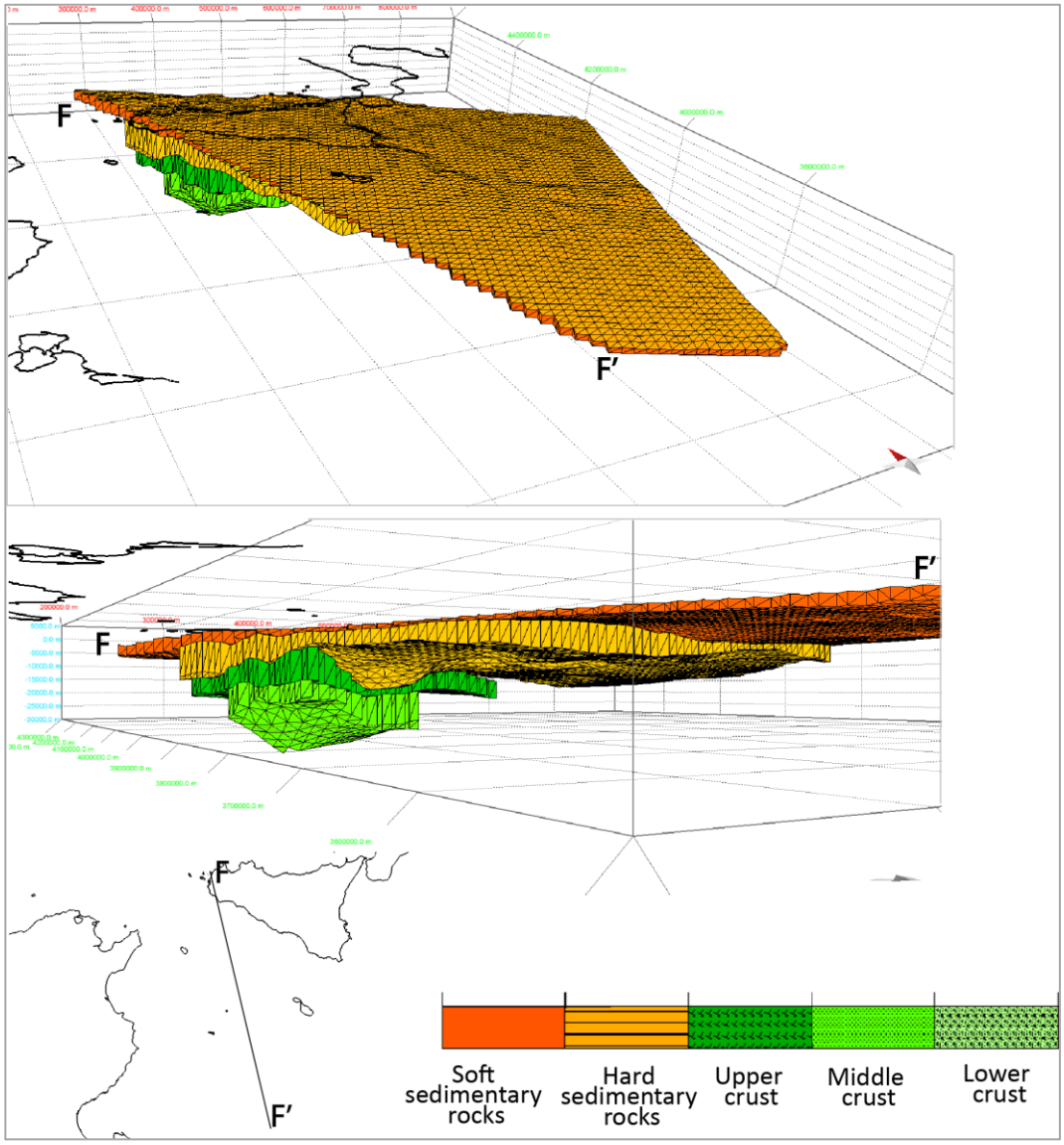

FIGURE 57. THE 3D LITHOSPHERIC MODELS OF THE SICILY CHANNEL. **SECTION F-F'** STARTS FROM THE SICILIAN COAST FROM THE MAZARA DEL VALLO AREA, CROSSING THE SICILY CHANNEL'S CENTRAL AREA TOWARDS THE LIBYAN COAST. THE LEGEND DIFFERENTIATES THE HORIZONS ACCORDING TO COLOR AND PATTERN (SOFT AND HARD SEDIMENTARY ROCKS, UPPER, MIDDLE, AND LOWER CRUST). AT THE BOTTOM LEFT IS THE LOCATION MAP OF THE SECTION. VERTICAL EXAGGERATION = 3 (MOVE SOFTWARE).

6.3. Map of Moho 3D

Following the realization of the lithospheric model, it was possible to reconstruct the map of the Moho. In Figure 58a, the Moho depth map, it is observed that at the SCRZ (Sicily Channel Rift Zone), there is a Moho (in seismic data at about 9-10 s/TWT) uplift at about 18-20 km in the Pantelleria graben (characterized by low P-wave velocity, about 7.6 km/s) (*Calò et al., 2013*).

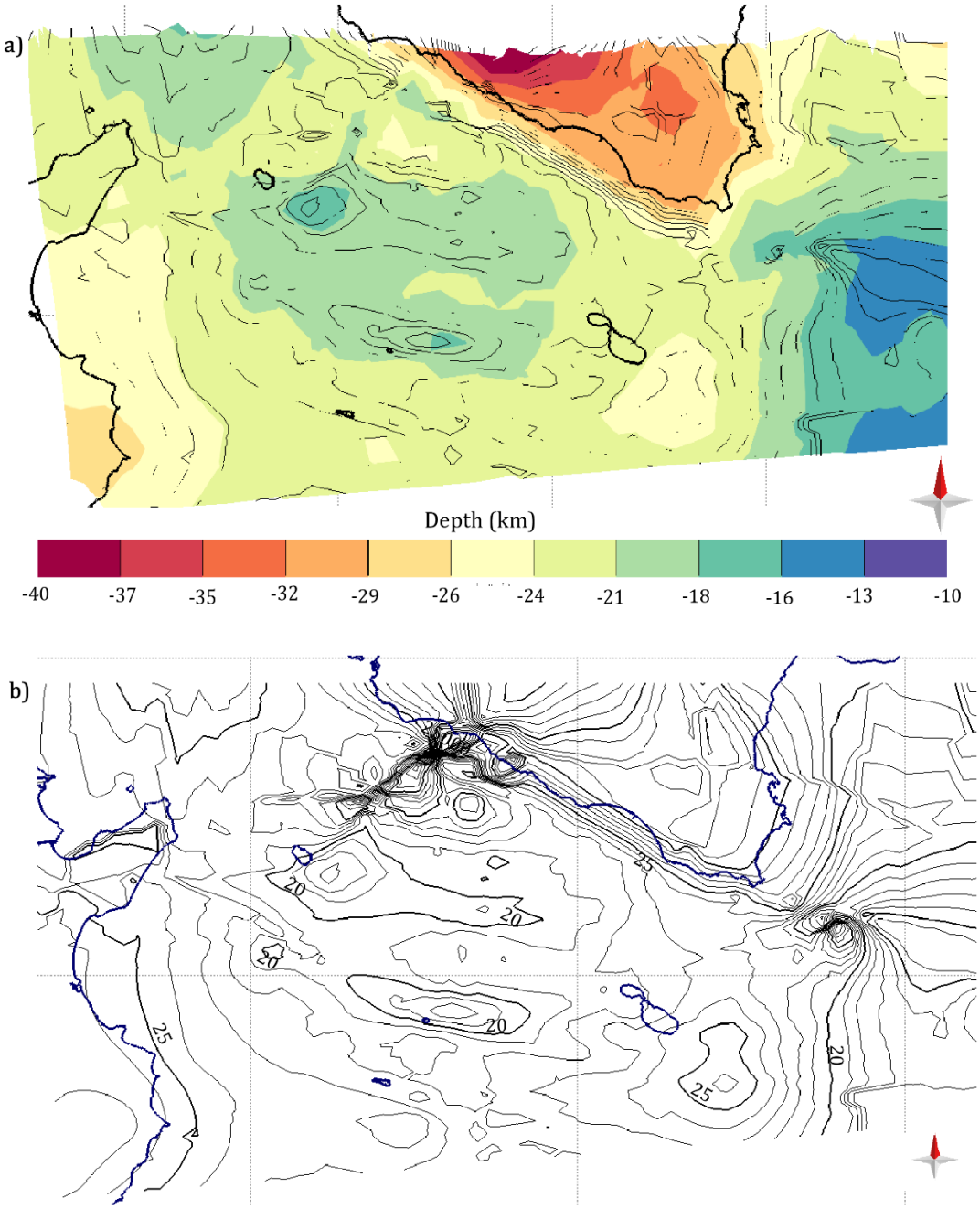

FIGURE 58. a) MAP OF MOHO FOR THE SICILY CHANNEL. THE COLOR SCALE SHOWS VARIATIONS IN DEPTH (KILOMETERS); **b)** MAP OF MOHO ISOBATHS OF THE SICILY CHANNEL. THE CONTOUR LINES ARE DRAWN WITH THICK AND THIN BLACK LINES EVERY 5 KM AND 1 KM DEPTH STEPS, RESPECTIVELY (MOVE SOFTWARE).

The depth of the Moho increases to about 25 km deep along the Sicilian offshore towards the Malta plateau. The data coverage is mainly concentrated in the central area of the Pelagian block, and there is a good agreement with the areas that cover the area of Sicily, an area widely studied by other authors. The realization of the qualitative and quantitative model of Moho for the area of the Sicily Channel is intended as an integration for the maps produced in literature by Mele et al. (2011) and Di Stefano et al. (2011), who created, respectively, a map of the isobaths of Moho of the Italian peninsula and a map of Moho 3D geometry for the Adriatic, the Tyrrhenian, and the Italian peninsula.

7. CONCLUSIONS

The activity of this work has led to the study and analysis of the area of the Sicily Channel. Based on previous works by several authors, a detailed study has been made of this area, collecting the available geological and geophysical data sets.

Thanks to the quantity and quality of data available, through the analysis of seismic reflection profiles, and structural analysis, geological analysis has been possible to create the crustal model of the Sicily Channel, to obtain a key to understanding the geological complexity of this area. From the sections that have been realized, it can observe how the crustal thickness model realized in this work compares well with the individual reflection profiles that were analyzed in the preliminary phase. The results shown in this work on the Moho map show a good coupling with the bathymetry of the area, and there is also a good connection with the creation of the 3D map of Moho, which is intensely detailed and consistent with the models from other studies which affect the surrounding areas of the Sicily Channel.

The study focused on the realization of a model of seismic tomography of the central Mediterranean; being the study area of seismic interest, an analysis of earthquakes was made. Past studies show that seismic activity in the Sicily Channel is moderate; however, this is closely related to the limited instrumental seismic coverage in the area. The problems of inversion are related to the area's seismic network coverage, as most of these are installed in Sicily and only a few to the south (for example, in Malta island) and can cover a small portion of the area. This means that to obtain a tomography model and reconstruct the raytracing of the

seismic rays from the hypocentre to the stations, it is necessary to have small distances (between source and receiver). Since the Sicily Channel area is located in an area where the nearest stations are tens of kilometers away, and even hundreds of kilometers, this does not return an acceptable and reliable tomography model. These conclusions were determined following a series of tests and tests that were made. Several inversion algorithms were used to test their effectiveness, and several earthquake catalogs were consulted, modifying the time interval of the data to be used. The geographical limits have also been changed to eliminate outlier data from seismic events in Etna Mt.

From the consultation of the available earthquake catalogues (INGV bulletin), it was possible to relocate seismic events. As a result, we have seen how the seismic events are well distributed and thicker within clouds of points, also in relation to the seismic volumes that affect the faults of the Sicily Channel. A distribution map of seismic events was obtained, relocating and distributing the events located at a fixed depth of 5 km and 10 km.

The three-dimensional mapping that has been realized in this work, with the Move software, could allow to define a more robust modelling method, creating different multidisciplinary datasets in order to constrain the final model. It is possible to include data of different nature, depending on the study to be carried out and the a priori information that can be available.

REFERENCES

Accaino F., Catalano R., Di Marzo L., Giustiniani M., Tinivella U., Nicolich R., Sulli A., Valenti V., Manetti P. (2011). A crustal seismic profile across Sicily. *Tectonophysics, 508*(1-4),52-61. doi.org/10.1016/j.tecto.2010.07.011

Agius M.R., Galea P., Farrugia D., D'Amico S. (2020). An instrumental earthquake catalogue for the offshore Maltese islands region, 1995-2014. *Annals of Geophysics,* 63(63),658. doi.org/10.4401/ag-8383

Aki K. (1965). Maximum likelihood estimate of b in the formula log N= a-bM and its confidence limits. *Bulletin Earthquake Research Institute, Tokyo Univ., 43,* 237-239

Amato A., & Mele F. (2008). Performance of the INGV National Seismic Network from 1997 to 2007. *Annals of Geophysics,* 51(2-3). doi.org/10.4401/ag-4454

Antonelli M., Franciosi R., Querci A., Ronco G., Vezzani F. (1988). Paleogeographic evolution and structural setting of the northern side of the Sicily Channel. *Memorie della Società Geologica Italiana*, 41, 141-157, 5 figg., 3 tavv., Roma

APAT, (2005). Gravity Map of Italy and Surrounding seas. 1:1 250 000, Agenzia per la protezione dell'ambiente e per I servizi tecnici, Dipartimento Difesa del Suolo, Servizio Geologico d'Italia, 2005

Argnani A. (2009). Evolution of the southern Tyrrhenian slab tear and active tectonics along the western edge of the Tyrrhenian subducted slab. *Geological Society, London, Special Publications, 311*(1), 193-212. doi.org/10.1144/SP311.7

Argnani A. (1990). The Strait of Sicily rift zone: foreland deformation related to the evolution of a back-arc basin. *Journal of Geodynamics, 12*(2-4), 311-331. doi.org/10.1016/0264-3707(90)90028-s

Argnani A., Cornini S., Torelli L., Zitellini N. (1986). Neogene-Quaternary foredeep system in the Strait of Sicily. *Memorie della Società Geologica Italiana*, *36,* 123-130

Belguith Y., Geoffroy L., Mourgues R., Rigane A. (2013). Analogue modelling of Late Miocene–Early Quaternary continental crustal extension in the Tunisia Sicily Channel area. *Tectonophysics, 608,*576-585. doi.org/10.1016/j.tecto.2013.08.023

Bello M., & Merlini S. (2000). Structural model of central eastern Sicily. In *EAGE Conference on Geology and Petroleum Geology of the Mediterranean and*

Circum-Mediterranean Basins (pp. cp-109). EAGE Publications BV. doi.org/10.3997/2214-4609.201405982

Blom N., Gokhberg A., Fichtner A. (2020). Seismic waveform tomography of the central and eastern Mediterranean upper mantle. Solid Earth, 11(2), 669–690. doi.org/10.5194/se-11-669-2020

Boccaletti M., Cello G., Tortorici L. (1987). Transtensional tectonics in the Sicily Channel. *Journal of Structural Geology*, *9*(7), 869-876. doi.org/10.1016/0191-8141(87)90087-3

Boschi E., Guidoboni E., Mariotti D. (1995). Seismic effects of the strongest historical earthquake in the Syracuse area. *Annals of Geophysic*s, 38(2), 223-253. doi: 10.4401/ag-4121

Boschi E., & Morelli A. (1994). The MEDNET Program. *Annals of Geophysics*, 37(5). doi.org/10.4401/ag-4197

Bottari A. (1973). Attività sismica e neotettonica della Valle del Belice. *Annals of Geophysics*, *26*(1), 55-84. doi.org/10.4401/ag-5008

Bozionelos G., Galea P., D'Amico S., Plasencia Linares M.P., Romanelli M., Rossi G., Parolai S., Vuan A., Sugan M., Agius M.R. (2019). An augmented seismic network to study off-shore seismicity around the Maltese Islands: the FASTMIT experiment, XJENZA, 7, 104-121, doi.org/10.7423/XJENZA.2019.2.03

Burollet P.F., Mugniot J.M., Sweeney P. (1978). The geology of the Pelagian block: the margins and basins off southern Tunisia and Tripolitania. *The Ocean Basins and Margins*, 331-359. doi.org/10.1007/978-1-4684-3039-4_6

Butler R.W.H., Lickorish W.H., Grasso M., Pedley H.M., Ramberti L. (1995). Tectonics and sequence stratigraphy in Messinian Basins, Sicily: constraints on the initiation and termination of the Mediterranean salinity crisis. *Geological Society of America Bulletin,*107(4), 425–439. doi.org/10.1130/0016-7606(1995)107<0425:TASSIM>2.3.CO;2

Calanchi N., Colantoni P., Rossi P.L., Saitta M., Serri G. (1989). The Strait of Sicily continental rift systems: physiography and petrochemistry of the submarine volcanic centres. *Marine Geology*, *87*(1), 55-83. doi.org/10.1016/0025-3227(89)90145-x

Calò M., & Parisi L. (2014). Evidences of a lithospheric fault zone in the Sicily Channel continental rift (southern Italy) from instrumental seismicity data. *Geophysical Journal International*, 199(1), 219-225, doi.org/10.1093/gji/ggu249

Calo M., Parisi L., Luzio D. (2013). Lithospheric P- and S-wave velocity models of the Sicilian area using WAM tomography: procedure and assessments. *Geophysical Journal International,* 195(1), 625–649. doi.org/10.1093/gji/ggt252

Caratori Tontini F., Stefanelli P., Giori I., Faggioni O., Carmisciano C. (2004). The revised aeromagnetic anomaly map of Italy. *Annals of Geophysics*, 47(5). doi.org/10.4401/ag-3358

Cassinis R., Scarascia S., Lozej A. (2005). Review of Seismic Wide-Angle Reflection–Refraction (WARR) Results in the Italian Region (1956–1987). In I.R. Finetti (Ed), *CROP PROJECT: Deep Seismic Exploration of the Central Mediterranean and Italy*, (Vol. chapter 2, 31-55). Elsevier

Catalano R., Valenti V., Albanese C., Accaino F., Sulli A., Tinivella U., Gasparo Morticelli M., Zanolla C., Giustiniani M. (2013). Sicily's fold–thrust belt and slab roll-back: the SI.RI.PRO. seismic crustal transect. *Journal of the Geological Society*, *170*(3), 451-464. doi.org/10.1144/jgs2012-099

Catalano S., Monaco C., Tortorici L., Paltrinieri W., Steel N. (2004). Neogene-Quaternary tectonic evolution of the southern Apennines. *Tectonics*, 23(2), n/a-n/a. doi:10.1029/2003TC001512

Catalano R., Doglioni C., Merlini S. (2001). On the Mesozoic Ionian Basin. *Geophysical Journal International*, *144*(1), 49-64. doi.org/10.1046/j.0956-540x.2000.01287.x

Catalano R., Franchino A., Merlini S., Sulli A. (2000). Crustal Structures from the Eastern Algerian Basin to the Ionian Ocean-Central Mediterranean. In *EAGE Conference on Geology and Petroleum Geology of the Mediterranean and Circum-Mediterranean Basins* (pp. cp-109). EAGE Publications BV. doi.org/10.3997/2214-4609.201405983

Catalano R., D'Argenio B., Torelli L. (1989). A geologic section from Sardinia to Sicily Straits based on seismic and field data. *The Lithosphere in Italy: Advances in Earth Science Research. Proceedings of the Convegni Lincei*, SLC-80. Academia dei Lincei, Rome, 109-127. *ISSN 2037-4631*

Catalano R., & D'Argenio B. (1981). Paleogeographic evolution of a continental margin in Sicily. *Guide Book of the field trip in Western Sicily*, 12-14

Cavallaro D., Monaco C., Polonia A., Sulli A., Di Stefano A. (2017). Evidence of positive tectonic inversion in the north-central sector of the Sicily Channel (Central Mediterranean). *Natural Hazards*, *86(s2)*, 233-251. doi.org/10.1007/s11069-016-2515-6

Cello G. (1987). Structure and deformation processes in the Strait of Sicily "rift zone". *Tectonophysics*, *141*(1-3), 237-247. doi.org/10.1016/0040-1951(87)90188-0

Chiappini M., Meloni A., Boschi E., Faggioni O., Beverini N., Carmisciano C., Marson I. (2000). Shaded relief magnetic anomaly map of Italy and surrounding marine areas. doi.org/10.4401/ag-3676

Chiarabba C., Jovane L., Di Stefano R. (2005). A new view of Italian seismicity using 20 years of instrumental recordings. *Tectonophysics*, *395*(3-4), 251-268. doi.org/10.1016/j.tecto.2004.09.013

Chironi C., De Luca L., Guerra I., Luzio D., Moretti A., Vitale M. & Sea Land Group. (2000). Crustal structures of the Southern Tyrrhenian Sea and the Sicily Channel on the basis of the M25, M26, M28, M39 WARR profiles. *Bollettino-Società Geologica Italiana*, *119*(1), 189-204

Civile D., Brancolini G., Lodolo E., Forlin E., Accaino F., Zecchin M., Brancatelli G. (2021). Morphostructural Setting and Tectonic Evolution of the Central Part of the Sicilian Channel (Central Mediterranean). *Lithosphere*, 2021(1). doi.org/10.2113/2021/7866771

Civile D., Lodolo E., Accaino F., Geletti R., Schiattarella M., Giustiniani M., Fedorik J., Zecchin M., Zampa L. (2018). Capo Granitola-Sciacca Fault Zone (Sicilian Channel, Central Mediterranean): Structure vs magmatism. *Marine and Petroleum Geology*, *96*, 627-644. doi.org/10.1016/j.marpetgeo.2018.05.016

Civile D., Lodolo E., Zecchin M., Ben-Avraham Z., Baradello L., Accettella D., Cova A., Caffau M. (2015). The lost Adventure Archipelago (Sicilian Channel, Mediterranean Sea): Morpho-bathymetry and Late Quaternary palaeogeographic evolution, *Global and Planetary Change*, 125, 36-47. doi.org/10.1016/j.gloplacha.2014.12.003

Civile D., Lodolo E., Alp H., Ben-Avraham Z., Cova A., Baradello L., Accettella D., Burca M., Centonze J. (2014). Seismic stratigraphy and structural setting of the Adventure Plateau (Sicily Channel). *Marine Geophysical Research, 35(1),* 37-53. doi.org/10.1007/s11001-013-9205-5

Civile D., Lodolo E., Accettella D., Geletti R., Ben-Avraham Z., Deponte M., Facchin L., Ramella R., Romeo R. (2010). The Pantelleria graben (Sicily Channel, Central Mediterranean): An example of intraplate 'passive' rift. *Tectonophysics*, *490*(3-4), 173-183. doi.org/10.1016/j.tecto.2010.05.008

Civile D., Lodolo E., Tortorici L., Lanzafame G., Brancolini G. (2008). Relationships between magmatism and tectonics in a continental rift: The Pantelleria Island region (Sicily Channel, Italy). *Marine Geology*, *251*(1-2), 32-46. doi.org/10.1016/j.margeo.2008.01.009

Colantoni P. (1975). Note di geologia marina sul Canale di Sicilia. *Giornale di Geologia*, s.2, 40(1): 181-207

Coltelli M., Cavallaro D., D'Anna G., D'Alessandro A., Grassa F., Mangano G., Patanè D., Gresta S. (2016). Exploring the submarine Graham Bank in the Sicily Channel. *Annals of Geophysics*, 59(2). doi.org/10.4401/ag-6929

Corti G., Cuffaro M., Doglioni C., Innocenti F., Manetti P. (2006). Coexisting geodynamic processes in the Sicily Channel. *Postcollisional Tectonics and Magmatism in the Mediterranean Region and Asia*. doi.org/10.1130/2006.2409(05)

Dart C.J., Bosence D.W.J., Mcclay K.R. (1993). Stratigraphy and structure of the Maltese Graben system. *Journal of the Geological Society*, 150(6): 1153–1166. doi.org/10.1144/gsjgs.150.6.1153

Della Vedova B., Bellani S., Pellis G., Squarci P. (2001). Deep temperatures and surface heat flow distribution. *Anatomy of an orogen: the Apennines and adjacent Mediterranean basins*. Kluwer Academic Publishers: 65-76, Dordrecht, The Netherlands. doi.org/10.1007/978-94-015-9829-3_7

Della Vedova B., Lucazeau F., Pasquale V., Pellis G., Verdoya M. (1995). Heat flow in the tectonic provinces crossed by the southern segment of the European Geotraverse. *Tectonophysics*, *244*(1-3), 57-74. doi.org/10.1016/0040-1951(94)00217-w

Della Vedova B.D., Pellis G., Pinna E. (1989). Studio geofisico dell'area di transizione tra il Mar Pelagico a la Piana Abissale dello Jonio, *Atti del VIII Convegno Nazionale GNGTS (CNR), Roma*, Esagrafica, 1, 543–558

Dellong D., Klingelhoefer F., Kopp H., Graindorge D., Margheriti L., Moretti M., Murphy S., Gutscher M.A. (2018). Crustal Structure of the Ionian Basin and Eastern Sicily Margin: Results from a Wide-Angle Seismic Survey. *Journal of Geophysical Research: Solid Earth*, *123*(3), 2090-2114. Portico. doi.org/10.1002/2017jb015312

Di Stefano R., Bianchi I., Ciaccio M.G., Carrara G., Kissling E. (2011). Three-dimensional Moho topography in Italy: New constraints from receiver functions and controlled source seismology. *Geochemistry, Geophysics, Geosystems*, 12(9), n/a-n/a. doi.org/10.1029/2011gc003649

Dziewonski A.M., Chou T.-A., Woodhouse J.H. (1981). Determination of earthquake source parameters from waveform data for studies of global and regional seismicity. *Journal of Geophysical Research: Solid Earth*, 86(B4), 2825–2852. Portico. doi.org/10.1029/jb086ib04p02825

Ekström G., Nettles M., Dziewoński A.M. (2012). The global CMT project 2004–2010: Centroid-moment tensors for 13,017 earthquakes. *Physics of the Earth and Planetary Interiors*, 200–201, 1–9. doi.org/10.1016/j.pepi.2012.04.002

Evans J.R., Eberhart-Phillips D., Thurber C.H. (1994). User's manual for SIMULPS12 for imaging vp and vp/vs; a derivative of the" Thurber" tomographic inversion SIMUL3 for local earthquakes and explosions (No. 94-431). *US Geological Survey*. doi.org/10.3133/ofr94431

Ferranti L., Pepe F., Barreca G., Meccariello M., Monaco C. (2019). Multi-temporal tectonic evolution of Capo Granitola and Sciacca foreland transcurrent faults (Sicily Channel). *Tectonophysics, 765,* 187-204. doi.org/10.1016/j.tecto.2019.05.002

Finetti I.R. (2005). CROP project: deep seismic exploration of the central Mediterranean and Italy. Elsevier. Finetti I.R., 1984. Geophysical study of the Sicily Channel Rift Zone. Boll. Geofis. Teor. Appl. 26, 3-28. ISBN: 0-444-50693-4

Finetti I.R., & Del Ben A. (2005). Crustal tectono-stratigraphic setting of the Pelagian foreland from new CROP seismic data. In *CROP Project: Deep Seismic Exploration of the Central Mediterranean and Italy*, (Vol. 1, pp. 581-596). Elsevier

Finetti I.R., Lentini F., Carbone S., Del Ben A., Di Stefano A., Forlin E., Guarneri P., Pipan M., Prizzon A. (2005). Geological outline of Sicily and lithospheric tectono-dynamics of its Tyrrhenian margin from new CROP seismic data. *In CROP Project: Deep Seismic Exploration of the Central Mediterranean and Italy*, 319-375. Elsevier

Finetti I. (1985). Structure and Evolution of the Central Mediterranean (Pelagian and Ionian Seas). *Geological Evolution of the Mediterranean Basin,* 215-230. doi.org/10.1007/978-1-4613-8572-1_10

Finetti I. (1984). Geophysical study of the Sicily Channel rift zone. *Bollettino di Geofisica Teorica e Applicata, 26,* 3-28

Finetti I. (1982). Structure, stratigraphy and evolution of central Mediterranean. *Bollettino di Geofisica Teorica e Applicata, 14*, 247-312

Fink P., Zimmer W., Punch S. (2012). A Mediterranean petroleum province on the North Africa Plate margin: The Sicily Channel. *The Leading Edge*, *31*(7), 794-801. doi.org/10.1190/tle31070794.1

Frohlich C. (1992). Triangle diagrams: ternary graphs to display similarity and diversity of earthquake focal mechanisms. *Physics of the Earth and Planetary Interiors*, 75(1–3), 193–198.doi.org/10.1016/0031-9201(92)90130-n

Gaidi S., Booth-Rea G., Melki F., Marzougui W., Ruano P., Pérez-Peña J.V., Azañòn J.M., Zargouni F., Chouaieb H., Galve J.P. (2020). Active fault

segmentation in Northern Tunisia. *Journal of Structural Geology, 139,* 104146. doi.org/10.1016/j.jsg.2020.104146

Galea P. (2007). Seismic history of the Maltese islands and considerations on seismic risk. *Annals of Geophysics,* 50(6). doi.org/10.4401/ag-3053

Gephart J.W., & Forsyth D.W. (1984). An improved method for determining the regional stress tensor using earthquake focal mechanism data: Application to the San Fernando Earthquake Sequence. *Journal of Geophysical Research,* 89(B11), 9305. doi.org/10.1029/jb089ib11p09305

Granath J.W., & Casero P. (2004). Tectonic setting of the petroleum systems of Sicily, in Deformation, Fluid Flow, and Reservoir Appraisal in Foreland Fold-and-Thrust Belts (Ed. By R. Swennen, F. Roure, J.W. Granath). *America Association in Petroleum Geologists Memoir*, 391–411

Grasso M., Torelli L., Mazzoldi G. (1999). Cretaceous–Palaeogene sedimentation patterns and structural evolution of the Tunisian shelf, offshore the Pelagian islands (central Mediterranean). *Tectonophysics, 315*(1-4), 235-250. doi.org/10.1016/s0040-1951(99)00285-1

Grasso M., Mazzoldi G., Torelli L. (1993). Structural and stratigraphic framework of the Tunisian shelf surrounding the islands of Lampione and Lampedusa (Pelagian Sea). *Geological Development of the Sicilian-Tunisian Platform. Report in Marine Science*, 58, 65-70

Grasso M., Reuther C.D., Tortorici L. (1992). Neotectonic deformations in SE Sicily: The Ispica fault, evidence of late Miocene-Pleistocene decoupled wrenching within the central Mediterranean stress regime. *Journal of Geodynamics*, *16*(1-2), 135-146. doi.org/10.1016/0264-3707(92)90023-l

Guidoboni E., Ferrari G., Tarabusi G., Sgattoni G., Comastri A., Mariotti D., Ciuccarelli C., Bianchi M.G., Valensise G. (2019). CFTI5Med, the new release of the catalogue of strong earthquakes in Italy and in the Mediterranean area. *Scientific Data*, 6(1). doi.org/10.1038/s41597-019-0091-9

Guidoboni E., Ferrari G., Mariotti D., Comastri A., Tarabusi G., Sgattoni G., Valensise G. (2018). CFTI5Med, Catalogo dei Forti Terremoti in Italia (461 a.C.-1997) e nell'area Mediterranea (760 a.C.-1500). Istituto Nazionale di Geofisica e Vulcanologia (INGV). doi.org/10.6092/ingv.it-cfti5

Guidoboni E., Comastri A., Traina G. (1994). Catalogue of ancient earthquakes in the Mediterranean area up to the 10th Century. ING, Roma-SGA, Bologna, 504 pp. doi.org/10.1163/221058785x01371

Gutenberg R., & Richter C.F. (1944). Frequency of earthquakes in California. *Bulletin of the Seismological Society of America*, 34(4), 185–188. doi.org/10.1785/bssa0340040185

Heidbach O., Custodio S., Kingdon A., Mariucci M.T., Montone P., Müller B., Pierdominici S., Rajabi M., Reinecker J., Reiter K., Tingay M., Williams J., Ziegler M. (2016): Stress Map of the Mediterranean and Central Europe 2016, *GFZ Data Service*, doi:10.5880/WSM.Europe2016

Holbrook W.S., Mooney W.D., Christensen N.I. (1992). The seismic velocity structure of the deep continental crust. *Continental lower crust*, *23*, 1-43

Illies J.H. (1981). Graben Formation — the Maltese Islands — a case history. In *Developments in Geotectonics* (Vol. 17, pp. 151-168). Elsevier. doi.org/10.1016/b978-0-444-41956-9.50018-6

International Seismological Centre (2022), Online Bulletin, doi.org/10.31905/D808B830

International Seismological Centre (2022), International Seismograph Station Registry (IR), doi.org/10.31905/EL3FQQ40

Ishimoto M., & Iida K. (1939). Observations of earthquakes registered with the microseismograph constructed recently. *Bulletin of the Earthquake Research Institute Tokyo*, 17, 443–478, 1939

ISIDe Working Group, (2007). Italian Seismological Instrumental and Parametric Database (ISIDe). Istituto Nazionale di Geofisica e Vulcanologia (INGV). doi.org/10.13127/ISIDE

Istituto Nazionale di Geofisica e Vulcanologia (INGV). (2005), December, 13. Rete Sismica Nazionale (RSN). Istituto Nazionale di Geofisica e Vulcanologia (INGV). doi.org/10.13127//SD/X0FXNH7QFY

Jallouli C., Mogren S., Mickus K., Turki M.M. (2013). Evidence for an east–west regional gravity trend in northern Tunisia: Insight into the structural evolution of northern Tunisian Atlas. *Tectonophysics*, *608*, 149-160. doi.org/10.1016/j.tecto.2013.10.003

Jia S. Q., Eaton D.W., Wong R.C. (2018). Stress inversion of shear-tensile focal mechanisms with application to hydraulic fracture monitoring. *Geophysical Journal International*, 215(1), 546–563. doi.org/10.1093/gji/ggy290

Jongsma D., Van Hinte J.E., Woodside J.M. (1985). Geologic structure and neotectonics of the North African Continental Margin south of Sicily. *Marine and Petroleum Geology*, 2(2), 156–179. doi.org/10.1016/0264-8172(85)90005-4

Kherchouche R., Ouyed M., Aoudia A., Mellouk B., Saadi A. (2020). Structure of the crust and uppermost mantle beneath the Sicily channel from ambient noise and earthquake tomography. *Annals of Geophysics*, 63(Vol 63 (2020). doi.org/10.4401/ag-8356

Khomsi S., Ben Jemia M.G., de Lamotte D.F., Maherssi C., Echihi O., Mezni R. (2009). An overview of the Late Cretaceous–Eocene positive inversions and Oligo-Miocene subsidence events in the foreland of the Tunisian Atlas: Structural style and implications for the tectonic agenda of the Maghrebian Atlas system. *Tectonophysics*, *475*(1), 38-58. doi.org/10.1016/j.tecto.2009.02.027

Kissling E. (1988). Geotomography with local earthquake data. *Reviews of Geophysics,* 26(4), 659–698. Portico. doi.org/10.1029/rg026i004p00659

Koulakov I. (2009). LOTOS Code for Local Earthquake Tomographic Inversion: Benchmarks for Testing Tomographic Algorithms. *Bulletin of the Seismological Society of America*, *99*(1), 194-214. doi.org/10.1785/0120080013

Ksentini A., & Romdhane N.B. (2013). Updated seismic hazard assessment of Tunisia. *Bulletin of Earthquake Engineering*, *12(2),* 647-670. doi.org/10.1007/s10518-013-9548-y

Lei J., & Zhao D. (2016). Teleseismic P-wave tomography and mantle dynamics beneath Eastern Tibet. *Geochemistry, Geophysics, Geosystems,* 17(5), 1861–1884. Portico. doi.org/10.1002/2016gc006262

Lentas K., Di Giacomo D., Harris J., Storchak D.A. (2019). The ISC Bulletin as a comprehensive source of earthquake source mechanisms. *Earth System Science Data,* 11, 565-578, doi.org/10.5194/essd-11-565-2019

Lentas K. (2018). Towards routine determination of focal mechanisms obtained from first motion P-wave arrivals. *Geophysical Journal International*, 212(3), 1665–1686. doi: 10.1093/gji/ggx503

Lipparini L., Scrocca D., Marsili P., Morandi S. (2009). Offshore Malta licence in the Central Mediterranean Sea offers hope of hydrocarbon potential. F*irst Break*, *27*(2). doi.org/10.3997/1365-2397.27.1296.28789

Locati M., Camassi R., Rovida A., Ercolani E., Bernardini F., Castelli V., Caracciolo C.H., Tertulliani A., Rossi A., Azzaro., D'Amico S., Antonucci A. (2022). Database Macrosismico Italiano (DBMI15), version 4.0. Istituto Nazionale di Geofisica e Vulcanologia (INGV). doi.org/10.13127/DBMI/DBMI15.4

Lodolo E., Civile D., Zanolla C., Geletti R. (2012). Magnetic signature of the Sicily Channel volcanism. *Marine Geophysical Research, 33(1),* 33-44. doi.org/10.1007/s11001-011-9144-y

Lu R., Liu Y., Xu X., Tan X., He D., Yu G., Cai M., Wu X. (2019). Three-Dimensional Model of the Lithospheric Structure Under the Eastern Tibetan Plateau: Implications for the Active Tectonics and Seismic Hazards. *Tectonics*, 38(4), 1292–1307. Portico. doi.org/10.1029/2018tc005239

Lund B., & Slunga R. (1999). Stress tensor inversion using detailed microearthquake information and stability constraints: Application to Ölfus in southwest Iceland. *Journal of Geophysical Research: Solid Earth*, 104(B7), 14947–14964. Portico. doi.org/10.1029/1999jb900111

Makris J., Nicolich R., Weigel W. (1986). A seismic study in the Western Ionian Sea. *Annales Geophysicae, Series B: Terrestrial and Planetary Physics,* 4(6), 665-678

Mahood G., & Hildreth W. (1983). Nested calderas and trapdoor uplift at Pantelleria, Strait of Sicily. *Geology*, *11*(12), 722-726. doi.org/10.1130/0091-7613(1983)11<722:ncatua>2.0.co;2

Martínez-Garzón P., Ben-Zion Y., Abolfathian N., Kwiatek G., Bohnhoff M. (2016). A refined methodology for stress inversions of earthquake focal mechanisms. *Journal of Geophysical Research: Solid Earth*, 121(12), 8666–8687. Portico. doi.org/10.1002/2016jb013493

Meccariello M. (2017). Tectonic evolution and current deformation of the NW Sicily Channel and the Lampedusa Plateau based on multi-resolution seismic profiles analysis (Doctoral dissertation, Ph. D. thesis, Università degli studi di Napoli Federico II)

MedNet Project Partner Institutions. (1990). Mediterranean Very Broadband Seismographic Network (MedNet). Istituto Nazionale di Geofisica e Vulcanologia (INGV). doi.org/10.13127/SD/FBBBTDTD6Q

Mele G. (2011). Mapping the Moho Across the Northern and Central Apennine Chain and Eastern Sicily-The Teleseismic Receiver Functions Method. *THE EARTH EXPANSION EVIDENCE–A Challenge for Geology, Geophysics and Astronomy*

Michael A.J. (1987). Use of focal mechanisms to determine stress: A control study. *Journal of Geophysical Research*, 92(B1), 357. doi.org/10.1029/jb092ib01p00357

Michael A.J. (1984). Determination of stress from slip data: Faults and folds. *Journal of Geophysical Research: Solid Earth*, 89(B13), 11517–11526. Portico. doi.org/10.1029/jb089ib13p11517

Micallef A., Camerlenghi A., Garcia-Castellanos D., Cunarro Otero D., Gutscher M.A., Barreca G., Spatola D., Facchin L., Geletti R., Krastel S., Gross F., Urlaub M. (2018). Evidence of the Zanclean megaflood in the eastern Mediterranean Basin. *Scientific Reports*, *8*(1), 1078. doi.org/10.1038/s41598-018-19446-3

Milano M., Kelemework Y., La Manna M., Fedi M., Montanari D., Iorio M. (2020). Crustal structure of Sicily from modelling of gravity and magnetic anomalies. Scientific Reports, 10(1), 1–18. doi.org/10.1038/s41598-020-72849-z

Mooney W.D. (2010). Crust and Lithospheric Structure – Global Crustal Structure. *Seismology and Structure of the Earth: Treatise on Geophysics*, *1*, 361-417. doi.org/10.1016/b978-044452748-6/00011-0

Mooney W.D., Laske G., Masters T.G. (1998). CRUST 5.1: A global crustal model at 5° × 5°. *Journal of Geophysical Research: Solid Earth, 103*(B1), 727-747. doi.org/10.1029/97jb02122

Morelli C. (1975). The Gravity Map of Italy. In L. Ogniben, M. Parotto, A. Praturlon (Eds.) *Structural Model of Italy*, CNR, Quad. Ric. Sci., 90, 427-447

Napoli G., Nigro F., Favara R., Renda P., Salvaggio G. (2015). Deformation history during chain building deduced by outcrop structural analysis: The case of the Sicilian fold-and-thrust belt (Central Mediterranean). *Journal of Geodynamics*, *91*, 26-38. doi.org/10.1016/j.jog.2015.08.003

Nuannin P., Kulhánek O., Persson L. (2012). Variations of b-values preceding large earthquakes in the Andaman–Sumatra subduction zone. Journal of Asian Earth Sciences, 61, 237–242. doi.org/10.1016/j.jseaes.2012.10.013

Orecchio B., Presti D., Totaro C., Guerra I., Neri G. (2011). Imaging the velocity structure of the Calabrian Arc region (southern Italy) through the integration of different seismological data. *Bollettino di Geofisica Teorica ed Applicata*, *52*(4)

Palano M., Ursino A., Spampinato S., Sparacino F., Polonia A., Gasperini L. (2020). Crustal deformation, active tectonics and seismic potential in the Sicily Channel (Central Mediterranean), along the Nubia–Eurasia plate boundary. *Scientific reports*, 10(1), 1-14. doi.org/10.1038/s41598-020-78063-1

Peccerillo A. (2005). *Plio-Quaternary volcanism in Italy* (Vol. 365). New York: Springer-Verlag Berlin Heidelberg. doi.org/10.1007/3-540-29092-3

Pondrelli S., Salimbeni S., Morelli A., Ekström G., Postpischl L., Vannucci G., Boschi E. (2011). European–Mediterranean Regional Centroid Moment Tensor catalog: Solutions for 2005–2008. *Physics of the Earth and Planetary Interiors*, 185(3–4), 74–81. doi.org/10.1016/j.pepi.2011.01.00

Pondrelli S. (2002). European-Mediterranean Regional Centroid-Moment Tensors Catalog (RCMT) [Data set]. Istituto Nazionale di Geofisica e Vulcanologia (INGV). doi.org/10.13127/rcmt/euromed

Reuther C.D., Ben-Avraham Z., Grasso M. (1993). Origin and role of major strike-slip transfers during plate collision in the central Mediterranean. *Terra Nova*, *5*(3), 249-257. doi.org/10.1111/j.1365-3121.1993.tb00256.x

Reuther C.D., & Eisbacher G.H. (1985). Pantelleria Rift — crustal extension in a convergent intraplate setting. *Geologische Rundschau*, *74(3*, 585-597. doi.org/10.1007/bf01821214

Reyes C., & Wiemer S. (2019). ZMAP7: a refreshed software package to analyze seismicity. *Geophysical Research Abstracts* (vol.21)

Rodríguez-Pérez Q., Márquez-Ramírez V.H., Zúñiga F.R. (2020). Seismicity characterization of oceanic earthquakes in the Mexican territory. *Solid Earth*, 11(3), 791–806. doi.org/10.5194/se-11-791-2020

Rodríguez-Pérez Q. & Zúñiga F.R. (2018). Imaging b-value depth variations within the Cocos and Rivera plates at the Mexican subduction zone. *Tectonophysics*, 734, 33–43. doi.org/10.1016/j.tecto.2018.03.019

Romagnoli C., Belvisi V., Innangi S., Di Martino G., Tonielli R. (2020). New insights on the evolution of the Linosa volcano (Sicily Channel) from the study of its submarine portions. *Marine Geology*, *419*, 106060. doi.org/10.1016/j.margeo.2019.106060

Rotolo S.G., Castorina F., Cellura D., Pompilio M. (2006). Petrology and geochemistry of submarine volcanism in the Sicily Channel Rift. *The Journal of Geology*, *114*(3), 355-365. doi.org/10.1086/501223

Rovida A., Locati M., Camassi R., Lolli, B., Gasperini P., Antonucci A. (2022). Catalogo Parametrico dei Terremoti Italiani (CPTI15), versione 4.0. Istituto Nazionale di Geofisica e Vulcanologia (INGV). doi.org/10.13127/CPTI/CPTI15.4

Rovida A., Locati M., Camassi R., Lolli B., Gasperini P. (2020). The Italian earthquake catalogue CPTI15. *Bulletin of Earthquake Engineering*, 18(7), 2953-2984. doi.org/10.1007/s10518-020-00818-y

Rovida A., Locati M., Antonucci A., Camassi R. (2017). Archivio Storico Macrosismico Italiano (ASMI). *Isituto Nazionale di Geofisica e Vulcanologia (INGV).* doi.org/10.13127/asmi

Rovida A., Camassi R., Gasperini P., Stucchi M. (2011). Catalogo Parametrico dei Terremoti Italiani (CPTI11). Istituto Nazionale di Geofisica e Vulcanologia (INGV), Milano, Bologna. http://emidius.mi.ingv.it/CPTI

Scarascia S., Cassinis R., Lozej A., Nebuloni A. (2000). A seismic and gravimetric model of crustal structures across the Sicily Channel Rift Zone. *Bollettino della Società Geologica Italiana*, *119*(1), 213-222

Scarascia S., Lozej A., Cassinis R. (1994). Crustal structures of the Ligurian, Tyrrhenian and Ionian seas and adjacent onshore areas interpreted from wide-angle seismic profiles. *Bollettino di Geofisica Teorica ed Applicata*, *36*(141-44), 5-20

Schorlemmer D., Wiemer S., Wyss M. (2005). Variations in earthquake-size distribution across different stress regimes. *Nature*, 437(7058), 539–542. doi.org/10.1038/nature04094

Schorlemmer D., & Wiemer S. (2005). Microseismicity data forecast rupture area. Nature, 434(7037), 1086–1086. doi.org/10.1038/4341086a

Scognamiglio L., Tinti E., Quintiliani M. (2006). Time Domain Moment Tensor (TDMT) [Data set]. Istituto Nazionale di Geofisica e Vulcanologia (INGV). doi.org/10.13127/TDMT

Stampfli G.M., Borel G.D., Cavazza W., Mosar J., Ziegler P.A. (2001). Palaeotectonic and palaeogeographic evolution of the western Tethys and PeriTethyan domain (IGCP Project 369). Episodes, 24(4), 222-228. doi.org/10.18814/epiiugs/2001/v24i4/001

Tan X., Liu Y., Lee Y.H., Lu R., Xu X., Suppe J., Shi F., Xu C. (2019). Parallelism between the maximum exhumation belt and the Moho ramp along the eastern Tibetan Plateau margin: Coincidence or consequence? *Earth and Planetary Science Letters*, 507, 73–84. doi.org/10.1016/j.epsl.2018.12.001

Torelli L., Carrara G., Sartori R., Zitellini N. (2000). Cenozoic collisional and extensional structures among Sardinia, Sicily and Tunisia (Central Mediterranean): examples and constraints from seismic reflection profiles. In *CIESM Workshop Ser* (Vol. 10, pp. 53-55)

Torelli L., Grasso M., Mazzoldi G., Peis D., Gori D. (1995). Cretaceous to Neogene structural evolution of the Lampedusa shelf (Pelagian Sea, Central Mediterranean). *Terra Nova*, 7(2), 200-212. doi.org/10.1111/j.1365-3121.1995.tb00689.x

Thurber C.H. (1993). Local earthquake tomography: velocities and Vp/Vs - Theory. *Seismic tomography: Theory and practice*, chapter 20, 563-583, eds Iyer, H.M., & Hirahara K., Chapman and Hall, London

University of Malta. (2014). Malta Seismic Network (Data set). International Federation of Digital Seismograph Networks. doi.org/10.7914/SN/ML

Vavryčuk V. (2014). Iterative joint inversion for stress and fault orientations from focal mechanisms, *Geophysical Journal International*, 199, 69-77, doi: 10.1093/gji/ggu224

Ventura B.M., Serpelloni E., Argnani A., Bonforte A., Bürgmann R., Anzidei M., Baldi P., Puglisi G. (2014). Fast geodetic strain-rates in eastern Sicily (southern Italy): New insights into block tectonics and seismic potential in the area of the great 1693 earthquake. *Earth and Planetary Science Letters*, *404*, 77-88. doi.org/10.1016/j.epsl.2014.07.025

Waldhauser F., & Ellsworth, W.L. (2000). A double-difference earthquake location algorithm: Method and application to the northern Hayward fault, California. *Bulletin of the seismological society of America*, *90*(6), 1353-1368

Washington H.S. (1909). Submarine Eruptions of 1831 and 1891 near Pantelleria. *American Journal of Science (1880-1910)*, *27*(158), 131-150. doi.org/10.2475/ajs.s4-27.158.131

Wiemer S. (2001). A software package to analyze seismicity: ZMAP. *Seismological Research Letters*, 72(3), 373-382. doi.org/10.1785/gssrl.72.3.373

Wiemer S., & Wyss M. (2000). Minimum magnitude of completeness in earthquake catalogs: Examples from Alaska, the western United States, and Japan. *Bulletin of the Seismological Society of America*, *90*(4), 859-869

Winnock E., & Bea F. (1979). D. -Structure de la mer Pélagienne/Structure of the Pelagian sea (Templeton R.S.M., & Desprat R.). *Géologie Méditerranéenne*, *6*(1), 35-40. doi.org/10.3406/geolm.1979.1068

Wu J., Suppe J., Lu R., Kanda R. (2016). Philippine Sea and East Asian plate tectonics since 52 Ma constrained by new subducted slab reconstruction methods. *Journal of Geophysical Research: Solid Earth*, *121*, 4670–4741. doi.org/10.1002/2016JB012923

Wyss M. (1973). Towards a Physical Understanding of the Earthquake Frequency Distribution. *Geophysical Journal International*, 31(4), 341–359. doi.org/10.1111/j.1365-246x.1973.tb06506.x

ACKNOWLEDGMENT

I want to thank those who supported me during these years of research. First, I would like to thank my tutor, Prof. Attilio Sulli, for his availability and professionalism. I thank the co-tutors for their cooperation and support, il Prof. Raffaele Martorana e il Prof. Sebastiano D'Amico. I would like to thank colleagues in the Department of Mathematics, Computers Sciences, Physics, and Earth Sciences of the University of Messina for their collaboration in the work and data integration. In particular, I would like to thank Dr. Cristina Totaro, Prof. Barbara Orecchio, Prof. Debora Presti, and Dr. Silvia Scolaro. I would also like to thank Prof. Agius Mattew of the Department of Geosciences, University of Malta, for providing much of the earthquake data I have been working on.

I thank those close to and supporting me, from family to friends.

Appendix A

TABLE A1. WELL LIST. ARE REPORTED THE NAME OF WELLS IN ALPHABETICAL ORDER, GEOGRAPHICAL COORDINATES (ETRS89), SEABED DEPTH (IN METERS, MEASURED BY THE DIFFERENCE BETWEEN ROTATION TABLE DEPTH AND THE SEABED UNDER THE ROTARY TABLE), AND TOTAL DRILLING DEPTH.

Well name	X (E)	Y (N)	Seabed depth (m)	Total drilling depth (m)
ACATE-001-DIR	442086	4094343.1	3	-3380.1
ACATE-002	441072.9	4095398.1	2	-3366.1
ACATE-003	439203	4097321.7	5	-3181.5
ALFA-001	255907.9	4148127.3	-60	-2715.5
ARCHIMEDES-001	467819.5	4054456.6	-71.5	-5020.5
ARETUSA-001	495445	4038791	-83	-3728
AVOLA-001	505771.3	4091674.3	503	-1958.7
BIDDINE-001	456157.8	4101606.4	240	-2105.4
BIDDUSA-001	292312	4184392.4	103	-2392.8
BIDDUSA-002	290917.5	4165365.5	160	-1843.3
BIMMISCA-001	507096.3	4073748.3	25	-3137.6
CAMPOBELLO-001	296509.5	4168339.9	80	-883.6
CAPO NEGRO-001	515512.6	4088502.4	24	-2096
CARLA-001	291447.9	4126246.4	-161.84	-3666.6
CARRUBO-001	496740.4	4069075.7	56	-3681.4
CASSIBILE-001	516623.2	4092772.9	56	-1451
CATANIA-011	504605.2	4146899.8	14	-1066.4
CATANIA-012	503378.1	4144310.8	15	-1106.4
CATANIA-013	505945.9	4143880.8	5	-691.4
CATANIA-014	505525.4	4148194.6	27	-839.4
CERNIA-001	512051.6	4018278.9	-96	-4331.7
CHELBI-001	286273.5	4182921.6	133	-1019
CIANCIANA-001	336932.7	4152090.6	55	-2148.2
CISINA-007	494483.4	4143788.2	20	-1386.6
CONTRADA TRIGLIA-001	282493.2	4173090.9	15	-2392.3
CONTRADA ULMO-001	449715.4	4107390.7	200	-2605.2
CORVI	281353.8	4191373.4	48	-1226
CORVINA MARE-001	228284.1	4136616.9	-95.5	-3073.5
COZZO SCALIA-001	501908.8	4069934	36	-3207.7
DELFINO-001	444858.7	4069558.1	-135.5	-4415
DITTAINO-001	492116.9	4141022.3	25	-1134
EGERIA-001	362780.7	4062909.1	-272.5	-4924
ERACLEA SICILIA-001	352288.8	4137113.7	13	-2009.2
ERMIONE-001	173683.6	4147166.8	-361	-2814
EVA-001	470736.8	4033552.2	-141.5	-3543.5
GABBIANO-001	477685.6	4041997	-114	-3322
GENZIANA-001	397410.9	4095303.1	-89	-3974
GENZIANA-001-DIR-A	397410.9	4095303.1	-89	-5574
GIADA-001	432883.9	4084284.5	-108	-2536.5
LEONE-001	370428.5	4118616	-27.7	-2653.9
LUCATA-001	470111.1	4054261.9	-83.2	-4393
MADDALENA-001	527809.6	4096623.1	54	-1706.9
MANFRIA-002	419037.5	4107475.9	6.5	-5894.2
MARINELLA-001	309462.3	4163113.5	50	-1347.2
MARINELLA-002	309786.5	4163877	55	-1343.1
MARINELLA-003	310179.2	4161740.2	30	-1166.6
MARZAMEMI-001	510251.5	4066433.2	2	-3510.6
MENFI-001	317752.9	4163876.7	95	-1581.7

MERLUZZO MARE-001	452081.7	4056909.2	-94	-2882.5
MILA-001	455981.8	4066001.8	-54.5	-3630.5
MILA-002	453378.4	4066108.2	-82	-3870.5
MILA-002-BIS	453378.4	4066108.2	-82	-3870.5
MILA-003	455991.9	4066371.6	-49	-3664.6
MILA-004	456421.7	4066281	-51.6	-3676.4
MILA-004-DIR	456421.7	4066281	-51.5	-3659
MILA-005	455633.8	4065849.6	-58.2	-3665.6
MILA-006	454456	4065715	-67	-3665
MILA-006-DIR	454456	4065715	-67	-3579
MILA-007	454456	4065715	-66	-3697
MILA-008-DIR	454456	4065715	-66	-3869
MILA-009	454456	4065715	-66	-3756
MONTEROSSO-001	477622.1	4105933.8	452	-763.2
MOZIA-001	278627.3	4196402.4	10	-2485.6
MS-A1	494966.4	3987870.8	-30	-5000
NADA-001	267004.6	4189271.5	-38	-3331
NAILA-001	233536	4160443.1	-124	-2049
NANDA-001	266597.6	4150532.8	-72.5	-2707
NARCISO-001-DIR	271666.8	4197591.6	-12	-2201.6
NARCISO-001-DIR-A	271666.8	4197591.6	-12	-1397.6
NARCISO-002	271215.2	4196379.7	-21	-844.6
NARCISO-003	270705.6	4196310.7	-21	-1678.5
NAUSICAA-001	238540.5	4165653.4	-174	-2228
NELLA-001	230361.8	4157274.4	-109.5	-1641
NERINA-001	241320.4	4160320.2	-93	-1902
NETTUNO-001	220008.5	4158958.6	-70	-1243
NILDE-001	227514.9	4159506	-107	-314
NILDE-001-BIS	227501.7	4159552.8	-106	-3488
NILDE-002	225319	4157161.9	-94.5	-2110
NILDE-003	228098.4	4160663.7	-105	-1700
NILDE-003-BIS	228098.4	4160663.7	-105	-2751
NILDE-004-DIR	226509	4157086.8	-100.5	-1778
NILDE-005	223861.1	4155811.5	-86	-1597
NILDE-006	225080	4157888.3	-93	-1667
NILDE-OVEST-001	228857.8	4165379.3	-107.7	-2196
NINFEA-001	263605.9	4187537.2	-77	-2454
NIOBE-001	248278.3	4172845.8	-117	-2082.5
NOEMI-001	256856.1	4190295.8	-143	-2440
NORA-NORD-001	246449.3	4161227.4	-96.4	-3836
NORMA-001	240554	4163929.6	-99	-2093
NUCCIA-001	266066.8	4169790.6	-120	-2442
NUNZIA-001	233643.6	4143018.3	-85.5	-2224
OLGA-001	312553.5	4123138.7	-150.5	-2526.5
ONDA-001	307403.8	4158905.6	-34.15	-1900.7
ORESTE-001	527069.4	4019669.7	-156	-2711
ORIONE-EST-001	321930.6	4142575.1	-78	-2178
ORLANDO-001	233107.2	4123177.1	-113	-3856
ORLANDO-002	235453.4	4123169.8	-102	-2252.5
OSCAR-OVEST-001	281341.8	4151070.4	-98	-2307
PACHINO-004	505230.9	4061388.9	22	-4975.5
PALAZZOLO-001	494328.5	4098151.5	611.4	-1814
PALMA-001	387255.5	4095719.3	-167.6	-4152.6
PALMA-002	382680.3	4099323	-162	-3795
PALMA-003	389708.1	4095560.6	-140.8	-3449.4
PAMELA-001	341658	4125884.8	-166	-527
PAMELA-001-BIS	342160.8	4125852	-156	-2970
PANCRAZIO-SUD-001	443061.4	4075943.5	-77.5	-3611

PAOLA-EST-001	279726.6	4098405.1	-113	-4977
PATTY-EST-001	408447.8	4094861.4	-69	-3806.7
PELLICANO-OVEST-001	439097	4071918.4	-145	-4515
PERLA-001	430308.4	4089981.7	-66	-4041
PERLA-002	428923.2	4089962.4	-75	-2700
PIERA-001	267197.9	4100490.7	-105	-1197
PILADE-EST-001	513283.7	4022182.5	-98	-3367
PINA-001	334667.9	4132149.3	-135	-2307.5
PLINIO-SUD-001	435007.2	4083314.2	-100	-4299.5
POGGI-003	431338.5	4110158.6	54	-793.4
POLPO-001	523766.9	4053128.9	-54	-5041
PONTE OLIVO-001	442119.3	4113941.9	80	-3594.6
PORTO PALO-001	509883.6	4058452	2	-1845.5
PREZIOSO-001	414956.3	4095669.1	-49	-4388.2
RABBITO-001	426408.2	4106422.2	7	-4962.6
REMO-NORD-001	281961.2	3937012.1	-94	-5005
RICCIO-SUD-001	254942.8	3931317.3	-70	-4951
RIGOLIZIA-001	493981.6	4096826.8	635	-1881.8
RIZZO-002	501191.5	4142769.4	9	-1252.1
RIZZO-003	499889	4141783.3	12	-888.4
ROSA-001	514098.8	4079426.3	-22.5	-3211
S. CROCE CAMERINA-001	456628.5	4079390.7	85	-826.6
S. CROCE CAMERINA-002	456315.7	4078760.6	80	-2865.5
S. DEMETRIO-001	502691.1	4134810	140	-1404.7
SAMANTA-001	221221.9	4143103	-87	-2517
SANTUZZA-001	223984.5	4148381.8	-89	-2407
SCICLI-001	477552.8	4069892.9	225	-4473.9
SCICLI-002	473862.2	4070797	225	-3078.5
SETTEFARINE-001	433855.9	4108671.6	75	-4630.7
SIMETO-001	499608.3	4142229.5	11	-965.75
SIRACUSA-001	508809	4095041.7	325	-2719
SIRIO-001	265939.7	4145894.3	-69.8	-2554.6
SOFIA-001	219477.6	4148360.1	-81.48	-2436.2
SPADA MARE-001	484536.4	4048692.9	-83.82	-3631.8
SPIGOLA MARE-001	505508.6	4013961.1	-86	-3275
TULLIA-001	243745.6	4176058	-284	-2009.5
ULISSE-001	485062.3	4026186.3	-108.5	-4656
URSITTO-001	444163.9	4115037.4	110	-3700.5
VALLE TORTA-001	441561.7	4098938.2	31.8	-3883.5
VALLO-001	255027.5	4157870.6	-68	-2724.2
VENERE-001	328749	4137255.3	-121	-2899.5
VERA-001	504360.4	4046732.7	-53	-1878
VITTORIA-003	451956	4095637	155	-2358.3
VITTORIA-004	459277.3	4096861.8	213	-2059.1
VITTORIA-OVEST-001	454923.4	4088995.4	151	-2262.1
ZAGARA-001	332039.7	4137816.1	-84.5	-2487.5

TABLE A2. EARTHQUAKE LIST. THE NUMBER DESIGNATED TO EACH EVENT ARE REPORTED, DATE, TIME (UTC), LATITUDE, LONGITUDE, DEPTH (KILOMETERS), MAGNITUDE, MAGNITUDE TYPE, AND CATALOG.

N.	Date	Time (UTC)	Lat	Lon	Depth (km)	Mag	Mag type	Catalog
1	2005-01-02	02:05:56.99	35.86	13.06	10	3.0	ML	INGV
2	2005-01-05	21:16:50.10	36.42	10.76	10	3.6	MD	ISC
3	2005-01-08	16:59:15.53	36.62	14.76	5	3.1	MD	INGV
4	2005-01-15	01:08:51.84	35.7	14.43	10	3.2	MD	INGV
5	2005-02-07	20:05:39.00	36.29	10.82	14	4.9	Mw	ISC
6	2005-02-07	20:46:26.91	36.26	10.83	10	5.1	Mw	ISC
7	2005-02-07	22:50:07.60	36.22	10.85	8.4	3.1	MD	ISC
8	2005-02-08	01:24:49.10	36.11	10.96	10	3.2	MD	ISC
9	2005-02-08	01:49:39.30	36.16	10.78	26.4	3.2	MD	ISC
10	2005-02-08	18:40:04.60	36.21	10.92	0.3	4.2	MD	ISC
11	2005-02-10	19:15:23.80	36.25	10.98	10	3.0	MD	ISC
12	2005-02-13	18:40:37.50	33.69	10.25	10	3.4	MD	ISC
13	2005-02-23	04:42:55.85	36.76	10.61	10	3.3	ML	ISC
14	2005-02-27	01:55:21.89	33.75	13.63	10	3.5	Mb	ISC
15	2005-03-17	18:57:15.95	37.41	15.96	10	3.1	ML	INGV
16	2005-03-20	02:18:17.08	36.63	14.38	10	3.0	MD	INGV
17	2005-03-22	09:51:53.70	36.41	10.69	19.1	3.4	MD	ISC
18	2005-04-09	09:55:32.30	34	10.33	5.2	3.5	MD	ISC
19	2005-04-13	13:19:19.88	37.5	16.33	24	3.4	ML	INGV
20	2005-04-19	08:47:35.30	37.9	14.71	26.4	3.0	ML	ISC
21	2005-04-20	10:03:10.80	37.14	14.52	48	3.1	ML	ISC
22	2005-04-20	16:56:13.20	34.24	10.02	10	4.4	MD	ISC
23	2005-04-21	12:53:40.09	37.83	14.99	21.7	3.0	ML	INGV
24	2005-04-21	17:11:52.70	37.83	14.96	24.3	3.1	ML	ISC
25	2005-04-22	15:40:49.90	35.47	15.17	7.2	3.9	Mb	INGV
26	2005-05-06	22:10:31.75	33.76	14.02	0	3.2	Mb	ISC
27	2005-05-13	15:19:50.70	37.64	15.15	4.1	3.0	ML	ISC
28	2005-05-20	03:11:12.20	35.88	10.28	2.5	3.3	MD	ISC
29	2005-05-22	20:20:31.51	37.8	14.64	24.2	3.4	ML	INGV
30	2005-05-23	21:30:39.10	37.67	15.7	34.1	4.1	ML	ISC
31	2005-05-30	21:19:37.99	36.26	15.28	17.5	3.0	ML	INGV
32	2005-05-30	22:19:14.17	37.68	10.96	9.4	3.6	Mb	INGV
33	2005-06-02	06:26:26.40	36.46	10.4	18.2	3.5	MD	ISC
34	2005-06-02	06:32:38.00	36.73	10.84	29.2	3.2	MD	ISC
35	2005-06-02	18:33:35.90	35.92	13.02	8.8	3.6	ML	ISC
36	2005-06-06	04:22:49.90	36.56	15.81	28.3	4.0	ML	ISC
37	2005-06-15	16:03:35.80	37.57	16.25	37.6	3.4	ML	ISC
38	2005-06-19	07:22:40.80	37.63	15.23	29.7	3.5	ML	ISC
39	2005-06-27	03:02:16.89	36.06	11.37	10	4.0	Mb	ISC
40	2005-06-27	04:53:20.80	35.7	11.26	10	3.2	ML	ISC
41	2005-06-27	05:11:15.79	35.93	11.49	10	3.6	Mb	ISC
42	2005-06-27	05:37:49.07	35.89	11.4	10	3.4	ML	ISC
43	2005-06-28	23:38:07.10	35.82	11.72	12.5	3.4	ML	INGV

44	2005-07-07	08:59:51.20	37.3	13.94	27.4	3.8	ML	ISC
45	2005-07-08	03:36:28.10	37.31	15.79	28.5	3.2	ML	ISC
46	2005-07-10	13:38:50.88	37.84	14.99	28.8	3.6	ML	INGV
47	2005-07-16	09:34:42.82	37.26	13.28	29.4	3.5	ML	INGV
48	2005-07-16	23:45:16.21	34.59	14.99	17.4	3.1	ML	INGV
49	2005-07-16	23:47:23.73	34	14.1	12.5	3.8	ML	INGV
50	2005-08-14	21:45:05.40	37.81	15.17	4.2	3.0	MD	ISC
51	2005-08-14	21:56:50.10	37.79	15.17	4.1	3.2	ML	INGV
52	2005-08-14	22:02:27.08	37.8	15.17	5	3.0	ML	INGV
53	2005-08-15	16:59:59.29	37.09	10.59	10	4.4	Mb	ISC
54	2005-08-18	16:59:55.20	36.48	10.1	33.8	3.6	MD	ISC
55	2005-08-29	16:46:08.30	36.68	10.67	3.7	3.1	MD	ISC
56	2005-08-29	21:19:33.77	36.2	16.14	9.1	3.0	ML	INGV
57	2005-08-31	03:49:22.80	36.72	10.59	5.3	3.3	MD	ISC
58	2005-09-04	18:59:38.11	35.53	15.64	12.5	3.2	ML	INGV
59	2005-10-01	08:35:21.43	36.79	14.3	21.3	3.6	ML	INGV
60	2005-10-01	08:41:43.92	36.79	14.31	20.5	3.6	ML	INGV
61	2005-10-21	22:13:00.18	37.66	15.13	5	3.2	ML	INGV
62	2005-10-27	19:19:26.93	35.82	11.51	12.5	4.0	Mb	INGV
63	2005-10-28	13:59:05.59	37.67	15.13	3.3	3.1	ML	INGV
64	2005-10-29	18:16:51.23	35.92	11.3	12.5	3.4	ML	INGV
65	2005-10-29	18:36:37.67	35.79	11.25	12.5	3.4	ML	INGV
66	2005-10-30	05:42:11.77	37.62	15.06	6.6	3.1	ML	INGV
67	2005-10-30	06:06:49.76	37.62	15.06	8	3.6	ML	INGV
68	2005-10-30	13:41:53.85	36.06	11.94	12.5	3.3	ML	INGV
69	2005-10-31	00:02:41.02	37.64	15.07	13.6	3.5	ML	INGV
70	2005-11-03	09:19:04.45	37.97	14.26	1.4	3.1	ML	INGV
71	2005-11-04	14:45:36.89	37.57	14.9	16.9	3.0	ML	INGV
72	2005-11-11	15:55:27.70	37.88	13	19.5	3.1	ML	ISC
73	2005-11-16	09:37:27.80	35.92	11.43	10	4.1	Mb	ISC
74	2005-11-21	10:57:40.23	37.6	14.11	63.2	4.6	Mw	INGV
75	2005-12-12	04:51:27.50	37.74	14.94	23.7	3.9	ML	ISC
76	2005-12-12	05:04:15.82	37.74	14.96	28.2	3.0	ML	INGV
77	2005-12-12	05:10:30.40	37.73	14.96	25.7	3.4	ML	ISC
78	2005-12-24	15:08:03.80	37.46	16.21	41.4	4.0	ML	ISC
79	2006-01-05	05:34:39.30	37.95	15.6	33.3	3.5	ML	ISC
80	2006-01-08	13:26:27.60	37.66	14.98	12.5	3.3	ML	ISC
81	2006-01-08	13:28:03.30	37.67	14.97	13.3	3.0	ML	ISC
82	2006-01-08	13:59:56.74	37.66	14.98	13.5	3.2	ML	INGV
83	2006-01-08	15:01:37.70	37.67	15.01	10	3.0	ML	ISC
84	2006-01-08	15:08:50.10	37.66	14.96	12.3	3.4	ML	ISC
85	2006-01-08	16:09:24.18	37.68	14.98	14.9	3.5	Mb	INGV
86	2006-01-08	17:12:41.09	37.67	14.99	12.3	3.1	ML	INGV
87	2006-01-08	17:21:58.14	37.67	14.98	13.4	3.3	ML	INGV
88	2006-01-08	18:21:21.70	37.67	14.96	13.8	3.1	ML	ISC
89	2006-01-09	01:15:57.70	37.72	15.14	5	3.5	ML	ISC
90	2006-01-16	13:53:24.63	36.68	10.98	10	3.2	ML	INGV
91	2006-01-19	05:58:37.50	36.99	12.89	0	3.7	Mb	ISC

92	2006-01-20	14:20:46.30	37.74	14.53	30.5	3.6	ML	ISC
93	2006-01-26	22:31:59.40	37.54	16.16	38.2	3.7	ML	ISC
94	2006-02-03	22:15:40.57	33.43	14.19	10	4.2	Mb	INGV
95	2006-02-05	18:34:32.42	36.8	12.77	10	3.2	ML	INGV
96	2006-02-05	21:15:58.75	36.84	12.84	10	3.9	ML	INGV
97	2006-02-24	13:25:09.90	35.82	10.8	19.7	3.1	MD	ISC
98	2006-03-02	20:35:38.08	37.8	14.94	24.7	3.4	ML	INGV
99	2006-03-13	15:38:54.55	36.22	12.99	10	3.2	ML	INGV
100	2006-03-13	18:04:55.46	35.15	12.57	10	3.8	ML	INGV
101	2006-03-15	20:33:12.25	36.05	13.04	10	3.3	ML	INGV
102	2006-03-21	19:39:02.10	35.62	10.51	1.4	3.0	ML	ISC
103	2006-03-24	20:07:22.00	37.81	14.84	26	3.7	ML	ISC
104	2006-03-29	20:19:59.74	37.7	13.84	5	3.9	Mw	INGV
105	2006-03-31	13:59:45.88	37.71	13.82	5	3.0	ML	INGV
106	2006-04-17	08:43:55.90	36.95	16.4	32.4	4.0	ML	ISC
107	2006-04-23	14:42:38.19	37.04	15.05	23.9	3.9	Mw	INGV
108	2006-05-03	21:37:50.69	37.06	16.1	8.7	3.2	ML	INGV
109	2006-05-07	15:47:48.00	36.33	12.79	10	3.3	ML	INGV
110	2006-05-08	04:05:11.83	36.32	12.78	10	3.5	ML	INGV
111	2006-05-08	20:42:59.50	36.19	12.81	10	3.0	ML	INGV
112	2006-05-20	05:50:44.60	37.65	14.99	10.2	3.0	ML	ISC
113	2006-05-20	05:56:39.46	37.66	14.97	13.6	3.0	ML	INGV
114	2006-05-20	06:05:59.61	37.66	14.98	11	3.0	ML	INGV
115	2006-05-20	07:05:56.16	37.66	14.96	17.7	3.7	Mw	INGV
116	2006-05-20	07:30:42.38	37.65	14.99	10.3	3.0	ML	INGV
117	2006-05-30	11:38:34.50	37.62	16.47	38.2	3.5	ML	INGV
118	2006-05-31	13:56:57.60	37.63	16.44	38.1	3.2	ML	ISC
119	2006-06-06	02:52:41.21	35.09	13.28	10	3.2	ML	INGV
120	2006-06-08	22:06:47.00	37.6	15.19	3	3.1	MD	ISC
121	2006-06-16	18:17:55.04	35.96	12.72	10	3.4	ML	INGV
122	2006-06-16	18:33:57.97	35.88	12.74	10	3.0	ML	INGV
123	2006-06-16	18:36:12.80	35.79	12.65	10	3.0	MD	ISC
124	2006-06-16	23:28:44.72	35.78	12.61	10	3.1	ML	INGV
125	2006-06-17	00:56:01.03	35.86	12.7	10	3.1	ML	INGV
126	2006-06-17	01:43:53.43	35.49	12.71	10	3.0	ML	INGV
127	2006-06-17	02:13:18.98	35.92	12.72	10	3.1	ML	INGV
128	2006-06-19	15:11:57.00	37.83	14.85	28.6	3.5	ML	ISC
129	2006-06-19	20:55:34.74	37.83	14.89	26.4	3.5	Mb	INGV
130	2006-06-19	21:20:12.93	37.83	14.88	26.8	3.0	ML	INGV
131	2006-06-19	21:27:12.38	37.82	14.87	25.5	3.0	ML	INGV
132	2006-06-20	13:16:35.48	37.83	14.86	25.4	3.2	ML	INGV
133	2006-06-21	07:17:49.63	37.83	14.83	25.4	3.2	ML	INGV
134	2006-06-28	19:39:44.30	35.23	14.57	10	3.0	MD	ISC
135	2006-06-29	07:54:15.84	35.56	14.68	10	3.1	ML	INGV
136	2006-07-05	23:32:30.80	35.42	10.48	10	3.3	MD	ISC
137	2006-07-13	13:20:36.13	35.82	10.49	10	3.3	MD	ISC
138	2006-07-20	06:05:22.33	35.59	12.7	10	3.1	ML	INGV
139	2006-07-20	22:58:10.40	37.62	14.2	58.6	3.1	ML	ISC

140	2006-08-04	16:15:10.00	37.73	10.94	10	3.4	ML	INGV
141	2006-08-05	16:15:15.40	36.96	10.37	10.8	3.2	MD	ISC
142	2006-08-09	10:38:50.00	36.08	13.89	10	3.1	MD	ISC
143	2006-08-30	07:53:55.10	37.67	16.24	35.2	3.4	ML	ISC
144	2006-10-10	21:07:17.97	36.45	11.57	10	3.3	ML	INGV
145	2006-10-14	23:55:31.25	37.29	14.83	9.4	3.1	ML	INGV
146	2006-10-18	18:25:34.54	33.8	14.09	10	4.3	Mb	ISC
147	2006-10-27	20:27:40.32	35.14	15.65	10	3.2	ML	INGV
148	2006-11-14	23:34:22.30	37.8	14.88	27.2	3.1	ML	ISC
149	2006-11-14	23:47:46.80	37.8	14.85	28	3.0	ML	INGV
150	2006-11-20	01:49:26.17	34.63	13.72	10	3.5	ML	INGV
151	2006-11-23	13:31:53.91	35.88	12.68	28.1	4.6	Mw	INGV
152	2006-11-23	13:55:43.47	35.94	12.69	32.5	3.6	ML	INGV
153	2006-11-24	04:37:39.73	36.23	15.8	11.7	4.2	Mw	INGV
154	2006-11-24	08:35:22.00	36.19	12.84	10	3.0	ML	INGV
155	2006-11-25	18:56:53.42	36.28	15.78	11.3	3.1	ML	INGV
156	2006-11-29	12:05:27.37	35.95	12.75	10	3.4	ML	INGV
157	2006-12-13	13:28:56.70	34.65	15.41	10	3.5	ML	INGV
158	2006-12-16	07:16:44.86	35.94	12.86	10	3.2	ML	INGV
159	2006-12-16	19:46:40.58	36.11	12.74	10	3.1	ML	INGV
160	2006-12-19	14:58:06.50	37.78	14.91	23.8	3.9	Mw	INGV
161	2006-12-20	01:46:24.07	37.77	14.91	20.3	3.2	ML	INGV
162	2006-12-21	05:29:51.42	35.92	16.44	10	3.2	ML	INGV
163	2007-01-07	12:04:15.45	34.85	15.05	7	3.1	ML	INGV
164	2007-02-06	10:52:00.41	36.2	12.87	10	3.2	ML	INGV
165	2007-02-11	17:11:53.99	35.24	16.07	10.5	3.9	Mw	INGV
166	2007-02-11	20:30:58.69	36.84	14.9	26.2	3.4	ML	INGV
167	2007-02-15	04:26:22.13	35.61	14.87	10	3.1	ML	INGV
168	2007-02-19	13:57:51.90	37.92	14.25	30.8	3.2	ML	INGV
169	2007-03-31	12:22:32.33	34.6	13.72	10	3.8	Mb	INGV
170	2007-04-10	19:17:32.07	36.93	12.91	21.6	4.1	Mw	INGV
171	2007-04-21	06:15:42.01	37.63	16.38	24.5	3.0	ML	INGV
172	2007-05-07	13:01:31.60	37.9	14.54	1.1	3.0	ML	ISC
173	2007-05-09	18:50:11.29	37.66	15.02	2	3.0	ML	INGV
174	2007-05-11	12:56:28.00	34.38	13.73	10	3.0	MD	ISC
175	2007-06-04	10:48:40.80	37.29	16.1	28.4	4.1	ML	ISC
176	2007-06-15	22:56:00.03	36.96	15.38	16.9	3.3	Mw	INGV
177	2007-06-20	07:54:11.80	31.37	14.91	37.2	3.1	ML	ISC
178	2007-07-05	23:43:35.40	36.88	14.3	19.9	3.0	ML	ISC
179	2007-07-11	14:10:13.00	36.8	14.25	10.4	3.1	ML	ISC
180	2007-07-13	16:25:10.68	34.46	15.17	10	3.3	ML	INGV
181	2007-07-30	19:52:00.90	37.47	14.75	28.1	3.2	ML	ISC
182	2007-07-31	06:53:16.15	37.47	14.74	27.8	3.1	ML	INGV
183	2007-08-01	23:38:17.29	37.64	15.17	3.6	3.0	ML	INGV
184	2007-08-16	08:36:25.80	36.63	14.9	2.8	3.0	ML	ISC
185	2007-09-03	11:58:39.32	31.65	11.34	10	4.0	Mb	ISC
186	2007-09-08	06:09:40.20	35.67	10.12	8.9	3.4	MD	ISC
187	2007-09-13	17:19:10.90	37.88	16.36	14	3.0	ML	ISC

188	2007-09-16	18:21:05.89	33.14	13.11	10	3.2	Mb	ISC
189	2007-09-18	06:11:02.99	35.21	13.27	10	3.3	ML	INGV
190	2007-09-26	04:19:10.70	37.44	16.16	10	4.0	ML	ISC
191	2007-09-26	21:12:01.62	35.91	11.64	10	3.6	Mb	INGV
192	2007-09-29	19:14:02.17	37.29	10.28	10	3.5	ML	INGV
193	2007-10-01	19:32:19.60	37.08	16.28	18.3	3.9	ML	ISC
194	2007-10-15	17:36:44.77	35.21	15.61	10	3.5	ML	INGV
195	2007-10-25	15:19:41.80	33.57	13.22	35.1	3.0	ML	ISC
196	2007-10-26	04:15:40.60	34.49	10.04	11.6	3.3	MD	ISC
197	2007-11-02	05:54:26.90	37	10.77	10	3.1	MD	ISC
198	2007-12-02	11:15:47.13	37.28	11.53	10	3.1	MD	INGV
199	2008-01-08	08:35:46.60	36.2	11.14	10.9	3.2	MD	ISC
200	2008-01-08	12:49:09.10	36.21	11.24	10	3.2	MD	ISC
201	2008-01-12	01:51:22.75	37.74	14.91	22	3.1	ML	INGV
202	2008-01-16	19:43:46.70	37.8	16.22	38.6	3.3	ML	ISC
203	2008-01-20	20:46:44.30	33.18	10.89	0	3.5	ML	ISC
204	2008-02-09	07:46:36.28	37.88	15.56	11	3.1	ML	INGV
205	2008-02-14	02:58:48.80	37.94	14.71	31.7	3.2	ML	ISC
206	2008-02-15	09:34:36.40	37.8	15.17	1	3.3	ML	ISC
207	2008-02-20	16:40:02.39	37.68	14.13	34.9	3.2	ML	INGV
208	2008-02-20	21:14:24.83	37.69	14.19	33.9	3.6	ML	INGV
209	2008-02-24	10:58:24.19	35.62	13.61	10	3.3	ML	INGV
210	2008-03-10	13:34:54.80	32.63	16.02	8.1	3.0	ML	ISC
211	2008-04-09	04:14:35.62	37.72	15.19	3.1	3.3	ML	INGV
212	2008-04-20	07:47:26.05	37.6	15.08	1.7	3.1	ML	INGV
213	2008-05-01	21:05:48.77	37.79	15.13	1	3.3	ML	INGV
214	2008-05-01	22:43:50.03	37.8	15.12	3	3.0	ML	INGV
215	2008-05-08	19:52:29.11	36.01	12.94	10	3.6	Mb	INGV
216	2008-05-13	09:22:08.32	37.74	15.03	1	3.0	ML	INGV
217	2008-05-13	09:24:15.66	37.75	15.02	2.1	3.0	ML	INGV
218	2008-05-13	09:28:06.55	37.76	15.02	4	3.5	ML	INGV
219	2008-05-13	09:56:39.48	37.78	15.03	2	3.1	ML	INGV
220	2008-05-13	10:07:48.39	37.75	15.07	1	3.6	Mb	INGV
221	2008-05-13	11:03:33.51	37.81	15.03	1	3.4	ML	INGV
222	2008-05-13	11:52:39.51	37.81	15.01	1	3.2	ML	INGV
223	2008-05-13	12:13:42.87	37.79	15.04	1	3.7	ML	INGV
224	2008-05-13	13:26:50.25	37.81	15.04	0.5	3.3	ML	INGV
225	2008-05-13	21:28:27.84	37.81	15.11	0.5	3.2	ML	INGV
226	2008-05-14	12:00:53.10	37.11	10.46	2	3.2	ML	ISC
227	2008-05-29	23:52:00.96	36.39	12.94	10	3.1	ML	INGV
228	2008-06-07	00:18:46.49	36.18	12.72	10	3.4	Mb	INGV
229	2008-06-07	13:54:51.05	35.77	12.72	10	3.3	ML	INGV
230	2008-06-12	07:46:32.90	36.2	12.75	10	3.4	ML	INGV
231	2008-06-20	13:25:15.70	33.81	10.22	6.5	3.1	MD	ISC
232	2008-06-21	15:37:27.06	37.3	11.12	10	3.5	Mb	INGV
233	2008-06-21	15:37:58.91	37.51	11.34	0	3.8	Mb	ISC
234	2008-06-23	01:28:57.11	37.32	11.13	10	3.3	ML	INGV
235	2008-07-02	09:17:50.22	36.15	12.67	10	3.7	Mb	INGV

236	2008-07-08	06:12:58.35	35.81	13.98	63.2	3.2	ML	INGV
237	2008-07-23	04:07:13.78	36.53	15.15	10	3.3	ML	INGV
238	2008-07-24	00:56:24.32	36.03	15.3	11.3	3.3	ML	INGV
239	2008-08-01	15:22:32.37	35	14.54	10	3.2	ML	INGV
240	2008-08-13	13:39:30.10	37.48	16.42	38.6	3.1	ML	INGV
241	2008-09-03	02:50:01.60	35.8	10.3	10	3.3	MD	ISC
242	2008-10-05	05:27:25.67	36.9	14.71	24	3.4	ML	INGV
243	2008-10-12	23:53:39.00	37.56	13.61	35.1	3.3	ML	INGV
244	2008-10-21	04:38:09.20	31.98	15.36	18.1	3.3	ML	ISC
245	2008-11-02	06:46:43.65	37.64	16.49	36.8	3.4	ML	INGV
246	2008-11-12	10:39:11.54	37	16.48	38.5	3.9	ML	INGV
247	2008-11-15	21:49:11.29	37.38	11.5	10	3.2	ML	INGV
248	2008-11-18	21:07:27.32	37.91	14.74	33.1	3.5	ML	INGV
249	2008-11-28	23:39:22.22	37.62	13.82	35.3	4.4	Mw	INGV
250	2008-12-15	18:38:57.57	36.27	12.78	16.3	3.4	ML	INGV
251	2008-12-16	02:30:14.05	37.66	14.97	4.8	3.7	Mb	INGV
252	2008-12-16	05:36:28.26	37.17	15.64	10	3.0	ML	INGV
253	2008-12-18	01:10:57.14	37.75	16.14	46.7	3.1	ML	INGV
254	2009-01-08	15:42:46.84	37.67	14.97	16.3	3.2	ML	INGV
255	2009-02-05	03:55:22.67	36.46	15.65	21.3	3.1	ML	INGV
256	2009-02-05	14:50:13.65	37.39	16.03	25	3.1	ML	INGV
257	2009-02-07	08:02:35.28	37.72	13.86	6.7	3.5	ML	INGV
258	2009-02-12	12:13:02.44	37.71	13.8	8.6	3.1	ML	INGV
259	2009-03-08	20:15:08.60	31.31	15.96	34.7	3.4	ML	ISC
260	2009-03-14	09:26:50.75	37.73	15.15	4.7	3.4	ML	INGV
261	2009-03-19	08:27:54.02	36.47	12.73	26.1	3.8	Mw	INGV
262	2009-03-19	09:29:19.16	36.25	12.86	20	3.0	ML	INGV
263	2009-03-19	10:25:57.24	36.44	12.62	84.3	3.5	ML	INGV
264	2009-03-20	01:15:16.10	36.47	12.72	30	3.5	ML	INGV
265	2009-03-23	18:44:49.28	35.34	14.16	20	4.0	Mw	INGV
266	2009-04-25	01:36:25.00	34.3	13.9	10	4.5	Mw	CSEM
267	2009-04-25	10:15:36.21	37.65	16.35	38	3.1	ML	INGV
268	2009-04-25	23:41:39.80	30.5	15.11	4.1	3.3	Mw	ISC
269	2009-04-26	04:50:18.76	37.24	14.09	22.1	3.0	ML	INGV
270	2009-05-13	14:13:47.91	37.68	15.18	2.5	3.4	ML	INGV
271	2009-05-17	22:23:50.00	34.91	10.28	10	3.0	MD	ISC
272	2009-05-20	14:31:17.26	35.06	15.08	10	3.0	ML	INGV
273	2009-05-21	03:17:44.80	35.01	15.12	10	3.0	MD	ISC
274	2009-05-21	03:19:43.55	35.05	15.12	10	3.0	ML	INGV
275	2009-05-26	21:17:55.22	35.11	15.11	9.9	3.0	ML	INGV
276	2009-07-05	18:52:15.14	34.99	13.59	40	3.3	ML	INGV
277	2009-07-23	00:10:42.55	37.6	14.75	26.4	3.5	ML	INGV
278	2009-07-29	19:30:03.07	35.04	15.12	9.7	3.0	ML	INGV
279	2009-07-29	21:58:25.17	35.04	14.86	9.2	3.1	ML	INGV
280	2009-07-30	02:58:35.64	35.02	15.16	9.9	3.0	ML	INGV
281	2009-07-30	05:38:54.46	35.11	15.14	10	3.3	ML	INGV
282	2009-07-31	17:35:48.70	34.72	10.74	34.3	3.3	MD	ISC
283	2009-08-04	16:17:16.39	37.12	15.71	22.5	3.7	ML	INGV

284	2009-08-05	12:26:04.50	37.13	15.66	24	3.0	ML	INGV
285	2009-08-07	09:06:23.44	35.83	14.9	10.4	3.4	ML	INGV
286	2009-08-16	07:49:42.91	35.11	15.15	10	3.1	ML	INGV
287	2009-08-25	12:06:54.30	35.82	10.25	1.1	3.0	MD	ISC
288	2009-08-25	16:58:02.92	37.8	15.18	1	3.1	ML	INGV
289	2009-08-29	19:23:45.80	32.36	15.04	12.6	3.0	Mw	ISC
290	2009-09-23	13:01:06.22	36.24	13.09	17.9	3.1	ML	INGV
291	2009-09-27	16:44:59.40	32.77	14.34	8	3.2	Mw	ISC
292	2009-09-27	16:56:01.27	32.94	14.39	10	3.8	Mw	ISC
293	2009-09-27	19:37:00.60	32.82	14.41	16.3	3.5	Mw	ISC
294	2009-10-02	00:05:33.63	35.53	13.81	10	3.2	ML	INGV
295	2009-10-09	07:05:45.98	37.41	14.46	23.8	3.3	ML	INGV
296	2009-10-10	14:55:00.28	36.5	12.75	11.9	3.0	ML	INGV
297	2009-10-12	20:07:49.00	37.23	15.96	18.3	3.4	ML	INGV
298	2009-10-18	03:44:50.08	37.01	15.23	20.4	3.3	ML	INGV
299	2009-10-18	08:06:09.67	35.01	14.72	10	3.6	ML	INGV
300	2009-11-07	07:10:05.56	37.63	13.85	34	3.7	Mb	INGV
301	2009-11-08	06:50:10.20	37.85	14.56	6.3	3.1	ML	INGV
302	2009-11-08	06:51:16.41	37.85	14.56	7.6	4.4	Mw	INGV
303	2009-12-07	04:31:17.10	32.55	14.88	11.3	3.1	Mw	ISC
304	2009-12-07	17:16:54.00	32.75	15.48	7	3.3	Mw	ISC
305	2009-12-19	05:27:24.99	37.77	14.93	27.5	3.0	ML	INGV
306	2009-12-19	05:36:19.00	37.77	14.94	27.5	3.1	ML	INGV
307	2009-12-19	05:36:28.79	37.77	14.95	24.7	3.9	Mb	INGV
308	2009-12-19	05:40:22.99	37.77	14.93	24	3.0	ML	INGV
309	2009-12-19	05:42:43.09	37.77	14.95	25.2	3.1	ML	INGV
310	2009-12-19	05:46:18.16	37.78	14.96	27.2	3.0	ML	INGV
311	2009-12-19	05:53:30.25	37.78	14.95	24.6	3.0	ML	INGV
312	2009-12-19	07:42:26.95	37.76	14.94	24.4	3.5	ML	INGV
313	2009-12-19	07:58:26.16	37.79	14.93	21.2	3.1	ML	INGV
314	2009-12-19	08:01:11.53	37.77	14.93	28.5	3.5	ML	INGV
315	2009-12-19	08:03:05.12	37.74	14.89	20.3	3.0	ML	INGV
316	2009-12-19	08:24:57.91	37.77	14.94	22.9	3.7	ML	INGV
317	2009-12-19	09:01:16.46	37.78	14.97	26.9	4.3	Mw	INGV
318	2009-12-19	12:35:40.91	37.77	14.95	24.7	3.2	ML	INGV
319	2009-12-19	12:43:11.39	37.79	14.96	24.3	3.6	ML	INGV
320	2009-12-19	14:02:31.11	37.78	14.95	29.9	3.2	ML	INGV
321	2009-12-19	14:11:04.03	37.78	14.95	26.8	3.0	ML	INGV
322	2009-12-19	14:37:33.27	37.79	14.96	27.3	3.2	ML	INGV
323	2009-12-19	15:40:00.55	37.78	14.95	27.6	3.1	ML	INGV
324	2009-12-19	17:24:36.12	37.79	14.96	25.5	3.2	ML	INGV
325	2009-12-19	18:08:33.94	37.79	14.97	24.7	3.4	ML	INGV
326	2009-12-20	04:33:29.97	34.7	13.79	10	3.7	Mb	ISC
327	2009-12-23	14:24:42.47	37.79	14.95	25.1	3.6	ML	INGV
328	2009-12-23	14:27:40.67	37.78	14.94	28.2	3.0	ML	INGV
329	2009-12-23	16:02:10.87	37.79	14.96	25.1	3.0	ML	INGV
330	2009-12-29	11:08:55.00	32.6	15	10	5.0	Mw	CSEM
331	2009-12-29	19:57:27.51	37.48	15.65	8.3	3.0	ML	INGV

332	2010-01-04	06:28:51.66	34	13.88	0	3.4	Mb	ISC
333	2010-01-05	11:23:23.11	34.12	14.97	10	3.9	Mb	INGV
334	2010-01-05	19:47:56.02	37.83	14.57	5.3	3.4	Mb	INGV
335	2010-01-11	22:15:45.40	37.74	15.15	1.4	3.0	ML	INGV
336	2010-01-23	18:00:46.80	34.13	11.26	3.5	3.4	MD	ISC
337	2010-02-09	02:51:54.68	36.43	13.44	10	3.0	ML	INGV
338	2010-02-16	06:42:15.98	35.15	14.09	9.7	3.5	Mb	INGV
339	2010-02-26	16:38:48.95	35.29	13.18	10	3.0	ML	INGV
340	2010-02-27	08:52:28.31	37.79	14.15	37.1	3.2	ML	INGV
341	2010-03-08	19:11:35.17	36.25	12.41	10	3.2	ML	INGV
342	2010-03-20	22:52:58.50	37.88	14.12	7.7	3.0	MD	ISC
343	2010-04-02	20:04:45.10	37.8	15.15	3.4	4.2	Mw	INGV
344	2010-04-03	00:05:13.24	37.78	15.13	2.3	3.2	Mb	INGV
345	2010-04-19	07:41:24.19	37.98	14.3	28.8	3.3	ML	INGV
346	2010-05-08	22:23:29.39	36.52	15.3	10	3.6	ML	INGV
347	2010-05-11	08:35:05.51	37.78	14.2	4.5	3.2	ML	INGV
348	2010-06-22	23:46:36.15	35.11	15.71	10	3.1	ML	INGV
349	2010-06-29	07:45:03.15	35.94	13.36	10.6	3.0	ML	INGV
350	2010-06-29	08:08:41.15	35.96	13.41	9.9	3.0	ML	INGV
351	2010-07-09	00:19:25.95	34.92	14.12	21.4	3.2	ML	INGV
352	2010-07-13	11:19:34.15	34.32	13.76	30	3.7	Mb	INGV
353	2010-07-14	00:35:39.48	34.29	13.92	30	3.3	ML	INGV
354	2010-07-15	17:38:48.25	34.38	13.95	20	3.0	ML	INGV
355	2010-07-26	01:48:24.27	35.25	16.45	0	3.6	Mb	ISC
356	2010-08-13	08:16:37.60	35.76	10.98	8.8	3.5	MD	ISC
357	2010-08-29	14:54:13.82	32.65	15.07	10	3.7	Mb	ISC
358	2010-10-08	17:26:58.47	36.91	16.33	38.1	3.6	ML	INGV
359	2010-10-22	05:59:02.06	37.62	16.11	48	3.1	ML	INGV
360	2010-10-27	11:10:14.08	37.36	12.24	10	3.5	ML	INGV
361	2010-11-10	08:22:45.22	35.16	14.2	10	4.0	ML	INGV
362	2010-11-12	04:43:35.84	35.1	14.55	14.8	3.8	ML	INGV
363	2010-11-18	08:20:08.97	35.12	14.16	10	3.3	ML	INGV
364	2010-11-19	19:24:58.95	35.1	14.48	20	3.3	ML	INGV
365	2010-12-01	11:41:53.42	34.51	15.32	10	3.9	Mb	INGV
366	2010-12-15	22:03:47.50	37.01	16.07	19.5	3.2	ML	INGV
367	2010-12-24	14:52:36.14	36.77	14.6	11.2	3.0	ML	INGV
368	2011-01-06	12:22:38.91	35.9	13.05	20	3.0	ML	INGV
369	2011-02-17	15:03:59.70	35.59	14.49	6.1	3.2	ML	INGV
370	2011-03-06	08:44:06.95	37.06	15.13	24.1	3.3	ML	INGV
371	2011-03-09	04:23:51.05	37.82	15.41	10.7	3.8	ML	INGV
372	2011-03-16	17:34:05.79	37.67	14.97	16.4	3.2	ML	INGV
373	2011-03-26	19:24:40.53	37.08	15.05	18.9	3.1	ML	INGV
374	2011-03-28	02:11:03.04	31.43	14.22	0	3.1	Mb1	ISC
375	2011-04-04	23:27:12.37	35.14	10.74	10	3.6	Mb	ISC
376	2011-04-07	07:27:40.60	32.37	12.33	5	3.0	ML	ISC
377	2011-04-23	22:10:58.26	35.88	14.88	5	3.5	ML	INGV
378	2011-04-24	01:34:00.87	35.84	14.89	10.5	3.3	ML	INGV
379	2011-04-24	04:38:59.44	35.85	14.89	9.4	3.4	ML	INGV

380	2011-04-24	09:21:18.43	35.82	14.91	8.9	3.7	ML	INGV
381	2011-04-24	09:25:28.01	35.83	14.89	8.8	3.7	ML	INGV
382	2011-04-24	13:02:12.03	35.83	14.91	9.7	4.2	Mw	INGV
383	2011-04-25	06:10:18.59	35.8	14.91	18.8	3.4	ML	INGV
384	2011-04-26	04:10:28.36	35.76	14.97	18.3	3.5	ML	INGV
385	2011-05-05	15:58:06.49	37.79	14.96	24.8	3.2	ML	INGV
386	2011-05-06	03:43:51.81	37.79	14.97	24.9	3.1	ML	INGV
387	2011-05-06	15:12:35.05	37.79	14.96	28.1	4.1	Mw	INGV
388	2011-05-06	15:15:23.00	37.8	14.98	26.6	3.4	ML	INGV
389	2011-05-06	15:17:37.26	37.79	14.96	25	3.2	ML	INGV
390	2011-05-06	15:18:30.86	37.79	14.95	24.9	3.3	ML	INGV
391	2011-05-06	15:27:37.50	37.79	14.97	26.1	3.1	ML	INGV
392	2011-05-06	16:54:49.07	37.79	14.97	25.9	3.1	ML	INGV
393	2011-05-06	19:28:49.81	37.79	14.96	25.7	3.5	ML	INGV
394	2011-05-11	01:45:35.69	37.79	14.96	26.7	3.5	ML	INGV
395	2011-05-11	01:46:48.14	37.79	14.97	25.3	3.4	ML	INGV
396	2011-05-11	02:12:25.96	37.79	14.97	27.3	3.2	ML	INGV
397	2011-05-11	02:17:08.02	37.79	14.96	26.5	3.4	ML	INGV
398	2011-05-11	15:17:10.60	35.68	14.58	5	3.3	ML	INGV
399	2011-05-23	01:01:03.08	37.69	10.77	10	3.4	Mb	INGV
400	2011-05-23	02:24:06.41	37.6	10.67	10	3.7	Mb	INGV
401	2011-05-23	02:26:02.36	37.82	10.85	10	3.9	Mb	INGV
402	2011-05-25	01:50:36.18	37.68	14.39	32	3.0	ML	INGV
403	2011-05-28	16:57:36.90	30.4	13.6	32	3.5	Mw	ISC
404	2011-07-02	13:49:43.46	36.7	15.6	28.6	3.1	ML	INGV
405	2011-07-10	03:07:03.78	36.67	15.65	15.8	3.7	Mw	INGV
406	2011-07-24	06:03:22.95	36.66	13.06	10	3.0	ML	INGV
407	2011-07-25	07:10:43.01	35.34	15.92	10	3.4	ML	INGV
408	2011-07-26	01:03:33.36	36.35	12.8	15.2	3.7	Mb	INGV
409	2011-08-12	11:15:42.98	35	15.81	10	3.1	ML	INGV
410	2011-08-20	06:48:10.80	37.73	15.97	29.5	3.5	ML	ISC
411	2011-08-31	16:33:19.66	37.11	14.7	4.7	3.1	ML	INGV
412	2011-08-31	22:10:23.81	37.27	16.04	21.9	3.1	ML	INGV
413	2011-09-09	22:23:45.50	37.81	14.87	28	3.9	ML	INGV
414	2011-10-09	08:28:26.65	36.98	15.1	9.8	3.3	ML	INGV
415	2011-10-09	17:25:00.08	36.98	15.04	8.6	3.1	ML	INGV
416	2011-10-10	09:19:19.65	36.99	15.03	8.9	3.1	ML	INGV
417	2011-10-16	07:02:53.60	35.18	10.76	10.4	3.5	MD	ISC
418	2011-10-26	07:15:49.48	34.85	13.91	20.8	4.0	ML	INGV
419	2011-11-08	14:50:32.54	34.12	13.62	10	3.5	Mb	ISC
420	2011-11-15	07:23:04.00	37.85	15.81	38	3.1	ML	INGV
421	2011-11-16	06:40:33.88	35.33	14.32	10	3.6	ML	INGV
422	2011-11-19	10:19:16.01	37.81	14.35	9.5	3.3	ML	INGV
423	2011-11-26	17:10:04.42	35.28	16.17	9.9	3.6	ML	INGV
424	2011-11-27	00:43:55.78	35.2	16.02	10	3.0	MD	INGV
425	2011-12-02	12:21:12.01	35.21	15.88	10	3.0	ML	INGV
426	2011-12-18	15:00:12.05	36.2	12.77	25.3	3.4	ML	INGV
427	2011-12-18	15:01:01.81	35.98	12.65	32.1	4.7	Mw	INGV

428	2011-12-18	15:30:03.62	36.17	12.66	29.6	3.0	ML	INGV
429	2011-12-18	17:57:47.96	35.98	12.64	38	3.5	ML	INGV
430	2012-01-01	04:17:03.05	37.86	14.91	30.4	3.4	ML	INGV
431	2012-01-26	06:48:15.98	37.79	14.62	27.2	3.2	ML	INGV
432	2012-01-29	11:14:50.16	37.88	14.27	11.1	3.1	ML	INGV
433	2012-02-01	14:28:37.94	37.89	14.28	9.9	3.1	ML	INGV
434	2012-02-03	08:25:54.75	34.47	13.98	30	3.9	ML	INGV
435	2012-02-04	14:53:13.54	37.13	15.34	21.3	3.1	ML	INGV
436	2012-02-08	16:15:56.36	37.89	14.3	4.8	3.0	ML	INGV
437	2012-02-18	14:42:22.64	36.41	12.73	30	3.1	ML	INGV
438	2012-02-26	16:17:23.15	37.3	16.06	22.1	3.9	Mb	INGV
439	2012-03-11	21:17:54.78	36.52	12.69	30	3.5	ML	INGV
440	2012-03-13	06:50:02.45	37.69	14.04	36.1	3.5	Mb	INGV
441	2012-03-23	10:28:36.00	35.95	14.26	10	3.9	Mb	INGV
442	2012-03-24	20:34:59.22	37.56	15.91	29.9	3.0	ML	INGV
443	2012-03-25	21:02:29.76	37.69	15.17	3	3.0	ML	INGV
444	2012-03-27	02:29:36.09	35.07	15.04	30	3.3	ML	INGV
445	2012-03-30	19:54:09.13	34.66	13.63	10	3.9	ML	INGV
446	2012-04-12	12:57:10.30	37.89	15.62	6.9	3.0	ML	INGV
447	2012-04-12	13:20:28.85	37.89	15.63	7.5	3.2	ML	INGV
448	2012-04-16	02:33:40.83	36.81	12.71	19.7	3.3	ML	INGV
449	2012-04-26	04:06:50.02	36.88	10.84	10	3.2	ML	INGV
450	2012-06-15	06:27:24.85	37.46	16.32	33.1	3.7	Mw	INGV
451	2012-06-25	10:52:51.01	37.01	15.15	7.9	3.1	ML	INGV
452	2012-06-26	11:13:54.35	36.49	11.94	10	3.1	ML	INGV
453	2012-06-27	01:14:20.24	37	15.06	5	3.7	Mw	INGV
454	2012-06-27	01:20:59.70	37	15.05	5	3.0	ML	INGV
455	2012-06-27	02:48:01.99	36.98	15.09	10.2	3.3	ML	INGV
456	2012-06-27	21:58:22.30	37.71	15.17	1.3	3.2	ML	INGV
457	2012-06-27	22:38:57.19	37.71	15.16	0.7	3.1	ML	INGV
458	2012-06-28	08:18:51.06	37.72	15.15	2.6	3.1	ML	INGV
459	2012-07-02	19:40:36.44	37.81	12.86	9.6	3.0	ML	INGV
460	2012-07-03	05:03:42.35	34.04	14.67	10	4.7	Mw	ISC
461	2012-07-26	14:20:04.03	37.96	16.3	27.6	3.0	ML	INGV
462	2012-08-01	17:13:52.88	35.57	10.8	1.8	3.3	MD	ISC
463	2012-09-14	22:19:23.02	36.35	13.07	35.7	3.8	Mb	INGV
464	2012-09-15	15:40:59.76	36.34	13.08	35.1	3.8	Mb	INGV
465	2012-09-24	02:40:43.05	34.06	10.09	10.7	3.1	MD	ISC
466	2012-10-16	17:02:07.12	34.94	13.93	10	3.6	ML	INGV
467	2012-10-22	03:34:48.72	36.66	12.85	30.4	3.3	ML	INGV
468	2012-10-29	03:53:00.04	37.11	16.44	25	3.0	ML	INGV
469	2012-11-20	05:25:13.19	35.2	12.74	10	3.5	ML	INGV
470	2012-11-22	09:10:41.53	37.8	14.96	24.4	3.9	Mw	INGV
471	2012-11-22	11:25:51.67	37.8	14.96	27.3	3.9	Mw	INGV
472	2012-11-22	11:28:55.59	37.79	14.95	24.5	3.9	Mw	INGV
473	2013-01-03	11:29:58.64	36.31	13.61	28.3	3.0	ML	INGV
474	2013-01-04	07:50:06.08	37.88	14.72	15.1	4.2	Mw	INGV
475	2013-01-08	01:27:05.91	34.93	15.86	10	3.2	ML	INGV

476	2013-01-20	06:03:36.41	36.73	14.86	28	3.0	ML	INGV
477	2013-02-28	20:14:36.95	37.56	16.02	38.1	3.2	ML	INGV
478	2013-03-02	04:22:10.53	36.28	12.62	55.1	3.6	Mb	INGV
479	2013-03-07	22:36:59.03	37.97	14.52	6.9	3.6	Mw	INGV
480	2013-03-11	10:18:21.08	37.23	15.43	18.1	3.3	ML	INGV
481	2013-03-19	07:50:06.15	37.98	14.52	7.9	3.4	Mw	INGV
482	2013-03-19	08:37:04.64	37.98	14.52	9.5	3.4	Mw	INGV
483	2013-03-21	09:45:55.07	36.55	14.8	8.3	3.1	ML	INGV
484	2013-03-21	22:03:06.12	37.27	15.31	14.7	3.4	ML	INGV
485	2013-03-24	15:47:21.95	37.71	16.47	38.2	4.4	Mw	INGV
486	2013-03-24	20:37:49.24	37.69	16.4	36.1	3.1	ML	INGV
487	2013-03-25	22:08:12.11	35.95	11.53	10	3.9	Mb	ISC
488	2013-04-16	21:57:13.28	35.36	12.74	10	3.2	ML	INGV
489	2013-05-02	18:43:08.00	35.46	12.67	10	3.0	ML	INGV
490	2013-05-11	04:42:38.14	32.78	12.54	20	4.8	Mw	INGV
491	2013-05-14	13:51:57.00	36.19	15.1	5.4	3.4	ML	INGV
492	2013-05-23	13:04:48.80	37.68	15.13	6.2	3.4	ML	INGV
493	2013-05-24	02:47:00.69	37.71	15.09	9.7	3.0	ML	INGV
494	2013-06-29	23:55:10.50	37.05	16.5	20.9	3.3	ML	INGV
495	2013-08-19	05:48:24.01	37.68	14.27	33.7	3.3	ML	INGV
496	2013-08-24	17:18:18.77	36.71	15.08	8.7	4.4	Mw	INGV
497	2013-08-26	03:45:27.58	36.63	14.12	4.7	3.7	ML	INGV
498	2013-10-09	08:33:21.99	37.61	15.07	8.1	3.0	ML	INGV
499	2013-10-09	17:22:47.97	33.32	15.7	10	4.1	Mw	ISC
500	2013-10-18	11:05:20.37	36.7	14.98	13.6	3.1	ML	INGV
501	2013-10-18	15:08:32.29	35.75	10.82	27	4.7	Mw	ISC
502	2013-10-19	05:33:34.55	35.84	10.63	21.8	3.6	MD	ISC
503	2013-10-21	03:52:37.25	35.84	10.6	5.31	3.3	MD	ISC
504	2013-10-21	19:37:01.74	35.69	10.97	10	4.5	Mw	ISC
505	2013-11-01	00:08:41.27	37.74	13.86	5.8	3.1	ML	INGV
506	2013-11-02	14:40:06.91	35.82	10.84	69.4	3.4	MD	ISC
507	2013-11-05	05:06:39.52	37.69	14.91	23.4	3.1	ML	INGV
508	2013-11-05	05:10:16.47	37.69	14.93	23.8	3.3	ML	INGV
509	2013-11-11	04:39:05.03	37.22	16.14	28.4	3.0	ML	INGV
510	2013-12-02	00:00:18.32	37.52	16.3	27.5	3.1	ML	INGV
511	2013-12-14	21:49:05.19	37.76	14.74	29.8	3.4	ML	INGV
512	2013-12-15	03:57:34.01	36.67	15.03	10.5	3.9	Mw	INGV
513	2014-01-13	18:01:14.80	37.77	14.42	32.1	3.0	ML	INGV
514	2014-01-18	06:17:40.95	37.89	16.15	37	3.1	ML	INGV
515	2014-01-20	22:45:12.95	37.87	15.53	51	3.2	ML	INGV
516	2014-02-15	22:11:31.28	37.09	11.7	10	3.1	ML	INGV
517	2014-02-18	21:44:18.75	37.61	13.79	4.9	3.1	ML	INGV
518	2014-03-08	20:52:50.84	37.92	14.86	36.7	3.8	Mw	INGV
519	2014-03-12	00:55:38.20	37.65	15.13	7.2	3.0	ML	INGV
520	2014-03-23	18:31:53.02	37.51	16.43	37.9	3.7	ML	INGV
521	2014-05-01	16:47:47.76	37.03	10	18.6	3.0	MD	ISC
522	2014-05-03	05:50:12.74	37.06	10	10	3.0	MD	ISC
523	2014-05-13	08:10:16.75	36.12	13.08	9.4	3.2	ML	INGV

524	2014-05-21	04:13:33.09	35.63	14.88	8.8	3.5	Mw	INGV
525	2014-05-27	05:00:03.24	35.57	14.92	22.2	3.0	ML	INGV
526	2014-06-18	03:07:10.59	37.94	15.88	59.9	3.5	ML	INGV
527	2014-06-23	17:50:42.37	36.23	13.19	26.4	3.1	ML	INGV
528	2014-06-27	02:56:49.22	37.83	14.63	21.5	3.1	ML	INGV
529	2014-07-01	00:08:20.73	37.74	15.95	33.1	3.1	ML	INGV
530	2014-07-11	22:03:15.73	36.5	15.24	23.8	3.0	ML	INGV
531	2014-07-15	21:43:54.75	36.98	12.9	21.8	3.0	ML	INGV
532	2014-08-26	01:19:45.32	37.94	14.33	26.7	3.7	Mw	INGV
533	2014-08-26	01:20:58.47	37.91	14.33	28.7	3.4	ML	INGV
534	2014-09-07	02:12:16.67	34.56	13.16	36.3	3.3	ML	INGV
535	2014-09-25	16:33:57.89	37.61	15.17	4	3.1	ML	INGV
536	2014-09-26	23:38:10.59	36.74	16.44	39.1	4.1	Mw	INGV
537	2014-10-13	11:56:40.50	36.21	11.31	25.4	3.7	Mb	INGV
538	2014-10-29	05:37:11.96	36.35	10.58	25.7	3.1	MD	ISC
539	2014-10-31	19:15:03.58	36.33	13.44	83.6	3.1	ML	INGV
540	2014-11-09	07:34:24.89	36.4	13.9	25.3	3.4	ML	INGV
541	2014-11-11	10:30:05.51	36.27	14.3	9.9	3.0	ML	INGV
542	2014-11-12	12:07:13.75	36.32	14.25	10.5	3.1	ML	INGV
543	2014-11-19	13:06:13.71	36.36	13.5	32.3	3.7	ML	INGV
544	2014-11-19	13:12:36.44	36.41	13.51	31.4	3.0	ML	INGV
545	2014-12-07	05:14:42.61	37.75	12.49	1.45	3.1	ML	ISC
546	2014-12-19	20:54:29.85	36.22	12.57	73.7	3.0	ML	INGV
547	2014-12-20	16:46:34.80	36.33	12.74	38	3.4	ML	INGV
548	2014-12-20	23:08:30.77	36.33	12.7	27.5	3.2	ML	INGV
549	2015-01-05	07:27:02.66	37.17	15.36	20.3	3.2	ML	INGV
550	2015-01-10	23:50:02.37	36.41	12.76	19.8	3.9	Mb	INGV
551	2015-01-28	17:53:10.75	34.27	11.15	0	3.3	Mb	ISC
552	2015-02-03	14:51:58.08	34.78	14.97	0	3.8	Mb	ISC
553	2015-02-04	08:14:08.66	36.87	16.19	30.2	3.0	ML	INGV
554	2015-02-08	19:39:21.93	37.34	15.26	20.3	3.1	ML	INGV
555	2015-02-23	02:58:27.28	37.42	14.75	24.6	3.1	ML	INGV
556	2015-02-25	15:04:12.58	37.3	16.49	31.8	3.0	ML	INGV
557	2015-03-19	14:15:51.03	36.21	13.59	20.7	3.0	ML	INGV
558	2015-03-28	08:21:54.55	37.62	16.12	35	3.1	ML	INGV
559	2015-04-20	01:07:43.25	37.81	15.15	3.1	3.3	ML	INGV
560	2015-04-29	04:28:42.69	35.48	16.26	10	3.8	Mb	ISC
561	2015-05-24	06:00:32.22	37.96	16.03	62	3.9	ML	INGV
562	2015-05-31	21:37:32.07	36.53	11.45	37.7	3.1	ML	INGV
563	2015-06-17	09:44:07.14	37.64	14.18	16.1	3.2	ML	INGV
564	2015-06-26	08:51:11.52	36.07	12.64	39.1	3.8	Mb	INGV
565	2015-07-15	16:29:48.95	37.6	15.04	9	3.0	ML	INGV
566	2015-08-01	02:46:50.62	37.65	15.9	32.9	3.2	ML	INGV
567	2015-08-03	13:52:37.35	37.41	16.14	29.2	3.8	Mb	INGV
568	2015-08-04	23:36:30.59	37.64	14.15	19.3	3.1	ML	INGV
569	2015-09-20	08:23:24.00	35	14.71	8.1	3.5	Mb	INGV
570	2015-09-20	22:27:58.50	37.16	15.61	22.6	3.5	Mb	INGV
571	2015-10-09	00:35:29.16	37.71	15.17	5	3.0	ML	INGV

572	2015-11-02	02:48:03.21	37.15	11.9	9.7	3.2	ML	INGV
573	2015-11-07	22:36:04.53	37.25	15.88	22.8	3.9	Mb	INGV
574	2015-11-19	09:43:37.44	37.72	13.89	36	3.1	ML	INGV
575	2015-11-22	13:55:28.32	34.73	10.8	10	3.7	MD	ISC
576	2015-11-24	03:07:45.26	36.69	16.23	38	3.1	ML	INGV
577	2015-12-08	09:28:30.89	37.79	15.09	2.5	3.4	ML	INGV
578	2015-12-08	10:53:55.42	37.79	15.1	1.5	3.1	ML	INGV
579	2015-12-12	18:15:13.51	37.43	16.3	24.8	4.0	Mb	INGV
580	2015-12-15	13:10:29.39	35.14	15.77	22.3	3.0	ML	INGV
581	2015-12-22	00:40:25.49	37.77	15.44	20	3.1	ML	INGV
582	2015-12-22	02:13:39.09	37.77	15.47	20.4	3.4	Mw	INGV
583	2015-12-22	03:31:58.23	36.73	10.2	10	3.5	MD	ISC
584	2015-12-22	05:35:09.89	37.78	15.43	22.6	3.4	Mw	INGV
585	2016-01-02	12:36:26.21	36.46	11.98	28.8	4.2	Mw	INGV
586	2016-01-10	07:33:25.52	36.46	11.89	34.9	3.5	ML	INGV
587	2016-01-10	07:43:38.70	36.47	11.8	38.2	3.4	Mb	INGV
588	2016-01-10	12:14:46.60	36.45	11.95	79.4	3.4	ML	INGV
589	2016-01-10	14:11:11.17	36.41	12.03	50	3.4	ML	INGV
590	2016-01-13	17:01:29.18	36.07	14.79	15.2	4.2	Mw	INGV
591	2016-01-16	05:58:53.87	36.7	12.69	24.5	3.4	ML	INGV
592	2016-01-17	16:36:05.20	36.48	12.71	19	4.0	Mb	INGV
593	2016-01-17	16:43:42.73	36.51	12.57	59.3	3.0	ML	ISC
594	2016-01-17	17:54:50.00	35.81	12.28	10	3.2	ML	ISC
595	2016-01-18	16:46:14.90	36.42	11.98	8	3.2	ML	ISC
596	2016-01-19	08:53:34.38	36.47	11.97	38.9	3.3	ML	INGV
597	2016-01-19	10:54:06.38	36.53	12.79	21.3	3.2	ML	INGV
598	2016-01-20	03:57:57.54	36.48	12.71	22.2	3.4	ML	INGV
599	2016-01-30	11:52:55.00	36.54	11.93	29.8	3.2	ML	INGV
600	2016-02-01	07:05:47.19	36.38	10.74	13.8	3.0	MD	ISC
601	2016-02-07	01:41:59.14	36.99	14.86	4.6	3.3	Mw	INGV
602	2016-02-08	15:35:43.39	36.97	14.87	7.4	4.2	Mw	INGV
603	2016-02-08	17:57:38.07	36.98	14.84	6.8	3.7	ML	INGV
604	2016-02-11	01:38:50.90	37.81	15.38	29.6	3.3	ML	INGV
605	2016-02-12	05:11:53.51	36.25	11.04	21.2	3.3	MD	ISC
606	2016-03-05	21:46:55.96	35.62	10.05	0	3.4	Mb	ISC
607	2016-03-07	21:25:17.04	37.62	15.85	29.9	3.6	Mb	INGV
608	2016-03-11	02:53:47.50	35.93	12.92	38.3	3.1	ML	INGV
609	2016-03-14	22:30:38.56	35.09	11.98	20	3.4	ML	INGV
610	2016-03-15	22:31:56.12	34.92	11.92	20	3.6	ML	INGV
611	2016-03-30	11:16:37.56	37.57	15.36	7.2	3.1	ML	INGV
612	2016-04-09	04:55:21.66	35.4	13.18	19.3	3.0	ML	INGV
613	2016-05-07	09:55:32.87	37.12	14.75	23.7	3.5	ML	INGV
614	2016-05-09	01:54:20.12	36.11	12.74	28.5	3.0	ML	INGV
615	2016-05-21	14:27:43.40	37.8	14.15	9.7	3.3	ML	INGV
616	2016-05-21	15:53:05.85	37.8	14.15	8.4	3.0	ML	INGV
617	2016-05-25	22:10:27.80	36.8	15.8	15.2	3.8	Mw	INGV
618	2016-06-02	10:49:13.10	36.39	11.14	19.5	4.4	Mw	INGV
619	2016-06-03	09:59:50.71	36.17	13.03	8.6	4.1	Mw	INGV

620	2016-06-07	09:39:23.15	35.24	10.34	45.4	3.3	MD	ISC
621	2016-06-25	17:55:51.30	36.74	10.89	14	3.7	Mb	ISC
622	2016-06-26	04:27:37.57	37.33	11.69	13.4	3.6	Mb	INGV
623	2016-06-27	12:14:39.79	35.47	10.55	19.5	3.6	MD	ISC
624	2016-08-17	10:52:05.20	36.08	14.87	11	3.5	ML	INGV
625	2016-09-02	19:11:12.33	36.68	11	12.7	3.6	MD	ISC
626	2016-09-25	08:42:41.13	37.74	15.14	10.3	3.0	ML	INGV
627	2016-10-11	07:38:14.60	36.51	10.84	4.99	3.2	MD	ISC
628	2016-10-15	13:37:53.24	36.31	12.63	38.1	3.2	ML	INGV
629	2016-10-29	10:39:02.40	37.85	14.71	29.9	3.2	ML	INGV
630	2016-10-30	09:27:07.44	35.15	16.21	41	3.8	Mb	INGV
631	2016-11-10	18:05:56.83	37.93	12.86	8.4	3.0	ML	INGV
632	2016-12-29	00:35:53.66	36.29	13.74	37.4	3.0	ML	INGV
633	2017-01-11	07:27:21.70	32.18	10.09	19.7	4.1	MD	ISC
634	2017-01-11	11:09:32.93	35.31	16.07	9.5	3.3	ML	INGV
635	2017-01-11	13:40:18.17	32.47	10.3	27.5	3.1	MD	ISC
636	2017-01-19	08:29:46.12	37.83	15.11	4.8	3.0	ML	INGV
637	2017-01-26	04:05:12.70	37.24	15.96	23.6	3.3	ML	INGV
638	2017-01-29	11:20:24.32	37.81	14.08	8.6	3.3	Mb	INGV
639	2017-01-30	08:15:33.24	37.67	14.99	17.9	3.4	ML	INGV
640	2017-01-30	08:51:51.64	37.67	15	17.1	3.3	ML	INGV
641	2017-01-30	09:44:56.41	37.67	14.98	16.4	3.4	ML	INGV
642	2017-01-30	09:51:07.70	37.67	14.99	18.8	3.9	Mb	INGV
643	2017-01-30	09:54:47.22	37.66	15	16.2	3.0	ML	INGV
644	2017-01-30	09:59:48.53	37.67	14.98	18.5	3.3	ML	INGV
645	2017-01-30	10:27:04.96	37.67	14.99	13.4	3.0	ML	INGV
646	2017-02-04	20:27:40.56	36.3	10.8	11.7	3.7	MD	ISC
647	2017-02-16	12:20:04.16	37.72	15.64	32.1	3.2	ML	INGV
648	2017-02-27	06:07:23.79	33.22	10.03	0	3.3	ML	ISC
649	2017-03-07	16:50:47.92	35.37	12.63	0	3.1	Mb	ISC
650	2017-03-20	00:35:12.13	35.55	10.01	7.64	3.2	MD	ISC
651	2017-03-27	09:03:45.66	37.07	10.8	18.6	3.3	MD	ISC
652	2017-05-04	08:26:56.27	33.66	11.25	10	4.5	Mw	ISC
653	2017-05-05	00:50:52.17	33.57	11.31	13.9	3.6	MD	ISC
654	2017-05-10	16:52:46.40	33.81	10.35	18.3	3.1	MD	ISC
655	2017-05-13	00:10:55.54	32.22	16.1	0	3.4	Mb	ISC
656	2017-05-18	16:59:31.81	35.96	11.37	8.98	3.4	MD	ISC
657	2017-05-21	07:56:44.84	36.33	13.35	79.2	3.0	ML	INGV
658	2017-05-30	05:45:21.17	36	12.59	89	3.1	ML	INGV
659	2017-06-19	15:11:14.72	37.13	10.06	16.9	3.2	MD	ISC
660	2017-07-19	20:16:53.46	36.12	13.07	18.3	3.1	ML	INGV
661	2017-07-27	08:30:32.72	37.53	14.98	9	3.0	ML	INGV
662	2017-08-08	14:29:25.79	35.61	14.84	13	3.3	ML	INGV
663	2017-08-19	11:38:10.69	37.67	14.89	24	3.0	ML	INGV
664	2017-08-20	08:06:01.93	35.15	10.83	92	3.7	MD	ISC
665	2017-08-21	17:37:13.53	35.58	14.81	18.3	3.0	ML	INGV
666	2017-08-23	09:16:24.35	35.66	14.86	12.5	3.8	Mw	INGV
667	2017-08-25	17:10:45.34	35.57	15.24	8.6	4.1	Mw	INGV

668	2017-08-25	21:57:47.35	37.6	14.99	6	3.1	ML	INGV
669	2017-08-26	20:46:21.21	37.68	14.89	23.8	3.0	ML	INGV
670	2017-08-29	02:10:01.47	33.55	11.02	27.3	3.0	MD	ISC
671	2017-09-02	00:45:31.35	35.48	15.24	11.3	3.4	ML	INGV
672	2017-09-06	01:52:12.73	35.43	15.23	16.8	3.0	ML	INGV
673	2017-09-18	07:21:27.94	37.73	14.93	8.5	3.2	ML	INGV
674	2017-09-23	22:30:41.63	35.41	12.77	11	3.3	ML	INGV
675	2017-10-05	18:04:50.05	37.92	14.99	29.6	3.1	ML	INGV
676	2017-10-08	11:48:32.62	35.46	15.17	22.1	3.2	ML	INGV
677	2017-10-15	09:51:48.17	36.95	16.4	36.6	3.9	Mb	INGV
678	2017-10-15	14:16:25.00	37.64	12.83	6	3.0	ML	ISC
679	2017-10-16	13:40:45.88	35.71	11.54	19	3.5	ML	ISC
680	2017-10-31	00:16:40.65	36.71	10.94	14	4.2	Mw	ISC
681	2017-10-31	09:46:05.71	36.67	11.12	14	3.2	Mb	ISC
682	2017-10-31	09:59:26.39	36.57	10.97	7.13	3.0	MD	ISC
683	2017-11-09	14:45:21.54	35.81	11.52	13.9	3.4	MD	ISC
684	2017-11-10	15:49:05.29	37.77	14.63	27.7	3.5	ML	INGV
685	2017-11-16	03:33:31.47	35.57	11.15	6.22	3.0	MD	ISC
686	2017-12-01	22:10:47.97	35.83	14.55	11.3	3.0	ML	ISC
687	2017-12-06	21:51:45.46	35.27	10.62	59.4	3.2	MD	ISC
688	2017-12-13	11:18:28.95	36.51	14.69	17.7	3.4	ML	INGV
689	2017-12-13	11:52:16.92	36.51	14.66	17.6	3.5	ML	INGV
690	2017-12-14	01:13:45.54	36.44	14.65	15.3	3.8	ML	INGV
691	2017-12-14	01:59:20.82	36.51	14.64	16	3.6	ML	INGV
692	2017-12-30	18:31:52.99	34.54	10.36	10	3.1	Mb	ISC
693	2018-02-27	12:35:13.08	37.84	15.52	8.2	3.0	ML	INGV
694	2018-02-27	12:44:18.82	37.84	15.53	9.8	3.0	ML	INGV
695	2018-03-08	08:49:54.81	37.62	15.06	1.6	3.0	ML	INGV
696	2018-03-08	08:50:47.00	37.69	14.94	0.1	3.3	ML	INGV
697	2018-03-08	16:42:37.87	36.94	10.26	19.5	4.3	Mw	INGV
698	2018-03-19	17:46:41.91	37.76	14.98	9.1	3.2	ML	INGV
699	2018-03-23	16:50:28.90	36.73	12.69	24.2	3.0	ML	INGV
700	2018-04-11	04:48:12.88	37.73	15.94	42.4	3.7	ML	INGV
701	2018-04-13	08:31:33.87	33.33	15.51	10	3.7	Mb	ISC
702	2018-05-12	11:31:06.62	37.95	15.2	22	3.0	ML	INGV
703	2018-05-12	14:04:50.10	34.38	14.82	10	3.5	Mb	INGV
704	2018-05-19	11:01:56.46	37.68	15.88	31	3.0	ML	INGV
705	2018-05-21	12:21:30.42	36	13.1	8.5	3.7	Mb	INGV
706	2018-05-22	05:15:38.14	37.41	16.41	38	3.3	ML	INGV
707	2018-05-25	10:28:11.83	37.74	15.12	18.9	3.1	ML	INGV
708	2018-06-02	07:40:54.20	37.71	15.15	7.7	3.4	Mw	INGV
709	2018-06-05	16:18:39.51	34.66	13.49	10	3.4	Mb	ISC
710	2018-06-06	05:26:56.72	37.17	16.1	19.5	3.0	ML	INGV
711	2018-06-21	18:53:05.90	32.94	16.01	10	3.6	Mb	ISC
712	2018-07-07	07:11:45.70	37.85	13.98	6.3	3.8	Mb	INGV
713	2018-07-07	18:51:37.60	37.84	13.95	4.4	3.3	Mb	INGV
714	2018-07-10	16:23:45.73	37.02	10.12	6.94	3.0	MD	ISC
715	2018-07-15	16:46:17.32	36.21	11.23	12	3.4	MD	ISC

716	2018-07-18	21:20:36.83	37.72	15.01	8.1	3.4	Mb	INGV
717	2018-07-18	21:20:54.45	37.72	14.97	7.4	3.4	ML	INGV
718	2018-07-29	12:48:15.80	35.77	10.61	4.2	3.4	MD	ISC
719	2018-08-03	23:28:50.04	34.4	13.61	69.1	4.3	Mb	INGV
720	2018-08-04	04:07:08.95	34.4	13.68	9.96	4.2	Mw	INGV
721	2018-08-08	16:20:18.62	35.9	12.62	8.3	3.0	ML	INGV
722	2018-09-30	06:23:06.03	37.64	14.49	36.1	3.3	ML	INGV
723	2018-09-30	17:24:06.10	37.82	15.09	2.7	3.2	ML	INGV
724	2018-10-06	00:34:19.79	37.61	14.94	4.5	4.6	Mw	INGV
725	2018-10-09	21:08:53.63	37.61	14.9	5.4	3.2	ML	INGV
726	2018-10-09	22:43:50.25	37.75	15.79	31.4	3.2	ML	INGV
727	2018-10-23	22:47:54.00	37.78	15.01	24.8	3.1	ML	INGV
728	2018-10-26	08:28:56.25	37.9	14.46	6.9	3.3	ML	INGV
729	2018-10-26	09:30:09.59	36.64	12.75	24.4	3.2	ML	INGV
730	2018-11-18	14:22:23.71	34.62	13.29	10	3.6	ML	INGV
731	2018-11-20	05:06:21.07	37.71	14.92	23.8	3.0	ML	INGV
732	2018-11-20	05:06:36.04	37.71	14.9	23.2	3.2	ML	INGV
733	2018-11-20	05:53:42.37	37.71	14.92	22.7	3.1	ML	INGV
734	2018-12-12	20:50:13.19	37.81	14.19	4	3.0	ML	INGV
735	2018-12-13	04:14:13.83	37.81	14.2	8.4	3.6	Mb	INGV
736	2018-12-16	19:29:33.78	37.74	15.03	1.6	3.2	ML	INGV
737	2018-12-24	09:59:31.00	37.75	15	1.5	3.1	ML	INGV
738	2018-12-24	10:08:57.00	37.76	15	1.3	3.1	ML	INGV
739	2018-12-24	10:27:01.00	37.81	15.11	0	3.5	ML	INGV
740	2018-12-24	11:01:50.00	37.74	14.97	1	3.6	Mb	INGV
741	2018-12-24	11:12:04.00	37.72	15.03	1.3	3.1	ML	INGV
742	2018-12-24	11:26:20.00	37.72	15.02	2.2	3.0	ML	INGV
743	2018-12-24	12:04:50.00	37.73	14.95	0.8	3.2	ML	INGV
744	2018-12-24	12:08:55.00	37.72	15.04	2.1	3.8	Mw	INGV
745	2018-12-24	12:19:28.00	37.72	15.04	0.6	3.4	ML	INGV
746	2018-12-24	12:31:51.00	37.73	15.03	1.9	3.0	ML	INGV
747	2018-12-24	13:49:51.00	37.72	15.04	1.8	3.3	ML	INGV
748	2018-12-24	15:43:12.00	37.72	15.05	0	3.2	ML	INGV
749	2018-12-24	16:50:10.00	37.72	15.04	2.2	4.5	Mw	INGV
750	2018-12-24	18:26:19.00	37.71	15.04	0.5	3.1	ML	INGV
751	2018-12-24	18:43:31.00	37.69	14.98	1.4	3.1	ML	INGV
752	2018-12-24	19:00:02.00	37.71	15.03	2.6	3.3	ML	INGV
753	2018-12-24	19:26:18.00	37.69	14.97	2.1	4.0	Mw	INGV
754	2018-12-24	19:45:44.00	37.7	15.02	1.6	3.0	ML	INGV
755	2018-12-24	19:59:30.00	37.67	14.99	7.3	3.3	ML	INGV
756	2018-12-24	22:37:24.00	37.72	15.01	0.4	3.2	ML	INGV
757	2018-12-25	12:45:44.00	37.67	14.91	0	3.4	ML	INGV
758	2018-12-26	00:09:17.00	37.64	15.13	1.2	3.3	ML	INGV
759	2018-12-26	02:19:14.00	37.64	15.12	-0.3	4.9	Mw	INGV
760	2018-12-26	13:14:54.00	37.75	15.13	8.2	3.0	ML	INGV
761	2018-12-30	18:30:50.00	37.73	14.97	1.9	3.4	ML	INGV
762	2019-01-03	23:01:15.00	37.66	14.94	0.6	3.0	ML	INGV
763	2019-01-04	03:54:03.00	37.7	14.94	0.9	3.0	ML	INGV

764	2019-01-04	04:10:36.00	37.7	14.94	0.1	3.5	ML	INGV
765	2019-01-05	01:47:36.33	37.14	15.02	4.2	3.2	ML	INGV
766	2019-01-08	23:50:34.00	37.8	15.05	2.2	4.1	Mw	INGV
767	2019-02-02	08:46:39.52	35.7	11.99	0	3.1	MD	ISC
768	2019-02-02	11:54:37.08	37.6	14.96	3.4	3.2	ML	INGV
769	2019-02-14	16:24:35.31	33.46	11.14	0	3.0	Mb	ISC
770	2019-02-19	03:52:06.44	37.79	14.32	67.3	3.2	ML	INGV
771	2019-03-27	17:14:22.11	37.73	15.15	6.7	3.0	ML	INGV
772	2019-04-20	19:14:24.27	37.37	15.19	8.8	3.3	ML	INGV
773	2019-04-27	00:44:55.71	37.8	15.16	1.6	3.3	Mw	INGV
774	2019-04-27	00:54:39.43	37.82	15.11	5.3	3.0	ML	INGV
775	2019-05-07	08:09:22.23	37.82	14.22	6.2	3.3	Mw	INGV
776	2019-05-07	13:29:31.55	37.83	14.22	4.5	3.1	ML	INGV
777	2019-05-29	14:21:53.34	37.67	15.15	6.7	3.0	ML	INGV
778	2019-06-02	21:52:10.66	35.19	13.29	10	3.6	Mb	ISC
779	2019-06-05	20:23:18.14	37.85	14.56	9.8	3.6	Mw	INGV
780	2019-06-27	23:06:16.17	36.23	11.24	40.5	3.4	ML	INGV
781	2019-07-08	04:38:28.62	37.67	14.89	21	3.8	Mw	INGV
782	2019-07-08	16:48:51.66	37.66	14.89	21.1	3.4	Mw	INGV
783	2019-07-10	07:44:15.75	34.91	16.31	39.9	4.1	Mw	INGV
784	2019-07-21	09:26:59.40	36.01	10.75	0	3.0	MD	ISC
785	2019-08-05	10:16:21.75	37.66	13.22	7.7	3.6	ML	INGV
786	2019-08-09	03:35:22.94	35.55	12.87	6	3.2	ML	INGV
787	2019-08-11	13:56:18.74	36.36	11.14	5.2	3.0	MD	ISC
788	2019-08-14	23:26:22.24	37.96	15.91	17.8	3.7	Mb	INGV
789	2019-09-04	15:52:24.17	37.88	14.99	28.9	3.1	ML	INGV
790	2019-09-17	18:40:49.78	37.74	14.89	7.5	3.0	ML	INGV
791	2019-09-17	21:32:34.84	37.74	14.89	6.9	3.1	ML	INGV
792	2019-09-23	22:44:24.65	37.75	14.97	10.8	3.0	Mbtmp	ISC
793	2019-09-27	14:26:54.32	35.89	15.27	21.9	3.2	ML	INGV
794	2019-10-08	20:24:07.11	36.14	14.31	10	3.3	ML	ISC
795	2019-10-18	01:06:07.75	37.73	15.17	5.9	3.1	ML	INGV
796	2019-10-19	01:03:56.12	37.05	15.48	22.5	3.1	ML	INGV
797	2019-10-26	01:17:51.62	37.74	15.13	8.8	3.2	ML	INGV
798	2019-11-09	00:38:25.26	35.02	13.1	10	3.6	Mb	ISC
799	2019-11-13	13:26:11.86	37.74	15.14	8.2	3.1	ML	INGV
800	2019-12-17	23:48:44.37	37.84	14.94	28.3	3.4	Mb	INGV
801	2019-12-20	16:31:54.02	37.28	16.42	38.1	3.0	ML	INGV
802	2020-01-06	20:25:31.43	32.13	10.31	0	4.0	MD	ISC
803	2020-01-10	02:24:09.04	37.42	14.8	10.7	3.1	ML	INGV
804	2020-01-23	14:27:56.31	35.89	15.31	20.6	3.0	ML	INGV
805	2020-01-31	07:19:56.65	33.97	13.62	10	3.4	Mb	ISC
806	2020-02-03	15:04:21.08	37.74	14.64	22.7	3.0	ML	INGV
807	2020-02-03	15:13:47.60	37.75	14.65	25.1	3.7	Mb	INGV
808	2020-02-03	15:14:11.54	37.73	14.64	18.4	3.1	ML	INGV
809	2020-02-11	01:08:17.91	35.84	11.4	9.7	3.4	MD	ISC
810	2020-02-12	21:14:20.35	35.67	12.14	17.7	3.1	MD	ISC
811	2020-02-16	15:30:23.24	37.86	13.95	5.9	3.0	ML	INGV

812	2020-02-20	01:19:37.34	37.85	13.94	6.9	3.6	Mb	INGV
813	2020-03-10	16:08:14.83	35.26	14.53	10	3.4	ML	INGV
814	2020-03-16	09:22:49.57	36.84	11.86	0	3.3	MD	ISC
815	2020-03-22	10:32:12.26	37.73	15.11	5	3.2	Mw	INGV
816	2020-03-22	18:34:14.18	36.39	10.97	0.1	3.1	MD	ISC
817	2020-03-28	00:26:19.43	35.13	14.66	13.5	3.2	ML	INGV
818	2020-04-10	21:52:34.25	36.38	15.54	17.2	3.3	ML	INGV
819	2020-04-23	11:46:50.16	37.75	14.61	23.5	3.0	ML	INGV
820	2020-04-24	14:28:15.39	37.77	14.09	36.1	3.8	Mw	INGV
821	2020-04-25	00:40:03.43	37.74	14.65	24.3	3.7	Mb	INGV
822	2020-04-25	07:21:54.48	37.75	14.62	23.5	3.6	Mw	INGV
823	2020-05-03	02:33:12.45	37.86	16.07	58.6	3.0	ML	INGV
824	2020-05-04	17:14:37.71	37.96	12.51	7.8	3.2	ML	INGV
825	2020-05-10	03:07:43.66	34.82	14.92	0	3.8	Mb	ISC
826	2020-05-13	17:03:46.74	35.21	15.24	10	4.6	Mb	INGV
827	2020-05-27	21:21:13.10	37.73	14.78	23.6	3.3	Mw	INGV
828	2020-06-12	07:13:02.62	35.16	12.75	65.1	3.2	ML	INGV
829	2020-06-12	09:40:43.92	36.25	11.3	2.2	3.0	MD	ISC
830	2020-06-21	21:25:23.14	37.75	14.85	29.4	3.0	ML	INGV
831	2020-07-02	15:28:00.78	37.04	15.65	29.7	3.6	Mb	INGV
832	2020-07-16	10:16:29.10	37.86	14.45	5.4	3.4	Mw	INGV
833	2020-07-19	20:58:50.89	35.75	13.54	18.5	3.3	ML	INGV
834	2020-07-26	08:22:47.51	37.76	15.04	8.6	3.0	ML	INGV
835	2020-08-22	08:44:00.80	30.82	14.68	10	4.1	Mb	ISC
836	2020-09-06	15:51:41.43	35.59	10.78	0	3.5	Mb	ISC
837	2020-09-09	04:56:58.51	37.84	12.83	14.8	3.5	Mw	INGV
838	2020-09-14	03:47:09.66	37.84	12.82	16.4	3.4	Mw	INGV
839	2020-09-18	01:16:45.31	37.91	16.46	34.9	3.3	ML	INGV
840	2020-09-23	20:50:11.37	37.84	12.82	11.8	3.1	ML	INGV
841	2020-09-27	18:10:39.19	37.81	15.12	1.7	3.2	ML	INGV
842	2020-09-27	19:15:44.98	37.82	15.1	0.7	3.1	ML	INGV
843	2020-09-29	05:30:38.39	37.78	14.83	30.6	3.1	ML	INGV
844	2020-09-29	18:23:54.61	35.57	14.52	16.4	3.1	ML	INGV
845	2020-09-30	01:01:00.74	35.67	14.38	8	3.9	Mb	INGV
846	2020-09-30	02:51:54.80	35.69	14.34	3.9	3.1	ML	INGV
847	2020-10-01	03:45:13.05	35.67	14.44	8.9	3.0	ML	INGV
848	2020-10-01	09:00:14.18	35.67	14.42	8.2	3.1	ML	INGV
849	2020-10-10	18:37:36.21	36.61	11.57	0	3.2	MD	ISC
850	2020-10-16	04:52:57.45	37.52	16.29	32.4	3.1	ML	INGV
851	2020-10-17	12:11:23.49	37.83	14.57	36.2	3.0	ML	INGV
852	2020-10-17	12:29:14.44	37.82	14.58	30.9	3.2	Mw	INGV
853	2020-10-18	02:15:55.30	37.83	14.59	30.7	3.0	ML	INGV
854	2020-10-18	06:02:22.13	37.82	14.58	31.6	3.2	ML	INGV
855	2020-10-20	07:36:40.40	35.64	14.54	4.1	3.0	ML	INGV
856	2020-10-24	01:00:32.73	37.82	14.58	33.1	3.1	ML	INGV
857	2020-10-27	19:28:07.60	37.82	14.56	35.1	3.1	ML	INGV
858	2020-10-28	03:53:16.94	37.75	15.08	8.7	3.0	ML	INGV
859	2020-11-05	20:08:10.79	37.75	15.06	9.6	3.1	ML	INGV

860	2020-11-18	02:06:25.22	37.82	14.59	31	3.3	ML	INGV
861	2020-12-15	22:51:14.90	37.18	15.92	20.9	3.3	Mb	INGV
862	2020-12-22	20:27:24.29	36.93	14.41	29.5	4.4	Mw	INGV
863	2020-12-31	20:02:07.82	37.66	14.95	15.5	3.1	ML	INGV
864	2020-12-31	20:25:51.26	37.66	14.98	15.2	3.2	ML	INGV
865	2020-12-31	20:28:01.78	37.67	14.98	14.7	3.4	ML	INGV
866	2020-12-31	20:30:52.16	37.67	14.97	16.2	3.3	Mb	INGV
867	2020-12-31	20:58:09.76	37.67	14.97	16.4	3.4	Mw	INGV
868	2020-12-31	21:51:22.45	37.67	14.98	16	3.3	ML	INGV
869	2020-12-31	21:54:39.46	37.67	14.97	16.9	3.8	Mw	INGV
870	2020-12-31	23:01:11.45	35.91	15.26	20.1	3.0	ML	INGV
871	2021-01-01	00:12:15.32	37.66	14.96	15.5	3.0	ML	INGV
872	2021-01-05	04:11:47.69	36.09	12.48	23	3.0	ML	INGV
873	2021-01-12	16:38:35.19	37.81	14.35	6.3	3.5	Mw	INGV
874	2021-01-14	07:18:49.17	37.31	16.48	42.6	3.4	ML	INGV
875	2021-01-16	15:21:10.66	37.82	15.08	23.1	3.1	ML	INGV
876	2021-01-16	17:47:37.87	37.75	15	2.8	3.4	Mb	INGV
877	2021-01-16	21:08:14.11	37.82	15.07	24.3	3.1	ML	INGV
878	2021-01-17	16:11:31.35	37.94	14.34	26.8	3.0	ML	INGV
879	2021-02-07	08:58:12.07	37.37	15.66	26.2	3.5	ML	INGV
880	2021-02-08	09:34:08.41	36.54	12.95	23.8	3.2	ML	INGV
881	2021-02-08	23:56:39.50	36.52	12.99	24.1	3.1	ML	INGV
882	2021-02-11	23:26:38.14	37.75	15	3.7	3.0	ML	INGV
883	2021-02-27	18:54:29.61	37.17	15.93	20.3	3.5	Mb	INGV
884	2021-03-01	15:57:43.89	37.74	11.73	0	3.7	Mb	ISC
885	2021-04-12	03:44:23.12	33.57	15.87	18.5	3.9	Mb	ISC
886	2021-05-05	12:11:55.21	37.53	14.9	8.8	3.0	ML	INGV
887	2021-05-08	18:09:11.50	37.76	15.12	8.6	3.0	ML	INGV
888	2021-05-08	18:13:24.90	37.76	15.12	8.6	3.1	ML	INGV
889	2021-05-30	19:31:42.77	37.36	16.46	38	3.0	ML	INGV
890	2021-06-28	22:58:19.20	37.31	14.74	25.2	3.2	Mw	INGV
891	2021-07-01	19:35:06.47	35.79	12.65	18	3.0	ML	INGV
892	2021-07-13	23:01:49.00	37.87	15.72	31.1	3.0	ML	INGV
893	2021-07-19	05:17:10.91	34.33	13.58	0	3.7	Mb	ISC
894	2021-07-20	09:43:55.37	36.64	13.31	33.4	3.1	ML	INGV
895	2021-07-27	20:56:34.99	36.72	14.4	6.4	3.4	Mw	INGV
896	2021-09-10	17:21:10.00	37.74	15.11	8.3	3.0	ML	INGV
897	2021-09-18	09:39:12.56	34.96	14.07	0	3.5	Mbtmp	ISC
898	2021-09-22	02:24:28.73	34.81	13.96	16.6	3.5	ML	INGV
899	2021-09-27	00:00:17.50	34.79	13.95	19.5	3.0	ML	INGV
900	2021-09-27	00:14:13.75	34.65	14.29	38	3.1	ML	INGV
901	2021-09-27	02:27:42.38	34.74	13.87	27.4	3.0	ML	INGV
902	2021-10-02	02:39:33.60	34.73	14.34	18.6	3.6	ML	INGV
903	2021-10-09	06:52:45.22	34.82	13.94	10.1	4.0	Mb	INGV
904	2021-10-09	14:57:54.43	34.78	14.01	15	3.6	ML	INGV
905	2021-10-19	10:26:08.54	37.64	16.3	34	3.1	ML	INGV
906	2021-10-26	17:52:48.65	36.89	12.96	0	3.8	Mb	ISC
907	2021-10-28	19:14:49.87	35.49	13.01	22.3	3.8	ML	INGV

908	2021-11-02	16:49:59.65	37.02	15.13	25.8	3.1	ML	INGV
909	2021-11-02	19:25:59.03	37.47	15.71	30.1	3.4	ML	INGV
910	2021-12-13	02:25:59.08	34.67	13.97	37.8	3.9	Mb	INGV
911	2021-12-18	21:24:46.21	37.77	14.63	29.1	3.5	ML	INGV
912	2021-12-23	20:38:40.36	37.48	14.92	9.3	3.3	ML	INGV
913	2021-12-23	21:33:45.56	37.48	14.93	17.3	4.3	Mw	INGV
914	2021-12-24	06:14:44.78	37.47	14.92	10.2	3.1	ML	INGV
915	2021-12-24	09:19:52.00	37.71	15.11	7	3.6	ML	INGV

TABLE A3. FOCAL MECHANISMS LIST. THE NUMBER DESIGNATED TO EACH EVENT, LATITUDE, LONGITUDE, DATE, TIME (UTC), DEPTH (KILOMETERS), MAGNITUDE (MW), STRIKE 1 (°), DIP 1 (°), RAKE (°), AND REFERENCE CATALOG ARE REPORTED.

N.	Lat	Lon	Date	Time	Depth (km)	Mag (Mw)	Strike 1 (°)	Dip 1 (°)	Rake1 (°)	Catalog
1	33.41	13.29	1988-03-26	07:36.40	15	5.1	176	61	-5	GCMT
2	35.79	11.80	1989-01-03	16:52:24	15	5.1	247	90	180	GCMT
3	33.73	12.28	1990-11-11	11:57:39	15	5.2	291	90	-180	GCMT
4	37.25	14.90	1990-12-13	00:24:34	15	5.6	274	64	174	GCMT
5	34.99	12.44	1993-09-10	16:02:36	26.1	5.3	200	78	1	GCMT
6	32.97	15.11	1999-02-10	05:51:50	10	5.2	75	88	179	RCMT
7	34.79	13.85	2000-01-19	16:21:30	10	4.3	241	54	177	RCMT
8	35.92	9.81	2001-08-12	14:22:25	33	4.6	10	25	122	RCMT
9	35.85	9.89	2002-06-24	01:20:36	10	5.1	174	29	83	RCMT
10	36.01	14.90	2003-07-07	15:08:12	10	4.3	350	62	4	RCMT
11	36.10	10.91	2005-02-07	20:05:37	10	4.8	67	44	128	RCMT
12	36.22	10.87	2005-02-07	20:46:26	10	5.1	51	41	124	RCMT
13	35.97	12.94	2006-11-23	13:31:56	10	4.8	357	70	-2	RCMT
14	36.26	15.76	2006-11-24	04:37:40	11	4.4	188	82	0	RCMT
15	36.93	12.91	2007-04-10	19:17:32	22	4.1	100	75	164	TDMT
16	36.96	15.38	2007-06-15	22:56:00	17	3.3	12	87	20	TDMT
17	36.52	12.72	2009-03-19	08:27:54	28	4.4	255	48	-180	RCMT
18	34.27	13.92	2009-04-25	01:36:25	10	4.5	283	39	-133	RCMT
19	32.63	14.95	2009-12-29	11:08:55	10	5.0	268	31	-131	RCMT
20	35.82	14.88	2011-04-24	13:02:12	20.3	4.2	28	34	-76	RCMT
21	36.02	12.98	2011-12-18	15:01:00	10	4.7	272	63	-171	RCMT
22	37.00	15.06	2012-06-27	01:14:20	5	3.7	187	87	-8	TDMT
23	33.99	14.65	2012-07-03	05:03:42	10	4.7	233	63	-174	RCMT
24	32.80	12.33	2013-05-11	04:42:39	15	4.8	205	44	-68	RCMT
25	36.71	15.00	2013-08-24	17:18:18	18.5	4.4	109	37	105	ISC
26	33.18	15.80	2013-10-09	17:22:47	10	4.1	294	31	-82	RCMT
27	35.61	10.98	2013-10-18	15:08:32	10	4.7	101	58	175	RCMT
28	35.60	10.93	2013-10-21	19:37:00	10	4.5	89	71	165	RCMT
29	36.67	14.94	2013-12-15	03:57:33	15	4.1	83	47	143	RCMT
30	35.63	14.88	2014-05-21	04:13:33	9	3.5	112	82	-148	TDMT
31	36.78	16.50	2014-09-26	23:38:11	40	4.2	267	75	170	ISC
32	36.46	12.03	2016-01-02	12:36:24	10	4.2	268	79	-178	RCMT
33	36.14	14.67	2016-01-13	17:01:30	10	4.2	262	79	175	RCMT
34	36.99	14.86	2016-02-07	01:41:59	5	3.3	193	89	13	TDMT
35	36.99	14.90	2016-02-08	15:35:43	10	4.5	280	42	178	RCMT
36	36.77	15.81	2016-05-25	22:10:28	20	4.1	224	34	139	RCMT
37	36.53	11.12	2016-06-02	10:49:13	10	4.4	184	66	9	RCMT
38	36.07	13.04	2016-06-03	09:59:52	30	4.1	11	44	-27	RCMT
39	33.50	11.29	2017-05-04	08:26:58	15	4.5	327	38	-104	RCMT
40	35.66	14.86	2017-08-23	09:16:24	13	3.8	350	86	-172	TDMT
41	35.34	15.49	2017-08-25	17:10:43	10	4.1	268	66	-167	RCMT
42	36.60	11.09	2017-10-31	00:16:39	11	4.2	270	85	178	RCMT
43	36.44	14.65	2017-12-14	01:13:45	15	3.8	26	80	134	TDMT

44	37.10	10.31	2018-03-08	16:42:36	10	4.3	281	33	110	RCMT
45	34.23	9.74	2018-05-21	00:18:34	10	4.9	302	74	-175	RCMT
46	34.33	13.65	2018-08-04	04:07:00	10	4.2	321	26	-79	RCMT
47	37.44	15.06	2018-10-06	00:34:20	10	4.7	268	64	8	RCMT
48	35.12	16.09	2019-07-10	07:44:17	32	4.1	55	85	-150	ISC
49	34.87	14.97	2020-05-10	03:07:45	10	4.1	326	36	-87	RCMT
50	35.66	14.42	2020-09-30	01:01:01	11	4.3	291	25	-133	RCMT
51	36.92	14.37	2020-12-22	20:27:24	30	4.5	93	72	-168	RCMT
52	37.31	14.74	2021-06-28	22:58:19	25.2	3.2	30	72	-44	ISC
53	36.72	14.40	2021-07-27	20:56:34	6	3.4	46	84	-16	TDMT
54	37.48	14.92	2021-12-23	21:33:45	11	4.5	119	66	-154	RCMT

TABLE A4. EARTHQUAKE RELOCATION LIST. ARE REPORTED THE NUMBER ASSIGNED TO EACH EVENT, DATE (YMD: YEAR, MONTH, DAY), TIME (HM, SEC: HOUR, MINUTE, SECOND, MILLISECOND), LATITUDE, LONGITUDE, DEPTH (KILOMETERS), MAGNITUDE, AND MAGNITUDE TYPE.

N.	ymd	hm	sec	Lat	Lon	Depth (km)	Mag
1	120	2016	55.32	37.50750	11.63950	34.2	3.3
2	501	1321	0.8	36.80133	11.57483	35.8	3.6
3	501	1324	37.99	36.49367	11.06867	18.2	3.4
4	10123	1655	32.41	37.19950	15.16717	19.8	3.3
5	10526	1330	48.4	36.96033	11.46200	5.0	3.3
6	10830	1351	40.24	36.54583	15.13067	2.2	3.3
7	10906	1241	37.47	36.99817	11.83050	1.4	3.1
8	20615	1232	34.19	36.24450	13.88033	28.3	3.0
9	21201	919	58.65	36.31183	11.00167	21.9	3.2
10	21201	926	18.95	35.71650	11.16683	10.0	3.3
11	30305	1721	27.6	37.34933	13.14383	10.4	3.3
12	30504	804	6.85	36.88383	13.67033	0.3	3.0
13	40411	37	28.01	35.27183	14.20383	40.0	3.2
14	40610	544	8.98	36.87867	12.65483	20.0	3.1
15	40610	605	24.67	36.25350	12.84950	11.6	3.4
16	40703	1052	46.04	36.37483	10.72100	10.0	3.1
17	40730	654	7.74	36.91317	14.40683	8.8	3.1
18	41126	1925	16.23	35.18100	12.82100	10.0	3.0
19	41230	404	50.07	36.94733	14.68367	26.5	3.5
20	50108	1659	14.56	36.66500	14.72100	5.5	3.1
21	50320	218	15.53	36.52867	14.33550	24.2	3.0
22	50422	1540	49.9	35.47400	15.17000	7.2	4.0
23	50530	2119	38.46	36.26950	15.25483	16.8	3.0
24	50628	2338	6.84	35.88833	11.46950	22.5	3.4
25	50707	859	51.2	37.30300	13.93800	27.4	3.8
26	50716	934	42.74	37.30550	13.32217	19.8	3.5
27	50831	349	23.27	36.73350	10.71467	11.9	3.3
28	51001	835	21.43	36.79200	14.29900	21.3	3.6
29	51001	841	43.74	36.84133	14.29033	8.7	3.2
30	60116	1353	25.63	36.88300	11.15583	5.4	3.2
31	60423	1442	37.59	37.08883	14.99200	19.1	3.9
32	60507	1547	51.93	36.73333	12.69033	7.1	3.3
33	60616	1833	59.94	36.28883	12.86550	1.0	3.0
34	60617	56	6.24	36.27767	12.71733	15.0	3.1
35	61010	2107	18.63	36.40183	11.73067	26.9	3.3
36	61014	2355	29.6	37.28617	14.80167	15.0	4.0
37	61216	716	50.58	36.02517	12.82933	27.4	3.2
38	61216	1946	43.27	36.01683	12.63100	20.0	3.1
39	70206	1052	1.06	36.41200	13.14317	0.0	3.2
40	70211	2030	58.61	36.92233	14.87650	24.5	3.4
41	70215	426	23.33	35.68767	14.81333	15.0	3.1
42	70410	1917	32.07	36.92600	13.72400	10.0	3.8
43	70615	2256	0.08	37.00950	15.28233	22.8	3.3
44	70705	2343	34.23	36.96433	14.32317	14.4	3.0

45	70711	1410	13.36	36.98217	14.32483	9.2	0.0
46	70730	1951	59.68	37.49017	14.75633	19.2	3.2
47	70731	653	16.15	37.46800	14.73800	27.8	4.0
48	70816	836	26.68	36.73900	14.87317	12.5	3.0
49	80224	1058	25.92	35.59983	13.77933	36.7	3.3
50	80607	18	46.49	36.17900	12.71600	10.0	3.4
51	80607	1354	53.21	35.85617	12.77867	11.9	3.3
52	80723	407	13.26	36.58533	15.14000	13.9	3.3
53	80724	56	25.48	36.05867	15.18867	37.3	3.3
54	81005	527	24.95	36.96950	14.69433	22.1	3.4
55	90426	450	17.39	37.27617	14.13033	15.7	3.0
56	90520	1431	17.26	35.06000	15.08000	10.0	3.0
57	90521	317	44.8	35.01000	15.12400	10.0	3.0
58	90521	319	45.39	35.23367	15.09200	4.3	3.0
59	90526	2117	57.44	35.40833	15.07683	0.0	3.0
60	90729	1930	4.45	35.40800	15.20917	1.7	3.0
61	90729	2158	27.8	35.22467	14.91733	0.0	3.1
62	90730	258	38.64	35.56250	15.07383	0.0	3.0
63	90730	538	55.71	35.20017	15.17717	0.0	3.3
64	90807	906	23.65	35.94117	14.82750	6.7	3.4
65	90816	749	42.91	35.11200	15.15000	10.0	3.1
66	90923	1301	6.22	36.23800	13.09300	17.9	3.1
67	91018	344	49.51	37.05450	15.15783	22.6	3.3
68	91018	806	10	35.03550	14.38450	40.0	3.6
69	100209	251	55.97	36.45567	13.45167	30.0	3.0
70	100216	642	17.9	35.43050	14.05167	3.1	3.5
71	100226	1638	51.49	35.37817	13.16033	11.1	3.0
72	100508	2223	29.88	36.59000	15.16650	16.4	3.6
73	100629	745	5.5	36.12117	13.74817	0.1	3.0
74	101110	822	45.22	35.16200	14.19500	10.0	4.0
75	101112	443	38.46	35.29267	14.32933	20.7	3.8
76	101119	1924	58.95	35.09600	14.48100	20.0	3.3
77	101224	1452	36.62	36.88800	14.66317	20.1	3.0
78	110217	1504	1.93	35.69917	14.31550	12.9	3.2
79	110306	844	6.24	37.09167	15.10800	24.8	3.3
80	110326	1924	39.31	37.10150	15.02900	18.6	3.1
81	110423	2210	59.38	35.87933	14.79467	20.6	3.5
82	110424	134	0.73	35.91000	14.89150	6.4	3.3
83	110424	439	0.13	35.88017	14.89217	10.7	3.4
84	110424	921	18.71	35.94967	14.86433	6.1	3.7
85	110424	925	27.2	35.96333	14.87567	4.2	3.7
86	110424	1302	12.64	35.87050	14.82133	22.1	4.2
87	110425	610	20.23	35.80183	14.86467	18.8	3.4
88	110426	410	30.28	35.87350	14.83350	25.7	3.5
89	110511	1517	12.37	35.81983	14.46533	5.4	3.3
90	110726	103	37.5	36.61867	12.88300	9.2	3.7
91	110831	1633	17.97	37.12450	14.69750	6.3	4.0
92	111009	828	25.64	37.03367	15.12900	7.6	3.3
93	111009	1724	59.1	37.00150	15.02600	8.4	3.1
94	111010	919	18.3	36.99367	15.03883	12.4	3.1
95	111116	640	36.15	35.33100	14.27633	10.0	3.6

96	111218	1530	5.88	36.48250	12.97833	4.8	3.0
97	120204	1453	12.49	37.14350	15.32267	22.0	4.0
98	120311	2117	54.78	36.51600	12.68500	30.0	3.5
99	120625	1052	49.68	37.02483	15.10550	8.7	3.1
100	120626	1113	55.38	36.91300	11.87283	20.7	3.1
101	120627	114	19.08	37.00617	15.08917	8.4	3.7
102	120627	120	58.4	37.01867	15.07767	6.8	3.0
103	120627	248	0.95	37.02950	15.06883	6.4	3.3
104	121120	525	15.58	35.61917	12.89017	0.0	3.5
105	130120	603	35.56	36.73033	14.87250	28.6	3.0
106	130311	1018	20.08	37.27100	15.39400	19.1	6.0
107	130321	945	54.38	36.61117	14.84050	10.5	3.1
108	130325	2208	12.11	35.94783	11.52917	10.0	3.9
109	130514	1351	57.19	36.20183	15.11517	19.2	4.8
110	130824	1718	17.95	36.73650	15.05017	8.7	4.4
111	130826	345	27.86	36.70183	14.13667	13.7	3.7
112	131018	1105	19.53	36.76083	14.97867	7.5	3.1
113	131215	357	33.48	36.76617	15.01350	5.5	3.9
114	140513	810	16.76	36.11950	13.00300	24.9	3.2
115	140521	413	34.36	35.87133	14.77817	0.5	3.5
116	140711	2203	16.94	36.64000	15.20117	27.2	3.0
117	140715	2143	56.5	37.12800	13.07317	23.4	3.0
118	141029	537	11.93	36.35000	10.57750	25.7	3.1
119	141111	1030	6.64	36.39550	14.31283	17.3	3.0
120	141112	1207	14.33	36.38933	14.27950	37.8	3.1
121	150105	727	1.84	37.19600	15.31517	23.4	5.0
122	150208	1939	20.73	37.35450	15.23217	20.7	4.0
123	150223	258	25.77	37.44500	14.74083	16.4	4.0
124	150531	2137	32.76	36.51383	11.67550	17.7	3.1
125	150626	851	10.5	36.24817	12.64983	19.1	3.8
126	150920	823	25.01	35.26733	14.71667	0.0	3.5
127	151102	248	5.61	37.32100	12.09783	23.9	3.2
128	160113	1701	29.05	36.11150	14.76650	18.6	4.2
129	160120	357	57.54	36.47600	12.70767	22.2	3.4
130	160207	141	57.8	37.01350	14.85117	5.6	3.3
131	160208	1535	42.11	37.01417	14.85233	6.1	4.2
132	160208	1757	36.76	37.01317	14.85083	5.9	3.7
133	160314	2230	39.98	35.46017	11.91983	14.0	3.4
134	160409	455	22.71	35.46717	13.13100	30.3	3.0
135	160507	955	31.65	37.13417	14.74667	19.5	3.5
136	160509	154	21.05	36.09533	12.87067	38.5	3.0
137	160626	427	36.69	37.38533	11.90400	3.4	3.6
138	160817	1052	4.8	36.12283	14.82417	14.1	3.5
139	161229	35	52.97	36.33517	13.76417	32.5	3.0
140	170719	2016	52.61	36.15167	13.03833	18.0	3.1
141	170808	1429	27.15	35.71850	14.77683	14.7	3.3
142	170821	1737	15.76	35.74583	14.69000	22.3	3.0
143	170823	916	25.41	35.81850	14.80133	8.5	3.8
144	170825	1710	47	35.76100	15.06950	2.5	4.0
145	170902	45	33.7	35.63650	15.11300	15.5	3.4
146	170906	152	15.61	35.60083	15.08867	20.0	3.0

147	170923	2230	42.36	35.57500	12.59850	29.3	3.3
148	171016	1340	46.93	35.66567	11.58750	13.5	3.5
149	171031	946	7.53	36.61200	10.96467	33.5	3.2
150	171213	1118	28.19	36.55317	14.68433	14.5	3.4
151	171213	1152	15.32	36.54483	14.66283	8.2	3.5
152	171214	113	44.53	36.51200	14.65300	8.1	3.8
153	171214	159	19.37	36.55350	14.65150	8.3	3.6
154	180521	1221	30.47	36.00767	13.02467	15.2	3.7
155	180808	1620	18.71	35.88400	12.68283	15.1	3.0
156	190105	147	35.26	37.17583	15.04733	8.5	3.2
157	190420	1914	24.27	37.36683	15.18500	8.8	6.0
158	190809	335	23.22	35.60000	12.76517	10.8	3.2
159	190927	1426	55.03	35.88683	15.21133	33.1	3.2
160	191019	103	55.76	37.09167	15.44267	22.7	4.0
161	200110	224	7.33	37.44183	14.80183	13.9	4.0
162	200123	1427	57.4	35.90767	15.24133	30.3	3.0
163	200211	108	18.62	35.84217	11.36967	18.5	3.4
164	200310	1608	16.5	35.54317	14.39583	0.0	3.4
165	200328	26	19.43	35.12600	14.66067	13.5	3.2
166	200410	2152	35.45	36.43300	15.44983	35.4	3.3
167	200513	1703	42.38	35.11817	15.35200	20.0	4.6
168	200929	1823	56.7	35.77550	14.43000	6.4	3.1
169	200930	101	2.6	35.77333	14.45683	9.4	3.9
170	201001	345	14.22	35.78700	14.42217	5.4	3.0
171	201001	900	15.32	35.76667	14.36767	8.0	3.1
172	201020	736	40.4	35.64100	14.54050	4.1	3.0
173	201222	2027	23.21	36.96717	14.36383	29.5	4.4
174	201231	2301	12.15	35.94567	15.19783	26.9	3.0
175	210105	411	47.69	36.08700	12.48450	23.0	3.0
176	210701	1935	6.47	35.79400	12.64617	18.0	3.0
177	210727	2056	34.72	36.73767	14.38383	9.5	3.4
178	211002	239	34.6	34.91767	13.83917	34.3	3.6
179	211009	1457	55.36	34.82150	13.97433	39.9	3.6
180	211028	1914	50.94	35.63650	12.95633	28.8	3.8
181	211102	1649	59.04	37.04200	15.12267	23.6	3.1
182	870727	1914	31.17	36.93500	13.31700	17.9	3.3
183	870903	756	28.86	37.26817	13.59417	27.7	3.3
184	871015	652	16.39	37.10400	15.49700	5.0	3.3
185	880516	2331	13.57	37.41917	14.46167	22.5	3.3
186	880518	422	24.01	35.91833	13.19083	0.0	3.6
187	880628	212	5.34	37.60733	14.00950	18.3	3.5
188	890729	444	50.25	36.12667	10.76750	10.0	3.0
189	890730	1113	18.24	36.81033	11.40283	0.0	3.0
190	890805	1314	41.2	36.67417	12.33467	20.0	3.1
191	890811	2231	59.17	36.34983	15.29083	27.7	3.3
192	891002	1214	19.79	37.59833	15.04900	25.0	3.2
193	891110	319	10.48	37.40750	15.11233	7.3	3.4
194	900325	2053	43.88	37.44600	12.47583	10.0	3.0
195	900407	608	21.23	36.98433	14.46000	19.5	3.1
196	900621	619	55.42	36.61650	13.75233	7.5	3.4
197	901029	821	8.94	37.02483	14.56583	0.0	3.5

198	901029	825	39.43	36.32400	14.95300	5.0	3.3
199	901029	831	16.28	37.05050	14.56083	0.0	3.4
200	901213	24	27.48	37.34900	15.20417	17.5	4.7
201	901216	1350	28.16	37.27050	15.23400	18.7	3.8
202	901226	2226	11.99	37.29933	15.21617	6.2	3.0
203	910218	2325	33.95	36.44150	15.02133	27.2	3.0
204	910306	117	23.32	37.33750	15.24817	17.6	3.2
205	910626	50	0.1	37.43350	12.29283	37.7	3.3
206	920112	1230	14.11	36.36683	12.80067	0.0	3.3
207	920318	306	8.09	35.61467	14.86767	10.0	3.4
208	920805	931	47.49	37.45817	13.30900	37.7	3.1
209	920805	2135	56.76	37.53650	13.24850	11.5	3.2
210	920806	212	5.24	37.47667	13.25450	19.5	3.2
211	920806	306	53.12	37.35650	13.16783	16.9	3.3
212	920806	423	12.69	37.19650	13.08117	23.4	3.6
213	921221	2312	17.08	36.91867	12.73200	0.0	3.7
214	930510	2317	26.97	36.64400	14.28800	10.0	3.3
215	930801	2139	44.08	36.70450	14.30450	39.7	3.2
216	931031	247	14.09	35.03117	15.29067	10.0	3.2
217	940426	2022	54.16	35.37350	13.31267	10.0	3.2
218	940508	716	21.38	36.08383	13.06833	28.5	3.2
219	940525	530	34.82	35.90933	14.71917	10.0	3.3
220	950309	736	19.44	37.25633	15.28600	10.4	3.1
221	950610	2150	18.35	37.05717	15.38283	0.0	3.1
222	950723	2256	15.16	36.65967	12.06433	28.4	3.7
223	960206	1406	16.17	36.68833	12.53850	0.0	3.1
224	960215	543	38.82	36.57883	12.78133	17.9	3.4
225	960524	103	58.38	36.95933	11.81833	0.0	3.3
226	960608	131	17.31	35.75100	15.21000	10.0	3.2
227	961116	2144	57.48	36.27200	15.11867	0.0	3.4
228	970730	1606	35.77	37.32783	14.70200	12.8	3.7
229	971022	26	53.19	37.42017	14.91100	21.8	3.2
230	981201	1901	33.09	37.27383	14.92867	9.2	3.1
231	990328	2146	21.28	36.25583	14.19000	23.0	3.2
232	990412	533	39.39	37.31267	14.25833	29.5	3.4
233	991021	1040	24.13	37.48600	14.87167	8.9	3.0